System Redundancy Evaluation for Steel Truss Bridges

Youyou Cao

Dissertation submitted to the Faculty of the
Virginia Polytechnic Institute and State University
in partial fulfillment of the requirements for the degree of

Doctor of Philosophy
In
Civil Engineering

Roberto T. Leon, Co-Chair
William J. Wright, Co-Chair
Cristopher D. Moen
Matthew R. Eatherton
Finley A. Charney

September 17th 2015
Blacksburg, Virginia

Keywords: Redundancy, Steel Truss Bridges, Fracture Critical, System Analysis

System Redundancy Evaluation for Steel Truss Bridges

Youyou Cao

ABSTRACT

In current bridge practice, all tension members in a truss bridge are identified as fracture critical members which implies that a collapse is expected to occur once a member of this type fails. However, there are several examples which show that bridges have remained standing and shown little distress even after a fracture critical member was completely damaged. Due to the high inspection cost for fracture critical members, it would be beneficial to remove fracture critical designation from some tension members. This could be achieved via considering system redundancy. Since there is no clear guidance in existing codified provisions for assessing system redundancy, this research is undertaken to develop simplified analysis techniques to evaluate system redundancy in truss bridges.

The proposed system redundancy analysis in this research starts with the identification of the most critical main truss members whose failure may significantly affect the system redundancy. The system redundancy is then measured by the remaining load capacity of a damaged bridge after losing one of the critical members. The bridge load capacity is checked using 3D models with nonlinear features that can capture the progression of yielding and buckling in a bridge system. The modeling techniques are validated through the case studies of the I-35W Bridge and one test span of the Milton-Madison Bridge. Reasonable correlations are demonstrated between the models and the measured data for these two bridges both in an undamaged and in a damaged state.

The feasibility of the proposed methodology for system redundancy evaluation is examined by applying the methodology blindly to two other simple truss bridges. The application shows that the proposed methodology can efficiently measure the system redundancy. To improve the system redundancy, this research also proposes sample retrofit strategies for the four example bridges.

ACKNOWLEDGEMENT

I would like to express my sincere appreciation and respect to the people who helped me on this journey. I am profoundly grateful to my advisors Dr. Roberto T. Leon and Dr. William J. Wright. I could not appreciate more that I can have the great opportunity to join their research teams. I especially feel it a great honor to gain tremendous help and continuous guidance from Dr. Roberto T. Leon. I appreciate that I can often learn new knowledge as well as critical thinking skills from him. I thoroughly enjoy working with him.

I would also like to give special thanks to my dissertation committee, Dr. Finley A Charney, Dr. Cristopher D. Moen, and Dr. Matthew R. Eatherton, for always willing to give me guidance and support. I am also strongly inspired by their passions to both research and education, their intense commitment to work, and their endless patience to international students.

Special thanks also go to Dr. Carin Roberts-Wollmann. She provided me with all the relevant documentations for the New River Bridge project. In addition to her help with my dissertation, her great effort in assigning me work as a teaching assistant is highly appreciated.

I am also indebted to my officemates and friends at Virginia Tech, Chia-Hong (Kenny) Fang, Yu Gao, Johnn P. Judd, Jeena Rachel Jayamon, Francisco Xavier Flores Solano, Amey Vivek Bapat, Mohammadreza Moharrami Gargari, David Alberto Padilla-Llano, Junle Cai, Tao Zou, Shaoqing Ge, and Qian Li. Without frequent discussions with these wonderful students, I would not accomplished this major milestone in my life.

I could not go without thanking my parents who never stop encouraging me and teaching me how to live a healthy life. Lastly, I would like to thank my boyfriend, Yuqi (Justin) Wang. He is incredibly supportive at all time.

Table of contents

List of Figures xi

List of Tables xxvii

1 Introduction 1

1.1 Background 1

1.1 Objectives 4

1.2 Methodology 4

1.3 Organization 9

1.4 Original Contributions 12

2 Literature Review 13

2.1 Introduction 13

2.2 Definition and Classification of Redundancy 13

2.3 Need for Redundancy Evaluation 16

2.4 Consideration of Redundancy in Bridge Standards 18

2.5 Methodologies for Redundancy Evaluation 20

2.5.1 Analytical Approaches 20

2.5.2 Modeling Details 24

2.5.2.1 Selection of Critical Loads 24

2.5.2.2 Simulation of Nonlinear Behavior 28

2.5.2.3 Identification of Critical Members 29

2.5.2.4 Rating of Critical Members 30
2.5.3 Destructive Tests 32
2.6 Key Findings and Limitations 34
2.7 Net Section Fracture at Connections 35
2.7.1 Fracture Failure Criterion 35
2.7.2 Finite Element Modeling Techniques 36
2.7.3 Guidelines for Net Section Fracture Simulation 40
2.8 Summary 40
3 Preliminary System Analysis 41
3.1 Methodology Overview 41
3.2 I-35W Bridge Description 42
3.3 System Model Development 46
3.4 System Model Validation 47
3.5 Consideration of Fracture Critical Connections 50
3.6 Modeling of Critical Live Loads 51
3.7 System Analysis of One Damaged Structure 55
3.7.1 Elastic System Analysis 56
3.7.2 Inelastic System Analysis 59
3.7.3 Result Comparison between Elastic and Inelastic System Analyses 61

3.7.4 Strain Rate Effect on the Yield Strength 64

3.7.5 Result Comparison between the Analyses with Static Yield Strength and with Dynamic Yield Strength 65

3.8 Conclusion 66

4 Evaluation of Connections 68

4.1 Introduction 68

4.2 Methodology 71

4.2.1 Identification of the Most Critical Connection 71

4.2.2 Modeling of the Truss Member with the Most Critical Connection 71

4.2.3 Simulation of Net Section Fracture 73

4.3 Verification 75

4.4 Net Section Capacity under a Combined Tension and Flexure 79

4.4.1 Net Section Capacity of a Single Plate 79

4.4.2 Net Section Capacity of a Box-Shape Truss Member 83

4.5 Conclusion 92

5 System Analysis with Refined Connection Details 94

5.1 Introduction 94

5.2 Modeling of Weak Connections 95

5.3 Effects of Weak Connections on System Behavior 99

5.4 Conclusion 102

6 System Anaysis with Bracing and Deck Effects 104
6.1 Introduction 104
6.2 Identification of Critical Brace Members 105
6.3 Material Plasticity 107
6.4 Initial Imperfections 110
6.5 Buckling Behavior Comparison 111
6.5.1 Deformation Comparison 111
6.5.2 Load-Deformation Comparison 112
6.6 Effect of Brace Buckling on Main Truss System 115
6.7 Significance of Nonlinear Concrete Deck Effect 118
6.8 Conclusion 120
7 Practical System Analysis 123
7.1 Introduction 123
7.2 Bridge Description 124
7.2.1 I-35W Bridge 124
7.2.2 M-Bridge 124
7.3 Modeling of Example Bridges 125
7.3.1 I-35W Bridge 125
7.3.2 M-Bridge 126

7.4 Model Calibration 134
7.4.1 I-35W Bridge 134
7.4.2 M-Bridge 146
7.5 Identification of Critical Members 152
7.6 Rating of Critical Members 159
7.6.1 Rating Factor Method 160
7.6.1.1 Load Rating for the I-35W Bridge 162
7.6.1.2 Load Rating for the M-Bridge 168
7.6.2 Strain Energy Method 174
7.6.3 Additional Findings from the Strain Energy Measures 181
7.7 Redundancy Evaluation for the Damaged Bridge Systems 186
7.7.1 P-M Interaction Failure 186
7.7.2 Buckling of Truss Member 187
7.7.3 Connection Failure 189
7.7.4 Damage on Deck 192
7.7.5 Investigation of Ultimate State for Damaged Bridge Systems 194
7.7.5.1 I-35W Bridge 195
7.7.5.2 M-Bridge 205
7.7.6 Examination of the Most Critical Live Load Condition for the Damaged Systems 211

7.8 A Step-by-Step Procedure for System Redundancy Analyses 213

7.9 Application of System Redundancy Analysis Methodology to Two Other Simple Truss Bridges 214

7.9.1 New River Bridge 214

7.9.2 Span No.4 of the Milton-Madison Bridge 224

7.10 Evaluation of the Proposed System Analysis Methodology 230

7.10.1 Appropriateness of Load Models 230

7.10.2 Efficiency of Nonlinear Analyses 232

7.11 Sample Retrofit Strategies 233

7.11.1 I-35W Bridge 233

7.11.2 M-Bridge 239

7.11.3 New River Bridge 241

7.11.4 Span No.4 of the Milton-Madison Bridge 245

7.12 Conclusion 248

8 Conclusions 252

8.1 Summary 252

8.2 Guideline for System Redundancy Evaluation 254

8.2.1 System Analysis Procedures 254

8.2.2 Critical Loading Condition 255

8.2.3 Redundancy Criteria 256

8.3 Key Findings from Example Bridge Studies 257

8.4 Redundancy Retrofit 261

8.5 Recommendations for Further Research 262

8.5.1 Probability of Failure on Each of the Critical Members 262

8.5.2 Model Sensitivity Studies 262

8.5.3 Reliability-Based Measure of System Redundancy 263

8.5.4 Further Experimental Studies for the Net Section Capacity under Combined Tension and Flexure 263

8.5.5 Improvement of Ultimate State Prediction in the Analytical Models 264

8.5.6 Improve the Design for New Truss Bridges with the Consideration of System Redundancy 264

References 265

Appendices 274

Appendix A: Details of the I-35W Bridge 275

Appendix B: Details of the Test Span of the Milton-Madison Bridge 280

Appendix C: Details of the New River Bridge 283

Appendix D: Details of Span No.4 of the Milton-Madison Bridge 285

List of Figures

Figure 1-1. Types of fracture critical bridges adapted from the National Bridge Inventory Database in 2010 (https://www.fhwa.dot.gov/bridge/britab.cfm) 3

Figure 2-1. Characteristics of one HS-20 truck. AASHTO (2010). LRFD Bridge Design Specifications. American Association of State Highway and Transportation Officials. Washington, D.C. Used under fair use, 2015. 25

Figure 2-2. Transverse configuration of two side-by-side HS-20 trucks with a minimum spacing of 4 feet on the Beech Creek Veterans Memorial Bridge. Reese, L. D. (2009). Critical Member Removal and Load Redistribution of a Deteriorated Truss Bridge. Civil Engineering. Pennsylvania State University. Master of Science. Used under fair use, 2015. 25

Figure 2-3. Live load model of TT-43 with a total truck weight=43tf. JRA (2002). Specifications for Highway Bridges Part I: Volume on Common Matters. Japan Road Association. Used under fair use, 2015. 27

Figure 2-4. Elevation view of the test span. Ocel, J. (2013). Evaluation of Member and Load-Path Redundancy on the US-421 Bridge over the Ohio River. Federal Highway Administration (FHWA). Washington D.C. Used under fair use, 2015. 32

Figure 2-5. Close-up view of Interstate 80 Sign Truss. Wipf, T. J. and B. M. Phares (2002). Evaluation of Interstate 80 Sign Truss. The Iowa Department of Transportation. The Bridge Engineering Center at the Center for Transportation Research and Education-Iowa State University. Used under fair use, 2015. 33

Figure 2-6. An illustration of the relationship between phantom nodes and original real nodes. Simulia (2010). Abaqus Analysis User Manual, Version 6.10, Providence, RI. Used under fair use, 2015..... 38

Figure 3-1. A side view of the I-35W Bridge. NTSB (2009). Collapse of I-35W Highway Bridge, Minneapolis, Minnesota, August 1, 2007. National Transportation Safety Board. Used under fair use, 2015. 42

Figure 3-2. Plan and elevation view of I-35W Bridge. Mn/DOT (2009). I-35W Bridge original plans & details. http://www.dot.state.mn.us/i35wbridge/history.html, Minnesota Department of Transportation. Used under fair use, 2015. 43

Figure 3-3. Major components in the bridge truss system viewing in a transverse direction. NTSB (2009). Collapse of I-35W Highway Bridge, Minneapolis, Minnesota, August 1, 2007. National Transportation Safety Board. Used under fair use, 2015. 44

Figure 3-4. 2D view of the idealized members and connections in the floor truss system. Ocel, J. M. and W. J. Wright (2008). Finite Element Modeling of I-35W Bridge Collapse Turner-Fairbank Highway Research Center. Used under fair use, 2015. 45

Figure 3-5. 3D view of a global model in ABAQUS for the I-35W Bridge. Ocel, J. M. and W. J. Wright (2008). Finite Element Modeling of I-35W Bridge Collapse Turner-Fairbank Highway Research Center. Used under fair use, 2015. 46

Figure 3-6. (a) Deflected shape of the bridge during collapse, looking northeast. NTSB (2009). Collapse of I-35W Highway Bridge, Minneapolis, Minnesota, August 1, 2007. National Transportation Safety Board. Used under fair use; (b) deflected shapes before and after the simulated failure at member U10'L9' in both trusses 48

Figure 3-7. Measured and predicted deflections of member L9L10 49

Figure 3-8. Simulation of a shear rupture failure at one gusset plate connection..... 51

Figure 3-9. Comparison of main truss deformation between the "AsBuilt" model and the HL-93 model..... 52

Figure 3-10. Lane load distribution of the HL-93 load..... 53

Figure 3-11. Transverse walkway loads 53

Figure 3-12. Elevation view of the center span between Piers 6 and 7 showing the HL-93 truck loads (unit: kips) that were applied to each of the eight traffic lanes 53

Figure 3-13. Close up 3D view of the HL-93 truck loads on eight traffic lanes 54

Figure 3-14. Load-deflection comparison between the undamaged and the damaged main truss structures..... 57

Figure 3-15. Beam-column interactions of the critical members in an elastic 3D system model (Note that all member interaction ratios result from sequentially applied dead load and the HL-93 load.) 58

Figure 3-16. Idealized stress-strain curves normalized by the nominal yield strength for a typical ASTM A572 Grade 50 steel 60

Figure 3-17. Von-Mises stress (unit: ksi) comparison between the elastic model (on the left) and the inelastic model (on the right) 62

Figure 3-18. Comparisons of load-deflection curves for the undamaged structure in the elastic analysis, as well as the damaged structure in the elastic and plastic analyses..... 63

Figure 4-1. Comparison of beam-column interactions at two ends of a critical member (U8U9) 69

Figure 4-2. Wreckage of member U10U11 on the East side of the main truss. NTSB (2009). Collapse of I-35W Highway Bridge, Minneapolis, Minnesota, August 1, 2007. National Transportation Safety Board. Used under fair use, 2015. 70

Figure 4-3. An elevation view of connection U9 of member U8U9. Sverdrup & Parcel and Associates Inc. (1965). State of Minnesota Department of Highway Construction Plan for Bridge No. 9340 – Balance of Bridge and Approaches. St. Louis, MO. Used under fair use, 2015..... 72

Figure 4-4. Simplified model for half-length of member U8U9 under a combined flexure and tension 72

Figure 4-5. Pure bending test set-up. Mohr, B. A. (2005). Investigation of Ultimate Bending Strength of Steel Bracket Plates. Masters of Science, Virginia Polytechnic Institute and State University. Used under fair use, 2015. 75

Figure 4-6. An elevation view of the simplified 3D model of the test specimen in pure bending 76

Figure 4-7. Failure mode comparison between (a) the test specimen Mohr, B. A. (2005). Investigation of Ultimate Bending Strength of Steel Bracket Plates. Masters of Science, Virginia Polytechnic Institute and State University. Used under fair use, 2015; (b) the FE model developed in ABAQUS 77

Figure 4-8. Strain gauge locations on the test specimen. Mohr, B. A. (2005). Investigation of Ultimate Bending Strength of Steel Bracket Plates. Masters of Science, Virginia Polytechnic Institute and State University. Used under fair use, 2015..... 77

Figure 4-9. Moment-strain curve comparison 78

Figure 4-10. Geometry of the critical net section of a single plate extracted from the built-up member in a box shape 80

Figure 4-11. Comparison of P-M interaction capacity between the net section and the gross section on one side plate of member U8U9 81

Figure 4-12. Moment-curvature relations for the net section and the gross section on one side plate of member U8U9 82

Figure 4-13. Meshed FE model of half box section of member U8U9 with member end U9 at the left side..... 84

Figure 4-14. Deflected shape of member U8U9 in the damaged structure with the removal of member U8L9 84

Figure 4-15. Equivalent plastic strain distribution when the first crack appears at the bottom edge of the side plate hole that is closest to the bottom cover plate (Note that all areas in gray represent the equivalent plastic strain that exceeds the 15% strain)..... 86

Figure 4-16. Out-of-plane bracing on each plate of the half-box-section model..... 87

Figure 4-17. P-M interaction comparison between net section and gross section..... 88

Figure 4-18. Equivalent section with a reduced thickness on the bottom cover plate..... 89

Figure 4-19. P-M interaction capacity predicted by FE model compared with that calculated using theoretical fiber analysis 89

Figure 4-20. (a) Original gross section of member U8U9 (b) Net section with access holes deducted in determining the section plastic capacity 90

Figure 4-21. P-M interaction capacity comparison among theoretical calculations using a gross section, an equivalent section, and a net section..... 91

Figure 5-1. Locations of plastic hinges that are displayed as dots near both ends of members U8U9 and L8L9 in the damaged structure 95

Figure 5-2. Net section used in determining the capacity of the critical section near U8 end of member U8U9..... 96

Figure 5-3. Net section used in determining the capacity of the critical sections near L8 and L9 ends of member L8L9..... 97

Figure 5-4. Idealized moment-curvature relation for plastic hinges..... 98

Figure 5-5. Comparison of P-M interaction behavior at each plastic hinge location 100

Figure 6-1. Location of the most critical brace member..... 106

Figure 6-2. Load-deformation curves compared to the theoretical buckling capacity 109

Figure 6-3. First mode shape of one critical brace member 110

Figure 6-4. Comparison between the undeformed shape (solid lines) and the deformed shape (dashed lines) of critical braces..... 112

Figure 6-5. Curves for compression versus lateral deformation at the brace member mid-point 113

Figure 6-6. Comparison of the axial-flexural interaction behavior at L9 of member L8L9..... 116

Figure 7-1. An aerial view of Milton-Madison Bridge (http://www.miltonmadisonbridge.com/the-project/)..... 124

Figure 7-2. A side view of the three-dimensional model for I-35-W Bridge in SAP2000. Lora, M. A. R. (2013). Study of the I-35W Highway Bridge Collapse Mechanism. Civil and Environmental

Engineering, Virginia Polytechnic Institute and State University. Master of Science. Used under fair use, 2015. 126

Figure 7-3. Cross sectional view of one beam element drawn align the deck plane in SAP2000. Diggelmann, L. M., et al. (2012). Evaluation of Member and Load-Path Redundancy on the US-421 Bridge over the Ohio River. Purdue University. Used under fair use, 2015. 127

Figure 7-4. Cross section with top center insertion point. Diggelmann, L. M., et al. (2012). Evaluation of Member and Load-Path Redundancy on the US-421 Bridge over the Ohio River. Purdue University. Used under fair use, 2015. 128

Figure 7-5. Cross section with insertion point offset and fictitious rigid links. Diggelmann, L. M., et al. (2012). Evaluation of Member and Load-Path Redundancy on the US-421 Bridge over the Ohio River. Purdue University. Used under fair use, 2015. 128

Figure 7-6. Load distribution diagrams (not to scale)..... 130

Figure 7-7. A side view of truss members and connections (http://www.miltonmadisonbridge.com/gallery/) 131

Figure 7-8. A close-up view of the connection details for a typical X-brace assembly. Diggelmann, L. M., et al. (2012). Evaluation of Member and Load-Path Redundancy on the US-421 Bridge over the Ohio River. Purdue University. Used under fair use, 2015. 132

Figure 7-9. Member end conditions in a typical X-brace assembly 132

Figure 7-10. Elevation view of main truss structure of I-35W Bridge 135

Figure 7-11. Influence lines for axial forces on member U9U10-West side (near loaded lanes)136

Figure 7-12. Influence lines for axial forces on member U9U10-East side (far from loaded lanes) 136

Figure 7-13. Influence lines for axial forces on member L9L10-West side (near loaded lanes) 137

Figure 7-14. Influence lines for axial forces on member L9L10-East side (far from loaded lanes) 137

Figure 7-15. Influence lines for axial forces on member L9U10-West side (near loaded lanes) 138

Figure 7-16. Influence lines for axial forces on member L9U10-East side (far from loaded lanes) 138

Figure 7-17. Nonlinear features in the ABAQUS model 140

Figure 7-18. Nonlinear features in the SAP2000 model 141

Figure 7-19. Behavior of nonlinear axial spring normalized by the yield properties 143

Figure 7-20. Behavior of each plastic hinge normalized by the yield properties: (a) axial behavior; (b) in-plane flexural behavior 144

Figure 7-21. Comparison of P-M interaction behavior at each plastic hinge location between SAP2000 model and ABAQUS model 145

Figure 7-22. Sand load distribution on the deck (highlighted in pink) 146

Figure 7-23. Nomenclature and location for each main truss member 147

Figure 7-24. Nomenclature and locations for the selected stringers and floor beam 148

Figure 7-25. Locations for the selected braces 148

Figure 7-26. Comparison of axial load demand for the main truss members in the I-35W Bridge under design dead load..... 153

Figure 7-27. Difference between the results from the 2D model and design values on the drawing for the I-35W Bridge..... 153

Figure 7-28. Comparison of axial load demand for the main truss members in the M-Bridge under design dead load..... 154

Figure 7-29. Difference between the results from the 2D model and design values on the drawing for the M-Bridge 154

Figure 7-30. A 2D model in SAP2000 for the I-35W Bridge showing critical diagonal and chord members..... 155

Figure 7-31. A 2D model in SAP2000 for the M-Bridge showing critical diagonal and chord members..... 156

Figure 7-32. A top view of the main truss and brace systems in the I-35W Bridge showing the locations of critical lower braces 165

Figure 7-33. Comparison of load distribution on the critical brace members between an undamaged structure and a damaged structure with the removal of member U8L9-W both under the same loading condition (0.20*DL when failure occurs on the critical lower brace connection)..... 167

Figure 7-34. Critical location on member U0L0, where a large in-plane bending effect can be observed as the ultimate failure mode 170

Figure 7-35. A simple illustration of the undeformed shape and the deformed shape of member U1L1 (Note: the red dot represents the location of plastic hinges formed in the ultimate state) 170

Figure 7-36. Comparison of the curves for the plasticity ratio versus loads on the ABAQUS models for the I-35W Bridge both in undamaged and damaged conditions 183

Figure 7-37. A close-up view for the cases: U10U11-damaged, U6L5-damaged, U10L10-damaged, U9L9-damaged, and Undamaged as plotted in Figure 7-36 184

Figure 7-38. Truss member connection details: (a) A shop drawing for a typical main truss to lower brace connection in the I-35W Bridge. Sverdrup & Parcel and Associates Inc. (1965). State of Minnesota Department of Highway Construction Plan for Bridge No. 9340 – Balance of Bridge and Approaches. St. Louis, MO. Used under fair use, 2015; (b) A photo showing a typical main truss connection and a typical main truss to sway brace connection in the M-Bridge (http://www.purdue.edu/newsroom/research/2011/110726ConnorBridge.html) 190

Figure 7-39. System load versus mid-span deflection curves for the I-35W Bridge in an undamaged condition 196

Figure 7-40. System load versus mid-span deflection curves for the I-35W Bridge with an initial damage on member L11L12 197

Figure 7-41. System load versus mid-span deflection curves for the I-35W Bridge with an initial damage on member L13L14 197

Figure 7-42. System load versus mid-span deflection curves for the I-35W Bridge with an initial damage on member U8U9 198

Figure 7-43. System load versus mid-span deflection curves for the I-35W bridge with an initial damage on member U7U8 198

Figure 7-44. System load versus mid-span deflection curves for the I-35W Bridge with an initial damage on member L9L10 199

Figure 7-45. System load versus mid-span deflection curves for the I-35W Bridge with an initial damage on member U14L13 199

Figure 7-46. System load versus mid-span deflection curves for the I-35W Bridge with an initial damage on member U10U11 200

Figure 7-47. System load versus mid-span deflection curves for the I-35W Bridge with an initial damage on member U6L5 200

Figure 7-48. System load versus mid-span deflection curves for the I-35W Bridge with an initial damage on member U10L10 201

Figure 7-49. System load versus mid-span deflection curves for the I-35W Bridge with an initial damage on member U9L9 201

Figure 7-50. 2D view of one main truss of the undamaged M-Bridge model in its ultimate state 205

Figure 7-51. 3D view of the M-Bridge model with an initial damage on member U1L0 in its ultimate state 205

Figure 7-52. 2D view of the damaged side of main truss for the M-Bridge model with an initial damage on member U1U2 in its ultimate state 206

Figure 7-53. 2D view of the damaged side of main truss for the M-Bridge model with an initial damage on member U2U3 in its ultimate state 206

Figure 7-54. 2D view of the damaged side of main truss for the M-Bridge model with an initial damage on member U3U4 in its ultimate state 206

Figure 7-55. 3D view of the M-Bridge model with an initial damage on member L3L4 in its ultimate state 207

Figure 7-56. 2D view of the M-Bridge model with an initial damage on member L1L2 in its ultimate state 207

Figure 7-57. 3D view of the M-Bridge model with an initial damage on member U1L2 in its ultimate state 207

Figure 7-58. 3D view of the M-Bridge model with an initial damage on member U2L3 in its ultimate state 208

Figure 7-59. 3D view of the M-Bridge model with an initial damage on member L2L3 in its ultimate state 208

Figure 7-60. 3D view of the M-Bridge model with an initial damage on member U2L2 in its ultimate state 208

Figure 7-61. 3D view of the M-Bridge model with an initial damage on member L0L1 in its ultimate state 209

Figure 7-62. 3D view of the M-Bridge model with an initial damage on member U0L0 in its ultimate state 209

Figure 7-63. 3D view of the M-Bridge model with an initial damage on member U1L1 in its ultimate state 209

Figure 7-64. 3D view of the M-Bridge model with an initial damage on member U3L3 in its ultimate state 210

Figure 7-65. 3D view of the M-Bridge model with an initial damage on member U3L4 in its ultimate state 210

Figure 7-66. The main span truss structure of the New River Bridge. Hickey, L. J., et al. (2009). Live Load Test and Failure Analysis for the Steel Deck Truss Bridge Over the New River in Virginia. Report No.: FHWA/VTRC 09-CR8. Virginia Transportation Research Council. Charlottesville, VA. Used under fair use, 2015. 215

Figure 7-67. Comparison of axial load demand (unit: kips) for the main truss members in the New River Bridge under design dead load between the results from a 2D elastic model and the values on the design drawing 216

Figure 7-68. Difference between the results from the 2D model and design values on the drawing for the New River Bridge 217

Figure 7-69. HL-93 load configuration I: only one span is assigned the HL-93 load 217

Figure 7-70. HL-93 load configuration II: two spans are assigned the HL-93 load (Note that both the truck load and the lane load in this model are 90 percent of their corresponding loads in the model shown in Figure 7-69 to account for a relatively low probability of this loading condition as specified by AASHTO (2012)) 218

Figure 7-71. A 2D model in SAP2000 for the New River Bridge showing critical chord and diagonal members 219

Figure 7-72. Comparison of axial load demand (unit: kips) for the main truss members in the New River Bridge under design dead load between the results from a 3D elastic model and the values on the design drawing 220

Figure 7-73. Difference between the results from the 3D model and design values on the drawing for the New River Bridge 220

Figure 7-74. Model calibration of the influence line for nodal deflections when the two HS-25 truck loads were moving along the centerline of the deck 221

Figure 7-75. Model calibration of the influence line for member axial forces when the two HS-25 truck loads were moving along the centerline of the deck 221

Figure 7-76. 3D system of the Span No.4 of the Milton-Madison Bridge modeled in SAP2000 224

Figure 7-77. Comparison of axial load demand (unit: kips) for the main truss members in the Span No.4 of the Milton-Madison Bridge under design dead load between the results from a 2D elastic model and the values on the design drawing 225

Figure 7-78. Difference between the results from the 2D model and design values on the drawing for the Span No.4 of the Milton-Madison Bridge 225

Figure 7-79. Comparison of axial load demand (unit: kips) for the main truss members in the Span No.4 of the Milton-Madison Bridge under design dead load between the results from a 3D elastic model and the values on the design drawing 227

Figure 7-80. Difference between the results from the 3D model and design values on the drawing for the Span No.4 of the Milton-Madison Bridge 227

Figure 7-81. Illustration of steel cable installation 234

Figure 7-82. Illustration on how an H-shape cross section was strengthened 239

Figure 7-83. A steel grid deck fully filled with lightweight concrete. Modjeski and Masters (2011). Winona Bridge - Deck Rehabilitation Options. Used under fair use, 2015..... 243

Figure 7-84. A half-filled steel grid deck. Modjeski and Masters (2011). Winona Bridge - Deck Rehabilitation Options. Used under fair use, 2015. 243

Figure 7-85. Exodermic deck. Modjeski and Masters (2011). Winona Bridge - Deck Rehabilitation Options. Used under fair use, 2015..... 244

Figure 7-86. 3D view of the main truss members (highlighted in blue) and top diagonal brace members (highlighted in red) in the Span No.4 of the Milton-Madison Bridge..... 246

Figure A-1. Overall geometry of the truss system. Sverdrup & Parcel and Associates, Inc. (1965). State of Minnesota Department of Highway Construction Plan for Bridge No. 9340 – Balance of Bridge and Approaches. St. Louis, MO. Used under fair use, 2015. 277

Figure A-2. Dimensions of brace members. Sverdrup & Parcel and Associates, Inc. (1965). State of Minnesota Department of Highway Construction Plan for Bridge No. 9340 – Balance of Bridge and Approaches. St. Louis, MO. Used under fair use, 2015..... 278

Figure A-3. Dimensions of floor truss members. Sverdrup & Parcel and Associates, Inc. (1965). State of Minnesota Department of Highway Construction Plan for Bridge No. 9340 – Balance of Bridge and Approaches. St. Louis, MO. Used under fair use, 2015..... 278

Figure B-1. Dimensions and design loads for floor truss members, stringers, and top lateral braces. J.G. White Engineering Corporation (1928). Used under fair use, 2015..... 280

Figure B-2. Dimensions and design loads for main truss members. J. G. White Engineering Corporation (1928). Used under fair use, 2015..... 280

Figure B-3. Dimensions and design loads for bottom lateral braces. J. G. White Engineering Corporation (1928). Used under fair use, 2015..... 281

Figure B-4. Dimensions and design loads for typical sway braces: (a) at the end panel points (U0 and U0'); (b) at intermediate panel points (U1 through U1'). J.G. White Engineering Corporation

(1928). Used under fair use, 2015……282
Figure B-5. Design loads for main truss members and lateral braces. J. G. White Engineering Corporation (1928). Used under fair use, 2015…… 282
Figure C-1. General information of the bridge geometry. The Commonwealth of Virginia, Department of Highways, Virginia Transportation Research Council (1941). Used under fair use 2015……283
Figure C-2. Dimensions and design loads for truss members. The Commonwealth of Virginia, Department of Highways, Virginia Transportation Research Council (1941). Used under fair use 2015……284
Figure D-1. Dimensions and design loads for truss members. J.G. White Engineering Corporation (1928). Used under fair use, 2015…… 285

List of Tables

Table 3-1. Critical stresses and strains for a typical ASTM A572 Grade 50 steel 61

Table 3-2. Strain rate effect on the interaction behavior of critical members 66

Table 4-1. Comparison of moment capacity between the FE model results and the measured test data 79

Table 4-2. Comparison of critical flexural capacities between the net section and the gross section (unit: in-k) 82

Table 4-3. Comparison of flexural and tensile capacity among theoretical calculations using a gross section, an equivalent section, and a net section 92

Table 5-1. Comparison of inelastic flexural stiffness of plastic hinges 98

Table 6-1. Comparison of critical brace member demand-to-capacity ratio 106

Table 6-2. Comparison of axial stiffness of the critical braces 110

Table 6-3. Geometric properties and theoretical buckling capacity of the critical braces 113

Table 6-4. Maximum principal stress comparison 119

Table 7-1. Member stress comparison on the main trusses in the undamaged structure (unit: ksi) 147

Table 7-2. Member stress comparison for the selected stringers and floor beam in the undamaged structure (unit: ksi) 148

Table 7-3. Member stress comparison for the selected braces in the undamaged structure (unit: ksi) 149

Table 7-4. Member stress comparison on the main trusses in the damaged structure (unit: ksi) 150

Table 7-5. Member stress comparison for the selected stringers and floor beam in the damaged structure (unit: ksi) 151

Table 7-6. Member stress comparison for the selected braces in the damaged structure (unit: ksi) 151

Table 7-7. Comparison of the ranking for critical members between the D/C ratio based method and the load rating method for the I-35W Bridge 156

Table 7-8. Comparison of the ranking for critical members between the D/C ratio based method and the load rating method for the M-Bridge 158

Table 7-9. System load capacities and governing failure modes for the I-35W Bridge in the undamaged and damaged conditions 163

Table 7-10. System load capacities and governing failure modes for the M-Bridge in the undamaged and damaged conditions 169

Table 7-11. Comparison of member axial stresses in the undamaged structure under sand loads to the stresses under 1.63 times of the HL-93 load 171

Table 7-12. Classification of critical members in the M-Bridge 173

Table 7-13. System strain energies for the I-35W Bridge in both undamaged condition (U_0) and damaged conditions (U_d) 176

Table 7-14. System strain energies for the M-Bridge in both undamaged condition (U_0) and damaged conditions (U_d) 177

Table 7-15. Critical member prioritization results using load rating factor compared with the prioritization results based on strain energy release for the I-35W Bridge 179

Table 7-16. Critical member prioritization results using load rating factor compared with the prioritization results based on strain energy release for the M-Bridge 180

Table 7-17. Prioritization of a selected number of critical damaged structures for the I-35W Bridge using load factors determined by the plastic strain energy based approach and the load rating method..... 185

Table 7-18. The critical member buckling load comparisons among SAP2000 model results, ABAQUS model results, and the theoretical buckling strength and yield strength..... 188

Table 7-19. Comparison between the maximum principal stresses on decks in the system models and the elastic stress limits of the smeared reinforced concrete deck in the I-35W Bridge 193

Table 7-20. Comparison between the maximum principal stresses on decks in the system models and the elastic stress limits of the plain concrete deck in the M-Bridge..... 194

Table 7-21. System ultimate load capacity comparison between the SAP2000 and ABAQUS models 203

Table 7-22. Load capacity reduction from an undamaged structure to a structure with two members damaged 204

Table 7-23. System load capacity comparison under various truck load conditions..... 212

Table 7-24. System load capacities and governing failure modes for the New River Bridge in the undamaged and damaged conditions 223

Table 7-25. System load capacities and governing failure modes for the Span No.4 of the Milton-Madison Bridge in the undamaged and damaged conditions 229

Table 7-26. Comparison of moment at the mid-span of the example bridges 231

Table 7-27. Comparison of nonlinear system models developed in SAP 2000 and in ABAQUS 232

Table 7-28. Comparison of cross section and capacity for each retrofitted member in the I-35W Bridge 236

Table 7-29. System load capacity comparison between the original and the retrofitted structures for the I-35W Bridge 237

Table 7-30. Dimension of the critical member cross section and the steel plates used in the retrofit 239

Table 7-31. Elastic section modulus comparison between the original H-shape and the strengthened tube-shape 240

Table 7-32. System load capacity comparison between the original and the retrofitted structures for the M-Bridge 241

Table 7-33. Comparison of dead load on the New River Bridge with different deck options ... 244

Table 7-34. System load capacity comparison between the original and the retrofitted structures for the Span No.4 of the Milton-Madison Bridge 245

Table 7-35. Comparison of cross section and capacity for each retrofitted member in the Span No.4 of the Milton-Madison Bridge 247

Table A-1. Dimensions of the main truss members 275

1 Introduction

1.1 Background

In 1967, the Silver Bridge, an eye bar chain suspension bridge built in 1928 and connecting Point Pleasant (WV) and Gallipolis (OH), collapsed while it was under rush-hour traffic, taking away 46 lives. Investigation of the wreckage revealed that the collapse was caused by a brittle fracture of one of the non-redundant eye bars supporting the main span (NTSB 1971). In response to this catastrophic collapse, the material, design, fabrication, shop inspection, and in-service inspection requirements for steel bridges were improved during the 1970's (Connor and Parr 2007). As an additional effort to prevent collapse in the event of fracture, Federal Highway Administration (FHWA) led the development of the first fracture control plan (FCP) for non-redundant bridges. In 1978, an improved FCP was implemented as a result of the publication of the AASHTO Guide Specification for Fracture Critical Non-Redundant Bridge Members (Wright 2002). This Guide Specification defined fracture critical members (FCMs) as members whose failure may lead to collapse of the structure. These FCMs were required to have a lower probability of brittle fracture than non-FCMs.

Unfortunately, about 76% of all bridges with FCMs presently in the United States' inventory were fabricated prior to the implementation of the FCP in 1978. Most of these fracture critical bridges (83%) are two-girder bridges and two-line truss bridges, and 43% of the FCMs are riveted. Hence, there is a considerable number of bridges in service whose FCMs were not designed with the aforementioned additional fracture reliability (Connor and Parr 2007). However, all FCMs in

existing structures, whether they are relatively new or old, are treated the same for inspection purposes in current bridge practice.

A major problem with the current FCM approach is that there are numerous examples of bridges with FCM members that have fractured, but the bridges did not even partially collapse. Typical cases for two-girder bridges (all designated as fracture critical) that sustained a full-depth fracture of one of its two girders include: (a) the US-422 Bridge over the Schuylkill River in Pottstown, PA, which did not collapse even after the entire bottom flange and approximately 9 in. of the web fractured in 2003 (Connor et al. 2004); (b) the Neville Island Bridge on I-79, whose full-depth fracture remained unnoticed until it was spotted by a nearby boater in 1977 (Fisher 1984); and (c) the Lafayette Street Bridge over the Mississippi River at St. Paul, Minnesota with a large crack on one girder did not close for repair until a 6.5 in. dip was detected to form at the road surface in 1976 (Fisher 1984). These damaged bridges provide evidence that, under certain circumstances, a redundant load path does exist in these structures to redistribute loads (Barnard et al. 2010). Thus members with fracture damage could be re-classified as non-fracture critical. There is a research need to develop robust methodologies to evaluate the redundant load carrying capacity of a damaged bridge system after one critical member fractured.

For truss bridges, the predominant type of Fracture Critical Bridges as seen from Figure 1-1, all tension members are currently identified as FCMs based on simplified analysis assumptions. However, this identification criterion is challenged by a recent accident on Mathews Bridge in Jacksonville, Florida (Scanlan and Gilliam 2013). Although one bottom chord truss member was basically removed after being hit by a US Navy transport ship, this major bridge did not collapse and no injuries were reported. Officials for the Florida Department of Transportation further determined that there was no potential danger to river traffic passing below. This is a clear example

that some tension members in a truss bridge may be removed from the fracture critical designation, as this failure did not lead to a collapse.

One direct benefit from a re-classification of truss members is significant inspection costs savings. According to Connor et al. (2005), inspections for FCMs are labor intensive and costly, requiring the traditional "arm-length in-depth" techniques to be performed every 24 months. Although hard data is not available, anecdotal evidence indicates that these costs can easily run in the $5K-$25K range and that these inspections need to be made every six months for cases of major bridges where fatigue cracks and similar problems exist. These costs are borne by the states, and thus there are powerful incentives to redefine FCM.

There is currently no clear guide for engineers on how to perform a system analysis to identify fracture critical members. Typically, members are classified as FCM based on very simplified 2D models and idealized boundary and connection conditions. The main aim of this study is to propose a rational and simplified methodology to evaluate system redundancy after one critical member fractured. This system redundancy evaluation forms the basis of identifying fracture critical members.

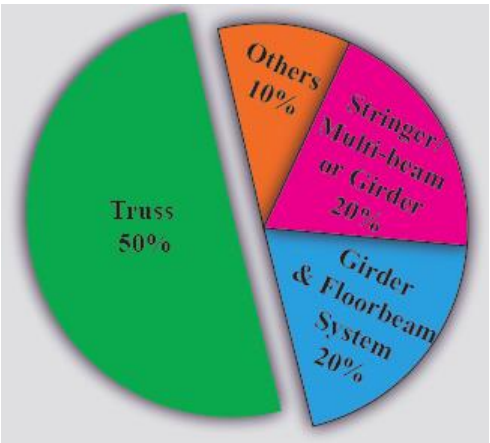

Figure 1-1. Types of fracture critical bridges adapted from the National Bridge Inventory Database in 2010 (https://www.fhwa.dot.gov/bridge/britab.cfm)

1.1 Objectives

The primary objectives of this dissertation are to improve methods to:

(1) identify critical main truss members whose failure can cause a significant reduction of system strength capacity;

(2) estimate the remaining load capacities for the damaged structures after losing one critical main truss member;

(3) evaluate system redundancy for truss bridges after failure of one critical main truss member; and

(4) retrofit an existing or damaged structure.

1.2 Methodology

There is limited experimental data available concerning the ultimate capacity of bridge systems, and even less experimental data addressing the capacity of damaged structures. Moreover, the analytical tools available to trace the failure of a structure from a local damage to a global system collapse present formidable modelling and computational obstacles. An infamous paradigm is the numerical simulation of the progressive collapse of World Trade Center towers (Bažant 2007). Due to a shroud of dust and smoke, it was impossible to determine the conditions within the building core from the photographic database. Thus even an extremely sophisticated analytical model could not provide acceptable reliability for key parameters such as the energy dissipation per unit height, the compaction ratio of a crushed story, and the fraction of mass shedding outside the building perimeter. As a result, this progressive collapse analysis can be viewed with skepticism if enough information about its real behavior is not available (Khandelwal 2008). Based on these constraints, the scope of this thesis had to be reduced to a manageable size as it constitutes

one of the first large-scale efforts on this topic for bridges. Thus this thesis is focused on the use of static analysis to estimate the residual strength of damaged truss bridges in the final stable state.

The analysis of dynamic impact on overloading members following a sudden fracture or buckling failure is beyond the scope of this research, as it will be a daunting task for bridge engineers to determine a rational damping ratio used in the simulation of dynamic behavior without conducting experiments on the specific structural configuration. Damping ratios are notoriously difficult to determine for bridges and similar structures as they are amplitude dependent. Tests tend to show large damping ratios as test amplitudes are small. In general, a 1% damping ratio is recommended as a default value.

For ease of analysis, the dynamic impact is accounted for by applying a dynamic amplification factor to a static load model. Since this dynamic amplification factor will also rely very heavily on the specific structural configuration, the recommendation of a representative dynamic amplification factor is not included in this study.

The static analyses proposed for system redundancy assessment can be divided into two parts. Part I performs a 2D and elastic analysis to identify critical main truss members. The proposed identification approach relies on selecting the main truss members with high Demand-to-Capacity (D/C) ratios for axial loads in an intact bridge structure. Since the skewed truss bridges are not included in this research, the behavior of the two lines of main truss structure can be considered symmetric about the deck longitudinal centerline. Thus it is adequate to simulate one line of main truss structure as a 2D model. Considering that a bridge in an undamaged condition is designed to behave elastically, nonlinear features are not needed for the 2D model.

Part II is primarily used for evaluating system redundancy in a damaged bridge after one of those critical members is removed from the structure. This study is focused on 3D inelastic analyses.

Because failure of a single member will make the two-line main truss structure asymmetric about the deck longitudinal centerline, a 3D model for an entire bridge system is necessary for analyzing the bridge behavior in a damaged state. In response to a member failure, the original load carried by the damaged member must be redistributed to the remaining members. As a result, some remaining members may be overstressed and deformation of the adjacent members will be increased. The behavior of a damaged bridge is thereby very likely to include a combination of nonlinear effects such as yielding, buckling, and large deformation. In this regard, the existence of nonlinear behavior is examined for main truss members, brace members and deck system. The possible failure modes on truss member connections are also analyzed. The first occurrence of failure on one of these structural components is captured through incorporating geometric nonlinearity and material plasticity into the 3D system models. The remaining load capacity of a damaged structure is determined as the minimum loads that cause the first component failure.

As an attempt to determine the worst single-member-out scenario associated with the lowest remaining load capacity of a damaged bridge, various damaged structures are modeled by removing the previously identified critical members one at a time. The most critical member can be considered as the member whose failure will lead to the least remaining load capacity in its associated damaged structure. As the remaining load capacity is a measure of the system redundancy, the structure rated as most critical is equated to the damaged system with less redundancy, making the structure more vulnerable to collapse. Thus a proper rating of critical members can bring significant economic benefits in that the allocation of inspection and maintenance resources can be prioritized to more critical members.

As previously discussed, there is very limited experimental data available concerning the ultimate capacity of bridge systems. It is even more difficult to test the capacity of damaged bridge systems

by conducting full scale experiments. This research thereby utilizes full 3D models developed in ABAQUS as "virtual" benchmarks to perform system redundancy assessment. Since the research team has a highly detailed working model of the I-35W Bridge, this bridge model is chosen as a baseline model to study the behavior of a damaged truss system.

From the search of available finite element analysis software at Virginia Tech, the ABAQUS program (Simulia 2010) is shown to provide the most robust nonlinear analysis features for bridge behavior simulation. The ABAQUS results will provide a basis for determining guidelines on how to perform a refined system analysis. To be specific, the results from the nonlinear ABAQUS model of the I-35W Bridge will make the bridge engineers clear about the appropriate selection of primary factors in a system redundancy analysis, such as the critical loading cases to be studied, location of the most vulnerable component after one member is damaged, the required level of details in modeling a truss member and its connections, and choice of element type and fineness of mesh.

Concerning the great modeling effort and long computational time in using ABAQUS software, simplified methodologies for system redundancy analysis are also explored for practical application by engineers. The SAP2000 program (CSI 2013) is selected as the platform for performing the simplified system analysis, as this software is most commonly used in current structural engineering projects for both building and bridge structures. The results from a simplified analysis using SAP2000 will be compared to the ones predicted from an advanced analysis using ABAQUS. Once adequate level of correlation between the results from these two types of analyses can be demonstrated, the modeling techniques for a simplified system analysis using SAP2000 will be applied to other truss bridges to determine potential limitations.

During a full scale demolition test conducted on one approach span of the Milton-Madison Bridge over the Ohio River, the bridge response to a complete damage on one main truss member was measured using field instrumentation. The experimental data can be used to confirm the ability of the modeling techniques used in SAP2000 to accurately predict the behavior of a damaged bridge structure. Once the modeling techniques are validated, the application of a simplified system redundancy analysis can be extended to more general truss bridges. Two simple truss bridges (the New River Bridge in Hillsville, Virginia, and the Span No.4 of the Milton-Madison Bridge), whose design plans are available to this research team, are thereby modeled in SAP2000 using the proposed methodology for a simplified system redundancy analysis. The feasibility and limitations of the proposed methodology will then be discussed.

Relevant details of the aforementioned four example bridges are provided in Appendices A through D. Because of the complexity of the models, it is not possible to fully describe them therein. To obtain the complete model files in PDF format, contact the author or her advisers.

From the maintenance prospective, a system redundancy analysis is also of great importance as it predicts the most vulnerable components to failure in the ultimate state of a structure. Retrofit resources can be allocated toward these most critical components to ensure sufficient system redundancy. In particular, effective retrofit strategies are needed for the most critical remaining components to protect the damaged structure from collapsing when a single member is damaged or under replacement. In light of this concern, a set of sample retrofit strategies will be provided following the system redundancy evaluation for the four example bridges studied in this research.

1.3 Organization

The remaining Chapters of this proposal are organized as follows. Chapter 2 presents a brief literature review, which explains (1) how redundancy is defined and classified; (2) why redundancy needs to be evaluated for existing bridge structures; (3) how to consider redundancy in the design of a new bridge. This chapter also discusses both analytical and experimental approaches for redundancy evaluation implemented by previous researchers. In addition, methodologies for identifying critical members that can greatly affect the system redundancy are assessed. This chapter also reviews the criteria and FE modeling techniques for predicting fracture at critical net sections of steel members. Lastly, key findings from the case studies of redundancy evaluation for truss bridges are summarized.

From Chapter 3 to Chapter 6, modeling techniques for performing refined system redundancy analyses using ABAQUS program are presented. The analyses discussed in these chapters rely heavily on a case study for the I-35W Bridge. These refined modeling techniques form the basis of a simplified system analysis for redundancy evaluation. The results predicted from the ABAQUS models provide insights on the key factors that are necessary to be considered in assessing system redundancy. Chapter 3 discusses the importance of considering material plasticity and geometric nonlinearity in properly capturing the behavior of the I-35W Bridge in a damaged state. This chapter also analyzes the system effects of failure on a gusset plate connection in the main truss structure. Additionally, the rate dependent material properties are investigated in this chapter primarily to ensure that a rational yield strength is assigned to the truss members. In Chapter 3, one limitation of performing a system analysis based on the existing 3D system model is identified as the inability of capturing failure at the critical net sections near the ends of the main

truss members after a single member is removed from the system because of the fixed end condition assumption used for main truss members.

To deal with the aforementioned limitation, Chapter 4 presents the studies about the behavior of main truss member connections in the ultimate state using highly detailed local models. The goal of this evaluation is to explore the actual capacity of the critical main truss member connections, where significant moments evident in the damaged system potentially enabled fracture to initiate at the net section due to tension and flexure interaction.

With the known net section capacities at the critical main truss connections, the modeling assumptions for these connections can be refined in the 3D system models. The approach of incorporating the critical connection capacities predicted in Chapter 4 into the system models is thereby discussed in Chapter 5. Prior to this discussion, Chapter 5 starts with the identification of the critical connections in the main truss system. The system effects of considering the actual net section capacities at the critical connections is also explored through comparing the different axial-flexural interaction behavior at these connections between the system models with and without a refined modeling assumption for these connections.

Chapter 6 examines the effect of damage on secondary load carrying components in the model for the I-35W Bridge after it loses one main truss member. This includes a study of buckling failure of the critical brace member, a prediction of failure progression from the brace buckling to the bridge collapse, and an investigation on plastic damage on the deck system. The goal for the assessments in this chapter is to determine if a brace member or a portion of deck will failure prior to a failure in the main truss system. If this is true, then the system models need to be further refined to ensure that the first component failure can be captured.

Chapter 7 proposes a simplified methodology for system redundancy evaluation. In this chapter the system analyses are performed using models developed in SAP2000. The approaches for identifying and rating critical members are discussed. The modeling techniques for simulating the behavior of a bridge system are validated through demonstrating reasonable correlations between the predicted member behavior and the measured data from the case studies of the I-35W Bridge and the test span on the Milton-Madison Bridge. Then this simplified methodology for assessing system redundancy is blindly applied to two other simple truss bridges whose system responses to a single member damage have not been tested. This application is undertaken to confirm the ability of using the simplified methodology for evaluating system redundancy in truss bridges with different configurations, as well as to explore potential limitations of this methodology. Furthermore, as an attempt to improve the system redundancy for those damaged structure that may be considered not functional due to insufficient ultimate load capacity, this chapter also discusses sample retrofit strategies for the four example bridges.

Chapter 8 begins with a review of the research objectives and scope of work, and then it proposes a guideline for system redundancy evaluation of existing truss bridges. In the proposed guideline, major procedures for conducting system analysis are presented. This guideline also emphasizes the importance of selecting a critical loading condition for a given structure when performing a system redundancy analysis. In addition, the criteria for determining the adequacy of system redundancy in a bridge structure is discussed. This chapter also summarizes the key findings from the system redundancy studies for the four example bridges. The feasibilities and potential limitations of the proposed methodologies in evaluating system redundancy for a truss bridge are discussed. This last Chapter also provides recommendations for future studies on this research topic.

1.4 Original Contributions

The original contributions in this research include the:

(1) development of methodologies in predicting the behavior in a 3D system of a truss bridge up to an ultimate state using both finite element analyses in ABAQUS (Chapters 3 to 6) and simplified system analysis in SAP2000 (Chapter 7);

(2) exploration of the feasibility of a strain energy based approach to rate critical members in a truss bridge (Section 7.6.2);

(3) discussion of possible applications of strain energy concepts to bridge system analyses in both undamaged and damaged conditions (Section 7.6.3);

(4) verification of the accuracy of fracture failure prediction using the extended finite element method in ABAQUS (Sections 2.7.2 and 4.3);

(5) prediction for net section capacity under a combination of tension and flexure (Section 4.4);

(6) investigation of the actual contribution of brace members to the system redundancy in a damaged structure (Sections 6.5 and 7.7.2);

(7) examination the existence of damage on deck system in response to a single truss member failure (Sections 6.6 and 7.7.4);

(8) demonstration of adequate level of accuracy in predicting the critical member deformation on the I-35W Bridge in a faulted state and the axial load behavior on the tested members in the Milton-Madison Bridge as compared to the measured data (Sections 3.4 and 7.4.2); and

(9) proposal for a guideline of performing system redundancy analysis for existing truss bridges (Section 8.2).

2 Literature Review

2.1 Introduction

As a prelude to this research, a comprehensive literature review of both the current state of practice and the existing research for evaluating system redundancy in steel truss bridges was conducted. In this chapter, a discussion of previous analytical and experimental research focusing on bridge system redundancy assessment is given first. These studies will provide the basis and validation for the system analysis methodology to be proposed later in this dissertation. A brief introduction into the main approaches for identifying members that are critical to the redundancy in a bridge system is then presented. Finally, research related to the prediction of net section fracture is provided, as this is identified as a very likely failure mode on a member after another single member is damaged.

2.2 Definition and Classification of Redundancy

Under the current Bridge Design Specification (AASHTO 2012), henceforth *Specification*, redundancy is defined as "the quality of a bridge that enables it to perform its design function in the damaged state." This redundancy definition is not specific about what type of damage, load type, damage magnitude, and/or damage distribution is being addressed. Important items such as whether dynamic impact is to be considered and which load factors are to be used in assessing the damaged structure are not specified (Connor et al. 2005). Even the definition of collapse, given as "a major change in the geometry of the bridge rendering it unfit for use", is less than precise. The *Specification* states that, a "component in tension whose failure is expected to result in the collapse of the bridge or the inability of the bridge to perform its function shall be designated as fracture

critical and the associated structural system as non-redundant." Although the *Specification* states that redundancy should be demonstrated using a refined analysis, it does not provide any criteria for that analysis. The level of rigor needed for a refined analysis is to be mutually agreed upon by the Owner and the Engineer. The *Specification* implies that the level of system redundancy is determined subjectively and that further improvements to these guidelines are anticipated.

By conducting an extensive survey of bridge owners and consultant inspectors, Connor et al. (2005) summarize that redundancy is often discussed in terms of three types: internal redundancy, structural redundancy and load-path redundancy, as follows:

Internal (member) redundancy exists within a member containing multiple parallel elements, such as a built-up member made from bolted or riveted elements but not from welded elements. A member with internal redundancy can prevent a crack in one element from propagating to the adjoining elements within the member. In other words, a fracture failure of one element will not result in the failure of other elements in the member if internal redundancy exists. An alternate means of providing internal redundancy is recognized when the member is fabricated with high toughness steel that assures crack arrest.

Structural (system) redundancy reflects external static indeterminacy due to continuity of a load path. It often occurs in two or more spans continuous girder or truss bridges. Furthermore, some bridge 3D action also contributes to structural redundancy, mostly through the participation of secondary members and deck.

Load-path redundancy represents internal static indeterminacy. This form of redundancy can be identified if more than two main load carrying components remain active in supporting the entire structure. Therefore, multi-girder bridges are classified as redundant, whereas two-girder bridges are deemed as non-redundant. As truss bridges are often comprised of two longitudinal lines of

main truss, they are regarded as non-redundant bridges. In fact, there is considerable debate on the existence of load-path redundancy in two-girder bridges, because two case studies of two-girder steel bridges that had suffered major fracture of one girder did remain serviceable under normal highway traffic (Fisher 1984). Likewise, the two-line truss bridges not always lack load-path redundancy. As mentioned in Section 1.1, the recent accident on the Mathews Bridge shows that a bridge can remain functional even after a primary truss member is damaged.

In the preparation of the NCHRP Synthesis 354, Connor et al. (2005) recognized that internal and structural redundancy were often neglected by agencies and designers. A recent Technical Memo published by FHWA (2012) reveals that only load-path redundancy is accounted for in current redundancy evaluation practice. This memo encourages the consideration of structural (system) redundancy, as some two-girder bridges and two-line truss bridges were found to gain redundancy from 3-dimensional system behavior via recent experimental and analytical research (Cha et al. 2014; Williamson et al. 2010). This memo also states that, "Engineers have begun to discover through modern analytical techniques that system redundancy may often exist, even though there are few apparent secondary load paths."

Guidance and recognition regarding structural (system) redundancy for bridges traditionally classified as fracture critical are also provided in this memo. However, the memo does not recognize that internal (member) redundancy from built-up details may affect the classification of a FCM. The potential benefits from internally redundant detailing are not considered sufficient to demonstrate that a bridge will still be safe for use after losing one FCM.

2.3 Need for Redundancy Evaluation

In response to the collapse of the Silver Bridge as introduced in Section 1.1, AASHTO published the first Fracture Control Plan (FCP) for bridges (AASHTO 1978). This plan officially established the terminology of fracture critical and the philosophy is still used today for fracture control in steel bridges (Wright 2002). The FCP provided many ways the fracture safety of structures could be improved including: provide higher material toughness, reduce weld defects, improve fatigue design reliability, increase in-service inspection requirements for fatigue, and require structural redundancy. There was considerable debate on the need for material toughness, as increasing toughness would have substantially raised the cost of steel production at that time. Thus a large emphasis was placed on the other four aspects of fracture control. Due to more stringent requirements for fracture critical bridge design, fabrication, and inspection, most bridge owners have been reluctant to build new fracture critical bridges. As a result, the majority of fracture critical bridges were fabricated prior to the implementation of the FCP in 1978. Thus the main need for bridge owners is further narrowed down to enhance inspection quality and frequency for existing bridges, as well as improve structural redundancy so that structures with certain level of damage can still fit for use.

Interestingly, other international codes do not address either fracture critical members or structural redundancy. For instance, there appears to be no special requirements for non-redundant members in Eurocode 3 (CEN 2005), as well as Chinese Steel Design Code (GB50017-2003 2003). Although the Canadian code (CAN/CSA-S6) and the Danish code (Danish Roads Directorate 2004) proposed different target member reliabilities, the criteria set in these first-generation attempts were based on subjective assessments of risk and were established based on the judgment of the code writers (Ghosn and Moses 1998). In addition, the Danish code merely required a reliability

analysis at the individual member level rather than at the system level. The main drawback of a reliability analysis is that it requires measures of statistical variation that are often not available. Estimations have to be made. Therefore, this reliability approach proposed in the Danish code can hardly serve as a practical tool. However, after comparisons among the main international structural steel design codes, it is found that modern steel bridge engineering practices and code provisions in Japan are the only ones, besides the U.S. ones, paying special attention to the redundancy of a structural system.

In the latest Japanese steel design code issued by JSCE (2010), the need to perform redundancy analyses in order to evaluate alternate load paths in a bridge system is suggested. The motivation to study the system redundancy originates from the fact that most existing bridges in Japan are deteriorated and over 50 years old. To properly rate the condition of older bridges, this code recommends engineers address safety of the structure at the system level, whereas the code acknowledges that common practice usually focuses on the capacity of individual members and connections. Neither is a direct encouragement for redundancy analyses nor a specific description on how to assess the system redundancy provided in this code. There is also a lack of special considerations for fracture critical members, though the code discusses special requirements for structures operating at low temperatures to control brittle fracture.

2.4 Consideration of Redundancy in Bridge Standards

To consider redundancy in the design philosophy, both the US bridge design specification (AASHTO 2010) and the Japanese code (JSCE 2010) use similar redundancy factors in the calculation of load effects on an individual member. A redundancy factor is applied as a multiplier to the load effect on a member. The value of a redundancy factor is selected from a range between 0.95 and 1.05 in AASHTO (2010), which is comparable to a factor varies from 0.8 to 1.1 in JSCE (2010). A redundancy factor greater than one is assigned to non-redundant members in order to amplify the load effects on these members. Whereas a redundancy factor less than one is used for exceptional levels of redundancy beyond girder continuity and a torsionally-closed cross section (AASHTO 2010).

Since the selection of a specific value of a redundancy factor is based on a case-by-case engineering judgment, the effect of redundancy is estimated subjectively. More importantly, these two standards do not consider redundancy at the system level. The interaction between individual members, which can greatly affect the system behavior is thereby ignored in a bridge design process.

As an attempt to bridge the gap between a member-by-member design and a system interaction based approach, both NCHRP 406 (Ghosn and Moses 1998) and the AASHTO Manual for Bridge Evaluation (MBE) (AASHTO 2011) introduced a set of system factors as a means to incorporate safety and redundancy of the entire bridge system in the design and rating process. A system factor (φ_s) is applied as a multiplier to the nominal member resistance. A value of φ_s less than one is assigned to the members in a bridge with low redundancy.

Although guidance on determination of the system factor is provided in both NCHRP 406 and MBE, they still have a number of limitations for the redundancy analysis of fracture critical bridges. In the report NCHRP 406, all given analytical studies and experimental tests were conducted to assess the level of system redundancy in undamaged bridges. Hence, the reserve system ratios and reliability indices limits might not be applicable to evaluate damaged bridges. Moreover, the calibration of a system factor in NCHRP 406 is based on a grillage model, which has limited ability to predict force redistribution in a damaged structure. In the commentary of the MBE, it is stated that, "Internal redundancy and structural redundancy that exists as a result of continuity are neglected when classifying a member as non-redundant." This commentary recommends that φ_s be taken greater than 1.0, up to a maximum of 1.2 in some instances if the Engineer can demonstrate the presence of adequate redundancy in a superstructure system but applicable situations are not defined.

2.5 Methodologies for Redundancy Evaluation

The topic of system analysis applied to undamaged bridge structures is addressed in many sources. This review targets the specific cases that could be found where system analysis was applied to damaged structures. Research that studied the system behavior in response to a single member failure will also be discussed herein.

2.5.1 Analytical Approaches

An overview of three approaches for measuring the system effect of a local failure, which can occur either on a member or a connection, is presented by Starossek (2009). This book introduces the terminology of "robustness" to assess the sensitivity of a structural system to a local failure. Thus "robustness" can be considered comparable to the term "redundancy" as discussed previously. One possible relation between robustness and redundancy was given as "Bridge robustness is measured by the so-called redundancy factors, which serve to compare the system's capacity to member capacity." (Wisniewski et al. 2006).

A robust structure is defined as a structure that is insensitive to a local failure. According to this definition, robustness is a purely structural property, and thus it is uncorrelated to the cause and probability of a local failure. This failure is assumed to have already occurred when the structure is carrying loads. Starossek (2009) suggests that robustness be measured in one of the three following ways:

(1) examine the stiffness reduction of the entire system after removing a structural element;

(2) quantify total damage resulting from initial damage; or,

(3) compare the energy release during an initial failure and the energy required for failure to progress.

Approach (1) measures the robustness using a factor expressed as R_s. The magnitude of R_s is:

$$R_s = \min_j \frac{det\, K_j}{det\, K_o} \tag{2-1}$$

where K_j is the system stiffness matrix for the structure after removing a structural element or constraint j, and K_o is the system stiffness matrix of the intact structure. The value of R_s ranges between 0 and 1. A fully robust structure is associated with R_s=1, while a structure that has no robustness is associated with R_s=0. One primary limitation of this approach is found to be its inability to reflect the change of system behavior in a damage event, because often the reduction in system strength capacity caused by failure on a structural element does not correlate very well with the stiffness reduction. Thus it remains unknown if a damaged structure can avoid collapse by demonstrating sound alternate load paths.

Under approach (2), robustness is measured by:

$$R_d = 1 - \frac{p}{p_{lim}} \tag{2-2}$$

where R_d is the damage-based measure of robustness, p is the maximum total damage resulting from the assumable initial damage (which, more precisely, can be any of the assumable cases of initial local failure), and p_{lim} is the acceptable total damage . If the value of R_d is no greater than one, then the robustness of a structure is satisfactory. Such value can be obtained when $p \leq p_{lim}$, which means the resultant damage in a worst case scenario does not exceed the limit of damage that can be tolerated by the structure to avoid progressive collapse. Under this situation, the remaining structure is most likely to possess a certain level of reserve strength capacity. In this

regard, this damage-based approach is somewhat analogous to a strength-based approach, which may be expressed as:

$$\mathrm{R} = 1 - \frac{\text{system strength demand}}{\text{sytem available strength}} \tag{2-3}$$

Since the system load capacity is regarded as the most important measure for evaluating both the design of a new bridge and the condition of an existing bridge, a strength-based approach seems more suitable for bridge practice as compared to a stiffness-based approach. It is further speculated that utilizing strength rather than damage to measure robustness of a structure may simplify the required analyses. As indicated by Starossek (2009), the total damage caused by a local failure is determined by carefully tracking the failure progression, which in turn can involve geometrically and materially nonlinear dynamic analyses in the time domain. In fact, dynamic impacts can be produced by sudden failure on a structural component, such as brittle fracture at a connection or buckling on a member. Analyses considering such dynamic effects will lead to high computational cost. The level of complexity in performing a nonlinear dynamic analysis of this type is beyond the current capabilities of most bridge engineers. Therefore, a simplified measure of robustness is needed.

Approach (3) considers the energy change in a system induced by an initial failure. The energy-based measure of robustness, expressed as R_e:

$$R_e = 1 - \max_j \frac{E_{r,j}}{E_{f,k}} \tag{2-4}$$

where "$E_{r,j}$ is the energy released during the initial failure of a structural element j and contributing to damaging a subsequently affected element k." (Starossek 2009). This term reflects the reduction in system energy from an undamaged state to a damaged state. This assumes that the damage in

the structure only exists in one structural element. "$E_{f,k}$ is the energy required for the failure of the subsequently affected element *k*." (Starossek 2009). This parameter represents the difference of system energy in a structure under two damaged states. One takes place when a single structural element loses its capacity, the other occurs when one of the most critical remaining structural elements begins to fail subsequently after the first element failure. For the sake of simplicity, this R_e reflects the system ability to absorb the energy released due to the first component failure. The advantage of this energy-based approach is its ability of considering both strength and stiffness effects of a system in a damage event. However, it is quite difficult to apply this approach to current bridge practice, owing to the fact that the energy concept is not considered in either the design or rating processes. Moreover, as the number of structural components to be examined for failure increases, the energy calculation will become more time consuming. It is also noteworthy that the calculation of energy in this approach assumes that the released energy during a component failure is completely absorbed by the remaining structure, or at least that the excess energy is not critical to cause damage on the subsequently affected component.

After comparing the three aforementioned measures using Equations (2-1), (2-2), and (2-4), Starossek (2009) concluded that "no approach stands out as clearly superior and practical.". Through a search for current steel bridge engineering practices that study the system behavior in a damaged condition, it was found that Nagai and Miyashita (2009) briefly described one approach for evaluating the system redundancy of truss bridges. This approach is focused on the system after the removal of one truss member. The level of redundancy is determined by quantifying by how much the resultant forces on the remaining members exceeded the ultimate strength of these members. By severing truss members one at a time, the most influential member could be

identified and then prioritized for monitoring and inspection. No detailed discussion about the basis for this methodology was presented in this paper.

2.5.2 Modeling Details

This section discusses the aspects needed to develop refined system models for redundancy analyses. It presents an overview on how previous researches addressed the key modeling issues in performing system redundancy analyses.

2.5.2.1 Selection of Critical Loads

There is no universal load model given in the existing studies with regards to system redundancy evaluation. It was found that the configuration and positioning of critical loads were selected on a case-by-case basis. In the report NCHRP 406 (Ghosn and Moses 1998), two critical traffic conditions are recognized: extreme loading and regular loading. The former one represents the maximum expected traffic loads in the design life of a bridge, which is normally equal to 75 years. The latter one corresponds to the recurrent loads expected under regular traffic conditions in the biennial mandatory inspection period for truss bridges. The load effects of these two traffic conditions can be expressed in terms of equivalent HS-20 truck load defined by older AASHTO LRFD Specifications. The HS-20 truck load used in this report consists of two side-by-side HS-20 trucks. The load configurations for one HS-20 truck and two side-by-side HS-20 trucks are illustrated in Figure 2-1 and Figure 2-2, respectively.

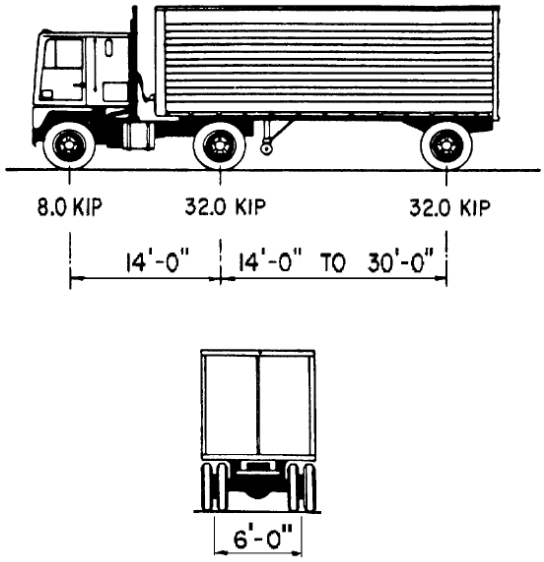

Figure 2-1. Characteristics of one HS-20 truck. AASHTO (2010). LRFD Bridge Design Specifications. American Association of State Highway and Transportation Officials. Washington, D.C. Used under fair use, 2015.

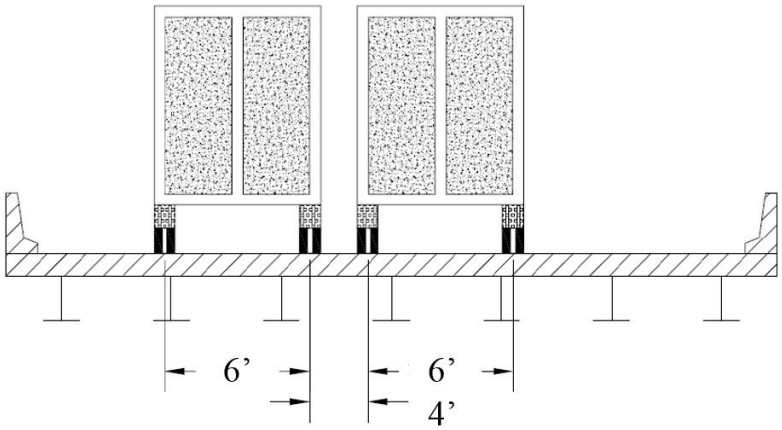

Figure 2-2. Transverse configuration of two side-by-side HS-20 trucks with a minimum spacing of 4 feet on the Beech Creek Veterans Memorial Bridge. Reese, L. D. (2009). Critical Member Removal and Load Redistribution of a Deteriorated Truss Bridge. Civil Engineering. Pennsylvania State University. Master of Science. Used under fair use, 2015.

This HS-20 truck load corresponds to the HL-93 load which is utilized in current bridge design and rating practices. Note that the HL-93 load is comprised of HS-20 truck load or HS-25 tandem

load and uniformly distributed lane load. In the HL-93 load model, each design lane should be loaded with one HS-20 truck or a pair of 25-kip loads, whichever produces a greater load effect. The two side-by-side HS-20 truck load is consistent with the HL-93 load when two traffic lanes exist in a bridge. If more than two traffic lanes are provided, the two side-by-side HS-20 truck load may not be regarded as the most critical loading per current AASHTO specification. Additionally, two side-by-side trucks may not be as critical as a single truck in the outside lane of a horizontally curved girder configuration. For a bridge with long span length, truck train loading that consists of both truck loads and lane loads may be more critical to the system.

The example bridges selected for previous redundancy analyses performed by Ghosn and Moses (1998), Ghosn and Fiorillo (2013), and Reese (2009) were typical short truss bridges with two traffic lanes. In these studies, the ultimate capacity of a bridge both in the undamaged and damaged states was determined via slowly increasing the two side-by-side HS-20 truck load until the first member failure occurs. As proposed by Ghosn and Moses (1998), the level of system redundancy can be measured by the ultimate capacity of a bridge and expressed as a multiple of HS-20 truck load.

In the two simple-supported Pratt truss bridges studied by Ghosn and Moses (1998) and Ghosn and Fiorillo (2013), the HS-20 truck load is positioned such that the middle axle loads align with the symmetric axis in the longitudinal direction, which represents the mid-span of a bridge. The overall configuration of this loading can be seen from Figure 2-1 with the only different spacing between the middle and rear axles. A uniform spacing of 14 feet is assigned to the three axle loads in these two studies. The location of the HS-20 truck load is determined in order to cause the worst load effect on the entire bridge rather than on any individual member. This philosophy is also applied to the redundancy study of the Beech Creek Veterans Memorial Bridge (Reese 2009). The

critical location of the truck load is determined by moving the two side-by-side HS-20 trucks in two traffic directions one at a time, because the large skew angle makes this bridge asymmetric about the mid-span. The most critical location is identified when the truck load gives maximum load effect on one line of the main truss.

Various live load models and positioning criteria are found in other redundancy studies. In the investigation on the behavior of a Japanese 3-span continuous truss bridge after one critical member fractured (Okui et al. 2010), the live load (TT-43 shown in Figure 2-3) is applied to trigger the maximum axial force in the member assumed to fracture in the undamaged bridge system. As a number of selected members are assumed to fracture one at a time, the truck loads are applied successively atop the damaged panel where fracture is assumed to have occurred.

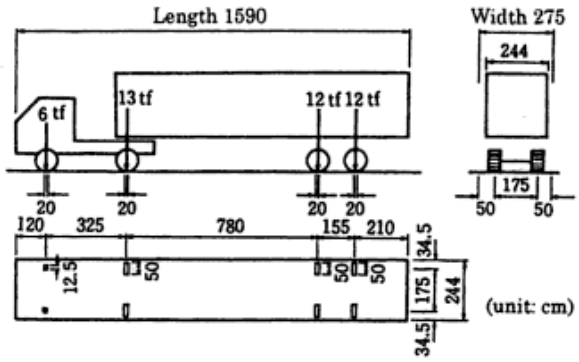

Figure 2-3. Live load model of TT-43 with a total truck weight=43tf. JRA (2002). Specifications for Highway Bridges Part I: Volume on Common Matters. Japan Road Association. Used under fair use, 2015.

In the load capacity evaluation of a 4-span continuous concrete bridge (Wisniewski et al. 2006), the critical traffic loads are comprised of not only a characteristic truck load (250kN) but a uniformly distributed lane load (80kN/m). The lane load is applied to the first and the third spans in order to trigger the failure of the mid-span section of the first span.

2.5.2.2 Simulation of Nonlinear Behavior

The system redundancy study for the Japanese 3-span continuous truss bridge reveals that a linear elastic analysis can predict misleading results (Okui et al. 2010). From the comparisons between the linear analysis and the nonlinear analysis, the authors concluded that the tension diagonal member identified as a fracture critical member through linear analysis was no longer fracture critical in the nonlinear analysis. In the nonlinear analysis, both geometric and material nonlinearity are incorporated into a limited number of critical members that were identified to be prone to yielding or buckling from the linear analysis. The material nonlinearity of these members is modeled using a bilinear stress-strain curve with a nonlinear secant stiffness that equals to one-hundredth of the elastic stiffness. After manually adjusting the stiffness of these members, the load analysis is repeated to find the next critical member that yields or buckles. A similar approach for simulating the nonlinear behavior is utilized by Reese (2009). This research assumes that the member load capacity will drop to zero immediately after yielding or buckling. This is achieved by assigning an axial force controlled hinge, a nonlinear analysis feature provided by SAP2000 (CSI 2013), to the critical members identified from the previous analysis. As compared to a full nonlinear analysis that considers nonlinear behavior of all truss members, the approaches of repeating the nonlinear feature assignment may not be able to properly capture the failure mechanism especially if the spread of plasticity after a local failure needs to be considered. The existing full nonlinear analyses proposals by Ghosn and Fiorillo (2013) and Cha et al. (2014) have had difficulty gaining acceptance among bridge engineers. In these two studies, all truss members and the entire deck system are modeled using 4-node thin-shell element (S4R) in ABAQUS (Simulia 2010), an advanced finite element software use mainly for research. The modeling effort and computational time may limit the full nonlinear analyses to be performed on short bridges with

simple geometry. Since no efficient approaches can be found from previous research, practical methods need to be developed in order to appropriately account for nonlinear behavior of a bridge system.

2.5.2.3 Identification of Critical Members

Since all truss members in tension are currently identified as fracture critical members, it is a daunting task to study the system effect of removing these members one at a time, especially for a large bridge with complex geometry like the I-35W Bridge. To avoid this predicament, an efficient method is needed to identify a subset of critical members and then analyze the system effect of failure on these members one at a time.

A general consensus among the bridge engineering community is that critical members can be identified as the members with high demand-to-capacity (D/C) ratios for axial loads in an intact structure. However, there is no agreement on what load model is appropriate for determining the member demand. Based on the objective of live load positioning, the load models utilized in the existing redundancy studies can be separated into two categories:

(1) one load model applies live load to cause the maximum load effect on a particular truss member (Azizinamini 2002; Okui et al. 2010). By moving the unit load along the chord members, the member with highest D/C ratio under each loading condition is recorded as one potential critical member. The member showing the greatest D/C ratio among all potential critical members is identified as the most probable member to fail (Hickey et al. 2009).

(2) another load model is selected to give the most critical system response (Ghosn and Fiorillo 2013). This load model seems to be more suitable for a system redundancy analysis, which focuses on the global behavior of a structure. Using this load model to perform an incremental analysis, the member that yields or buckles first will be regarded as the most critical member.

2.5.2.4 Rating of Critical Members

A major difficulty in rating damaged structures is that if the critical members are identified based on the behavior of an undamaged structure, there is no assurance that the failure of this member will exert the greatest influence on the remaining structure at the system level. In addition, it is worth noting that zero-force members such as vertical members are not considered critical due to their zero D/C ratios in an undamaged structure. However, it is uncertain whether failure of one zero force member will significantly affect the redundancy of the damaged structure. Therefore, it is necessary to further investigate the system effect of failure on the critical members as well as zero-force members one at a time.

One practical measure is to assess the residual strength capacity of a damaged structure after losing one critical member (Ghosn and Fiorillo 2013). Although this research does not give direct guidance on how to rate critical members, it provides insight into where are the critical locations that greatly affect the system redundancy based on a case study of a short Warren truss bridge. The study further implies that the most critical member may be identified as the member whose failure will result in the largest reduction of system load capacity. One concern is that this approach does not account for the stiffness change in a system from an undamaged state to a damage state. In fact, it is possible that a damaged structure fails due to large plastic deformation. This deformation-controlled failure will take place if the critical structural components can exhibit ductile nonlinear behavior such as post-yielding on a steel member, hinging effect near a connection, and/or block shear on a gusset plate. To examine if the removal of the most critical member will cause the maximum deflection of a bridge system, a method based on principle of virtual work may be helpful. This virtual work method developed by (Charney 2003) can serve as an effective measure of how much each member contributes to the maximum deflection of a structure. The analysis of

a system effect after changing the volume of a particular member is included in this method. The reason to use volumetric change stems from the fact that as all external work produced by forces moving through a certain displacement is always fully transformed to internal work done by each member. This internal work is stored as a form of strain energy filling the volume of each member under a static loading condition. Using this method, critical members may be identified as the members whose volumetric change will greatly affect the maximum deflection of a truss system. However, this method cannot predict if the strength of a system is equally affected by changing the volume of a critical member.

Perhaps a more robust measure to account for the influence of both strength and stiffness of a system following the failure of one critical member can be indirectly found to be the strain energy release from a system after the removal of one critical member. As the strain energy considers the whole volume of a member, the combined effect of the cross sectional properties, corresponding to the resultant forces, and the member length, directly relating to the deformations, can be assessed simultaneously (Guo and Gilsanz 2003). The authors concluded that a higher strain energy a member has, the more significant the member is to the redundancy of a structure. Similarly, it has been suggested that the ratio of strain energy in different states can serve as a structural robustness indicator (Tavakoli and Kiakojouri 2012). As far as the dynamic impact triggered by a sudden removal of one critical member is concerned, a strain energy based approach was proved to provide more reliable results than an approach measuring either force or deformation alone (Szyniszewski and Krauthammer 2012).

2.5.3 Destructive Tests

Among a very limited number of full-scale destructive tests that address redundancy of truss bridges, the demolition test of Milton-Madison Bridge over the Ohio River presents valuable information regarding the behavior of the bridge system after a main truss member is damaged (Cha et al. 2014; Diggelmann et al. 2012; Ocel 2013). This test monitored the bridge system response after a brittle fracture in the lower chord member at the mid-span, as highlighted in Figure 2-4.

Figure 2-4. Elevation view of the test span. Ocel, J. (2013). Evaluation of Member and Load-Path Redundancy on the US-421 Bridge over the Ohio River. Federal Highway Administration (FHWA). Washington D.C. Used under fair use, 2015.

The test section is a 149 feet simple span truss on the northernmost approach span of the bridge. More details about this truss structure will be given in Chapter 7, as the test data will serve as a key reference to verify the results from the system models developed in this research.

In the test, fracture was simulated by cutting the lower chord member using explosive demolition. By installing strain gauges on a selected number of steel members, the redistribution of forces and deflections of the structure were measured. The post-fracture measurements showed that the

structure remained standing after the chord member was severed. None of the measured members reached their critical strength capacity under the test loading condition. This indicates that the damaged truss is still partially effective in carrying load and the bridge system is compensating somewhat for the damaged truss member. It is also surprising that the damage of this chord member merely increased the vertical deflection of the structure by 0.39 inches. This level of deflection would not be noticeable unless a bridge inspection is conducted. Thus it can be inferred that sufficient system redundancy exists in this damaged structure.

There are three destructive tests conducted to evaluate the post-fracture reserve strength of four-chord trusses (Connor and Altstadt 2013; Wipf and Phares 2002). These type of trusses are widely used to support traffic message signs over many highways. A photo of one of the tested sign truss can be seen in Figure 2-5.

Figure 2-5. Close-up view of Interstate 80 Sign Truss. Wipf, T. J. and B. M. Phares (2002). Evaluation of Interstate 80 Sign Truss. The Iowa Department of Transportation. The Bridge Engineering Center at the Center for Transportation Research and Education-Iowa State University. Used under fair use, 2015.

The studies of system behavior after a member failure on these structures provide insights into whether collapse will be triggered by a tension chord failure. Results from the destructive load tests on the three sign trusses revealed that cutting one of the selected tension chord did not bring immediate safety concerns in that the damaged structure still exhibited a considerable amount of reserve strength. The system behavior of the Interstate 80 Sign Truss after cutting the most heavily loaded tension chord also indicates that lateral braces played an essential role in transferring axial forces from the damaged side of truss to the undamaged side of truss.

2.6 Key Findings and Limitations

Through reviewing benchmark case studies pertaining to system redundancy analysis of truss structures, it is worth noting that not all tension members deserve the FCM designation. For instance, the chord members investigated in the previously discussed destructive tests might be re-classified as non-FCMs. Results from the analytical case studies indicate that the location of damaged member greatly affects the system redundancy (Ghosn and Fiorillo 2013). A good agreement regarding one conclusion is identified from the results presented by Ghosn and Fiorillo (2013) and Yamaguchi et al. (2010). The conclusion is that in a simple-supported Warren truss bridge the closer the damaged diagonal member is to the support, the greater influence it will exert on the system strength capacity. The likelihood of collapse is highest if an end diagonal fails.

A number of limitations are also identified from the analytical redundancy studies. In most redundancy analyses, failure of a damaged system was determined by checking if the capacity of a member in the main truss structure was exceeded. This failure criterion may not be true given the fact that either a brace member failure or a connection failure could occur prior to a main truss member failure. In particular, an increase in axial stress was found on some lateral braces in the

damaged Milton-Madison Bridge and the Interstate 80 Sign Truss under the destructive test loading. This result indicates that brace members are also likely to be overstressed in a damaged structure. However, the possible nonlinear behavior of lateral braces has not been adequately addressed in the analytical redundancy studies conducted thus far. Thus, a research need exists to study the behavior of brace members in a damaged structure and explore how brace members affect the system redundancy.

Likewise, potential connection failures are also neglected in the existing system redundancy analyses. In most system models, the truss member connections were idealized as rigid nodes that can fully transfer moments and axial loads. The accuracy of this assumption was challenged by results showing that significant in-plane moments were observed near the critical member connections in the damaged main truss structure (Diggelmann et al. 2012; Okui et al. 2010; Yamaguchi et al. 2010). Large moment effects in the vicinity of truss member connections could even result in serious plastic damage as demonstrated by Ghosn and Fiorillo (2013). In fact, damage can be even worse than these predicted results if rivets or bolts were used in the truss member connections. Due to the presence of rivet or bolt holes, the resulting net section may fracture when it is subjected to large tension and flexure. This failure could separate the connected truss member from the bridge system suddenly.

2.7 Net Section Fracture at Connections

2.7.1 Fracture Failure Criterion

One commonly employed fracture failure criterion for ductile metals was proposed by Lemaitre (1985). The Lemaitre criterion is based on equivalent plastic strain (Chi et al. 2006). In fact, fracture, in the form of ductile tearing, of a ductile material is triggered by plastic damage. The

strain on a structural steel member varies significantly while the stress remains nearly unchanged. Hence, the rupture process is strain-controlled (Lemaitre 1985). Merely measuring plastic strain is not sufficient to predict fracture failure in ductile metals where the fracture initiation is also strongly influenced by the stress state (Gurson 1976; Panontin 1994). Results from analytical and experimental studies (Hancock 1976; Rice and Tracey 1969) have shown that tri-axial hydrostatic or mean stresses facilitate volume increase of a ductile metal. Consequently, the inside voids can grow and coalesce much faster and finally initiate a crack. Rice and Tracey (1969) also found that the void growth rate was an exponential function of the stress triaxiality. This was later confirmed by Kanvinde and Deierlein (2004) with a statement that fracture initiates at critical plastic strains depending on stress triaxialities. This critical plastic strain is often assumed to be the ultimate plastic strain of a ductile material defined from its true stress–strain curve. Moreover, a constant triaxiality ratio during static loading is postulated by Lemaitre (1985), whose studies placed a solid foundation for current research work for fracture failure prediction.

Given the fact that there is very limited full scale experimental data dealing with the ultimate behavior of structural steel members, a reliable alternative is to make use of the Lemaitre criterion to simulate ductile fracture damage and further estimate the ultimate capacity of a target steel member. Through comparisons with other conventional criteria, Girão Coelho (2013) concluded that the Lemaitre criterion can be most readily applied to finite element analyses without additional modeling effort and it does not require any model parameter calibration.

2.7.2 Finite Element Modeling Techniques

In current structural engineering practice, neither AISC nor AASHTO gives explicit guidance on the determination of net section fracture resistance to a combined tension and flexure (Altstadt 2008). Estimations of net section capacities in combined loading heavily depend on simplified

engineering idealization due to the lack of published experimental data. A rational modeling technique plays an essential role in verifying such estimated capacities. Through reviewing previous reported numerical simulations of fracture failure, two modeling techniques in ABAQUS turned out to be most prevailing among major 3D nonlinear finite element analyses.

One is called as element deletion method. Fracture failure is achieved by deleting the element whose average effective plastic strain computed from all integration points on this element exceeds the material rupture strain (Szyniszewski and Krauthammer 2012). A Dynamic/Explicit scheme is utilized to implement the element deletion process. In spite of the fact that using this scheme can avoid potential solution convergence problems for models with large deformations and considerable plasticity, there are numerous obstacles that prevent this scheme from a wide and practical application in real industry.

To be specific, this scheme by its nature was originally applied to analyze the structural performance under dynamic loading conditions, whereas the loads to initiate fracture at net sections are almost static, at least within the scope of the investigation in this thesis. A quasi-static analysis has to be ensured to minimize the effects of the inertial force, as this force is not expected to affect fracture failure. According to ABAQUS documentations (Simulia 2010), a quasi-static loading condition can be achieved if a series of stringent requirements for determining a proper loading rate and mass scaling factor are satisfied. Therefore, many sophisticated parametric studies need to be performed. It is rather time consuming to carry out a fracture failure analysis using this dynamic scheme. To make matters worse, solutions from this dynamic analysis may not be stable, and thus a rational engineering judgment is necessary. In addition, as an element deletion inevitably causes a loss of some energy and mass from a system, most fracture failure analyses using this method usually underestimate the capacities of the test specimens.

The other modeling technique, known as extended finite element method (XFEM), is implemented with a Static/Stabilize scheme. The analyses are performed under a pure static environment. Fracture damage is simulated through modifying the cohesive behavior of the critical elements that are most likely to fracture. Each node of the critical elements is assigned a phantom node. As the prescribed crack initiation criterion is reached, each phantom node, which is originally constrained to its corresponding real node, will gradually reduce its cohesive strength down to zero. After completely losing the cohesive strength, the phantom node will move away from the real node, resulting in a crack across an entire element. This approach maintains the element mass, contrary to what happens when using an element deletion approach. The principle of this phantom node is illustrated in Figure 2-6.

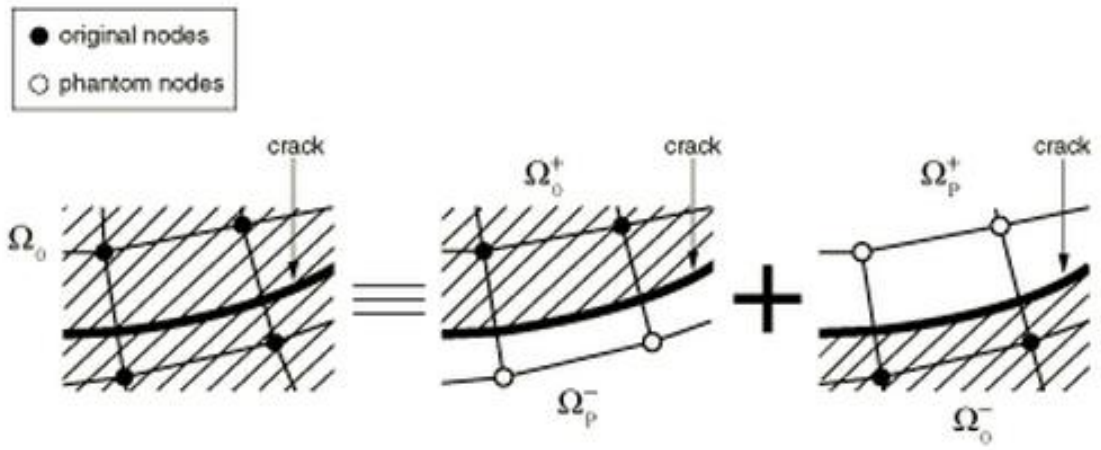

Figure 2-6. An illustration of the relationship between phantom nodes and original real nodes. Simulia (2010). Abaqus Analysis User Manual, Version 6.10, Providence, RI. Used under fair use, 2015.

Since a crack is captured through splitting one element into two parts, there is no need to re-meshing the cracked elements. Many conventional crack simulation approaches require each cracked element to be meshed with a smaller size after every crack propagation step, because the

crack line is formed along the element boundaries in a particular mesh. Unlike these approaches, the XFEM carries out the crack propagation without disturbing any element boundary. As a result, the mesh of a cracked element can keep unchanged and the propagation path of a crack becomes arbitrary and independent of mesh.

This mesh independency was further confirmed by Areias and Belytschko (2005). Their analytical results have shown that both coarse and refined mesh of cracked elements can accurately depict the load-deformation histories recorded from experimental tests at the critical locations. In contrast with the element deletion method, which requires that the mesh has to be refined until the change in global behavior is negligible, the XFEM may get rid of mesh sensitivity analysis, leading to a more efficient numerical analysis of fracture damage. The accuracy of using the XFEM for fracture failure prediction was well verified by Davila and Camanho (2003), and Krueger et al. (2000). Their numerical simulations of the onset of delamination in the flange of composite bonded skin/stringer specimens were in good agreement with the published experimental data for uniaxial tension, three-point bending, and combined tension and bending coupon tests.

As discussed previously, the net section fracture process is strain-controlled. Thus a strain based failure criterion can capture a more realistic status of an element undergoing a fracture damage than a stress based failure criterion. Moreover, when using the maximum principal strain criterion, a crack will automatically propagate along the path that is orthogonal to the maximum principal strain direction, whereas other criteria still require users to specify the crack propagation path.

2.7.3 Guidelines for Net Section Fracture Simulation

The review of fracture failure criterion and modeling techniques forms the basis of the following guidelines which will be implemented for the net section fracture studies discussed later in this dissertation:

(1) The Lemaitre criterion is selected for use in this research for fracture failure prediction;
(2) It is necessary to postulate both an equivalent plastic strain and a constant stress triaxiality ratio to properly capture the occurrence of fracture damage in a finite element model; and
(3) The process of fracture, which consists of crack initiation and propagation, will be simulated using the extended finite element method with a Static/Stabilize scheme in ABAQUS.

2.8 Summary

The goal of this literature review was to provide an understanding of the definition of fracture critical members, background knowledge about current fracture critical practice and bridge system redundancy evaluation. From this literature review, two problems will need to be addressed to attain the objectives of this research:

(1) As current codified provisions lack clear criteria on how to identify fracture critical members, this research will develop detailed procedures to properly assign the fracture critical designation to truss bridge members while not unnecessarily penalizing bridge owners; and
(2) A further development of analytical models with refined assumptions and nonlinear features to capture the system response post fracture is required.

These issues are addressed in the rest of this dissertation.

3 Preliminary System Analysis

3.1 Methodology Overview

Since a typical two-line truss structure like the I-35W Bridge is designed to carry loads primarily via the main truss system, the system analysis presented in this chapter will focus on modeling member behavior on the main longitudinal trusses. Prior to a system analysis based on the existing bridge model developed by Ocel and Wright (2008), a validation study is carried out to provide sufficient level of confidence in the model. Because of the vast number of truss members in the two main trusses, it would be a daunting task to study nonlinear system behavior after removing each member one at a time. Thus the first phase of the system analysis is to identify the members that are most critical for the system strength of the structure. Then the system response after failure at these critical members is investigated. The possible failure at truss member connections is analyzed to determine if some connections can be classified as fracture critical components.

From a practical perspective, a linear elastic static analysis is commonly utilized in design to assess bridge capacity in an intact condition. With the implementation of a set of rigorous limit states, a linear analysis can provide acceptable accuracy in estimating the design strength of a bridge. However, the results from a linear analysis may not be reliable if the ultimate strength of a damaged system is to be determined, because the ultimate failure of a system typically includes a combination of nonlinear effects such as yielding and buckling. In this chapter, the adequacy of utilizing linear analyses are examined by comparing their results with nonlinear analyses, which consider geometric nonlinearity, material plasticity, and strain rate effect on yield strength.

3.2 I-35W Bridge Description

In 1967, the I-35W Bridge (see Figure 3-1) was constructed over the Mississippi River in Minneapolis, Minnesota. The bridge carried eight lanes of traffic in two directions (see Figure 3-2) on the Interstate Highway 35 West, thus being designated as the I-35W Bridge. The main structure of this bridge was comprised of a three span (266 feet-456 feet-266 feet) continuous deck truss. The total length of this bridge, including approach spans at each end of the central deck truss structure, was 1,907 feet.

The complexity of the bridge structure is illustrated in Figure 3-1 and Figure 3-3. The superstructure is primarily supported by the two main longitudinal trusses continuous over three spans. The lateral braces, which framed into the main trusses, supported floor longitudinal stringers, which in turn supported the reinforced concrete deck of the bridge. There were eight traffic lanes on the bridge deck with six lanes between the main trusses and two lanes, one on each cantilever (A. Astaneh and Asla 2008).

Figure 3-1. A side view of the I-35W Bridge. NTSB (2009). Collapse of I-35W Highway Bridge, Minneapolis, Minnesota, August 1, 2007. National Transportation Safety Board. Used under fair use, 2015.

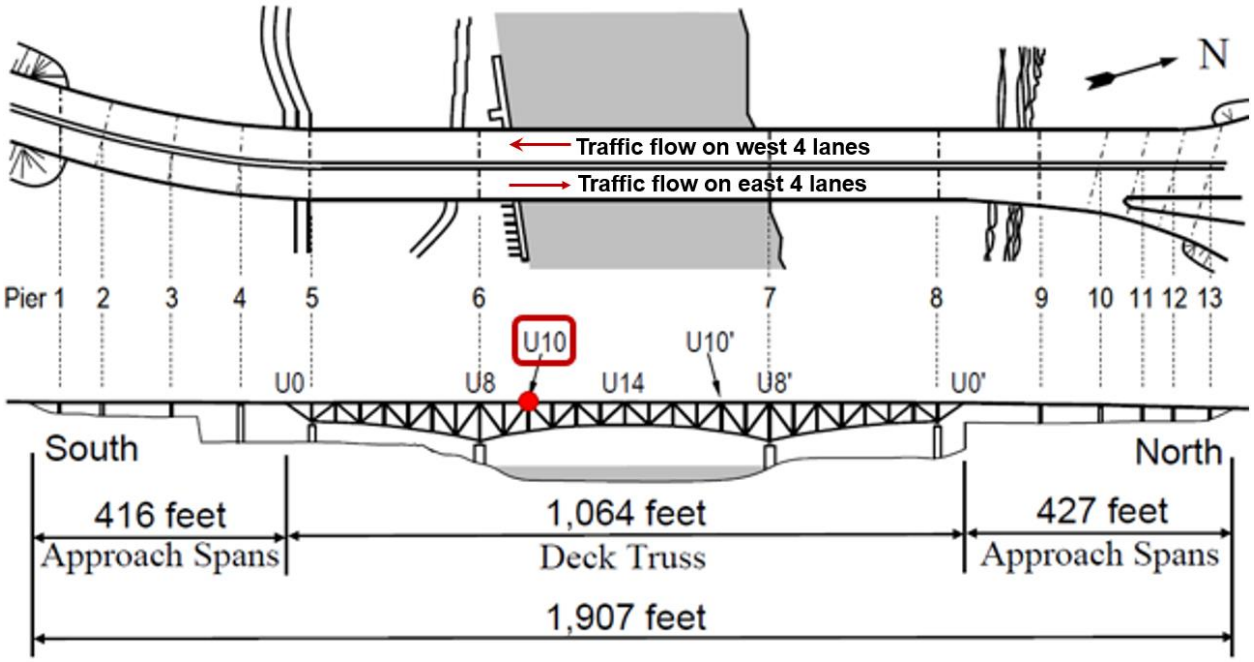

Figure 3-2. Plan and elevation view of I-35W Bridge. Mn/DOT (2009). I-35W Bridge original plans & details. http://www.dot.state.mn.us/i35wbridge/history.html, Minnesota Department of Transportation. Used under fair use, 2015.

As shown in the plan and elevation view of the entire bridge in Figure 3-2, there were 13 piers, numbered from the south end, supporting the entire bridge structure. The central deck truss consisted of 28 panels, each of which was 38 feet long (Liao and Okazaki 2009). Starting from the south end, the panel points were labeled from U0 to U14 at the center of the bridge, and then from U14, U13' down to U0'.

The East and West sides of main trusses were transversely connected through the floor trusses, sway frames, and brace members illustrated in Figure 3-3 and Figure 3-4. The floor trusses supported longitudinal stringers, which in turn supported the reinforced concrete deck and traffic. Underneath the floor trusses, sway frames in a chevron configuration connected the two sides of

main trusses. Lateral bracing spanned between the upper chords and lower chords of the main trusses. The reinforced concrete deck was separated longitudinally for the southbound and northbound traffic. Each deck was 54 feet wide, consisting of four 12-foot-wide traffic lanes and two 2-foot-wide shoulders. In 1977, the bridge was modified by adding a 2-inch-thick concrete overlay to the original 6.5-inch-thick deck. In 1998, a new concrete face was added to the inside of the original rails along the exterior edges of the deck, and new median barriers replaced the rails on the inside edges of the deck.

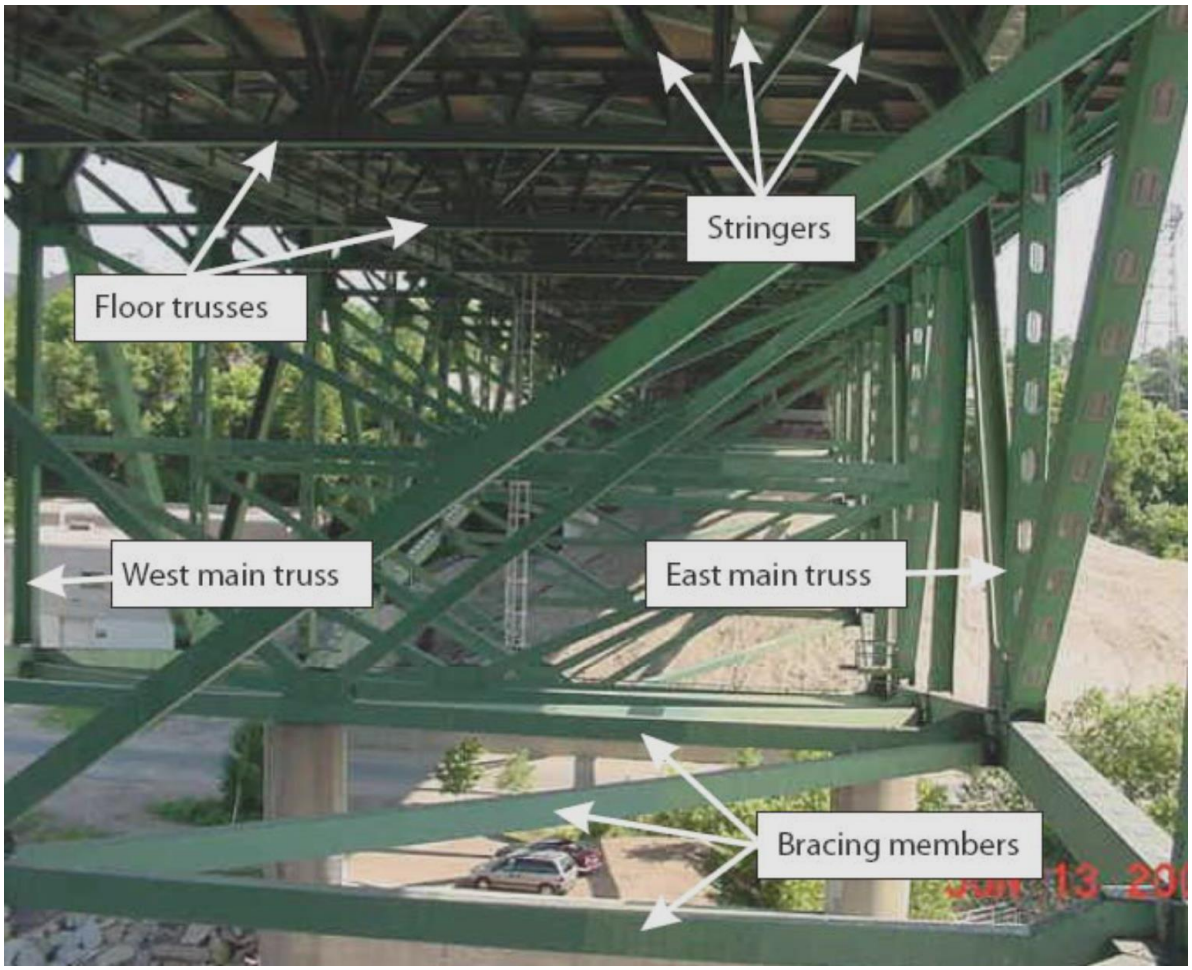

Figure 3-3. Major components in the bridge truss system viewing in a transverse direction. NTSB (2009). Collapse of I-35W Highway Bridge, Minneapolis, Minnesota, August 1, 2007. National Transportation Safety Board. Used under fair use, 2015.

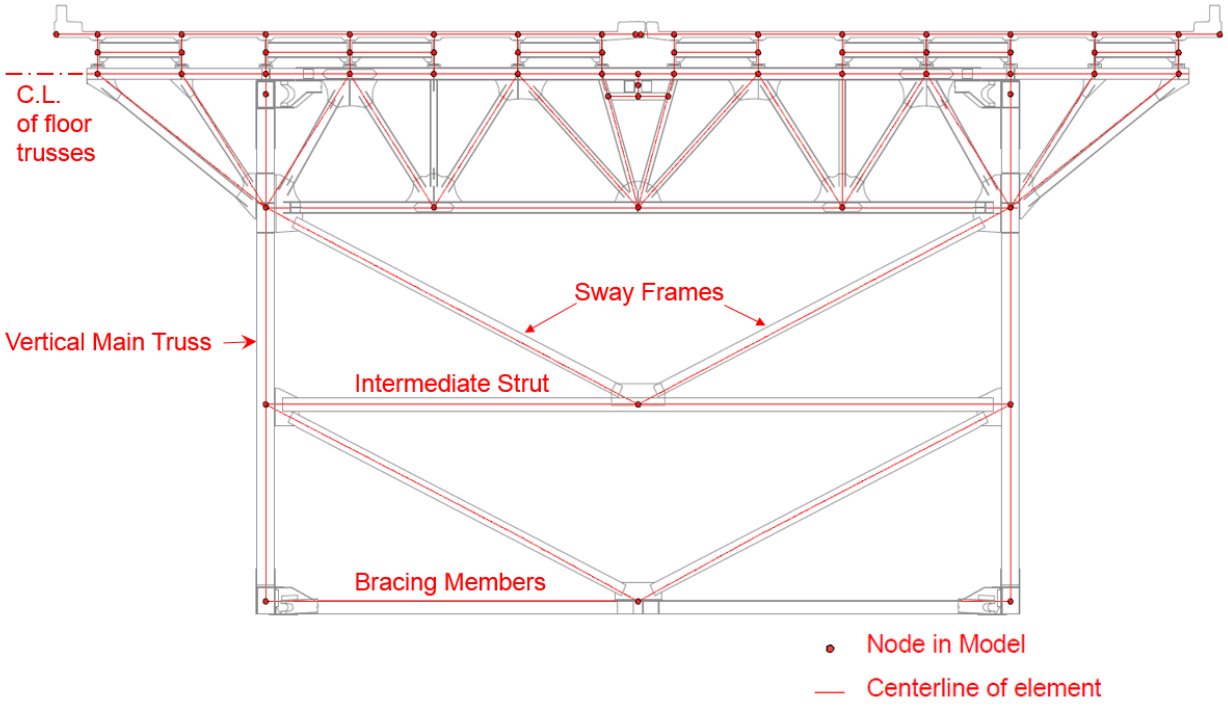

Figure 3-4. 2D view of the idealized members and connections in the floor truss system. Ocel, J. M. and W. J. Wright (2008). Finite Element Modeling of I-35W Bridge Collapse Turner-Fairbank Highway Research Center. Used under fair use, 2015.

On August 1, 2007, the bridge suffered a tragic collapse, with the 456-foot-long central deck truss falling into the Mississippi River. This bridge collapse took away 13 lives, and injured 145 people. A forensic investigation led by the National Transportation Safety Board (NTSB) concluded that inadequate design of a particular pair of gusset plates played an essential role in the collapse of the bridge (NTSB 2009). These gusset plates were located at the panel point U10 on both East and West sides of main truss structure (highlighted in Figure 3-2), and they connected two adjacent top chord members, two diagonal members, and a vertical member.

3.3 System Model Development

To assist the National Transportation Safety Board (NTSB) investigation into the bridge collapse, a highly detailed 3D system model for the I-35W Bridge was developed by the Federal Highway Administration (FHWA) (Ocel and Wright 2008). Since this 3D model was used to simulate the behavior of the undamaged bridge structure in the service condition prior to its collapse, nonlinear features were not introduced into this model. The modeling work was implemented based on the geometry and member sizes outlined in the design plans (Sverdrup & Parcel and Associates Inc. 1965). A 3D view of this model is shown in Figure 3-5. All main trusses, floor trusses, and cross-frames were modeled with 5 beam elements (B33 in ABAQUS) along their lengths. The stringers were modeled with 10 elements between the floor trusses because they were modeled with lower order linear elements (B31). The deck and piers were modeled with linear shell elements (S4R). This bridge model was calibrated to match the live load data collected by the research team at the University of Minnesota (O'Connell et al. 2001).

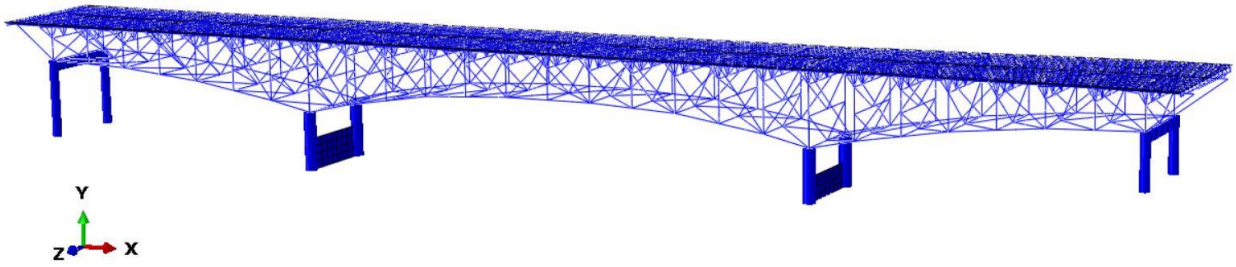

Figure 3-5. 3D view of a global model in ABAQUS for the I-35W Bridge. Ocel, J. M. and W. J. Wright (2008). Finite Element Modeling of I-35W Bridge Collapse Turner-Fairbank Highway Research Center. Used under fair use, 2015.

It is worth noting that in this 3D model all the joints between truss members were considered perfectly rigid. Thus it would have difficulty in predicting failure at connections unless highly

detailed local models were used (Ocel and Wright 2008). These highly detailed models are needed to incorporate net section fracture and local buckling effects, thus require dense meshing. This level of meshing, which is orders of magnitude greater than that needed to properly capture member behavior, will result in both numerical convergence problems and very long computational times. Thus a two-step approach will be used in this research. In step I, very extensive local studies will be used to characterize the behavior of critical sections in a selected number of members and connections. In step II, the results of these local studies will be used to define critical sections or hinge properties in the global system model, avoiding the need for dense meshes at connections. Clearly, the robustness of this two-step approach depends on the ability to properly calibrate the behavior of local sections. The implementation of this two-step approach will be explicitly described in Chapter 4 for step I and Chapter 5 for step II.

3.4 System Model Validation

As discussed in section 2.7, a highly detailed FE model of the I-35W Bridge will be used in this research. Prior to implementing a system analysis based on this existing model, it is essential to insure that the model can provide a credible prediction of the system behavior in a damaged condition. Since the ultimate deformations of the main trusses can be inferred from the wreckage collected after the bridge collapse, an effective means to validate the damaged truss system model is to compare the simulated deformation in the FE model with the field data measured on site by Dr. William Wright during the FHWA investigation.

As the bridge collapsed due to simultaneous failure at the connections of the compression diagonals (U10L9) on both trusses, it is worthwhile to simulate this failure using the existing model under the construction and vehicle loads known to be present at the time of collapse. Considering

that only the deformed shape at the north end of the center span was captured by a motion-activated surveillance video camera, the comparison between the evidence and the analytical results thereby focuses on the deflected shape of the damaged structure with failure at member U10'L9' simulated by separating the diagonal members from their nodal connections at member ends U10' on both sides before applying dead and live loads.

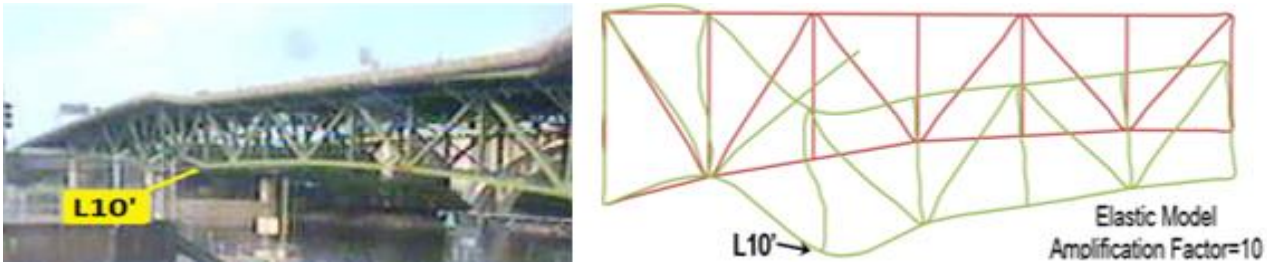

(a) (b)

Figure 3-6. (a) Deflected shape of the bridge during collapse, looking northeast. NTSB (2009). Collapse of I-35W Highway Bridge, Minneapolis, Minnesota, August 1, 2007. National Transportation Safety Board. Used under fair use; (b) deflected shapes before and after the simulated failure at member U10'L9' in both trusses

Figure 3-6 compares the deflected shape of the real bridge recorded by the video camera with the simulated deformation change on a major part of the main truss system around the failure location. It is obvious that the deflected shape in the model (green curve in Figure 3-6 (b)) is consistent with the actual deformation observed from Figure 3-6 (a). In particular, the very pronounced downward deflections at member end L10' depicted in the model were in agreement with those captured by the video camera.

To quantitatively validate the damaged system model, the deflections of some main truss members were compared between analytical results and evidence from the wreckage. As permanent deformations of the members adjoining the U10L9 diagonal were measured during the failure investigation (Hill et al. 2008), the comparison is concentrated on this location. From the

observation of the wreckage, it is conceivable that most members in the measured location had undergone inelastic deformation early in the collapse sequence. Therefore, the material plasticity for a typical ASTM A572 Grade 50 steel (Frank et al. 2000) was added to the members connecting the U10L9 diagonal in the system model. The results from this nonlinear collapse analysis indicate that first plastic behavior occurs on the L9L10 segment of the L9L11 bottom chord member.

The comparison between the calculated and the measured final deflections along the length of the member are plotted in Figure 3-7. This figure shows that the analytical results match the measured data reasonably well. The main discrepancy between the predicted and measured deflections is near the L10 end of L9L10.

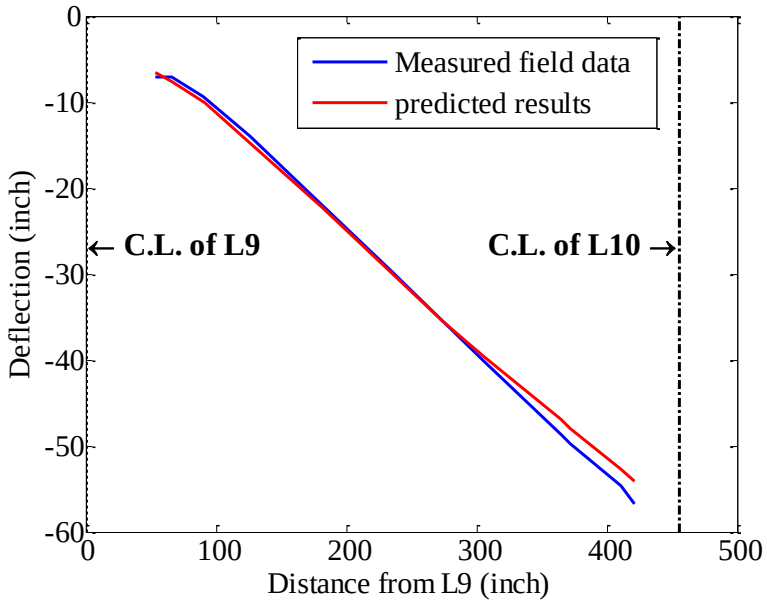

Figure 3-7. Measured and predicted deflections of member L9L10

Several factors may lead to the difference between the analytical results and evidence from the wreckage especially near L10. On the one hand, it is impossible to know the exact changes in the magnitude of plastic deformations when the members begin to fracture. On the other hand, the

wreckage collected may have been damaged by strong impact loads. This impact damage is most likely caused by a combined effect, including the amplified loads due to a sudden fracture, the impact loads induced from the immediate contact between the falling members and the river, and possible additional damage during the recovery process. Given these possible sources of uncertainty, the nonlinear damaged system model is considered capable of reasonably predicting the early collapse sequence.

3.5 Consideration of Fracture Critical Connections

The importance of considering gusset plate failure in assessing existing bridge load capacity was heightened in the aftermath of the I-35W Bridge collapse, which was caused by failure at a connection and not in any main truss member. The possible failure modes on gusset plate connections in the main truss structure of this bridge were identified during the completion of NCHRP 12-84 (Ocel 2013). From a fracture critical perspective, the tension failure mode of a typical gusset plate connection was found to produce a very similar system consequence to failure of the connected tension member. Likewise, the compression failure mode such as plate buckling in the early collapse event that occurred at the end of a diagonal member made the system behave as if the diagonal compression member was removed from the structure. Thus, for modeling purposes, tension or compression failure of the member or connection will be considered as identical phenomena.

The one mode that may act somewhat like a fracture is a shear failure along the chord line as demonstrated in the left part of Figure 3-8. However, this mode will be accompanied by significant shear deformation before ultimate failure occurs. Severe section loss due to corrosion may allow failure with low ductility and shear rupture could act somewhat like brittle fracture: both

phenomena might jeopardize the system integrity. A preliminary system analysis is thereby performed to explore the system effect of a shear failure at one connection.

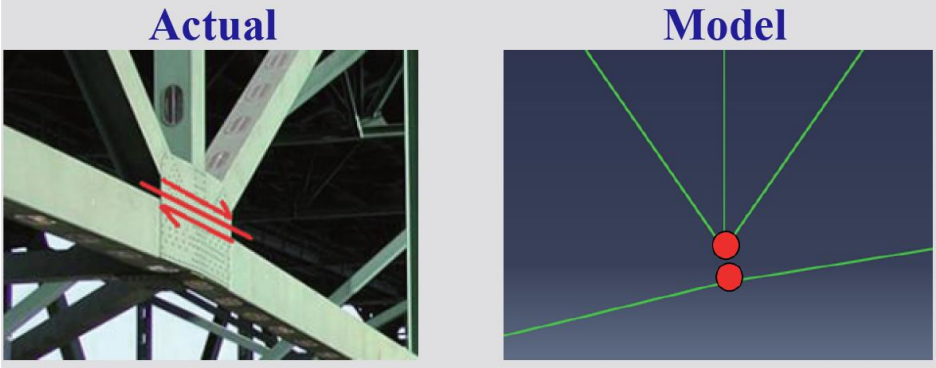

Figure 3-8. Simulation of a shear rupture failure at one gusset plate connection

A shear failure is modeled by disconnecting the diagonal and vertical members from the chord members as shown in the right part of Figure 3-8. This shear failure was simulated at every five-member joint in the center span of the main trusses. The investigations revealed that the shear failure did not cause any of the truss members to exceed the member design capacity. A properly designed gusset plate without severe corrosion section loss is unlikely to have a low ductility shear rupture. Hence shear fracture failure at connections will not need to be included in a refined fracture critical system analysis.

3.6 Modeling of Critical Live Loads

In order to exert an extreme load effect on the entire bridge system, the HL-93 load specified by AASHTO (2010) is chosen to replace the measured traffic loads and construction loads at the time of I-35W bridge collapse. A deformation comparison on the undamaged main trusses under the HL-93 load and under the “AsBuilt” load is plotted in Figure 3-9. This figure also indicates that

an approximately 16% increase in the maximum deflection of the main truss structure results from the change of live loads from the "AsBuilt" load to the HL-93 load.

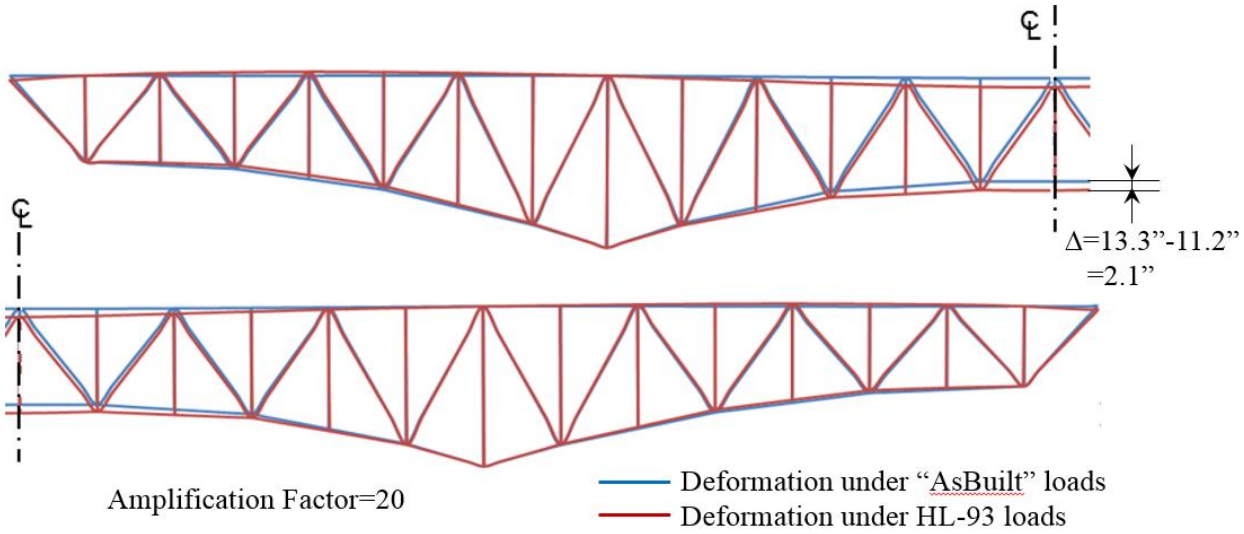

Figure 3-9. Comparison of main truss deformation between the "AsBuilt" model and the HL-93 model

In accordance with this research objective, the HL-93 load is positioned to cause the maximum effect for the entire bridge system rather than an individual member. Thus the design lane loads are applied to the center span, as well as two overhangs shown in Figure 3-10. Likewise, the design truck loads are assigned in the middle of the center span with a uniform spacing of 14ft. Due to the presence of transverse walkway loads as a source of asymmetric loading (see Figure 3-11), the south side of the center span near Pier 6 has most critical load effects. Therefore, the truck loads are placed in a manner that the centroid of the load group is located at the south side of the center span as illustrated in Figure 3-12. Furthermore, to account for multiple presence of four traffic lanes in each direction on the bridge, both the truck loads and the lane loads discussed above are reduced by a factor of 0.65. These reduced loads with their magnitudes shown in Figure 3-10 and Figure 3-12 are modeled in the system analysis.

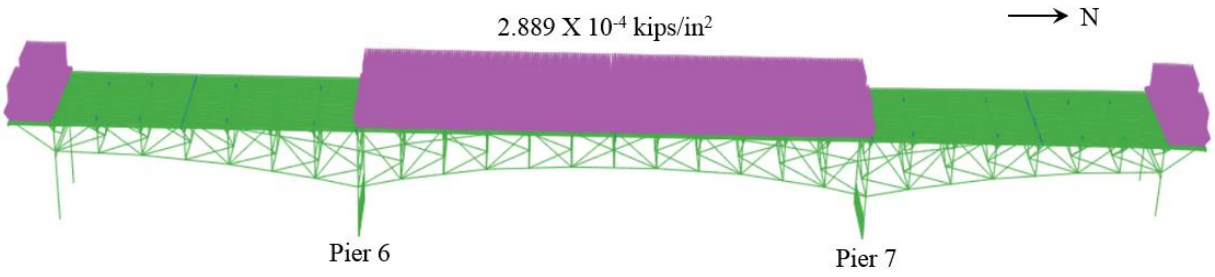

Figure 3-10. Lane load distribution of the HL-93 load

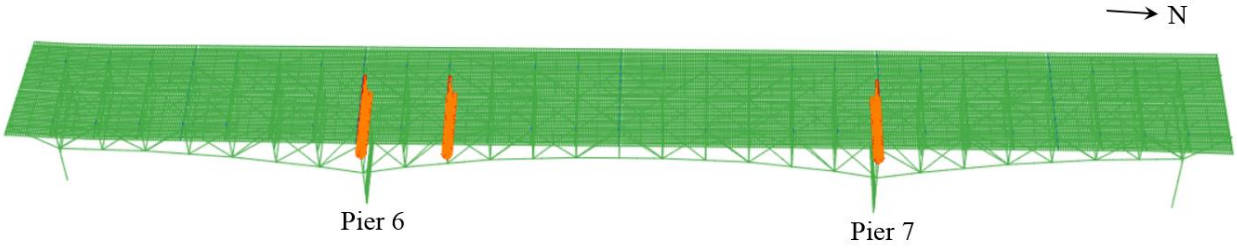

Figure 3-11. Transverse walkway loads

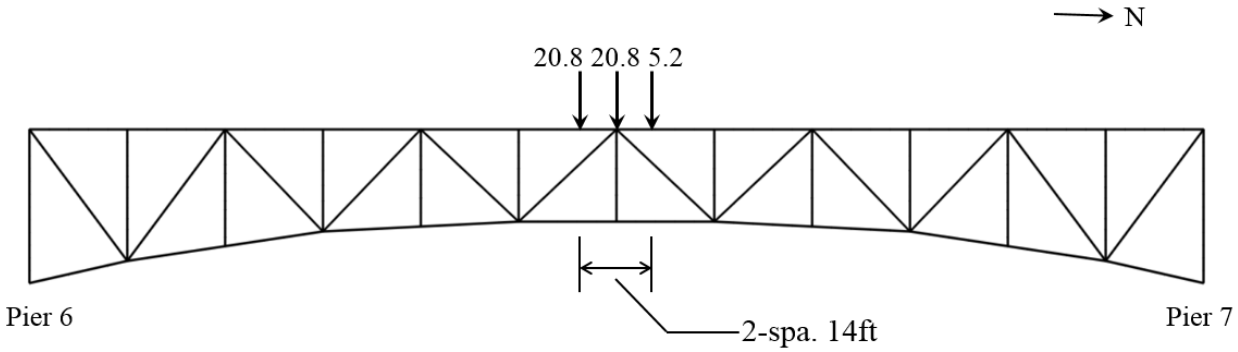

Figure 3-12. Elevation view of the center span between Piers 6 and 7 showing the HL-93 truck loads (unit: kips) that were applied to each of the eight traffic lanes

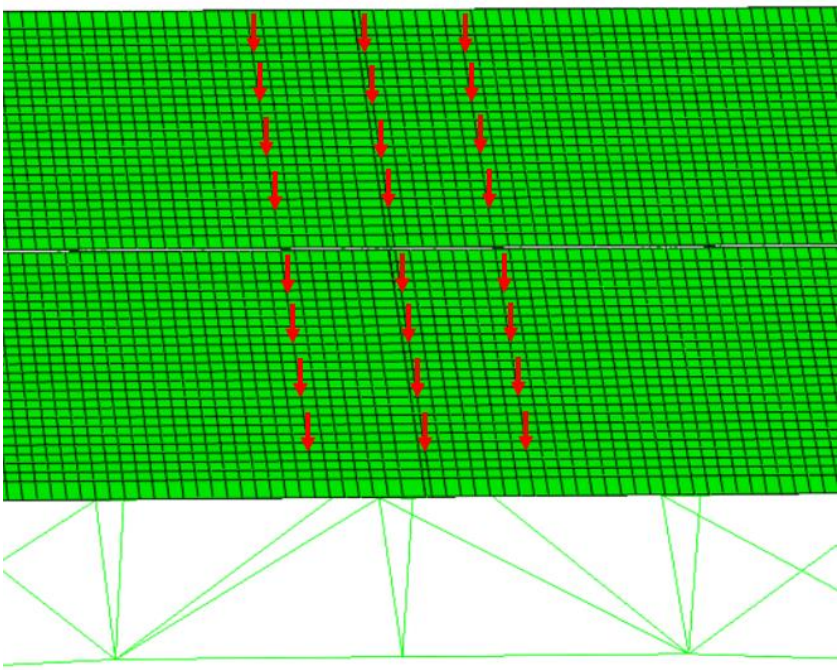

Figure 3-13. Close up 3D view of the HL-93 truck loads on eight traffic lanes

In addition, it should be noticed that two approach spans of the I-35W Bridge are excluded in the current system model. In order to account for the load effects on these spans, the end reactions from all dead load and live loads on the approach spans are applied as concentrated forces atop four edge panel points (i.e. U0, U0' on both sides of the main truss structure in Figure 3-2).

3.7 System Analysis of One Damaged Structure

As the first phase of a system analysis, the effect of failure on a truss member that is expected to be most critical for the system strength capacity will be explored. By studying the behavior of the damaged structure after losing the most critical member, the following questions can be answered:

(1) Will the damaged structure be able to withstand failure on this critical member?

(2) Will failure of this critical member trigger a progressive collapse?

(3) What will be the ultimate failure mode of the damaged structure?

(4) Can the analyses properly capture the ultimate failure modes in the system models?

Since a methodology to accurately identify the most critical member has not been developed so far, the preliminary system analyses will study the behavior of the I-35W Bridge structure after the presumably most critical member is completely damaged. This damaged member is selected based on the conclusion in the previous research for the system effects of failure on a truss member in various locations (Okui et al. 2010). This research revealed that in a truss bridge a diagonal main truss member close to the support will exert the greatest system effect. From a fracture critical perspective, the tension diagonal member U8L9 that is closest to the interior support will therefore be assumed to be most critical to the system redundancy. In fact, this assumption will be proved to be true after the modeling improvements to be discussed in Chapter 7.

Since the system analysis is focused on the estimation of the residual strength capacity of a damaged system, member U8L9 was assumed to have completely lost its strength capacity prior to the application of loads. In this regard, the system models used for the analyses to be discussed in the remainder of this chapter were created by removing the member U8L9 on one side of main truss from the 3D bridge system in a no load condition.

3.7.1 Elastic System Analysis

In typical bridge design practice, a system strength capacity is determined based on a set of elastic limit states. Even the latest guidelines for performing bridge analysis (AASHTO/NSBA 2011) do not address non-linear analysis procedures. Therefore, the damaged system behavior will first be analyzed assuming that all truss members are perfectly elastic during the entire loading process.

One of the most straightforward measures to reflect a change in system response is the stiffness reduction of the main trusses due to the damage on member U8L9. The comparison between the undamaged and the damaged main truss structures is plotted in Figure 3-14, which shows the dominating role that dead load are playing as these dead load are 93% of the total applied loads.

Figure 3-14 shows the slopes plotted as secant lines to particular load levels, not the exact loading path, which is affected by construction sequence. Moreover, it is important to note that the difference in stiffness between dead load and live load (the HL-93 load in this case) is due to the differences in load position and magnitude, not inelastic action. In Figure 3-14, there is about a 26% increase in dead load deflection due to the member removal. This underscores the criticality of member U8L9.

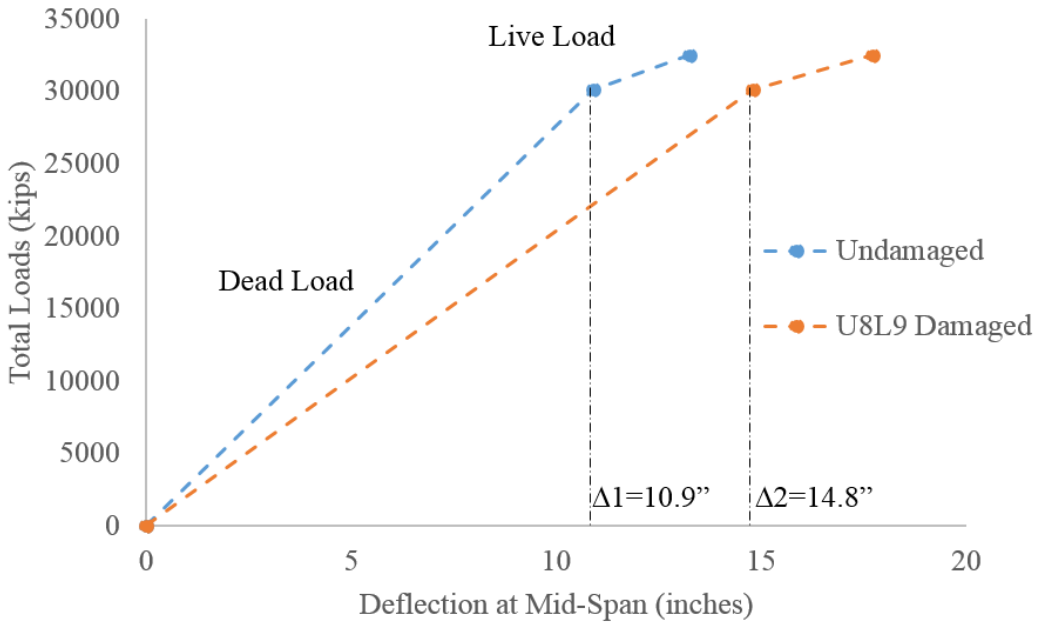

Figure 3-14. Load-deflection comparison between the undamaged and the damaged main truss structures

It seems unrealistic that the damage of member U8L9 causes such small additional deflection when the live load is applied, as shown Figure 3-14. It is probable that the deflection of the damaged structure is underestimated using a linear elastic system analysis.

Another limitation of a highly simplified elastic analysis is its inability to capture the effective stresses due to a combined flexural and axial loading. In such simplified model, a node is postulated to represent the centroid of the cross section. The stress from an elastic analysis is thereby calculated only at the centroid of the cross section, where the bending stress is zero. With this regard, the stress output merely reflects the axial stress, leading to an underestimation of the maximum stress on a cross section. Meanwhile, the exact profile of a cross sectional stress distribution is unknown.

As an alternative way to investigate the actual stress state of critical members, their interaction ratios under a combination of flexure and axial load are compared to the member first yield limit and the full plastic limit illustrated in Figure 3-15.

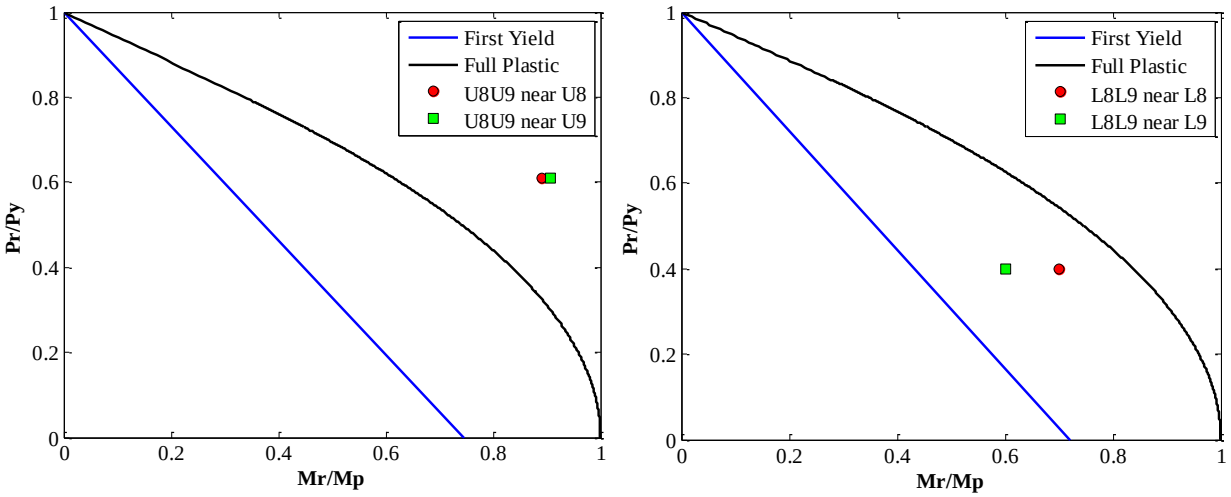

(a) Member U8U9 at U8 and U9 ends (b) Member L8L9 at L8 and L9 ends

Figure 3-15. Beam-column interactions of the critical members in an elastic 3D system model (Note that all member interaction ratios result from sequentially applied dead load and the HL-93 load.)

From Figure 3-15, it is apparent that both ends of the critical members U8U9 and L8L9 have already yielded with interaction ratios far beyond their first yield limits. However, the maximum axial stress on these members is 35.8ksi, indicating that there is no yielding on the critical members. From this stress result, it will be inferred that all main trusses in the damaged structure with failure of member U8L9 can still behave elastically under sequentially applied dead load and the HL-93 load. This deduction apparently conflicts with the inelastic interaction ratios shown in Figure 3-15. As explained previously, this elastic stress output is not the real effective stress on a cross section under a combined loading effect. Thus it is imperative to refine the current simple elastic model in order to directly obtain a realistic stress result.

It is also worth noting that even though the interaction ratios at two ends of member U8U9 exceed the full plastic limit by an ample margin, the structure can still escape from collapse, primarily owing to 3D system action. In other words, the members in the deck and floor systems spanning out-of-plane could provide adequate residual strength to support the structure after the failure of member U8U9 resulting from an initial damage at member U8L9. The contribution of these out-of-plane members, commonly recognized as secondary members, will be discussed in detail in Chapter 6.

3.7.2 Inelastic System Analysis

An inelastic system analysis is utilized as an approach to improve the ability to capture the ultimate structural behavior, which generally features a plastic damage mechanism. The material plasticity for a typical ASTM A572 Grade 50 steel (Frank et al. 2000) is introduced to the members that have most significant interaction ratios computed from the elastic analysis, since these members are expected to yield first. The members modeled with both elastic and plastic properties are the chord members U8U10 and L8L9, which used to connect the damaged diagonal U8L9.

Figure 3-16 shows the idealized stress-strain curves normalized by the nominal yield strength for a typical ASTM A572 Grade 50 steel.

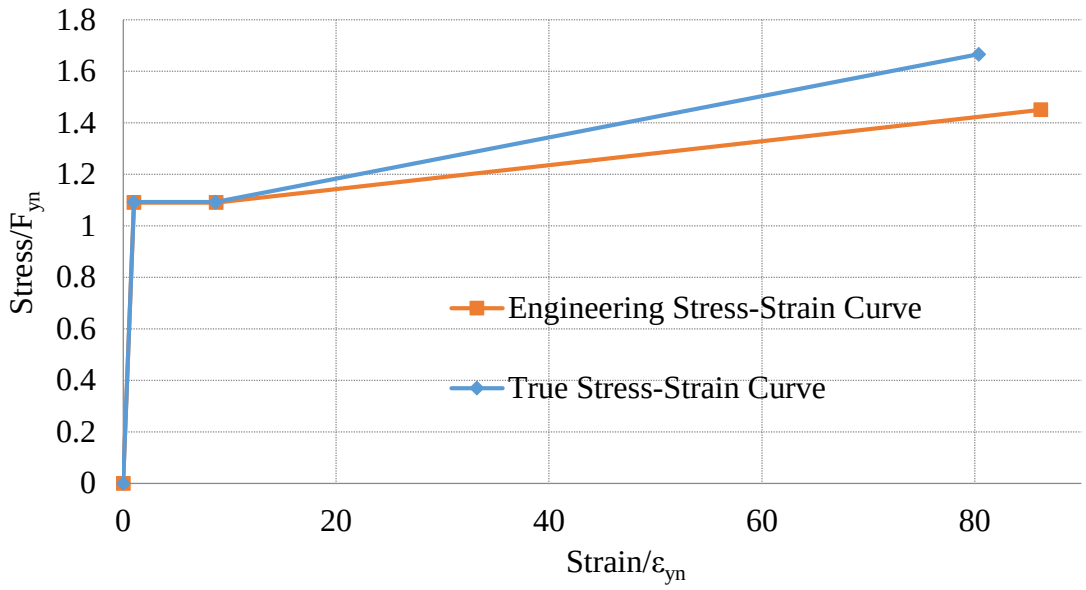

Figure 3-16. Idealized stress-strain curves normalized by the nominal yield strength for a typical ASTM A572 Grade 50 steel

Considering that the nonlinear analysis performed in ABAQUS program requires a true stress-strain curve, the critical characters in the engineering stress-strain curve are converted to true stresses and true strains using equations (3-2) and (3-3):

$$\sigma_{true} = \sigma_{en}(\varepsilon_{en} + 1) \tag{3-2}$$

$$\varepsilon_{true} = \ln(\varepsilon_{en} + 1) \tag{3-2}$$

The critical characters in both the engineering stress-strain curve and the truss stress-strain curve are summarized in Table 3-1. The strain is arbitrarily capped at 15%.

Table 3-1. Critical stresses and strains for a typical ASTM A572 Grade 50 steel

Critical characters	Engineering (Frank et al. 2000)		True	
	Stress/F_{yn}	Strain/ε_{yn}	Stress/F_{yn}	Strain/ε_{yn}
Beginning of the yield plateau	1.09	1	1.09	1
End of the yield plateau	1.09	8.73	1.09	8.66
Ultimate strength	1.45	86.2	1.67	80.4

One key advantage of inelastic analysis is the improved stress calculation for a member cross section. Unlike the elastic system analysis, the inelastic system analysis considers the exact profile for the cross section of a truss member with plastic properties. The stresses computed from an inelastic analysis are based on the points at all corners of a cross section. For the box shape members U8U10 and L8L9 assigned with plasticity, four corner points on each cross section are utilized as the stress output points. Since each corner point is located on the extreme fiber of a cross section, the stress result from a corner point will include both bending and axial stresses, which can correctly predict the maximum stress on a cross section under a combined loading condition.

3.7.3 Result Comparison between Elastic and Inelastic System Analyses

Since in the damaged structure the critical members U8U10 and L8L9 are carrying combined flexure and axial loads, it is appropriate to choose a Von-Mises stress output to analyze the effective stress due to both axial and bending stresses. The Von-Mises stresses for the critical members U8U9 and L8L9, where yielding first occurs, are compared to the results from the elastic model in Figure 3-17.

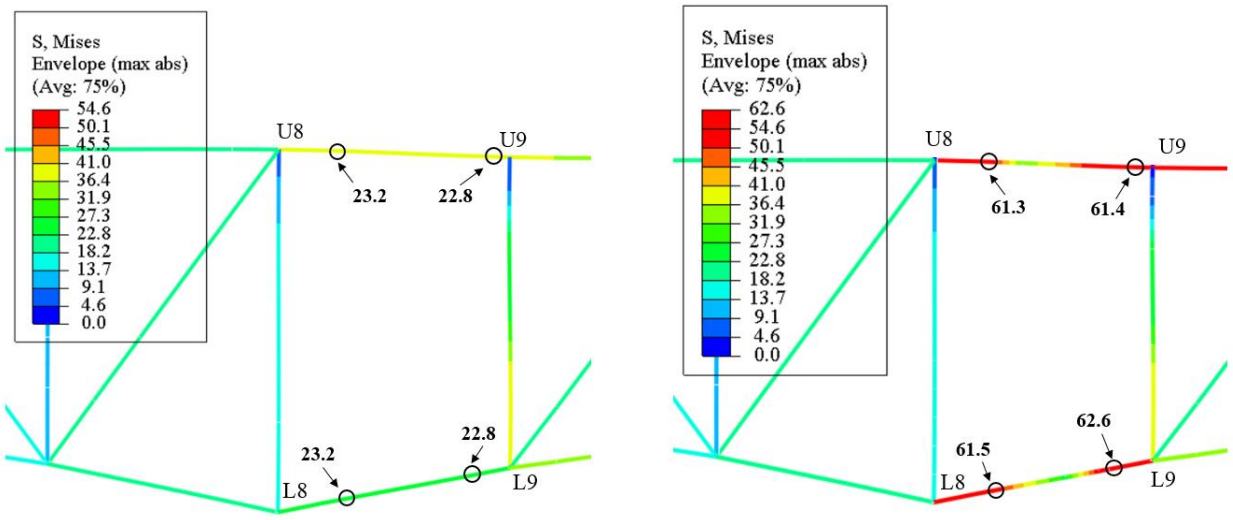

Figure 3-17. Von-Mises stress (unit: ksi) comparison between the elastic model (on the left) and the inelastic model (on the right)

Notes:

- The output of Von-Mises Stress on each cross section was obtained by taking the maximum value of the Von-Mises Stresses on all section points of that cross section. This means that the Von-Mises Stresses displayed in Figure 3-17 can basically represent the stress results on the extreme fiber of a cross section, where yielding will occur first.

- The yield limit is set as 54.6ksi for the main truss members that were made of Grade 50 Steel, as it is not the engineering yield stress (50ksi) but the true yield stress (54.6ksi) is used in an inelastic analysis in ABAQUS.

- The critical sections with Von-Mises Stress values displayed in this figure are located at *d*/2 from the outmost edge of the gusset plate connection (*d* represents the depth of the member L8L9).

Obviously, only the inelastic model is able to capture the member post-yielding behavior. It can be seen from Figure 3-17 on the right that the inelastic Von-Mises stresses occur at both ends of the chord members U8U9 and L8L9. This further implies that a plastic Vierendeel mechanism will form in the damaged panel following the failure of a diagonal member. The locations exhibiting plastic behaviors are consistent with those displayed in Figure 3-15. This indicates that an inelastic model is able to reflect the actual effective stress under a combined loading.

Along with the occurrence of plastic stresses on the critical members, the stiffness of these member reduces. As a result, the ultimate mid-span deflection of the structural system predicted by an inelastic analysis will be larger than that computed by an elastic analysis. This statement is confirmed by comparing the ultimate deflections of the elastic damaged model and the plastic damaged model plotted as the final points of the last two curves in Figure 3-18.

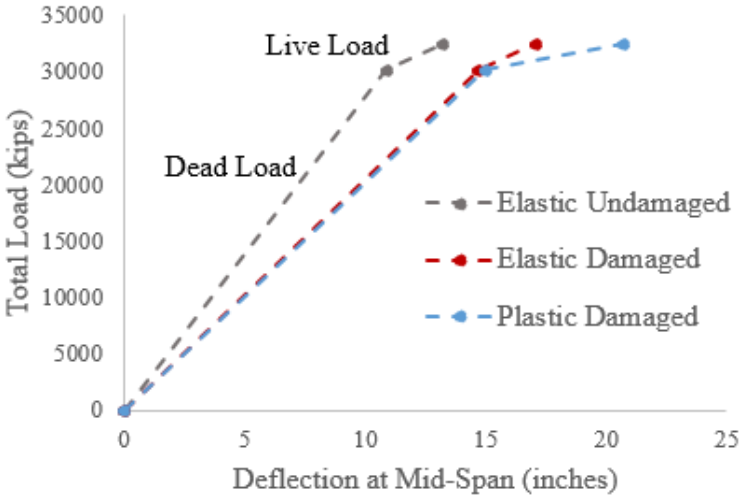

Figure 3-18. Comparisons of load-deflection curves for the undamaged structure in the elastic analysis, as well as the damaged structure in the elastic and plastic analyses

It is also observed from Figure 3-18 that there is little difference between the stiffness of the elastic damaged model and the one of the plastic damaged model before applying live load. In fact, the stress history of the critical members reveals that the first yielding appears when dead load are almost completely applied to the structure. With the accumulation of plastic behaviors, the stiffness difference between the elastic damaged model and the plastic damaged model becomes larger and larger after live load is incrementally applied as demonstrated in Figure 3-18.

Furthermore, through the comparison of stiffness in the live load phase among the three models labeled in Figure 3-18, the stiffness reduction in the plastic damaged model is more perceptible

than that in the elastic damaged model. Clearly, an inelastic model is needed to obtain realistic stiffness of a damaged system.

3.7.4 Strain Rate Effect on the Yield Strength

Since all gravity loads reflecting the effect of member self-weight on the bridge system are applied instantaneously at a rate much higher than the one assumed in a typical static analysis, yielding slip planes on the main steel members do not have adequate time to develop, resulting in an elevated yield strength. This yield strength at a given load rate and temperature can be estimated using Equation (3-1) (Madison and Irwin 1974):

$$\sigma_{yd} = \sigma_{ys} + \frac{174{,}000}{log(2 \times 10^{10} t)(T + 459)} - 27.4 \qquad (3\text{-}1)$$

where σ_{yd} represents the dynamic yield strength with a high strain rate and a specific temperature; σ_{ys} is the standard 0.2% offset yield strength at a static load rate at room temperature; t stands for the total duration from the initial no-load condition to the end of the loading process measured in second; T is the ambient temperature.

For a standard Grade 50 structural steel at a static loading rate, σ_{ys} is the calculated true yield stress, which is equal to 54.6ksi (Frank et al. 2000). The total load duration t can be determined by a free fall formula (Equation 3-2), assuming that the bridge system is a single degree of freedom system and the self-weight of all members is concentrated as a lumped mass at the place where maximum vertical deflection (term h in Equation 3-2) occurs in the damaged structure after losing U8L9. In addition, a typical room temperature T = 70°F is utilized to exclude temperature effect on the yield strength.

$$t = \sqrt{2h/g} = \sqrt{2 \times 12.167/386.4} = 0.25sec \quad (3\text{-}2)$$

By substituting the above parameters into Equation (3-1), the dynamic yield strength is obtained as σ_{yd} = 61.11ksi for the trusses in the damaged system model. An increase of 6.52ksi is found compared to the static yield strength. This calculated increase is reasonable compared to experimental data provided by Frank et al. (2000).

3.7.5 Result Comparison between the Analyses with Static Yield Strength and with Dynamic Yield Strength

Table 3-2 shows that it makes little difference to consider the strain rate effect or not in predicting the behavior of critical members. As the yield strength increases when the strain rate effect is taken into consideration, the member available strength increases. At the same time, the resultant forces and moments are also elevated, which is detected from the results of the system analysis. Since the interaction behavior of critical members is not sensitive to the strain rate effect, the inclusion of rate dependent yield strength is considered not necessary.

Table 3-2. Strain rate effect on the interaction behavior of critical members

Critical Member	P_r / P_y		M_x / M_{px}		M_y / M_{py}		P-M interaction ratio	
	no strain rate effect	with strain rate effect	no strain rate effect	with strain rate effect	no strain rate effect	with strain rate effect	no strain rate effect	with strain rate effect
U8U10-U8W	1.0	1.0	0.6	0.7	0.0	0.0	1.6	1.6
U8U10-U9W	1.0	1.0	0.6	0.7	0.0	0.0	1.6	1.6
L8L9-L8W	1.0	1.0	0.8	0.8	0.1	0.0	1.8	1.8
L8L9-L9W	1.0	1.0	0.8	0.8	0.0	0.1	1.7	1.7

3.8 Conclusion

This chapter provides preliminary system analyses results based on an existing 3D model that has been validated to match the behavior of an actual bridge system in a collapse event. The system analyses performed so far are focused on the behavior of one damaged structure after losing the diagonal main truss member U8L9. This main truss member is the tension diagonal member closest to the interior support. A hypothesis based on previous literature is that failure on this member would cause the worst system effect.

In response to the failure of member U8L9, the chord members U8U9 and L8L9 that used to connect this damaged diagonal member become flexural members. Large in-plane bending moments are induced at both ends of the chord members. Thus a combined flexure and axial load has to be carried by these chord members. As a result, yielding occurs first at these chord member ends where most significant beam-column interaction is observed. This eventually forms a plastic mechanism that would make the entire structure unstable if only a 2D system behavior is considered. The presence of this plastic mechanism did not cause a bridge collapse, as the

structural behavior is analyzed using a full 3D model. This indicates that the out-of-plane members in deck and floor system are making vital contributions to the residual strength of a damaged system. Therefore, it is imperative to perform system analyses based on a 3D model.

To capture the formation of this plastic mechanism, an inelastic analysis is required as the nonlinear effects after yielding must be considered for the critical chord members above and below the damaged diagonal member.

Considering fracture critical connections, either tension or compression failure on gusset plate connections are found to have the same system consequence as failure of the connected truss member. Meanwhile, a shear rupture along the chord line on any five-member member joint does not cause any of the truss members to exceed their strength capacity. This implies that a connection failure due to shear rupture in the horizontal plane is not as critical as a member failure to the system redundancy.

Since all system models discussed in this chapter do not account for connection details of the truss members, the progressive failure of connections in the vicinity of a damaged member was not modelled. The required limit state checks for the connections around the damaged member can follow the proposed procedures in NCHRP 12-84 (Ocel 2013), as this recently completed report has already intensively analyzed all possible connection failure modes. This progressive failure of connections is thereby beyond the scope of work in this thesis.

4 Evaluation of Connections

4.1 Introduction

All previously discussed system analyses were performed using 3D truss models with a rigid end assumption for every truss member connection. Although the use of fixed-fixed connectivity for each truss member enables every truss member to carry bending moment, the system model might still fail to reflect the actual ultimate failure mode of the critical truss member under a combined loading. The current system model does not consider the presence of rivet holes at both ends of each truss member, and thus the member strength capacity has been assumed equal to its capacity based on a gross section. This assumption is reasonable for a compression member as it does not have a rupture failure mode. However, this assumption may not be valid for a tension member, since the occurrence of rivet holes at a connection subjected to tension and flexure may alter the failure mode from gross section yielding to net section rupture. Tension on the gross section allows the member to remain active at its yield strength through relatively large displacement while a rupture failure will deactivate the member suddenly at low elongation.

In the damaged structure with failure of member U8L9, the top chord U8U9 was identified as the most critical tension member due to excessively large beam-column interaction ratios near the member ends (see Figure 3-15 (a)). The interaction history curves at these critical locations were plotted in Figure 4-1. This figure displays the difference of interaction behavior predicted from an elastic model as compared to a plastic model. These interaction curves are also compared with the first yield and full plastic limits.

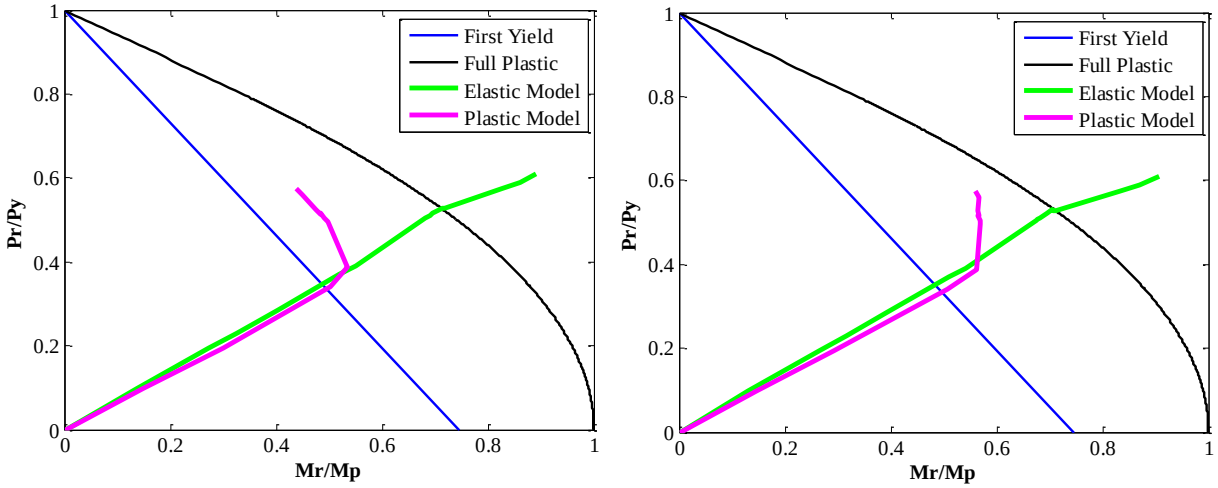

(a) P-M interaction curves near U8 (b) P-M interaction curves near U9

Figure 4-1. Comparison of beam-column interactions at two ends of a critical member (U8U9)

It is apparent that the plastic interaction curves of the member U8U9 fall below the curve for full plastic limit state which represents the ultimate capacity for a gross section of this member. As rivet holes are not taken into consideration in this plastic system model, the level of reduction in the ultimate capacity as a result of introducing rivet holes remains unknown. In this regard, it is essential to determine the net section capacity for member U8U9 so that the possibility of failure due to excessive axial-flexural interaction at any one of the two critical connections for this member can be properly predicted.

Another equally important motivation to study the net section capacity of beam-column interaction originates from the observation of the wreckage for a similar tension chord connection. Figure 4-2 displays an actual fracture failure at a net section, which indicates that it is possible to initiate net section failure at a critical connection of a truss member.

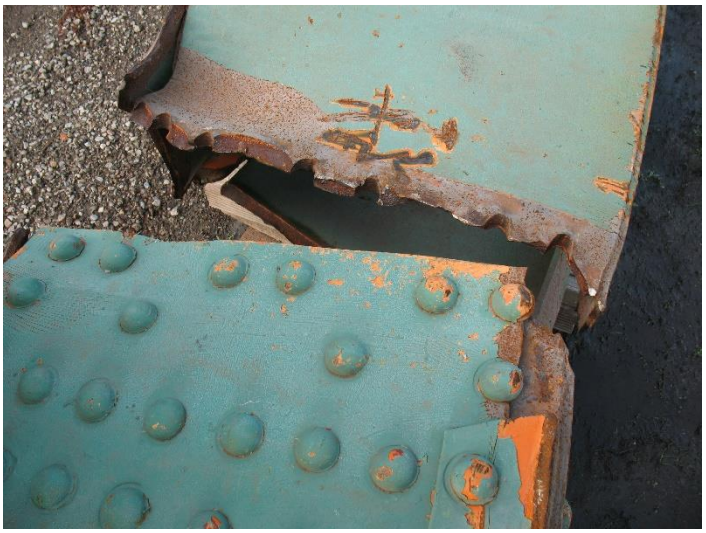

Figure 4-2. Wreckage of member U10U11 on the East side of the main truss. NTSB (2009). Collapse of I-35W Highway Bridge, Minneapolis, Minnesota, August 1, 2007. National Transportation Safety Board. Used under fair use, 2015.

In the actual collapse sequence, member U10U11 was recognized as the most critical tension chord with significant beam-column interaction near its two end connections after the removal of a compression diagonal U10L9. Figure 4-2 clearly shows that the chord member was completely separated from its connection following a failure path along the centerline of the rivet holes at the outmost edge of the connection. It can be further assumed that this failure was most likely triggered by tension rupture at the net section under combined tension and bending effects. The existence of flexural behavior can be detected in the form of local buckling on the compression side of the net section shown in the top left of Figure 4-2.

The occurrence of failure at critical member connections must be checked based on the net section capacity of beam-column interaction. However, the calculation of such net section capacity under combined tension and flexure for built-up sections is not addressed specifically in either AISC or AASHTO. There are few published studies on the topic of net section capacity under a combined flexure and tension (Altstadt 2004; Altstadt 2006; Dexter et al. 2002). Therefore, an appropriate

methodology to analytically predict this net section capacity needs to be explored. In the following sections in this chapter, one methodology proposed by the author is discussed in detail.

4.2 Methodology

4.2.1 Identification of the Most Critical Connection

Due to the lack of experiments addressing the net section capacity under a combined flexure and tension, a finite element analysis has to be utilized to predict the ultimate fracture failure at a net section. The idea is to analyze the ultimate capacity of the connection whose interaction ratio is largest among all remaining trusses in the damaged structure under full dead load and HL-93 load, as this connection is most critical to failure. From both Figure 3-15 (a) and Figure 4-1, it can be seen that the connection near the end member end U9 of member U8U9 has highest interaction ratio, thereby becoming the target connection whose net section capacity is required to be elaborately studied.

4.2.2 Modeling of the Truss Member with the Most Critical Connection

A similar failure path to the one shown in Figure 4-2 is expected to occur at the outmost edge of connection U9 of member U8U9. The most critical net section is found along the failure path highlighted in Figure 4-3, which is exact centerline of the outmost rivet holes on a side plate. Although there are multiple lines of rivet holes at the connection U9, only the rivet holes on the failure path are explicitly simulated in the finite element model of member U8U9. The negligence of the rest rivet holes is believed not to affect the ultimate capacity of this U9 connection, as results from previous tests conducted by Munse (1970) indicate that the behavior of a truss member end with only one column of holes along the critical failure path is the same as the behavior of a truss member end with all staggered holes at the connection.

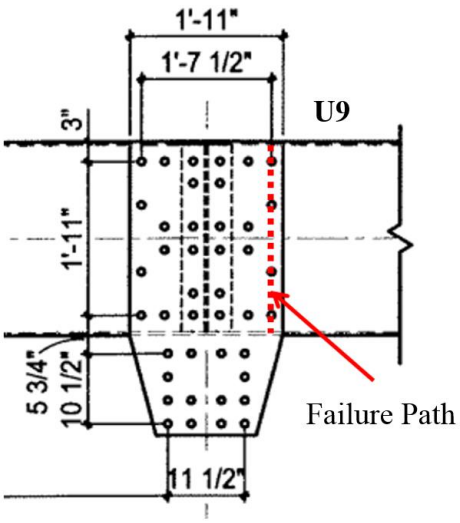

Figure 4-3. An elevation view of connection U9 of member U8U9. Sverdrup & Parcel and Associates Inc. (1965). State of Minnesota Department of Highway Construction Plan for Bridge No. 9340 – Balance of Bridge and Approaches. St. Louis, MO. Used under fair use, 2015.

As the in-plane bending moment distribution of the damaged system shows that the inflection point on member U8U9 is close to its midpoint, a zero moment can be assumed to occur at the mid-span of U8U9. Thus the FE model for member U8U9 can be simplified as a cantilever beam with a fixed end at the centerline of the connection U9 and a free end at the midpoint of U8U9. Each rivet hole in the model is assigned 1-1/16 in. diameter to accommodate 1 in. rivets. The geometry of the simplified FE model for half-length of member U8U9 is plotted in Figure 4-4.

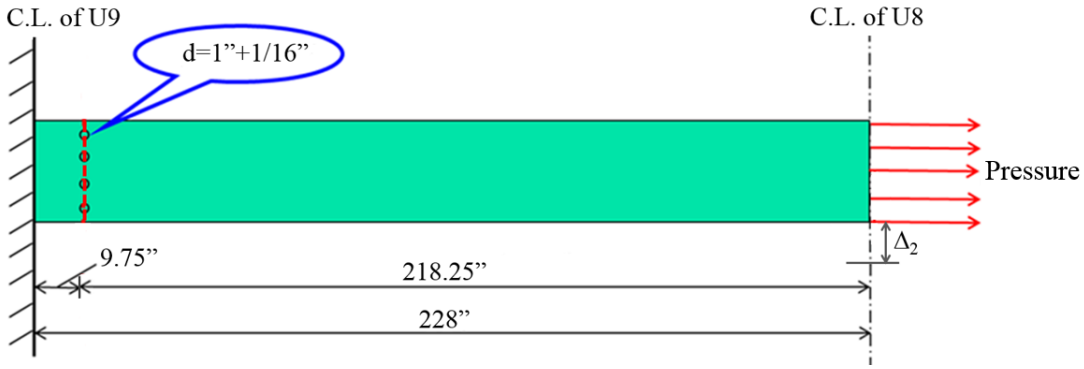

Figure 4-4. Simplified model for half-length of member U8U9 under a combined flexure and tension

For a static finite element analysis, the combined loading is gradually applied to the face of the free end as a ramp loading. The tension force is simulated as uniform surface pressure, while the in-plane bending moment is produced by applying vertical displacement loading (Δ_2). As the damaged system response indicated that the in-plane bending and tension on member U8U9 shared the same rate of increment, it is reasonable to apply the pressure load and the deflection simultaneously with the same load amplitude function in ABAQUS.

The FE model for member U8U9 utilized linear continuum solid elements in order to precisely capture the through-thickness deformation behavior. An element type of C3D8I with full integration (8 Gauss points) and incompatible modes was chosen to improve the accuracy of the prediction of flexural behavior, as Bursi and Jaspart (1998) and Citipitioglu et al. (2002) found a best match of moment-rotation curve between the analytical models using C3D8I and test specimens.

4.2.3 Simulation of Net Section Fracture

In light of the lack of published experimental data on net sections subjected to a combined loading, the ultimate capacity of the critical net section is estimated through simulating fracture failure in the FE model for member U8U9. An approximate and conservative failure strain is imposed to define the initiation of a fracture failure. It is assumed that the material of member U8U9 cannot sustain stress once the equivalent plastic strain of the material reaches 15% strain. This 15% strain is smaller than the typical strain at the onset of necking for any of the commonly used steel grades (Altstadt 2008). This 15% failure strain is comparatively low for regular steel grades that have had net section axial tests and net section flexure tests reported in the literature. Therefore, the 15% failure strain is expected to underpredict the occurrence of fracture when compared to experimental tests and eventually give a conservative estimation of the ultimate capacity of the net section.

In addition to the 15% failure strain, a constant stress triaxiality ratio has been identified as another key factor to affect fracture initiation (see Section 2.7.1). Based on an assumption that a fracture failure will initiate in a stress state for which a uniaxial tensile stress is predominant, a constant stress triaxiality ratio of 1/3 (Lemaitre 1985) is used in simulating the fracture failure in the FE model. The use of a 1/3 stress triaxility ratio in the numerical simulations was found to be satisfactory compared to the real test results by Bao and Wierzbicki (2004) and Zhou et al. (2013).

Fracture is a process of separating a solid into pieces, which involves two basic stages: crack initiation and propagation (Girão Coelho 2013). Therefore the simulation of a net section fracture is herein carried out with both crack initiation and propagation characteristics. The crack initiation is implemented by separating one phantom node from its originally attached real node as explained in section 2.7.2. This separation is automatically imposed to an element whose plastic strain just exceeds 15% strain and stress triaxiality ratio is kept at a constant value of 1/3. The crack propagation follows a critical crack opening displacement criterion, where the critical crack opening displacement is computed as the product of the 15% strain and the element characteristic length (length of the shortest side of the element before cracking). As this critical displacement is reached, a full crack cutting throughout the element will be formed. The ultimate capacity of the critical net section is conservatively approximated to occur when the first element gets fully cracked, as there are many uncertainties in determining the additional capacity after the appearance of the first full crack.

4.3 Verification

The accuracy of the proposed failure criteria used for fracture simulation is verified by comparing the analytical results with the data from pure flexure tests conducted by Mohr (2005). A schematic diagram of the test setup is shown in Figure 4-5. The net section flexural capacity is determined as the measured maximum applied moment on the bolted splice plate attached to the web of a simply supported beam. Since this web splice plate is located at the mid-span of the simply supported beam, only a constant bending moment exists on the splice plate.

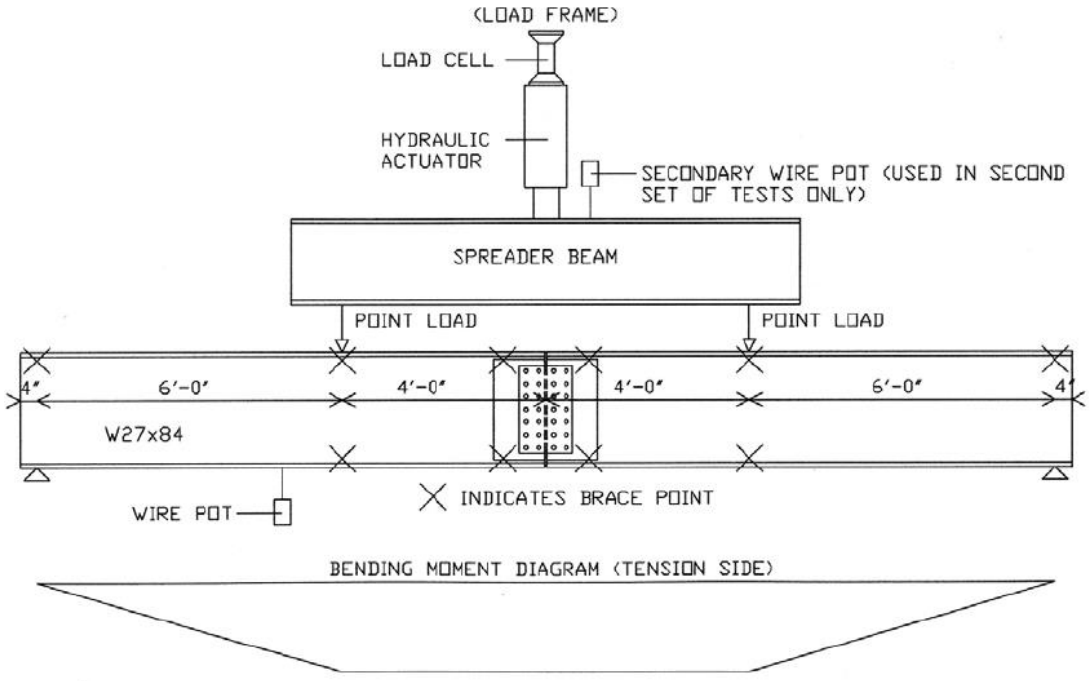

Figure 4-5. Pure bending test set-up. Mohr, B. A. (2005). Investigation of Ultimate Bending Strength of Steel Bracket Plates. Masters of Science, Virginia Polytechnic Institute and State University. Used under fair use, 2015.

Following the same configuration of the test specimen, a simplified FE model was constructed in ABAQUS and shown in Figure 4-6. Because the objective of the FE analysis is to explore the flexural capacity of the splice plate, neither the W27X84 beam nor the contact between the beam

and the splice plate needs a refined modeling. For ease of modeling, the test configuration is simplified as a beam in a rectangular shape with its depth and thickness the same as the splice plate. In lieu of attaching the splice plate to the web of the beam, the splice plate is treated as an embedded portion of the simplified beam, whose mid-span is assigned an equal amount of holes in the same pattern as the one in the original splice plate. As an attempt to prevent out-of-plane distortion, continuous lateral bracing is also assigned to the top and bottom edges of the simplified beam. As a point load in an ABAQUS model often results in extreme local effects around the loading point, a uniformly distributed displacement loading is used as a substitution for a point load.

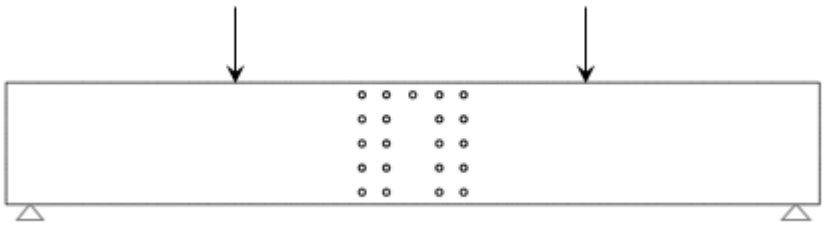

Figure 4-6. An elevation view of the simplified 3D model of the test specimen in pure bending

The predicted failure mode when the first through thickness crack can be detected is compared to the actual deformed shape of the test specimen in Figure 4-7.

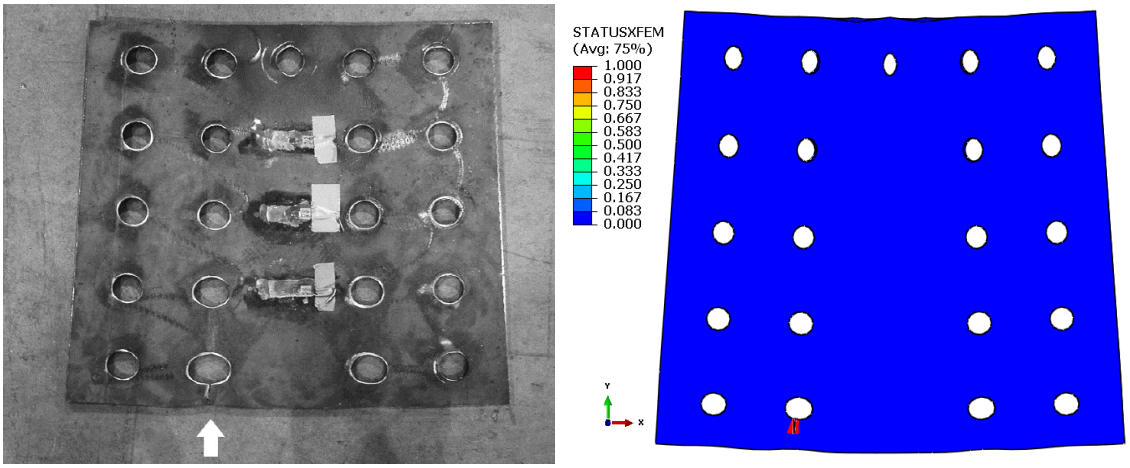

(a) (b)

Figure 4-7. Failure mode comparison between (a) the test specimen Mohr, B. A. (2005). Investigation of Ultimate Bending Strength of Steel Bracket Plates. Masters of Science, Virginia Polytechnic Institute and State University. Used under fair use, 2015; (b) the FE model developed in ABAQUS

Note that in the FE model a full crack appears when STATUSXFEM equals one. Thus the region with a fracture failure is marked in red as shown in Figure 4-7 (b). The failure mode comparison clearly illustrates that the FE model is able to properly capture the fracture failure at the critical net section. This comparison also confirms that the first crack always appears at the edge of the hole that is closest to the extreme tension fiber of the critical net section.

To further quantitatively examine the correlation between the analytical simulation and the test result, the moment-strain relation of the critical net section is used for a comparison between the analytical prediction and the test results. The experimental data selected for the moment-strain curve comparison is acquired from strain gauge 8 highlighted in Figure 4-8.

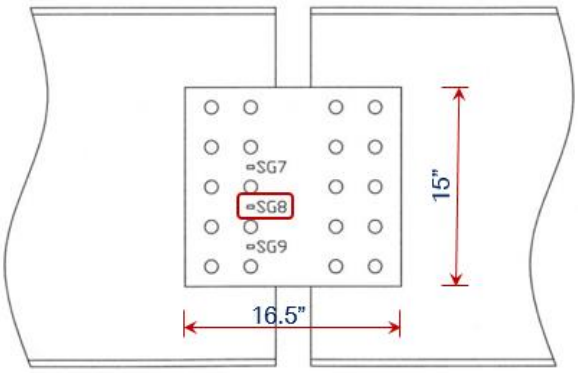

Figure 4-8. Strain gauge locations on the test specimen. Mohr, B. A. (2005). Investigation of Ultimate Bending Strength of Steel Bracket Plates. Masters of Science, Virginia Polytechnic Institute and State University. Used under fair use, 2015.

According to the moment diagram displayed in Figure 4-5, the moment acting on the critical net section in the FE model can be calculated as the product of the reaction force at one support and the distance between the end support and its adjacent loading point. The strain at the location of

strain gauge 8 can be directly output from the analysis results. With the known moment and strain, the comparison of the moment-strain curve is plotted in Figure 4-9.

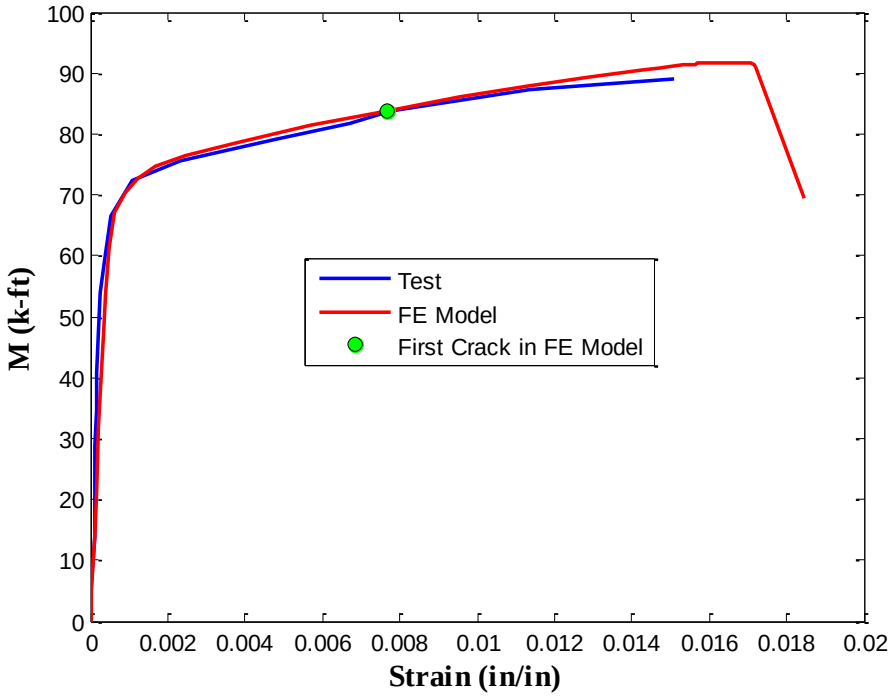

Figure 4-9. Moment-strain curve comparison

A close match between the analytical prediction and the test results is observed from Figure 4-9. The primary difference is found near the ultimate status. The FE model is able to simulate the flexural capacity degradation after the first crack occurs, while there is no descending trend from the test results as the strain gauge was found to stop functioning prior to the occurrence of rupture failure. Critical moments for yielding and ultimate limit states are compared in Table 4-1.

Table 4-1. Comparison of moment capacity between the FE model results and the measured test data

Unit (k-ft)	Test	FE model	Discrepancy
My	67.0	67.1	0.13%
Mu	88.8	91.7	3.24%
Moment when the first element fully cracked in FE model		83.8	6.0% ($=\frac{88.8-83.8}{83.8}$)

It is worthwhile to notice that the moment of the critical net section when the first element gets fully cracked is around 6% lower than the last measured moment in the real test. Therefore, it is reasonable and conservative to assume that the net section ultimate capacity is reached when the first element gets fully cracked.

4.4 Net Section Capacity under a Combined Tension and Flexure

4.4.1 Net Section Capacity of a Single Plate

In most cases, fracture will first occur on one single plate of a built-up member. For member U8U9, for which the most critical net section is shown in the left of Figure 4-10, fracture is expected to initiate on one of the side plates. Thus the analysis of net section capacity starts with the investigation of ultimate axial-flexural interaction of a single plate (see the right side of Figure 4-10) under a combination of tension and flexure. The goal of this analysis is to determine whether there is a member capacity reduction due to the effects of rivet holes. If the reduced member capacity falls below the factored design capacity, it is necessary to further discuss an appropriate approach to incorporate the net section effect on the critical truss member to the system analysis.

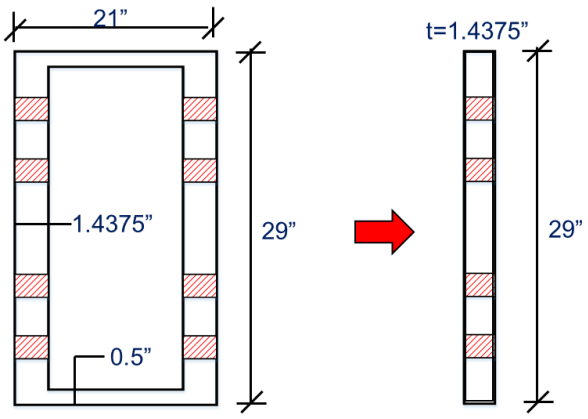

Figure 4-10. Geometry of the critical net section of a single plate extracted from the built-up member in a box shape

The ultimate failure of a single plate with the net section shown in the right of Figure 4-10 was analyzed by making use of the FE model, whose geometry is displayed in Figure 4-4. The ultimate state of the single plate was assumed to occur when the first element in the FE model was fully cracked. The beam-column interaction curve representing such ultimate limit state can be obtained by applying various combinations of tension and flexural loading to the FE model. The predicted interaction ratio is plotted as dotted curve and compared to the interaction limit of a single plate without any net section (see Figure 4-11).

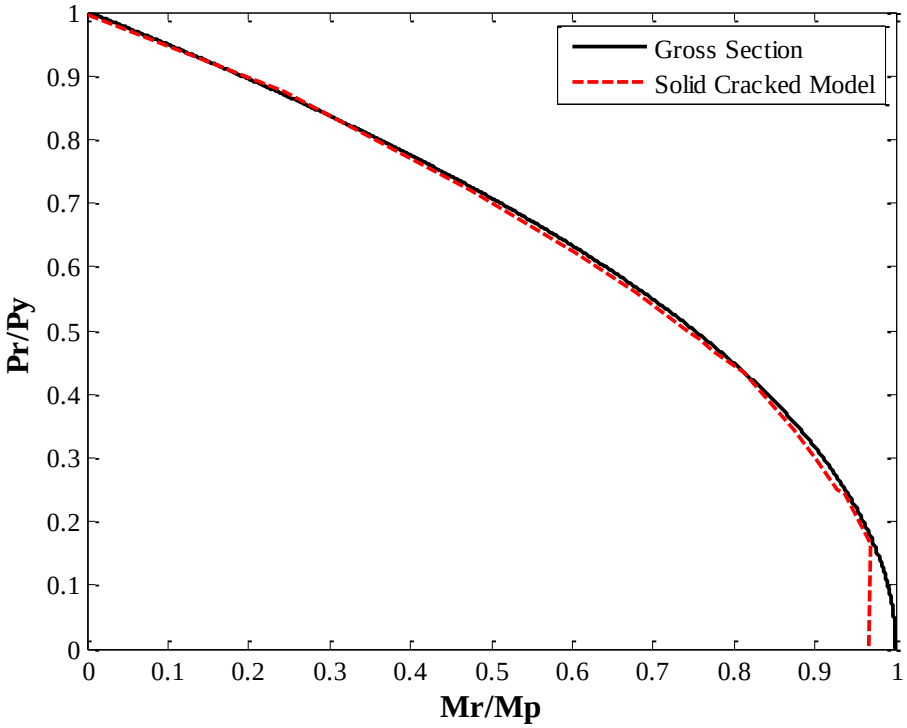

Figure 4-11. Comparison of P-M interaction capacity between the net section and the gross section on one side plate of member U8U9

It can be clearly seen from Figure 4-11 that the two interaction curves are very close to each other except in the bending dominant region. Therefore, the flexural behavior under bending moment alone is analyzed. The moment-curvature relation is compared between the net section and the gross section, and the curves predicted from the ABAQUS models using solid elements (C3D8I) are plotted in Figure 4-12.

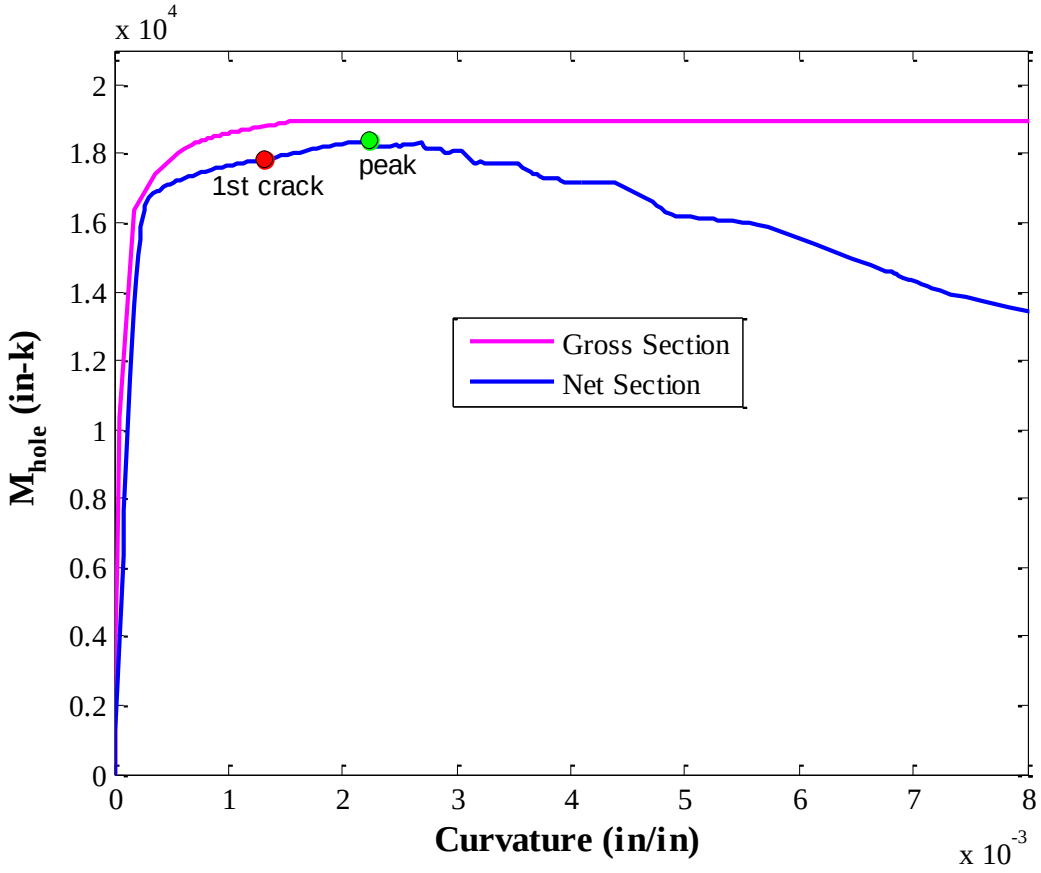

Figure 4-12. Moment-curvature relations for the net section and the gross section on one side plate of member U8U9

The critical moments at the occurrence of the first crack and the peak value in the entire loading history are also compared with the gross section yield capacity, as shown in Table 4-2.

Table 4-2. Comparison of critical flexural capacities between the net section and the gross section (unit: in-k)

Net Section ($M_{,net}$)		Gross Section ($M_{,gross}$)		Difference
Yield	16489	Yield	16374	1%
1st crack	17834	Maximum	18931	6%
peak	18392			3%

Since the critical flexural properties of the net section are close to the characters of the gross section, the reduction of flexural capacity due to the presence of rivet holes on the single plate can be neglected. This implies that the reduction of the interaction capacity of a net section under a bending dominated loading condition, as displayed in Figure 4-11, can be ignored, and that it is valid to determine the ultimate capacity of this single plate based on a gross section. Moreover, it can be also inferred that even though there are rivet holes in the single plate, yielding on a gross section will occur prior to rupture at a net section. Given that the ratio of net to gross area is 0.853, which is greater than 85%, this predicted failure mode as gross section yielding also corroborates the 15% rule in the current steel design manual published by AISC (2011).

4.4.2 Net Section Capacity of a Box-Shape Truss Member

To analyze the ultimate behavior of the critical member U8U9 under a combination of tension and in-plane bending, which is observed in previous system analysis, a local FE model with C3D8I elements is developed. Due to the symmetry about the weak axis, only one half of the box section is modeled. The rivet holes at the U9 end of member U8U9 being explicitly simulated are those on the outmost line on every plate. This FE model also includes a series of regularly spaced access holes on the bottom cover plate. A 3D view of the meshed model in a partial length is illustrated in Figure 4-13. From the actual deflected shape of U8U9 shown in Figure 4-14, one can infer that the vicinity of member end U9 is subjected to a bending effect such that the top of a cross section is in compression while the bottom is in tension. Thus the moment applied to member U8U9 in the local FE model is supposed to cause tension force on the bottom cover plate, where access holes are regularly spaced along the member length.

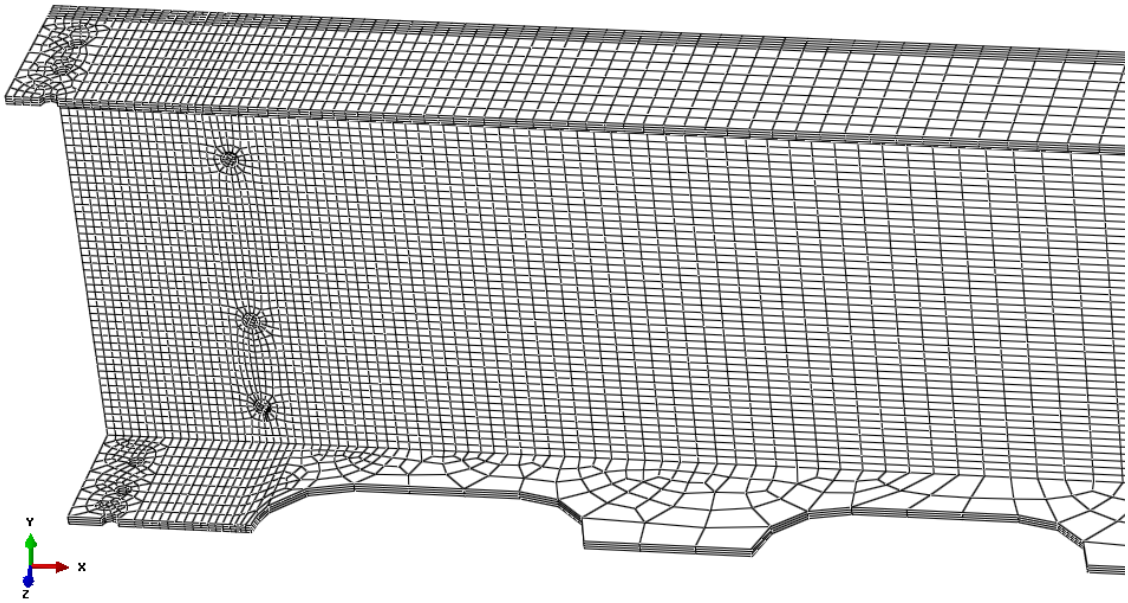

Figure 4-13. Meshed FE model of half box section of member U8U9 with member end U9 at the left side

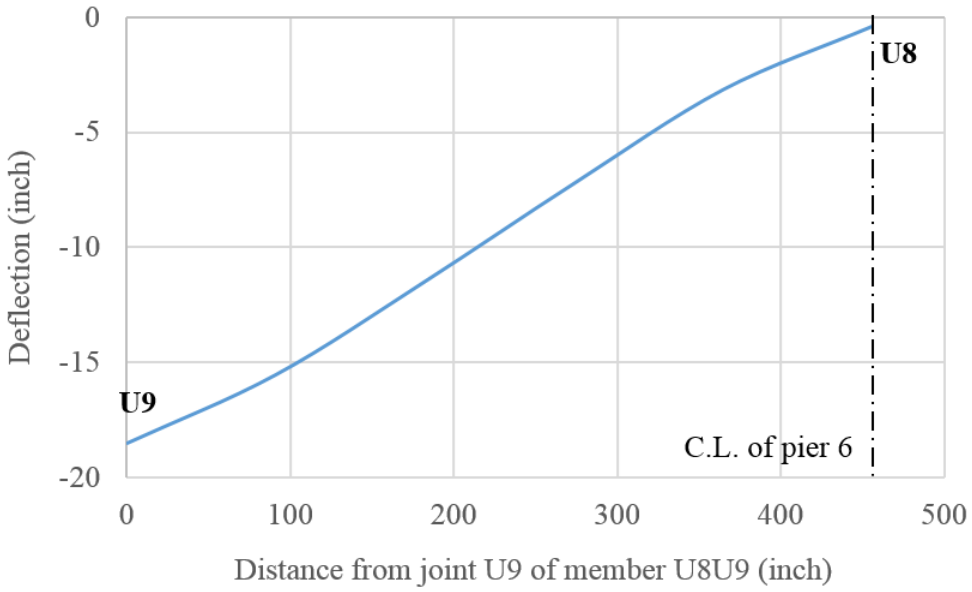

Figure 4-14. Deflected shape of member U8U9 in the damaged structure with the removal of member U8L9

The ultimate failure features the occurrence of the first crack at the extreme tension edge of the side plate hole that is closest to the bottom cover plate. This hole with crack through its thickness is shown in Figure 4-15. The deformed shape shown in Figure 4-15 also exhibits a local distortion on the top cover plate, which turns out to be caused by the sudden change of bracing conditions. To be specific uniform out-of-plane bracing is imposed to the outer surface around the rivet holes on every plate highlighted in Figure 4-16, whereas the rest portion of each plate displayed in gray is set free to deform in an out-of-plane direction. This bracing condition is used to account for the effect of the attached gusset plate at the riveted connection. With two boundary sides restrained but the third boundary side and the surface free to deform out-of-plane, the region adjacent to the lateral bracing on the top cover plate is most susceptible to a local distortion along the y-axis under an in-plane bending moment. Although this local distortion appears prior to the fracture at the tension hole edge, the member capacity does not start decreasing until the fracture begins to propagate through the plate thickness. This confirms the statement in section 4.2.2 that the most critical section governing the ultimate failure of member U8U9 is the net section cutting through the side plate holes. The profile of this critical net section is the same as that shown in the left of Figure 4-10.

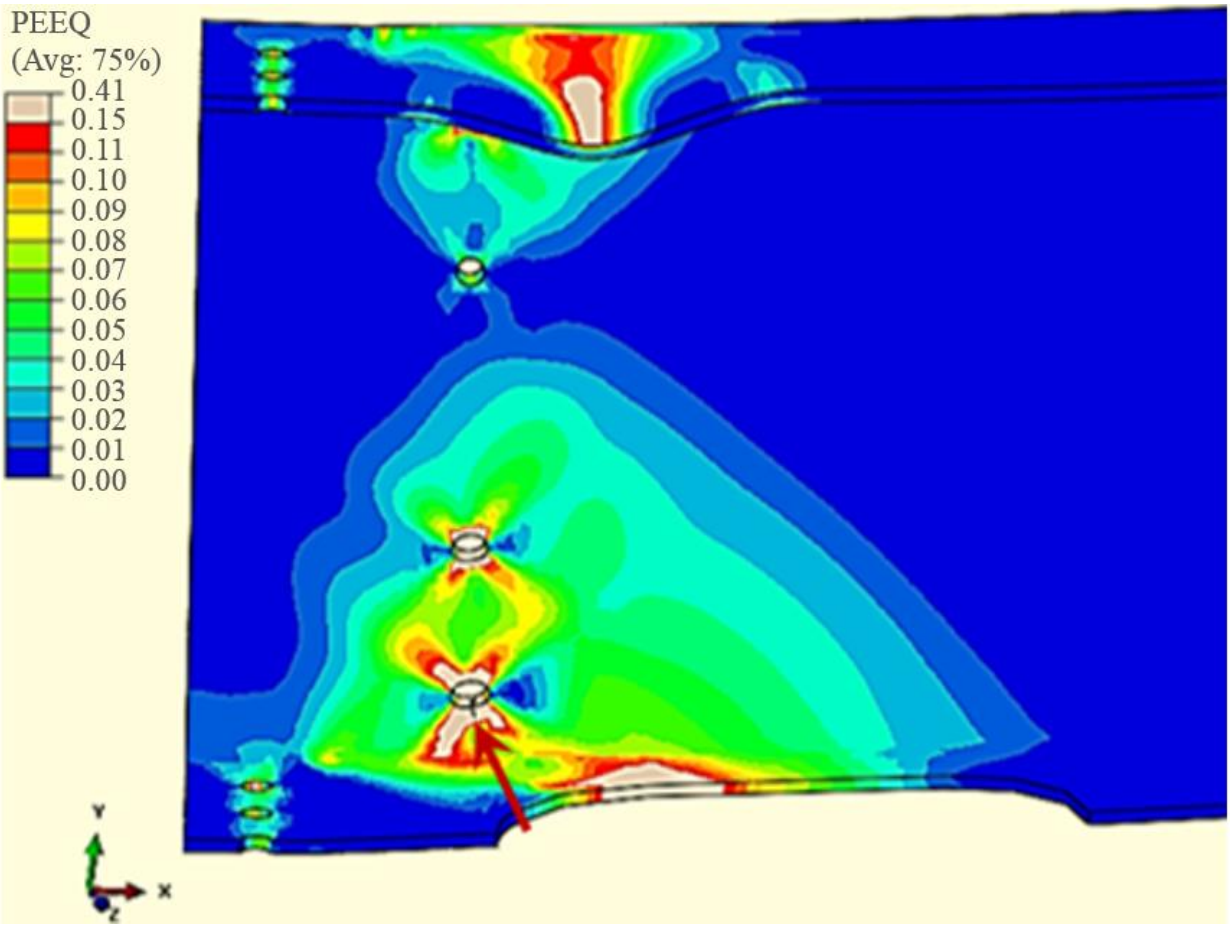

Figure 4-15. Equivalent plastic strain distribution when the first crack appears at the bottom edge of the side plate hole that is closest to the bottom cover plate (Note that all areas in gray represent the equivalent plastic strain that exceeds the 15% strain)

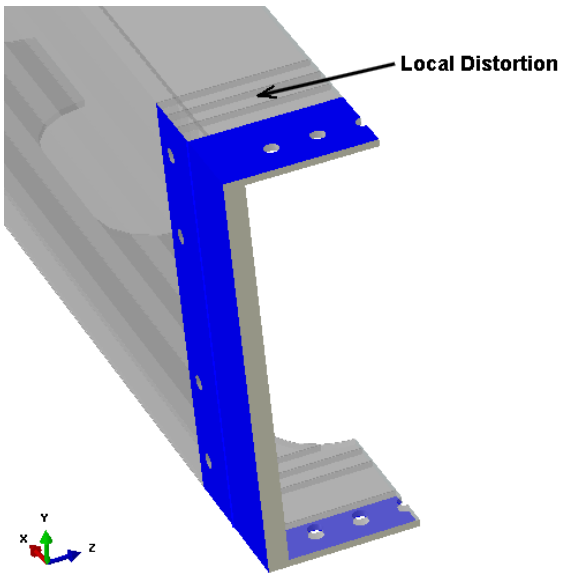

Figure 4-16. Out-of-plane bracing on each plate of the half-box-section model

The ultimate beam-column interaction behavior of the FE model under various combinations of tension and flexure is plotted as a dashed curve in Figure 4-17. This figure apparently shows that current unfactored AISC Equations (H1-1a and H1-1b) are no longer conservative in both tension dominated region ($P_r/P_y>0.9$) and flexure dominated region ($P_r/P_y<0.2$). Therefore, it is imperative to provide a safe prediction of the interaction capacity for the member with net sections.

$$\text{For } \frac{P_r}{P_c} > 0.2 \qquad \frac{P_r}{P_c} + \frac{8}{9}\left(\frac{M_{rx}}{M_{cx}} + \frac{M_{ry}}{M_{cy}}\right) \leq 1.0 \qquad \text{AISC Equation (H1-1a)}$$

$$\text{For } \frac{P_r}{P_c} \leq 0.2 \qquad \frac{P_r}{2P_c} + \left(\frac{M_{rx}}{M_{cx}} + \frac{M_{ry}}{M_{cy}}\right) \leq 1.0 \qquad \text{AISC Equation (H1-1b)}$$

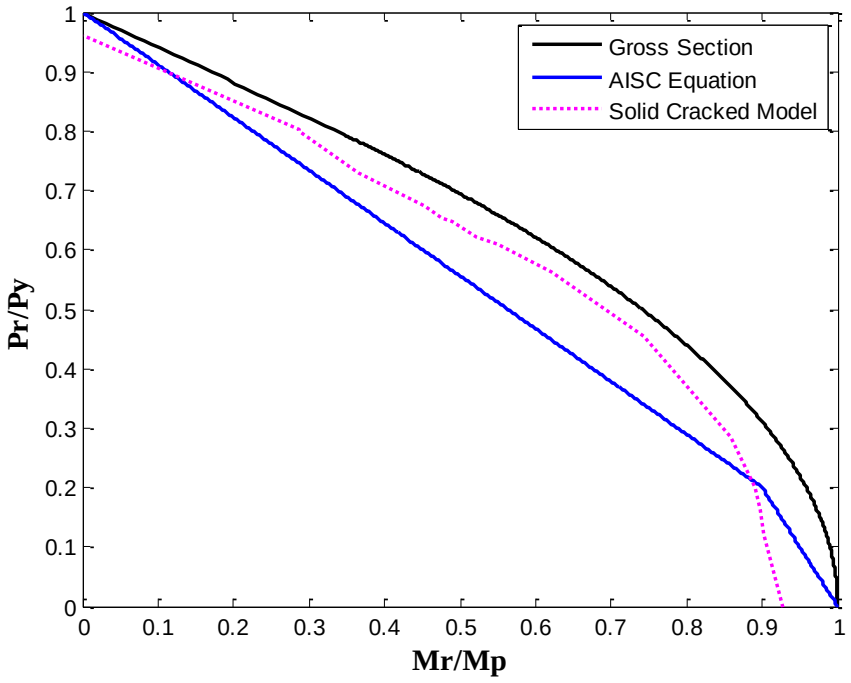

Figure 4-17. P-M interaction comparison between net section and gross section

Since analytical results for a single plate in the previous section indicate that the rivet holes on every side plate of member U8U9 do not reduce the capacity of their associated side plate, the section capacity reduction will be caused by the presence of regularly spaced access holes on the bottom cover plate. In the damaged structure, this bottom cover plate is found to behave as a tension flange under the combined tension and flexure. As the access holes decrease the tension flange area by more than 15%, it is reasonable to have reductions in both the tensile and flexural capacities.

To account for the effect of access holes, the bottom cover plate is idealized as a solid plate. The width and length of this plate is the same as the original plate, but the plate thickness is replaced with an effective thickness. The principle for determining this effective thickness is to obtain a solid plate with equivalent longitudinal stiffness in tension as compared to the original plate with

regularly spaced access holes. A new cross section with this effective thickness at the bottom cover plate is presented in Figure 4-18.

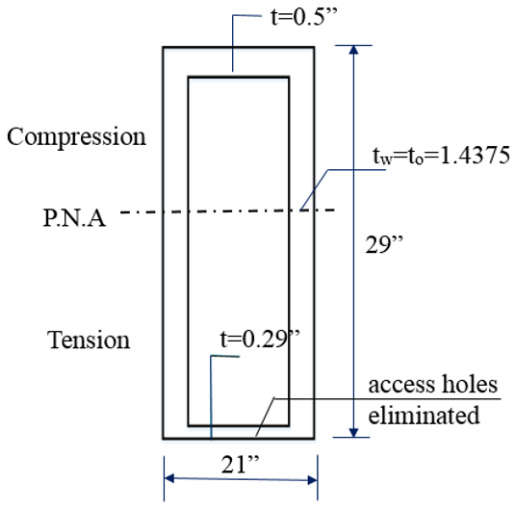

Figure 4-18. Equivalent section with a reduced thickness on the bottom cover plate

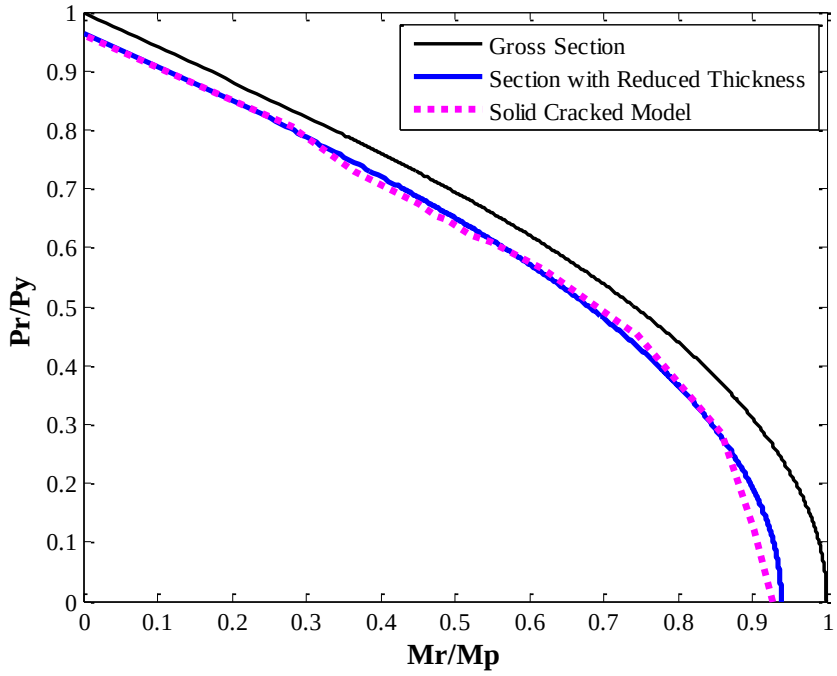

Figure 4-19. P-M interaction capacity predicted by FE model compared with that calculated using theoretical fiber analysis

Based on the equivalent box section shown in Figure 4-18, the ultimate interaction capacity is calculated using a typical fiber analysis and then plotted as a blue curve in Figure 4-19. This curve is found to closely match the curve that reflects the actual of the real member when the first crack is detected on a solid element of the local FE model. In the moment dominant region, the interaction limit predicted from the FE model is slightly lower than the one computed based on the equivalent cross section with a reduced thickness in the bottom cover plate.

To further verify the feasibility of this equivalent section based approach, the plastic capacity predicted using this equivalent section is compared with the theoretical lower bound estimation using a net section as shown in Figure 4-20 (b). The use of this net section in determining the capacity of member U8U9 will be required if this member is designed per AASHTO (2010). The comparison of the plastic capacity under P-M interaction, pure tension and pure bending of the original gross section, the equivalent section, and the net section is plotted in Figure 4-21.

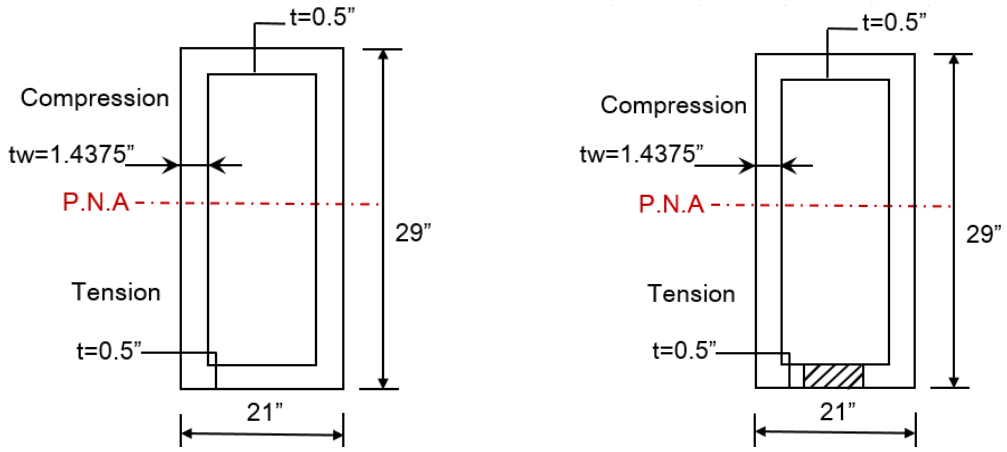

(a) (b)

Figure 4-20. (a) Original gross section of member U8U9 (b) Net section with access holes deducted in determining the section plastic capacity

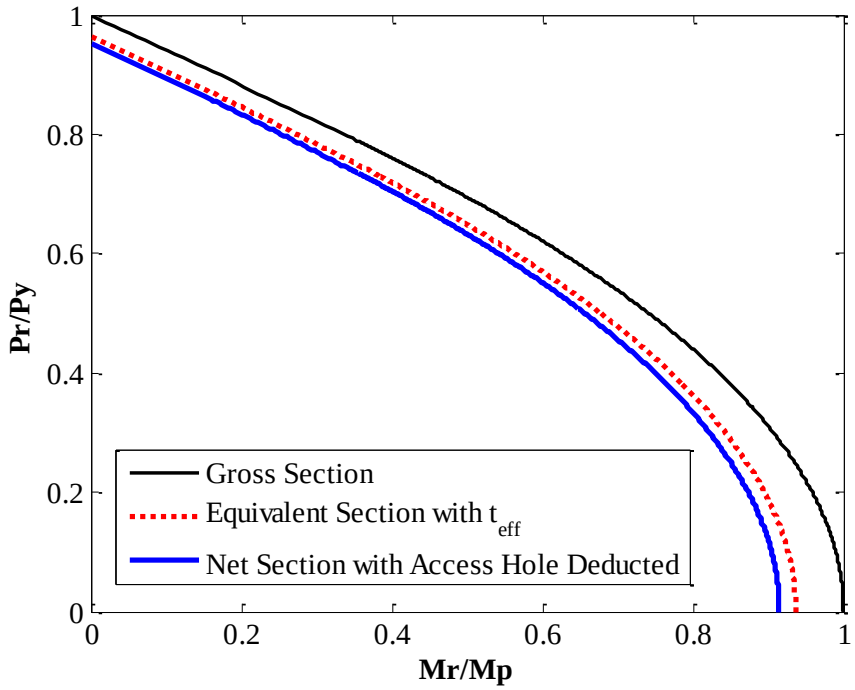

Figure 4-21. P-M interaction capacity comparison among theoretical calculations using a gross section, an equivalent section, and a net section

It can be seen from Figure 4-21 that the plastic capacity determined based on the equivalent section (dashed curve) is slightly higher than the one calculated using the net section (blue curve), but the difference between the two interaction curves is very small. It can be observed that the minimum difference occurs in the pure tension condition, while the maximum difference exists in the pure bending condition. Table 4-3 quantifies the difference in both pure tension and pure bending conditions.

Table 4-3. Comparison of flexural and tensile capacity among theoretical calculations using a gross section, an equivalent section, and a net section

Cross Section	Figure	$t_{f,bot}$ (in)	Section with Hole?	$\frac{M_{reduce}}{M_{p,original}}$	$\frac{P_{y,reduce}}{P_{y,original}}$
Original gross	Figure 4-20 (a)	0.50	No	1.00	1.00
Equivalent	Figure 4-18	0.29	No	0.94	0.96
Net	Figure 4-20 (b)	0.50	Yes	0.91	0.95

The above comparison implies that the plastic capacity based on an equivalent section will be very similar to the capacity determined using a net section with access holes deducted. As there is not much benefit gained from using this equivalent section, it is reasonable and recommended to still follow the use of a net section as required in AASHTO (2010).

4.5 Conclusion

This chapter focused on the discussion of connection details among main truss members that are modeled based on simplified assumptions in the preliminary system analyses performed in Chapter 3. The motivation of analyzing the main truss member connections originated from the fact that a significant increase of in-plane bending moments was observed in some of these connections in the damaged structure after losing member U8L9.

The evaluation of connection details among main truss members is targeted at the most critical end (U9) of the tension member U8U9 that used to connect the damaged member U8L9. Large in-plane bending moment along with high tension is detected at this connection. As significant flexure and tension interaction is likely to initiate fracture at the net section in which rivet holes are located, the actual capacity of the connection U9 of member U8U9 is investigated. An ultimate interaction capacity is conservatively estimated through a fracture simulation approach using strain controlled

failure criteria. This approach shows sufficient accuracy as compared to a test of a steel plate under pure flexural loading.

Through the results of the ultimate P-M interaction capacity predicted using the local FE models with crack initiation and propagation features, it was found that the rivet holes on every side plate of member U8U9 did not give rise to a decrease in the ultimate interaction capacity of this single plate. This indicates that, for this side plate, gross section yielding will appear prior to fracture failure on its net section. Given the fact that the ratio of net to gross area for a cross section of each side plate is greater than 0.85, this gross section yielding controlled failure is in a good agreement with the 15% rule defined in current steel design specifications.

This 15% rule is also corroborated by the fact that there is an apparent reduction of P-M interaction capacity for member U8U9, whose bottom cover plate, behaving as a tension flange, has a ratio of net to gross area less than 0.85 due to the presence of regularly spaced access holes on it. The reduced interaction capacity for member U8U9 could be predicted using an equivalent section with a reduced thickness, which is determined to provide the same tensile stiffness as that of the original member. Furthermore, this equivalent section is found to provide a plastic capacity that is very close to the capacity based on a net section with access holes deducted but without any reduction of thickness. Since the use of this net section is required in AASHTO (2012), it is reasonable and recommended to determine the plastic capacity for member U8U9 using the net section.

The above findings about the member interaction capacity under a combined tension and flexure are still preliminary and cannot be generalized to other cross section configurations nor other grades of steel with various yield to tensile strength ratios due to the lack of robust experimental data.

5 System Analysis with Refined Connection Details

5.1 Introduction

The analyses discussed in Chapter 4 reveal that the actual end conditions for a typical truss members are not as rigid as it was assumed in the preliminary system analyses performed in Chapter 3. In that preliminary system model, the assumption of a rigid connection and elastic behavior results in unrealistic moments at the end of a truss member. However, limit states such as gross section yielding or net section fracture will limit, reduce or eliminate the flexural stiffness at the member end connection as the failure progresses. In order to properly capture such softening effects, the assumption of rigid connections needs to be modified. As the stiffness reduction will undoubtedly first appear at the connections with the highest resultant moments in a damaged structure, the modification of flexural stiffness will be made to only these few connections; it would be computationally prohibitive and unnecessary to model all truss connections to this level of detail. According to the preliminary system analyses, the most significant resultant moments were detected at the ends of members U8U9 and L8L9. The high moments and axial forces carried by these truss members make connections at both ends of members U8U9 and L8L9 the most vulnerable to failure. Therefore, these four connections can be regarded as "weak" connections that are supposed to be modeled with more refined flexural properties. The term "weak" as used here is relative; it is only meant to separate connections where inelastic action is modelled from those where the behavior will be assumed as elastic.

5.2 Modeling of Weak Connections

From the wreckage shown in Figure 4-2, it is obvious that the failure path at the end connection of a bolted or riveted built-up truss member goes through the centerline of the outmost set of holes. Thus it is reasonable to consider such location as the weakest cross section at an end connection of a typical large truss member. Post-yielding behavior is thereby expected to first appear at this weakest cross section. To simulate the softening effect after yielding at this critical section, a zero-length element serving as a plastic hinge is introduced into the damaged system model. The location of each hinge-point corresponding to the distance from the center of the connection to the centerline of the outmost set of holes is shown in Figure 5-1. (Note that the relatively small distance from the hinge location to U9 is due to the fact that U9 is an intermediate point of the continuous chord member U8U10. The gusset plate connection at U9 is designed to hold the vertical member U9L9 in place.)

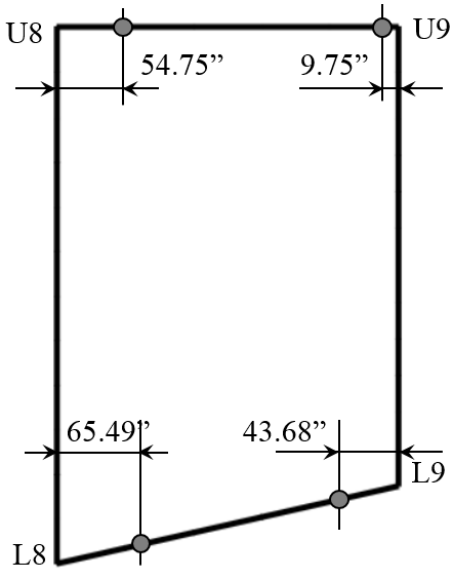

Figure 5-1. Locations of plastic hinges that are displayed as dots near both ends of members U8U9 and L8L9 in the damaged structure

As discussed in Chapter 4, the plastic capacity of the critical section near U9 end of member U8U9 can be estimated using a net section with the access hole deducted as shown in Figure 4-20 (b). As for the critical section near the U8 end of member U8U9, the access hole on the bottom cover plate will be in compression due to the deflected shape in the damaged structure under full loads depicted in Figure 4-14. The capacity of this cross section is determined using the net section shown in Figure 5-2.

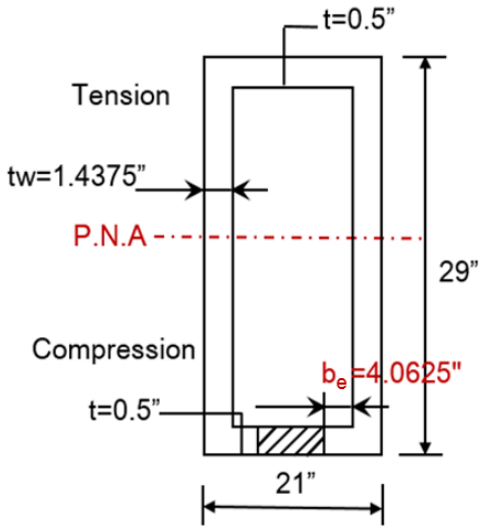

Figure 5-2. Net section used in determining the capacity of the critical section near U8 end of member U8U9

As the projecting length from the inner face of the web to the near edge of the access hole (**b_e** in Figure 5-2) is used in determining the compression flange slenderness, this compression flange is found to be compact. This indicates that local buckling will not occur on this net section, and both yielding and plastic moment capacities can be reached on this cross section.

Since member L8L9 is in compression under full loads in the damaged structure, the critical sections near both ends of this member are thereby subjected to an interaction of compression and flexure. All rivet holes on the side plates will be neglected in calculating the section capacity. This is because holes in compression will not rupture, and even if some holes will be in tension due to

the tensile bending stress and the compressive axial stress, the effective tensile stress will not reach the rupture stress prior to the yielding on the extreme compression fiber of the cross section. For these reasons, the net section used in calculating the capacity of critical sections near L8 and L9 ends will only consider the presence of access holes as shown in Figure 5-3.

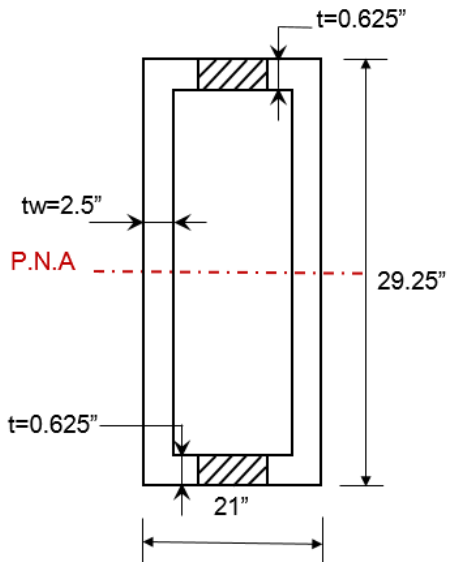

Figure 5-3. Net section used in determining the capacity of the critical sections near L8 and L9 ends of member L8L9

Similarly, as each flange is found to be compact, this net section is also able to develop yielding and reach its full plastic capacity. Thus the critical flexural capacities of the critical sections near L8 and L9 ends are determined using the elastic and plastic section modulus of the net section shown in Figure 5-3.

With the assumed yield and plastic flexural capacities, the flexural behavior of the plastic hinges in the system model can be idealized as bilinear models as illustrated in Figure 5-4, where a zero yield curvature (φ_y) as well as a 0.023 in/in ultimate curvature (φ_u) is assumed. These plastic hinges were modeled using zero-length elements, so the elastic component of the flexural deformations is taken by adjacent elements. Note that the critical members U8U9 and L8L9 are assigned material

plasticity for the entire member length, which ensures that the nonlinear axial behavior on these members can still be captured even if the plastic hinges are not incorporated into the system model.

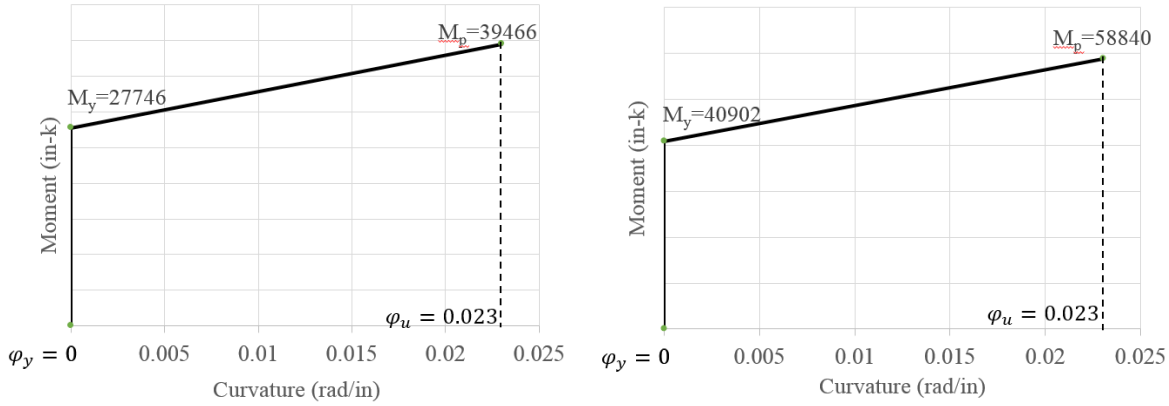

(a) Plastic hinges on member U8U9 (b) Plastic hinges on member L8L9

Figure 5-4. Idealized moment-curvature relation for plastic hinges

The accuracy of using the idealized bilinear models to reflect the flexural behavior at critical member end connections is confirmed by comparing the inelastic flexural stiffness with the theoretical values as shown in Table 5-1.

Table 5-1. Comparison of inelastic flexural stiffness of plastic hinges

Hinge locations	EI/L (Net Section; unit: in-k)	$K= (M_u-M_y)/\varphi_u$	Difference
On member U8U9	537776	509579	6%
On member L8L9	742505	779916	5%

5.3 Effects of Weak Connections on System Behavior

The objective of introducing plastic hinges into the damaged system is to determine if the lower flexural stiffness in a post-yielding regime alters the interaction behavior at the hinge point. To investigate the system effects resulting from introducing these plastic hinges, the beam-column interaction history from a no-load condition to a full load condition is explored at each hinge point and then compared with the interaction history at the same location with the no-hinge system model. The final interaction ratios at four hinge points in the damaged system under full dead load and HL-93 load is plotted in Figure 5-5. Also shown in the figures are the plastic capacities of the critical net sections and the corresponding gross sections, where the determination of each net section capacity is explained in section 5.2.

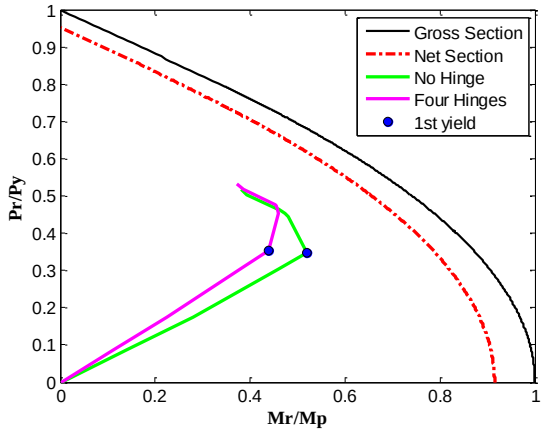

(a) Critical section near member end U8

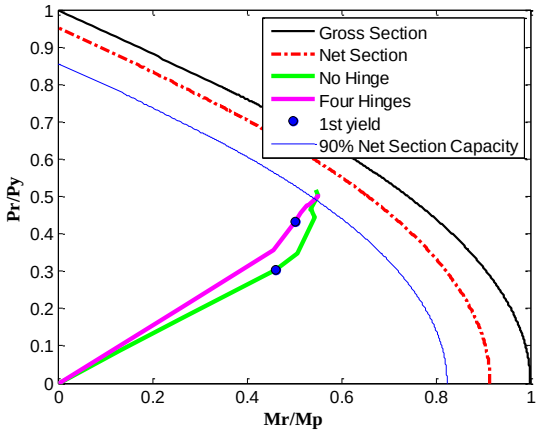

(b) Critical section near member end U9

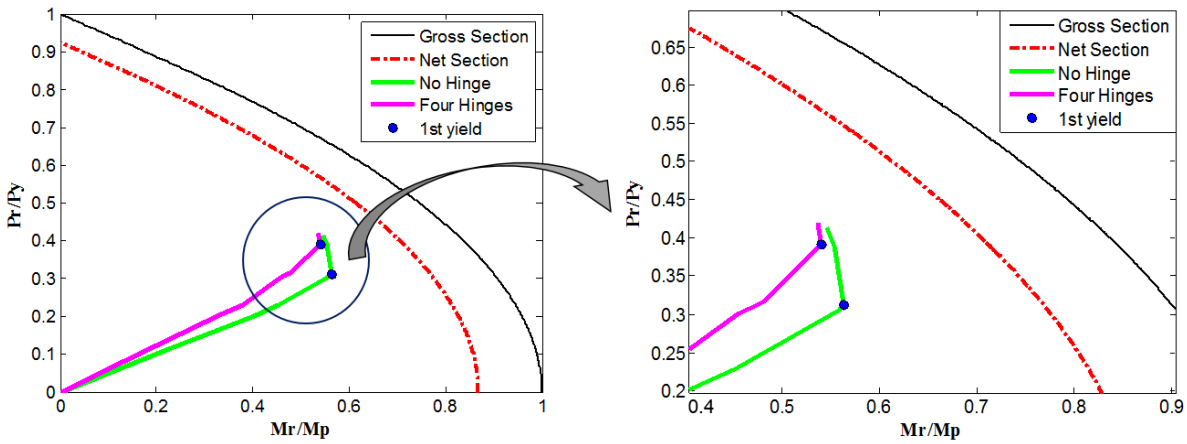

(c) Critical section near member end L8 (d) Zoom-in view around first yield points

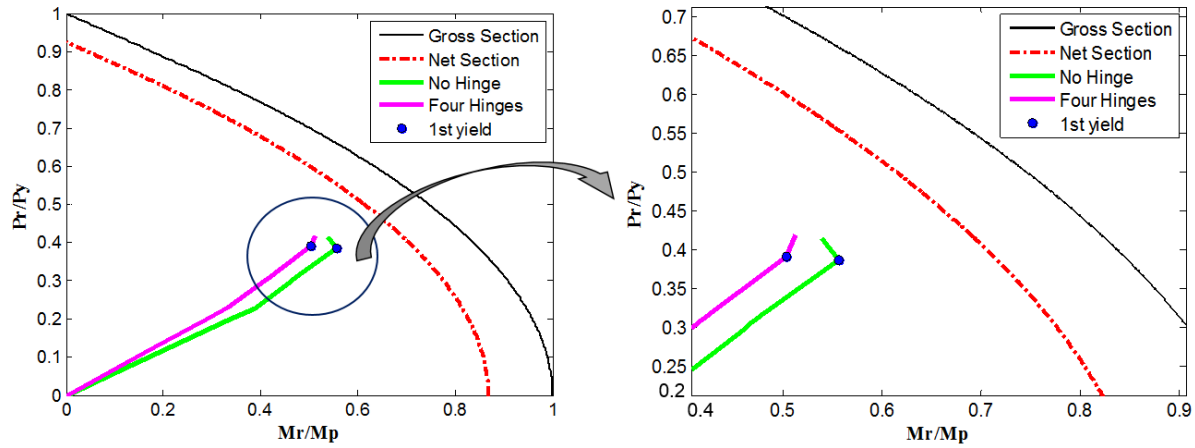

(e) Critical section near member end L9 (f) A zoom-in view around first yield points

Figure 5-5. Comparison of P-M interaction behavior at each plastic hinge location

From Figure 5-5, it is obvious that the final interaction ratios under full dead load and HL-93 load at the four critical sections are still within their ultimate strength envelopes. This implies that the bridge system after losing one diagonal main truss member can remain standing and even functional when it carries the HL-93 load. Note that this analysis ignores the weak U10 and U10' connections.

Among these critical sections the one near U9 is most likely to fail if loads go beyond one HL-93 load. As seen from Figure 5-5 (b), both models predicted that the interaction ratios resulting from

one HL-93 load exceeded 90% of the net section capacity. If any of the defects during construction, such as residual stresses and initial imperfections, a failure at this cross section may take place. As a consequence, the member U8U9 will lose its stability. Eventually, the entire structural collapse will follow. This result underscores the significance to study the net section capacity of critical tension members.

Although the interaction history curves in Figure 5-5 are different between the no-hinge and four-hinge models, the curves from these two models tend to converge to the same interaction behavior after the first yielding at the extreme fiber has been initiated. This indicates that introducing plastic hinges exerts little impact on the inelastic system behavior at the final stage for the damaged structure.

Through the comparison of the interaction history curves between the no-hinge and four-hinge models, it can be also found that under the same resultant axial load, the resultant moment from the model with four plastic hinges is lower than that from the no-hinge model. This probably reflects the fact that a lower flexural stiffness at the hinge point will lead to a lower resultant moment compared to the original model without plastic hinges.

It can be also seen that an obvious change of slope on each interaction history curve occurs when the extreme fiber of a cross section reaches yielding. This moment is denoted by "1^{st} yield" in Figure 5-5. After this point, the change of the resultant stresses on the cross section will be very small. As these resultant stresses are caused by an interaction between axial force and bending moment, an increase in axial force ratio will lead to a decrease in moment ratio, which further results in a reversal in the interaction history curve exhibited in Figure 5-5.

5.4 Conclusion

This chapter primarily studied the effects of modeling "weak" connections with lower flexural stiffness in the post-yielding phase. The weak connections discussed here are located at the end regions of critical main truss members U8U9 and L8L9, where the greatest In-plane bending effects are detected in the structure after member U8L9 is damaged. The critical section of each weak connection is simulated using a plastic hinge. Examination of the results obtained from the ABAQUS models for this particular damaged structure would lead to the following conclusions:

(1) Introducing plastic hinges exerts little impact on the inelastic system behavior at one HL-93 load;

(2) Both no-hinge and four-hinge models consistently indicate that interaction behavior at all four critical connections is still below the full plastic capacity;

(3) Under full dead load and HL-93 load, the damaged system still remain stable with a plastic panel mechanism formed near both ends of the critical chord members;

(4) The possible formation of a plastic collapse mechanism at the damaged panel U8-U9-L9-L8 can be inferred given the fact that each of the four critical sections studied in this chapter had already yielded under the full load condition. However, the analysis shows that the structure can still remain stable, a result that seems unlikely if a standalone 2D system is analyzed. Therefore, it can be inferred that the lateral braces framing from out-of-plane into the critical main trusses must have shed significant loads so as to keep an equilibrium condition in the 3D system. This further prompts the need to investigate the actual contribution of brace members to the residual strength of the damaged system, which will be addressed in the next chapter.

(5) From a system perspective, the removal of the tension diagonal member U8L9 leads to a local stiffness reduction within the panel 8-9. Consequently, the worst system response might be

triggered by placing the truck loads atop U8U9. However, the system model with such truck load position is found to have very similar effects as the model with truck loads at the mid-span, in terms of the P-M interaction behavior for all critical sections of weak connections. This fact probably eliminates the need to change the live load model by moving the truck loads from mid-span to the top of the damaged panel. This result is not surprising given that for a typical long bridge it is not the live load but the dead load that plays a predominant role in the system response.

6 System Anaysis with Bracing and Deck Effects

6.1 Introduction

Results from previous system analyses show that high beam-column interaction ratios at "weak" connections can enable the development of a plastic collapse mechanism in the main truss system around the damaged diagonal member. However, the damaged structure is still able to remain stable, even though plastic deformations have propagated through all "weak" connections. It can be inferred that without the contribution from the lateral system, the damaged structure would not had escaped from collapse. This further prompts the need to investigate the system's post-fracture response with consideration of 3D actions. As stated by Connor et al. (2005), the participation of secondary members and deck can also contribute to structural redundancy. This chapter examines the contribution of lateral braces and deck system, respectively, to system redundancy.

Since both lateral braces and deck are modeled with linear elastic assumptions in the previous system analyses, the contribution of these members may have been overestimated. In this regard, it will be of great significance to vet the adequacy of considering elastic properties alone for these members. In the following analyses, the post buckling behavior will be taken into consideration for the brace members with compression forces that exceed the member elastic buckling capacity.

The need to model the deck with plastic damage properties will also be studied, as the deck can play a crucial role when considering 3D action. In the case of the I-35W Bridge, due to the non-composite connection used between the main trusses and the deck, it was assumed that the deck would not be significantly affected by the damage on the main trusses. In this chapter this assumption is investigated.

6.2 Identification of Critical Brace Members

Critical brace members were identified as the brace members with demand-to-capacity (D/C) ratios for axial loads greater than 0.9. Figure 6-1 shows the critical brace members in the I-35W Bridge after losing the diagonal member U8L9 on the West side of the main truss. These members are the sway braces in panel 9 and lower braces between panels 8 and 9. The sway braces in panel 8 are aligned with the Pier 6, thus they contribute to the integrity of the interior support. The cross section of these braces are much larger than the braces elsewhere. As a result, the D/C ratios of the sway braces in panel 8 are less critical than those of the sway braces in panel 9. Figure 6-1 also highlights the most critical brace members whose D/C ratios exceed one. In the calculation of the member D/C ratios, the axial force demand was obtained from the system model where inelastic behavior was not considered for all braces. The critical brace member D/C ratios obtained from such elastic brace model are summarized in Table 6-1.

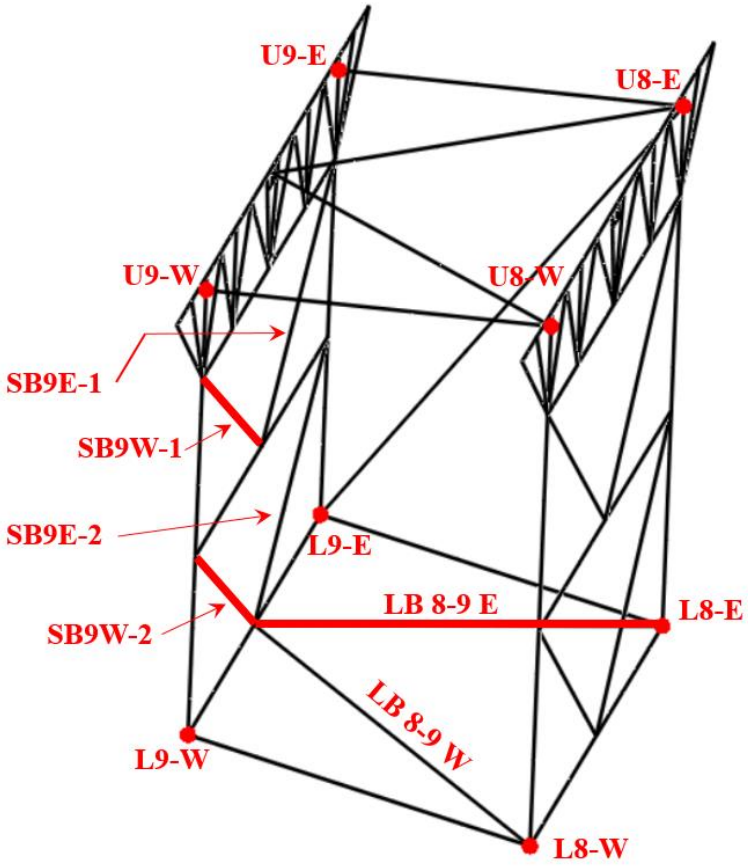

Figure 6-1. Location of the most critical brace member

Table 6-1. Comparison of critical brace member demand-to-capacity ratio

Critical Brace Members	Demand (kips)	Capacity (kips)	D/C
SB9W-1	-797.73	576.14	1.38
SB9W-2	-863.63	576.14	1.50
SB9E-1	813.04	900.00	0.90
SB9E-2	836.80	900.00	0.93
LB8-9W	900.38	975.00	0.92
LB8-9E	-912.23	514.40	1.77

For brace members in compression, the buckling capacity is estimated assuming a **K** factor of 0.75 for a typical bolted connection as specified in AASHTO (2010). It is noteworthy that the **K** factor of 0.75 is valid for determining the brace member strength capacity assuming that the brace

member connection can provide adequate capacity to avoid a connection failure prior to a member failure. This assumption still needs to be checked, and will be explicitly discussed in Section 7.7.3.

6.3 Material Plasticity

Considering that the post buckling behavior of a member always displays a nonlinear relation between compression force and displacement, the effect of introducing material plasticity to the critical brace members in compression will be investigated. For ease of computation, local models for the critical brace members are selected for the buckling behavior study. A pin-roller support condition is used for each local model. Since the geometry of all critical sway braces in Table 6-1 is identical, the local models are developed for one of the critical sway braces (SB9W-2) and the lower brace LB8-9E.

The buckling behavior of these members are analyzed using the Dynamic Explicit scheme in ABAQUS (Simulia 2010). This scheme is chosen because it does not have the potential solution convergence problems for models with large deformations, which will take place in the post-buckling phase of compression members (Altstadt 2006). In other words, the strength degradation in a buckling event can be properly captured by using this analysis scheme in ABAQUS. Although this scheme is commonly used for dynamic problems, it has the ability to provide solutions to a static model under a displacement-controlled loading. This can be achieved by applying very small velocities as boundary conditions so that the effects of the inertial force will be minimal. In the local models a velocity of 1 in/sec is applied to the roller support, as the member lengths for SB9W-2 and LB8-9E are 494 inches and 638 inches, respectively.

Since the Euler-Bernoulli beam elements (B33 in ABAQUS), which were used for modeling the brace members in the system model for the I-35W Bridge, are not available in the Dynamic

Explicit scheme, the Timoshenko beam elements (B31 in ABAQUS) are selected for the local models (Simulia 2010). Then these model are meshed to have six elements along the member length. Since the difference between these two types of beam element is that B33 neglects transverse shear deformation but B31 does not, the effect of considering such deformation is investigated. This is implemented by comparing the eigenvalue of the first buckling mode, which represents the critical elastic buckling load, between the models constructed by B33 elements and B31 elements, respectively. The results from elastic buckling analyses for the two critical braces show that the buckling loads predicted from the B31 models are 2.9% higher than those from the B33 models on the average. It can be inferred that the transverse shear deformations on these brace member are insignificant. It is true given the fact that these brace members have a span-to-depth ratio greater than 15, which makes them behave like slender beams. This result also indicates that the selection of beam element types between B31 and B33 is not an important factor in the buckling analyses for this case.

Using the Dynamic Explicit scheme and B31 elements, the buckling behavior is analyzed for brace members LB8-9E and SB9W-2. The effect of incorporating material plasticity to the local models are evaluated by comparing the difference of critical buckling capacity as shown in Figure 6-2.

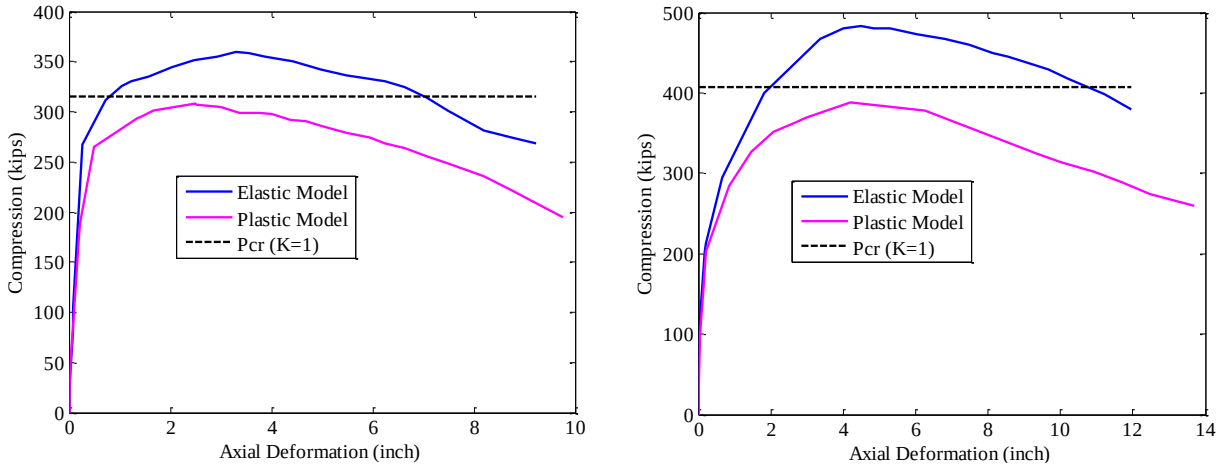

(a) P-Δ curves for member LB8-9E (b) P-Δ curves for member SB9W-2

Figure 6-2. Load-deformation curves compared to the theoretical buckling capacity

Figure 6-2 shows that critical buckling strength obtained from the plastic model is much closer to the theoretical limit as compared to the elastic model. In fact, as the elastic model cannot capture yielding on the member, the resultant force will keep increasing until the nonlinear deformation becomes so large that stability of the member is lost. As seen from Figure 6-2, the descending trend of the curves in both elastic and plastic models initiates at a very similar deformation. As the critical buckling load predicted from the plastic model is obviously lower than the one from the elastic model, it can be inferred that it is the material plasticity that causes this buckling strength reduction. This can be explained by the fact that local yielding at the critical section of the member will occur as the nonlinear deformation grows. To properly capture this yielding effect, a model with plastic braces will be necessary.

In addition, the comparison of member axial stiffness in the elastic phase, as shown in Table 6-2, further confirms the accuracy of the predicted results from the plastic models.

Table 6-2. Comparison of axial stiffness of the critical braces

Critial Braces	K_e from FE model (kips/in)		EA/L (kips/in)	Difference	
	Elastic	Plastic		Elastic	Plastic
LB8-9E	1041	900	889	17%	2%
SB9W-2	1249	994	1056	18%	6%

6.4 Initial Imperfections

To initiate a buckling failure, it is necessary to introduce an initial imperfection in a compression member. The initial imperfection is modeled as a continuous out-of-straightness along the member length. The shape of the out-of-straightness is determined as the first mode shape obtained from each of the local models for the two critical brace members. Each local model consists of six Euler-Bernoulli beam elements in ABAQUS. Figure 6-3 illustrates the first mode shape of one critical brace member. To simulate an extreme condition in a brace member, the magnitude of the out-of-straightness is computed by scaling the mode shape by a factor such that maximum out-of-straightness at the middle of the brace member equals to one-thousandth of the member length, which is the out-of-straightness limit specified by ASTM (2010).

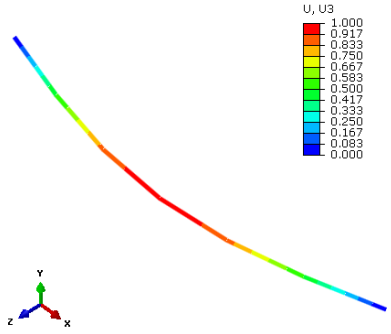

Figure 6-3. First mode shape of one critical brace member

Results from the local models for the two critical braces show that introducing an initial imperfection to the plastic model further reduces the member peak compressive strength but the average reduction is merely 2.4%. Hence, the model without the initial imperfection can still provide enough accuracy in predicting the system response in a faulted state. It is assumed that for a real case, a survey of the structure will be made in order to detect if actual initial imperfections are significantly larger than the ASTM limit.

As discussed previously, the consideration of material plasticity is essential to properly reflect the post buckling behavior of critical braces. Thus the effect of introducing post buckling behavior to the critical braces in the damaged structural system is studied by comparing the results between the model with elastic braces and the one with plastic braces.

6.5 Buckling Behavior Comparison

6.5.1 Deformation Comparison

The difference of deformed shapes between an elastic brace model and a plastic brace model can be seen in Figure 6-4. In the latter model, all sway braces in panel 9 and the two lower braces between panels 8 and 9 are assigned material plasticity in the system model with the removal of member U8L9 on the West side of main truss. Figure 6-4 confirms that it is necessary to introduce material plasticity in order to properly capture the nonlinear behavior of the most critical braces LB8-9E and SB9W-2.

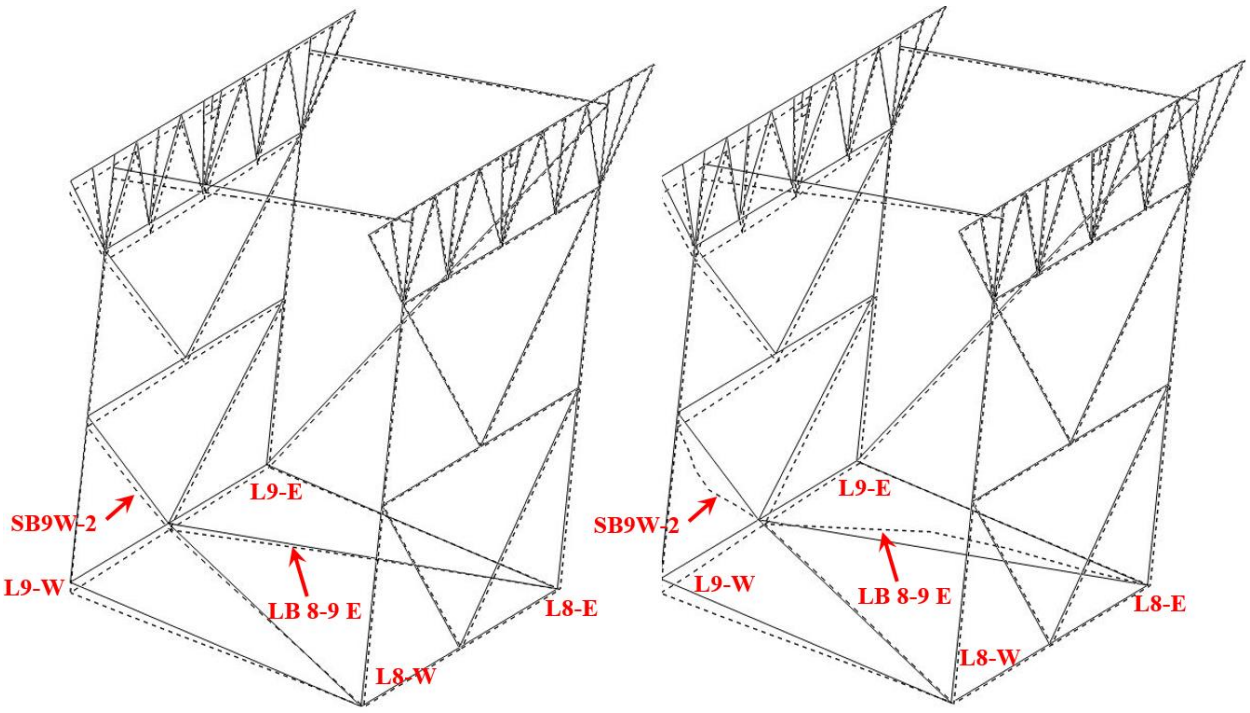

(a) System model with elastic braces (b) System model with plastic braces

Figure 6-4. Comparison between the undeformed shape (solid lines) and the deformed shape (dashed lines) of critical braces

6.5.2 Load-Deformation Comparison

As seen from Figure 6-4 (b), the most noticeable nonlinear lateral deformations appear on the members LB8-9E and SB9W-2. The large deformation implies that these members might have buckled in the damaged system under full dead load and HL-93 load. Ascertaining the buckling failure on these members, the entire buckling process of these members from an initial no load condition to full dead load and HL-93 load is depicted with the use of the load-deformation history curve shown in Figure 6-5.

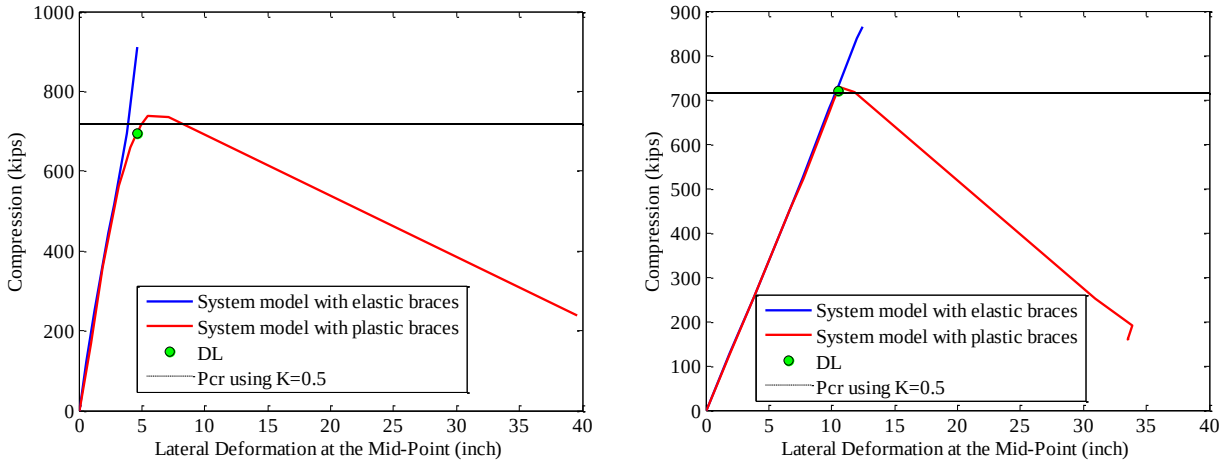

(a) Curves for member LB8-9E (b) Curves for member SB9W-2

Figure 6-5. Curves for compression versus lateral deformation at the brace member mid-point

Figure 6-5 confirms the ability of the plastic brace models to accurately simulate the strength variation before and after the buckling on these two critical braces. Considering that the brace member connection was modeled as a rigid joint in the system model, the **K** factor used in the determination of theoretical buckling capacity (P_{cr}) was selected as 0.5. Table 6-3 summarizes the geometric properties of members LB8-9E and SB9W-2 used in the determination of the theoretical buckling capacity (P_{cr} in Figure 6-5).

Table 6-3. Geometric properties and theoretical buckling capacity of the critical braces

Critical Braces	LB8-9E	SB9W-2
F_y (ksi)	50	50
D (in)	14	12
W (in)	12	12
$t_w=t_f=t$ (in)	3/8	3/8
I (in^4)	510	393
A (in^2)	18.94	17.44
r_y (in)	5.19	4.75
L (in)	638	495
K	0.5	0.5
KL/r_y	61	52
P_{cr} (kips)	719	715

Interestingly, Figure 6-5 also reveals that the two brace members are highly likely to reach their peak strength capacities under full dead load. Even though member LB8-9E seems to buckle earlier than member SB9W-2 at a relatively smaller lateral deformation, the latter one will buckle subsequently in a very short time. Moreover, the resultant compression forces on these members under full dead load are very close to both the theoretical and the predicted buckling loads. This implies that either one or both of these braces will probably buckle when the damaged system is carrying 100% of dead load given the modeling uncertainties or any of the defects during construction.

6.6 Effect of Brace Buckling on Main Truss System

This section studies the effect of brace member buckling failure on the main truss system aiming to see if failure on secondary members will directly impair the integrity of primary load carrying members in the damaged system. Since previous system analysis discussed in Chapter 3 identified the most critical remaining components in the main truss structure were located in the ends of chord members U8U9 and L8L9 in the damaged panel, the study of brace buckling effect on the main truss system is thereby focused on the behavior of these critical members. Damage on these members was examined by comparing the axial-flexural interaction behavior at each critical net section near the member end with the plastic interaction capacities determined at the moment when the entire cross section reaches yielding limit.

It was found from such comparison that the most critical interaction behavior occurred at the cross section near L9 of member L8L9. This result is reasonable considering the specific location of this cross section (L9-W in Figure 6-4). As seen from Figure 6-4 (b), large buckling deformations on the brace members SB9W-2 and LB8-9E will directly exacerbate the deformation on member L8L9. This results in an increase of P-M interaction ratio at the critical sections of this main truss member. In addition, as the critical cross section near L9 is closer to the truss member connection as compared to the cross section near L8 (see Figure 5-1), the bending effect near L9 can be greater, leading to a more critical axial-flexural interaction behavior.

The interaction behavior of the cross section near L9 of member L8L9 from initial no load condition to full dead load and HL-93 load is depicted in Figure 6-6. This figure compares the predicted interaction curves from an elastic brace model with that from a plastic brace model. As the study is meant to compare the difference of interaction behavior at L9 for member L8L9 caused

by member plasticity, the two interaction history curves were obtained from the system models both with plastic main truss member L8L9 but one with elastic braces and the other with plastic braces.

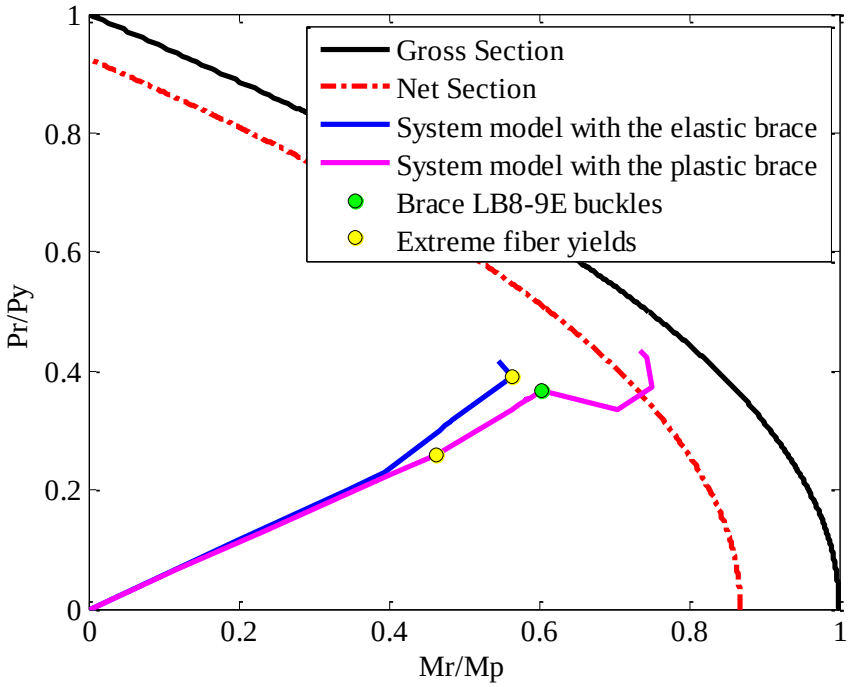

Figure 6-6. Comparison of the axial-flexural interaction behavior at L9 of member L8L9

Figure 6-6 shows that in an immediate response to the brace member buckling, the axial load on the critical cross section L9 of main truss member L8L9 begins to decrease. However, this load decrease is found to be temporary and may not necessarily lead to a failure. Although the interaction ratio at the end of the plastic brace curve falls below the gross section plastic limit, this ratio does well exceed the net section interaction capacity, which is determined considering the presence of access holes as discussed in Section 5.2. Due to such excessive interaction ratio, a

failure at L9 of L8L9 is likely to take place. As a consequence, the main truss member L8L9 will lose its stability. Eventually, the entire structural collapse will follow.

It is also obvious to see from Figure 6-6 that prior to the occurrence of extreme fiber yielding on the plastic brace model, the elastic interaction behavior is quite similar between these two models. After this point, the difference of interaction behavior keeps increasing. As the curve for the plastic brace model is below the elastic one, it can be inferred that the stiffness of the system model with plastic brace is less than that of the elastic brace model. This further implies that the plastic brace model predicts a larger deformation near L9-W of member L8L9-W. This implication can be confirmed through the comparison of the deformation shapes between the elastic brace model and the plastic brace model as illustrated in Figure 6-4. In particularly, the flexural deformation on member L8L9-W seems to be more significant in the plastic brace model. Therefore, the plastic brace model provides a larger bending ratio when both models produce the same axial force ratio in the interaction curves as shown in Figure 6-6. Lastly, the fact that the extreme fiber on the critical section yields much earlier in the plastic brace model may also imply that buckling on the critical braces can exacerbate plastic damage on a main truss member.

In brief, the above results reflect that brace member buckling in the damaged structure can significantly impair the system redundancy so that a bridge collapse is likely to occur. This indicates that brace members are the key load carrying components in a damaged structure after

losing one critical main truss. Hence the consideration of brace member failure is necessary in performing system analyses for a damaged bridge.

6.7 Significance of Nonlinear Concrete Deck Effect

Apart from brace members, the reinforced concrete deck is also a key component in the lateral system and that can provide system redundancy through 3D action. It is therefore crucial to properly model the deck system in order to figure out the actual contribution of deck. To achieve this, there is a need to vet the sufficiency of modeling the deck with only linear elastic properties. One approach is to compare the maximum principal stress on deck in the damaged structure with the elastic limits of both tensile and compressive stresses. If a large exceedance of the elastic limits is found, then the nonlinear concrete behavior such as cracking and crushing should be taken into consideration.

Since the reinforced concrete deck in most conventional two-line truss bridges is not designed to withstand large plastic damage, the bridge deck in the existing system model was assumed to remain linear elastic throughout the service life even after failure of a fracture critical member. In an effort to simplify the model of deck system, an equivalent modulus of elasticity is used to represent the smeared properties of the 4ksi plain concrete blend with Grade 40 reinforcing steel. This equivalent modulus of elasticity is determined through testing the cores drilled from above through the entire depth of the deck. These cores contained reinforcing steel which was encountered during the drilling (Fassil Beshah et al. 2008). The average test value of this equivalent modulus of elasticity is 4800 ksi, which gives rise to a 7.09 ksi compressive strength as well as a 0.63 ksi tensile strength of the reinforced concrete. Based on the assumption that concrete will remain linear elastic until one half of its compressive strength is reached in compression and

until its full tensile strength is reached in tension, the elastic limits of the reinforced concrete with equivalent modulus can be determined and are shown in the second column of Table 6-4, while the peak stresses from the analysis are shown in the last column.

Table 6-4. Maximum principal stress comparison

Unit: ksi	Elastic Limit with Equivalent Modulus	Plain Concrete Elastic Limit	Peak Stress on Deck
Compression	3.55	2.00	0.36
Tension	0.63	0.47	0.54

From Table 6-4, it is obvious that the reinforced concrete deck in compression still displays a linear elastic behavior after the critical diagonal main truss is damaged, which eliminates the need to consider the nonlinear concrete crushing effect for the deck. For the reinforced concrete deck in tension, the maximum tensile stress on deck in the damaged structure falls in between the elastic limit of the reinforced concrete with equivalent modulus and the plain concrete. As this maximum tensile stress is still close the elastic limit of the actual reinforced concrete deck, there will be of little significance to model the nonlinear effect of tension damage for the deck.

Furthermore, the fact that there is little plastic damage on the deck system after failure of one critical truss member indicates that deck is not sensitive to the change in the main truss system. This is reasonable considering the non-composite connectivity between the deck and truss system. For this condition, it can be confirmed that damage to the truss system will not greatly affect the deck system.

6.8 Conclusion

This chapter discusses the contribution of secondary members spanning out-of-plane to the system redundancy. Since these secondary members, comprised of brace members and reinforced concrete deck, are primarily designed to provide sufficient stiffness to the undamaged system, their strength capacities are not expected to be exceeded in the service life. However, in response to a fracture failure of a main truss member, the adjoining secondary members will probably be so overstressed that failure or plastic damage of these members will occur. This chapter thereby investigated the possibility of secondary member damage.

Brace members were found to be highly vulnerable to be overstressed in response to failure on a main truss member. In particularly, the braces that frame into the damaged panel are very susceptible to buckling prior to a failure on the remaining main trusses. Such failure on the brace members further implies that braces in the lateral system can have a great effect after one main truss member is damaged. In this regard, a proper simulation of the brace member behavior with the consideration of the member buckling strength will be of great significance in performing system analysis for a bridge in a damaged condition. This can be achieved by incorporating material plasticity of the critical brace member into the system model.

As a consequence of buckling failure on the critical braces, a main truss member in the damaged panel may fail due to a high P-M interaction demand at the member end. Thus the integrity of primary load carrying system will be severed, which will eventually lead to the bridge collapse. This progressive failure implies that brace members can be crucial to provide load redistribution path once a critical main truss member is damaged. It is also worthy to note that the above

progressive collapse mechanism cannot be captured without considering the plastic properties of the critical braces. Therefore, a refined plastic brace model is necessary.

As for the reinforced concrete deck, its behavior is found to remain linear elastic in the damaged structure. One could infer that modeling the deck with elastic property alone can provide sufficient accuracy. Although it is true for this case where the deck was non-composite, it is uncertain if this implication will still be applicable to a truss bridge with composite deck system. Hence, the deck behavior in a bridge that has composite actions between deck and truss systems will be investigated through the case study of the test span of Milton-Madison Bridge in Chapter 7.

At the completion of this chapter, a more realistic system behavior of the example damaged structure with the loss of a tension diagonal member is predicted. Through the examination of the predicted results, the answers to the questions presented in the beginning of Section 3.7 can be determined as below:

(1) The damaged structure will not be able to withstand failure on member U8L9, as the structure can barely sustain the dead load. In this regard, the tension member U8L9 can be considered as a fracture critical member.

(2) Failure on member U8L9 will trigger a progressive collapse. The progression of failure will start from buckling on a lower brace in the damaged panel between points 8 and 9 under dead load. A subsequent buckling failure could occur on one sway brace that frames into the vertical member U9L9. Following the brace buckling failure, the main truss member L8L9 will get separated from the system due to the axial-flexural interaction failure at the critical net section. As a result, a collapse mechanism will develop so that the entire system will lose stability.

(3) The ultimate failure modes of the damaged structure could be:

a. Buckling on the critical braces if the connections between brace members and main truss members will produce higher strength capacities than that of the connected members;

b. Axial-flexural interaction failure at the critical net section of a main truss member given that both brace members and connections will not fail prior to a main truss member;

c. Failure on either the connections between brace members or the connections that transfer loads from brace members to main truss members. Such connection failure will be explicitly studied in Chapter 7. Noted that the failure modes on main truss member connections for the I-35W Bridge has been intensively analyzed in NCHRP 12-84 (Ocel 2013), thus it will not be discussed in this research.

(4) To appropriately capture the possible ultimate failure modes I and II in the system models, it is necessary to assign critical truss members material plasticity, which is found to play an essential role in simulating nonlinear actions in the ABAQUS models.

7 Practical System Analysis

7.1 Introduction

Due to the high level of complexity present in the system models developed in ABAQUS, the system redundancy analyses discussed in the previous Chapters need to be simplified for practical application in the bridge engineering industry. In this chapter, system analyses will be performed using models constructed in SAP2000, a structural analysis program in common engineering use that includes easy visual input/output interfaces.

Searching the very limited database on measured behavior of truss bridges in a damaged condition, this research identified two bridges that experienced major fracture events and had their post-fracture deformations measured. One is the I-35W Bridge and the other is the northernmost approach span of the Milton-Madison Bridge, which will be referred as the M-Bridge in the remainder of this thesis. Using the field data, the models developed in SAP2000 can be calibrated to the measured behavior in the real structure. Based on these validated models, simplified system analyses will be performed, and approaches for identifying and rating critical members will be proposed. As an attempt to extend the methodology for evaluating system redundancy to other truss bridges with different configurations, this methodology is then blindly applied to two other simple truss bridges whose system responses to a single member damage have not been tested. These two bridges are the New River Bridge in Hillsville, Virginia, and the Span No.4 of the Milton-Madison Bridge. Lastly, to further improve the system redundancy for some critical damaged structures, sample retrofit strategies will be discussed on a case by case basis.

7.2 Bridge Description

7.2.1 I-35W Bridge

See Section 3.2 for a detailed description of this structure.

7.2.2 M-Bridge

In 1921, the US-421 Bridge was constructed over the Ohio River between Milton, KY, and Madison, IN, thus being referred to as the Milton-Madison Bridge. The bridge structure was comprised of 19 spans of riveted, built-up truss members. Figure 7-1 shows an aerial view of the 3180-foot-long bridge structure, including five main spans crossing the river and fourteen approach spans leading up to the river span. Not all the approach spans are captured in Figure 7-1.

Figure 7-1. An aerial view of Milton-Madison Bridge
(http://www.miltonmadisonbridge.com/the-project/)

The northernmost approach span on the Indiana shore is the focus of this research study, as it was tested using explosive demolition (Cha et al. 2014). This approach span was located with easy access over land and its collapse would not present any logistical or safety concerns. This structure was briefly described in Section 2.5.3, and a photograph of the test span can be seen in Figure 2-4. The test span is a simple-supported structure with a seven-panel Pratt truss configuration. Each panel is 21 feet in length. The superstructure width is 24 feet and the truss height is 22 feet. The deck system is located 4.75 feet below the top chord of the truss and consists of six lines of stringers spaced at 3.67 feet on center. Floor beams are attached below the deck and therefore are not coincident with the upper truss joints. In 1996, the original deck was replaced with an Exodermic deck system, which is a precast, partially filled grid deck system consisting of an overlay that is composite with the stringers and floor beams. Details pertaining to the deck and structural configuration will be discussed in Section 7.3.2.

7.3 Modeling of Example Bridges

7.3.1 I-35W Bridge

A basic three dimensional model was constructed in SAP2000 by Lora (2013). The geometry of the model was based on the General Management Plan, Elevations & Sections (Allied Structural Steel Company, 1966) and T.H. 35W State of Minnesota Department of Highways, Bridge no. 9340 Design Drawings (Sverdrup & Parcel and Associates, Inc., 1965). The material mechanical properties used are as reported by Beshah et al. (2008). The boundary conditions of this model had already been calibrated to match the field data presented by O'Connell et al. (2001). In this model, frame elements were used to simulate the behavior of main trusses, floor trusses, sway frames, stringers, and brace members. Shell elements were selected to model the reinforced concrete deck,

spandrels, and walls of the concrete piers. The bridge deck was modeled to be non-composite with the stingers and the main trusses, as the deck was allowed to move longitudinally relative to the stringers and the main trusses. Four axial springs were attached to panel points U0 and U0' on both the East and West sides of the main truss structure to account for the stiffness of the approach spans. An overall view of this model is presented in Figure 7-2. More details pertaining to the modeling of individual members and particular components are given in Lora (2013).

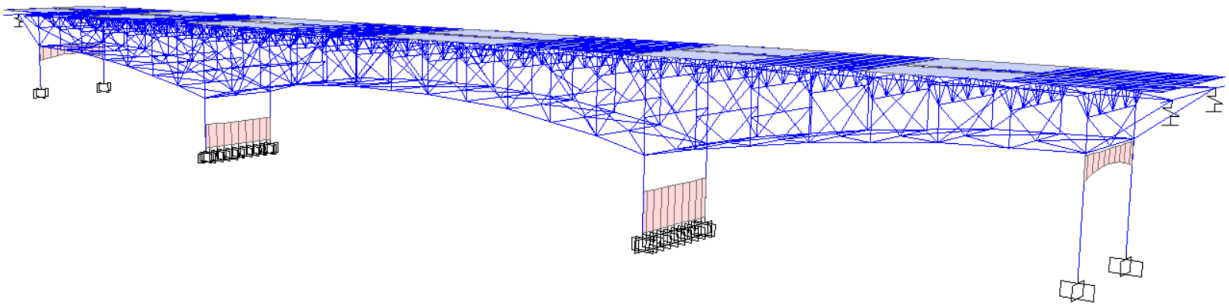

Figure 7-2. A side view of the three-dimensional model for I-35-W Bridge in SAP2000. Lora, M. A. R. (2013). Study of the I-35W Highway Bridge Collapse Mechanism. Civil and Environmental Engineering, Virginia Polytechnic Institute and State University. Master of Science. Used under fair use, 2015.

7.3.2 M-Bridge

Structural analysis of the M-Bridge (the test span of Milton-Madison Bridge) was performed using a three-dimensional model constructed in SAP2000 by the author. Frame elements were selected to represent the main trusses, stringers, floor beams, and brace members. The reinforced concrete deck was modeled using shell elements.

As mentioned, the original deck was replaced with an Exodermic deck system, leading to a change of deck weight and stiffness. Given the weight of the Exodermic deck system, the thickness of an equivalent plain concrete deck was determined to have the same weight. A thickness of 6.25 inches was thereby used in modeling the deck. The concrete deck in the model has a compressive strength

of 4,000psi and a unit weight of 150pcf. The stiffness of the Exodermic deck system was determined by Mizzen (2011). Results show that the stiffness of the Exodermic deck in the strong direction is 71,700 kip-in^2/in while the stiffness in the weak direction is 19,990 kip-in^2/in. The 6.25-inch-thick equivalent concrete deck, which was used in the system model, has a stiffness of 73,300 kip-in^2/in in both strong and weak directions. To convert this stiffness to that of the Exodermic deck, a stiffness modifier of 0.98 was used in the strong direction while a stiffness modifier of 0.29 was used in the weak direction.

During long-term data collection, the Exodermic deck was confirmed to behave compositely with the stringers and floor beams (Diggelmann et al. 2012). The composite action in the model was achieved by introducing rigid links between the deck and the supporting beam elements. The modeling of rigid links was implemented using a two-step approach. First, changes needed to be made to the insertion points that were automatically generated at the centroid of a beam element when it was drawn to align it to the elevation of the deck centroid. By default, the insertion point of a beam element will coincide with the centroid of the deck's cross section as illustrated in Figure 7-3.

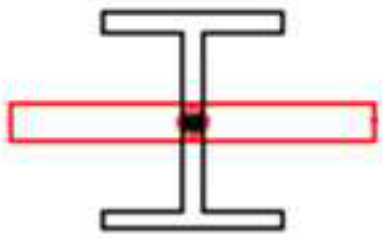

Figure 7-3. Cross sectional view of one beam element drawn align the deck plane in SAP2000. Diggelmann, L. M., et al. (2012). Evaluation of Member and Load-Path Redundancy on the US-421 Bridge over the Ohio River. Purdue University. Used under fair use, 2015.

Clearly, the cross section shown in Figure 7-3 cannot reflect the actual geometric relation between the deck and its support beam. To simulate the actual cross section, the insertion point of the beam element was changed to be in the middle of the top edge. This was achieved by selecting the top center insertion point for the beam element. This new insertion point is highlighted in Figure 7-4.

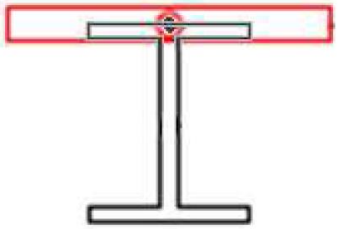

Figure 7-4. Cross section with top center insertion point. Diggelmann, L. M., et al. (2012). Evaluation of Member and Load-Path Redundancy on the US-421 Bridge over the Ohio River. Purdue University. Used under fair use, 2015.

The second step in developing rigid links is offsetting the top center insertion point downward to make the top edge of the beam element align with the bottom edge of the deck. Once the beam element has been shifted down with the top flange below the deck, two fictitious rigid link elements will be automatically generated to reflect the presence of shear studs. Thus full composite action between the deck and the beam element was obtained. The desired cross section after offsetting the top center insertion point is demonstrated in Figure 7-5.

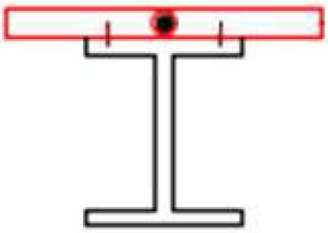

Figure 7-5. Cross section with insertion point offset and fictitious rigid links. Diggelmann, L. M., et al. (2012). Evaluation of Member and Load-Path Redundancy on the US-421 Bridge over the Ohio River. Purdue University. Used under fair use, 2015.

It is also worth noting that the composite action will not be developed along the entire length of a beam element if the deck is not meshed appropriately. To ensure the compatibility between the deck and each supporting beam element, the edges of the deck element must align with the surrounding stringers and floor beams. In this regard, the deck element was divided into a number of small area elements based on the lines of stringers and floor beams.

After dividing the deck element, a uniform area load of 78psf, representing the weight of the concrete deck, was applied to each small area element using a two-way distribution. In this way, SAP2000 will convert the uniform area load on a deck element to the effective line loads on the surrounding stringers and floor beams. The load distribution diagrams of these effective line loads are shown in Figure 7-6. The reason for using these effective line loads to account for the weight of deck is that this approach can eliminate the need to consider the load transfer within each panel that is enclosed by stringers and floor beams. Thus there is no need to mesh each panel, resulting in savings in computational time. It is also worth noting that a refined mesh of deck will become necessary if significant stress concentration and plastic damage is identified on the deck. The existence of such effects will be examined in Section 7.7.4 to ensure that the current area elements do not need to be meshed.

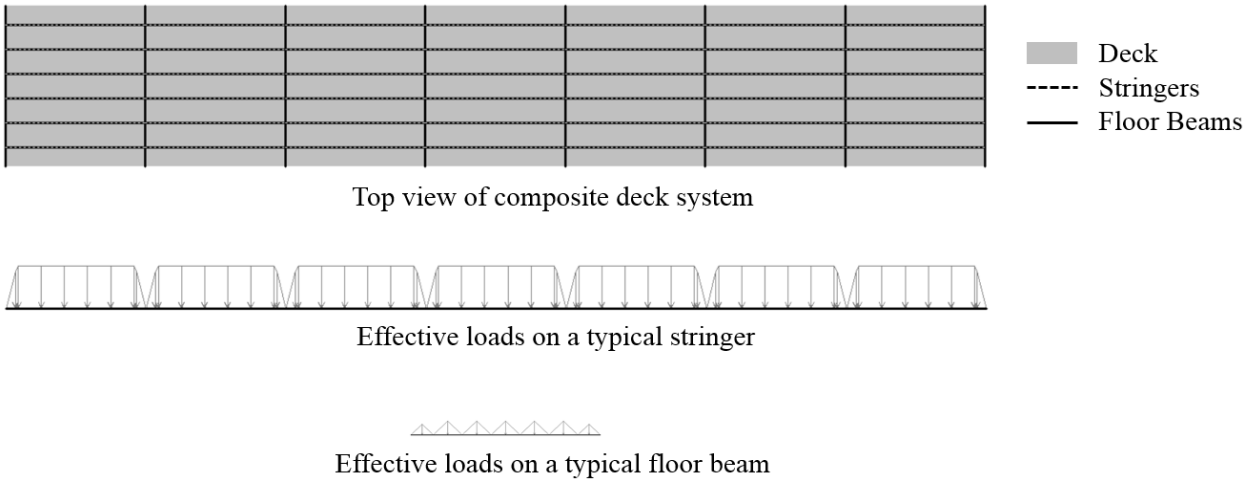

Figure 7-6. Load distribution diagrams (not to scale)

According to the original design plans, each steel member was assigned a particular material type and a cross section. A typical elastic-to-plastic stress-strain curve for Grade A36 steel was used for all steel members. The cross section of each steel member was drawn using the section designer tool in SAP2000, as many of the members were built-up members consisting of angles, cover plates, and lacing members as shown in Figure 7-7. For the sake of simplification, all lacing members were not modeled. Being designed as a secondary component of a built-up member, a lacing member was not expected to significantly affect the axial and flexural behavior of the built-up member. The primary purpose of installing lacing members is to ensure that the individual components of the built-up member can behave as one unit. This can be achieved without modeling the lacing members as long as each component is drawn in one cross section, which ensures that the relative distance between individual components will not change during the analysis.

The end restraints for steel members were specified based on the actual member connection details displayed in Figure 7-7. As it can be seen, main truss members were connected to one another by riveted gusset plates at the joints. Considering that this type of connection will provide large

moment restraint at each joint, fixed connections were specified at each end of a main truss member. Connections between stringers and floor beams were selected to be pinned connections with both axial and flexural release, because simple shear tabs were used in all these connections. Similar modeling was used for the floor beams framing into the vertical main trusses with simple shear tab connections.

Figure 7-7. A side view of truss members and connections
(http://www.miltonmadisonbridge.com/gallery/)

Since brace members were small in cross sectional area and were connected to main trusses with small gusset plates, flexural restraint at these connections can be neglected. Thus pinned end conditions were specified for the ends of each brace member. It is also a noteworthy to point out details used in modelling the X-brace assemblies for the sway brace members. As seen from Figure 7-8, the two brace members in an X-brace assembly were connected to each other through a steel plate at the crossover point. Since this mid-connection was able to provide support to resist out-of-plane buckling of each brace member, the unbraced length for each brace member could be

reduced. To account for this effect, a steel bridge design handbook for bracing system design published by FHWA (2012) sets the effective unbraced length as the distance from the crossover point to one end of a brace member. The approach to simulate the reduced unbraced length of each brace member in an X-brace assembly is dividing each brace member at the crossover point in the SAP2000 models. In this way, the two originally continuous brace members were changed into four discontinuous members that were connecting to one another through rigid joints shown as red dots in Figure 7-9.

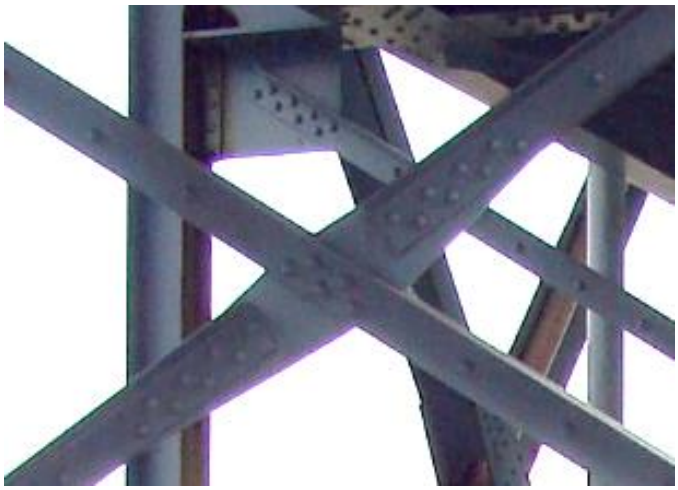

Figure 7-8. A close-up view of the connection details for a typical X-brace assembly. Diggelmann, L. M., et al. (2012). Evaluation of Member and Load-Path Redundancy on the US-421 Bridge over the Ohio River. Purdue University. Used under fair use, 2015.

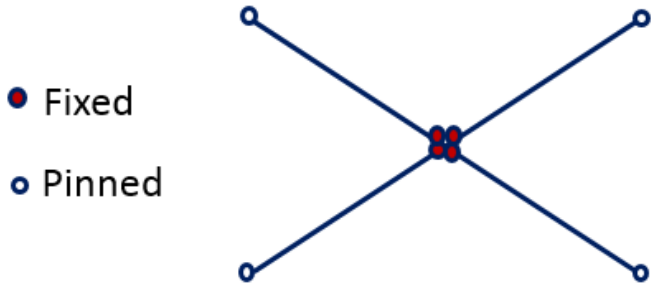

Figure 7-9. Member end conditions in a typical X-brace assembly

7.4 Model Calibration

The model calibration was implemented using a two-step approach. First, full 3D models for the two example bridges were developed based on the original design plan and were calibrated to match the measured member behavior under a particular loading condition used in the field tests. Next, the damaged structures for these two bridges were simulated by removing one of the main truss members from each of the previous 3D models in a no-load condition. These models for the damaged structures after losing one member were then calibrated to ensure that the damaged system behavior could be predicted with acceptable accuracy. As there was no records reflecting the behavior of I-35W Bridge with one main truss member removed from the system, the damaged model for this bridge was verified through demonstrating a correlation between the SAP2000 model and the ABAQUS model under the same loading condition. On the other hand, for the M-Bridge, the damaged structural behavior was measured during the destructive test. Thus the calibration for the damaged model of M-Bridge was performed by comparing the predicted member behavior with the measured test data.

7.4.1 I-35W Bridge

The first part of model calibration is for the 3D model of the I-35W Bridge in an undamaged condition. Since the bridge model with linear elastic features had been calibrated by Lora (2013) to match the live load data reported by O'Connell et al. (2001), this model was used as a baseline model for further incorporating nonlinear features that are essential to properly capture the system behavior in a damaged condition. To ensure the addition of nonlinear features to this existing model will not degrade the level of confidence in the model, the 3D nonlinear model was also calibrated to demonstrate a correlation between the linear and nonlinear models. The nonlinear

features added to the linear model include plastic hinges at each of two ends of main truss members, as well as nonlinear axial springs in the middle of each main truss member. Detailed descriptions of these nonlinear features will be presented later in the discussion about the verification of the model in a damaged condition.

The calibration for both linear and nonlinear models in an undamaged condition was performed by comparing the influence lines with the recorded test data for the axial forces on main truss members U9U10, L9U10, and L9L10 displayed in Figure 7-10. The influence lines were obtained from the bridge structure when it was subjected to the moving loads, which consisted of three sand trucks, each weighing 51 kips (O'Connell et al. 2001). In the test the member strain data was recorded when these three trucks were running side-by-side in the three lanes close to the West side of main truss and passing across the center span (between Pier 6 and Pier7). The influence lines from the test for member axial forces were derived from the stress histories that were elastically converted from strain gauge records.

The influence lines predicted from both linear and nonlinear models were plotted and compared with the influence lines obtained from the test data, as shown in Figure 7-11 to Figure 7-16. It is clear that the influence lines from the nonlinear model can be considered the same as the ones from the linear model. This indicates that the addition of nonlinear features did not affect the structural behavior in an undamaged condition. This is reasonable in that all the members were expected to behave linear elastically if there was no damaged on the bridge.

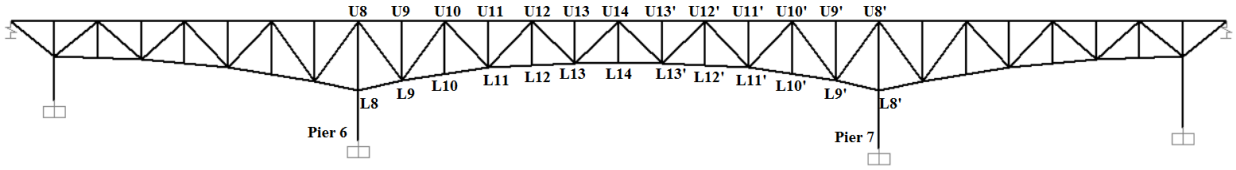

Figure 7-10. Elevation view of main truss structure of I-35W Bridge

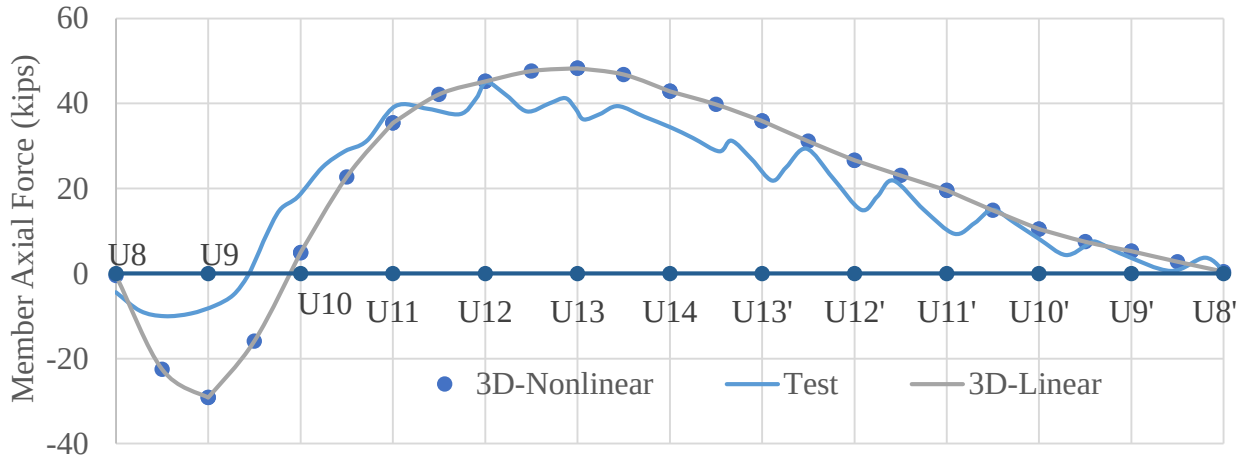

Figure 7-11. Influence lines for axial forces on member U9U10-West side (near loaded lanes)

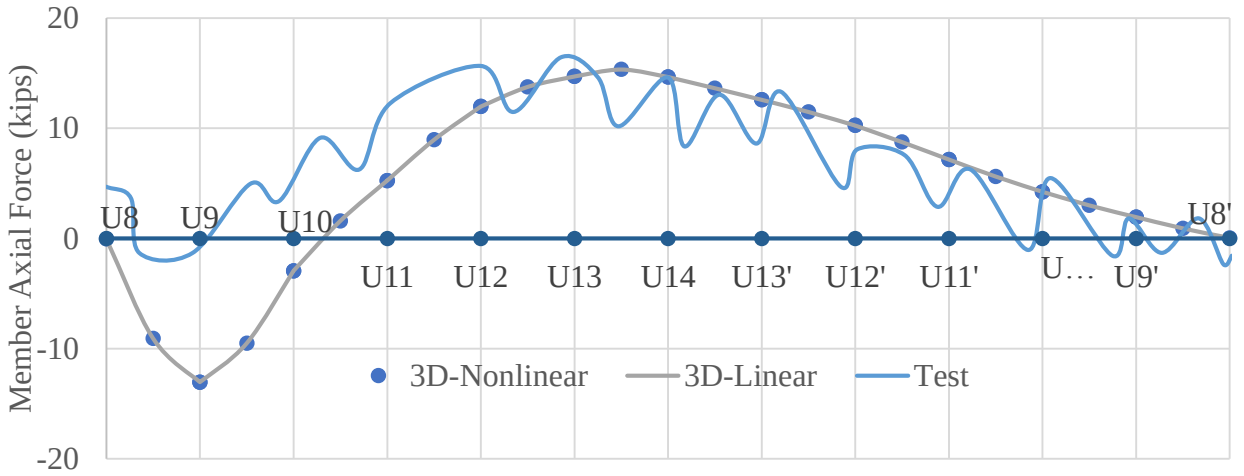

Figure 7-12. Influence lines for axial forces on member U9U10-East side (far from loaded lanes)

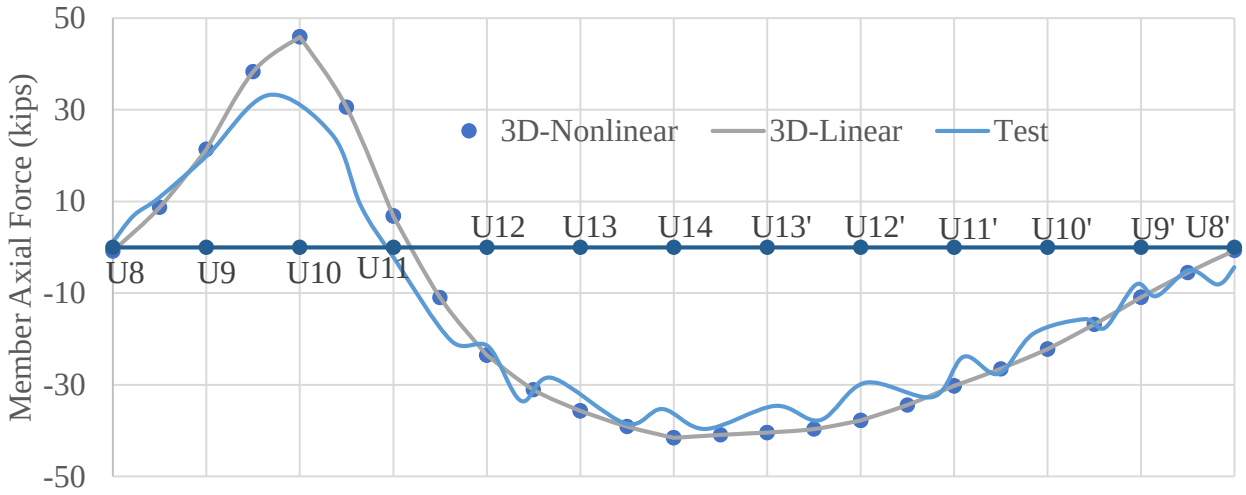

Figure 7-13. Influence lines for axial forces on member L9L10-West side (near loaded lanes)

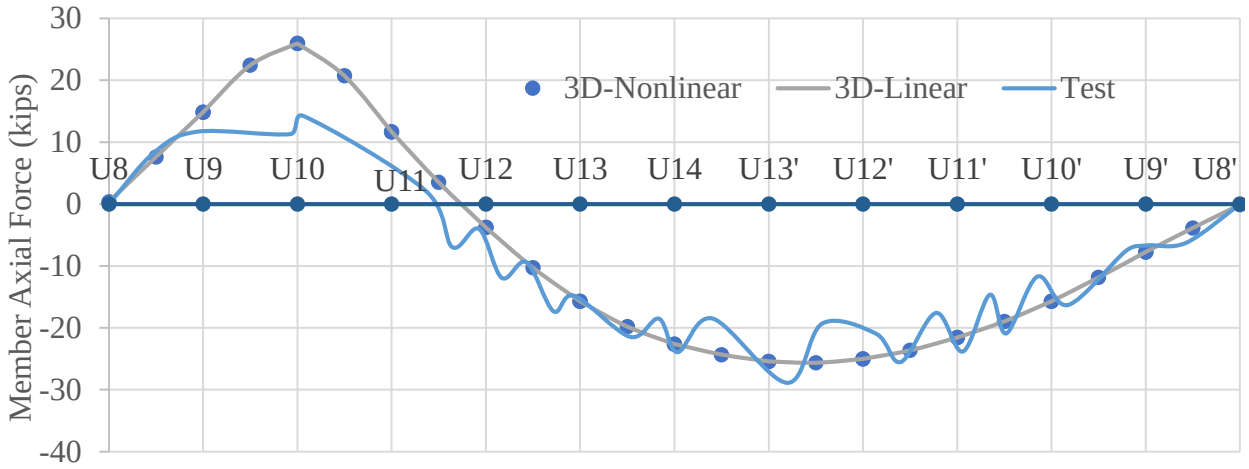

Figure 7-14. Influence lines for axial forces on member L9L10-East side (far from loaded lanes)

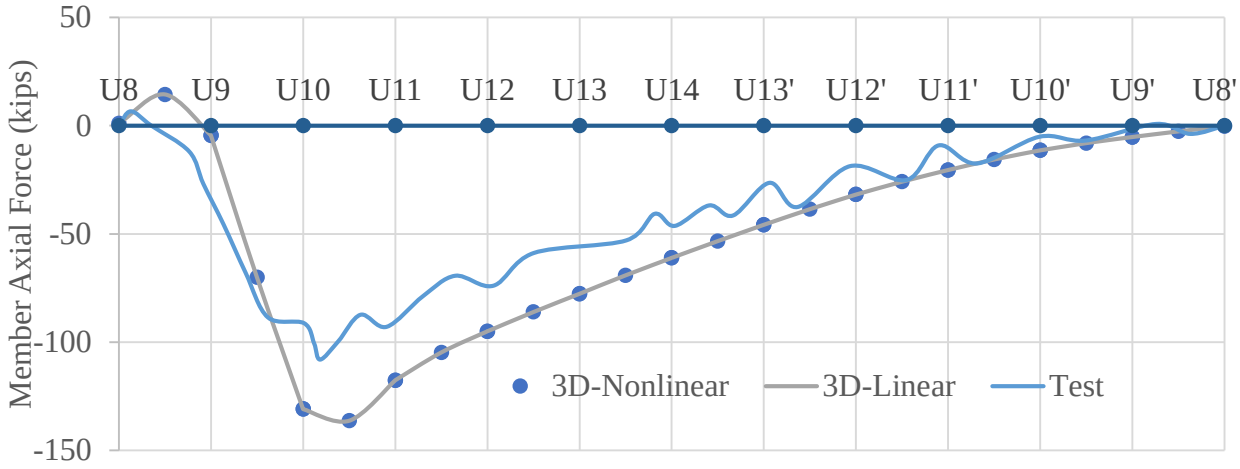

Figure 7-15. Influence lines for axial forces on member L9U10-West side (near loaded lanes)

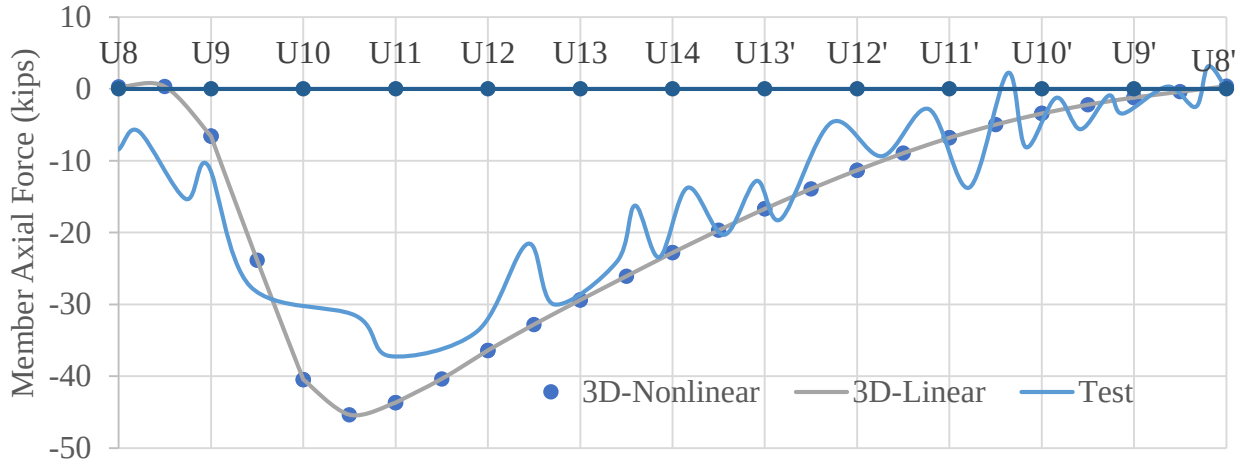

Figure 7-16. Influence lines for axial forces on member L9U10-East side (far from loaded lanes)

The model for the damaged bridge structure was verified through comparison of the resultant forces and moments on the critical main truss members between the SAP2000 model and the ABAQUS model. The accuracy of modelling the bridge structure in a damaged condition in ABAQUS with nonlinear features was verified through the comparison between the simulated deformations with the data measured from the wreckage on the damaged structure after the two

main trusses failed simultaneously. This model validation study is discussed in Section 3.4. It is worth noting that the deformation comparison approach was not used for validating the SAP2000 model because this analysis stopped when a plastic mechanism develops. In other words, once two or more hinges went into the post-yielding phase, the structural model could not continue to simulate the progression of plastic deformations. However, considering the fact that after a steel truss member yields large changes in member deformation will be observed but little change in member resultant forces can be found, the predicted member forces at the end of the analysis from SAP2000 model were expected to be close to the member forces in a realistic condition.

The member force comparison was performed using the models for the damaged structure with one diagonal main truss U8L9 on the West side being removed from the system in the initial no-load condition, as the behavior of the critical members in this damaged structure had been previously studied using the ABAQUS model with nonlinear features.

The simulation of this live load condition in the SAP2000 model was as follows:

- The uniform lane loads were applied directly to the deck as area loads. The distribution and magnitude of lane loads were the same as those used in the ABAQUS model.
- The three truck loads designed to be acting in each of the eight traffic lanes were converted to point loads on each stringer using the lever rule. The positions of these truck loads in one traffic direction were the same as that defined in the ABAQUS model, as illustrated in Figure 3-12 and Figure 3-13.

Since the preliminary system analyses presented in Chapter 3 revealed that it was essential to assign nonlinear features to properly capture the behavior of critical members in the ABAQUS model with member U8L9 damaged, the plastic stress-strain data for typical Grade 50 steel was assigned to the critical members U8U10 and L8L9, where the failure mechanism initiated. This

plastic properties were associated with individual fibers at the cross sectional level, and one truss member was comprised of a series of cross sections connecting to one another continuously. In this regard, the plasticity is continuous along the entire member length. As discussed in previous sections, with the plasticity assigned to the critical members, not only the member post yielding behavior (see Section 3.6.2) but also the member buckling failure (see Section 6.3-6.4) can be captured. Additionally, as in the damaged structure, large in-plane moments were identified at the ends of each critical member, and therefore nonlinear flexural hinges were utilized to simulate the softening flexural stiffness after the yield moment had been exceeded in the ABAQUS model. The positions of these hinges are illustrated in Figure 7-17. The exact distance from each hinge to the member end was given in Figure 5-1.

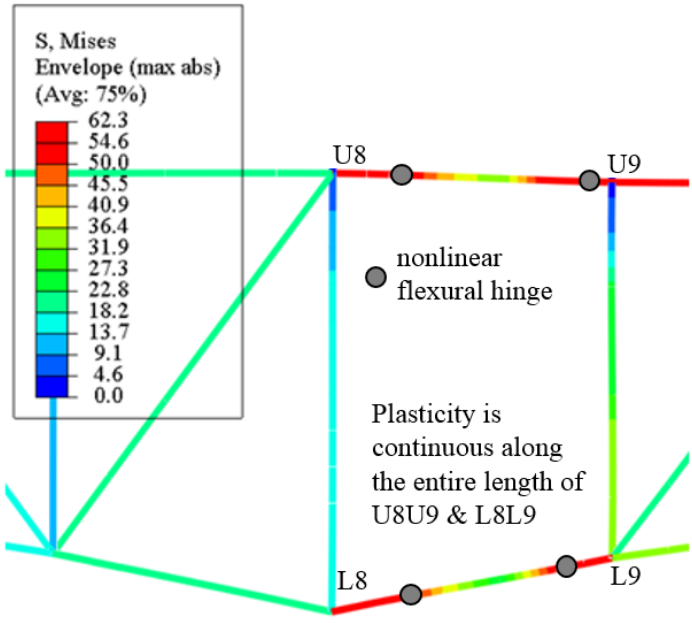

Figure 7-17. Nonlinear features in the ABAQUS model

To keep the SAP2000 model consistent with the ABAQUS model, similar nonlinear effects were taken into consideration in the SAP2000 model. To be specific, the nonlinear axial behavior such

as post yielding and buckling on the critical members were simulated through modeling nonlinear axial springs at the mid-point of each critical member. Unlike the ABAQUS model, the plasticity incorporated in the SAP2000 model was not continuous but lumped at one point. This means that on one critical member the nonlinear behavior will only occur at the point where the spring is located. The nonlinear flexural behavior was considered through incorporating plastic hinges at the ends of each critical members. The location of each plastic hinge in the SAP2000 model was the same as the location of each nonlinear flexural hinge in the ABAQUS model. Figure 7-18 displays the placement of nonlinear axial springs and plastic hinges in the SAP2000 model.

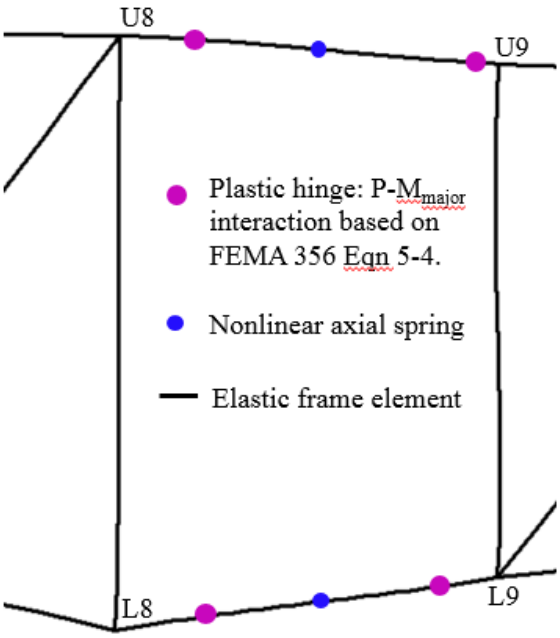

Figure 7-18. Nonlinear features in the SAP2000 model

The axial behavior of each axial spring can be idealized as the curve shown in Figure 7-19. The correctness of the curve in the compression region was confirmed through a separate study for member buckling strength. The study compared two different compressive curves to simulate member buckling in a 3D system. One curve is shown in the third quadrant in Figure 7-19. This

curve had a peak compression strength equal to the yield strength P_y. The other curve used the same critical deformation parameters but with a different peak compression strength that was equal to the flexural buckling strength P_{cr}. The buckling study focused on the 3D models for the damaged structures in which the buckling failure on one particular truss member can be identified as the governing failure mode that triggers the progression of damage on other remaining members. In these 3D models it was found that using the first curve provided a closer correlation between the predicted buckling strength of the critical truss member and the theoretical buckling strength. Apart from the use of these two curves, a different way to define the compressive behavior of the axial spring was also implemented to predict the buckling strength for W shapes and built-up double angles. The axial spring was defined by selecting the auto-hinge type for typical steel braces from Table 5-5 in FEMA 356 (FEMA 2000). Since this auto-hinge is used to capture the behavior at a particular cross section rather than a length of a member, the peak strength for braces loaded in compression is specified as the yield load while the peak strength for braces loaded in tension represents the tensile rupture strength. This feature is available in SAP2000 for quick modeling of nonlinear axial springs on the members whose cross sectional shapes can be found from Table 5-5 in FEMA 356. Through comparisons it was found that the predicted buckling strength on the critical member from the 3D model with the auto-hinges was very similar to the buckling strength obtained from the model using the first curve as shown in Figure 7-19. The difference between these two approaches was less than 1%. Considering the fact that there are many built-up members in compression for both I-35W Bridge and M-Bridge but the steel braces with built-up cross sections were not included in the FEMA table, it was decided to use the curve shown in Figure 7-19 rather than the auto-hinge to capture the buckling failure of main truss members.

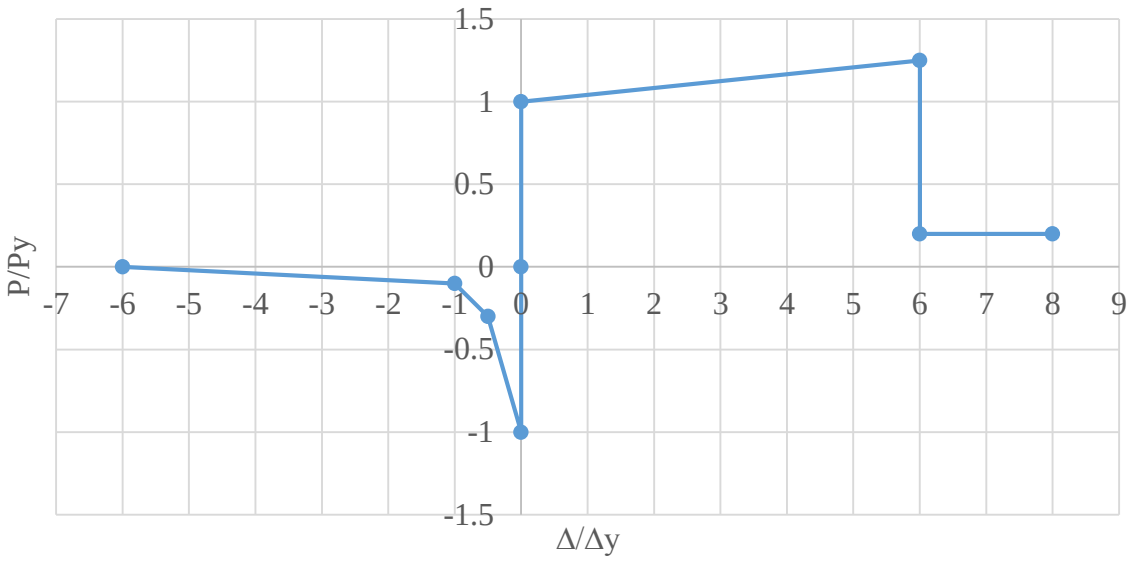

Figure 7-19. Behavior of nonlinear axial spring normalized by the yield properties

To consider the large in-plane bending effect that may lead to high axial-flexural interaction behavior at the ends of critical truss members, plastic hinges with idealized elastic perfectly plastic properties were incorporated to the SAP2000 model (see Figure 7-18). The nonlinear properties defined for each plastic hinge are shown in Figure 7-20. These curves depict the strength variation paths for each hinge before the P-M interaction surface is reached. For ease of modeling, the P-M interaction for each hinge utilized the limit defined by the FEMA 356 Equation (5-4): $M_{CE}=1.18ZF_{ye}\ (1-P/P_{ye}) \leqslant ZF_{ye}$. This equation is used to examine failure on steel columns subjected to various P-M interaction effects.

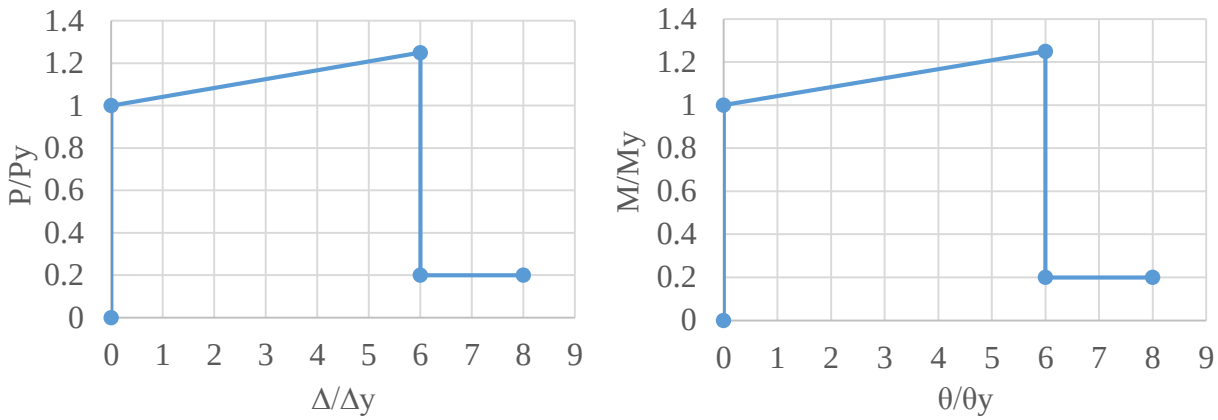

Figure 7-20. Behavior of each plastic hinge normalized by the yield properties: (a) axial behavior; (b) in-plane flexural behavior

The accuracy of applying the interaction limit using FEMA 356 Equation (5-4) was examined via comparing the interaction curves of the four critical sections where large in-plane bending and axial force effects were acting simultaneously. In Figure 7-21, the interaction curves defined by FEMA 356 Equation (5-4) for members U8U9 and L8L9 are compared with the interaction capacities determined by the net sections and the gross sections separately. In the region where the resultant interaction curves approach the interaction limit defined by the FEMA equation, second-order effects began to become important even for the relatively stocky members under consideration. This interaction is not properly captured by the SAP2000 models, resulting in the differences shown in Figure 7-21 between the SAP and ABAQUS results near ultimate strength. In general, there is a good correspondence between the SAP and ABAQUS results. The use of FEMA 356 Equation (5-4) can be considered as a reasonable approach to predict the ultimate failure at a cross section under axial-flexural interaction.

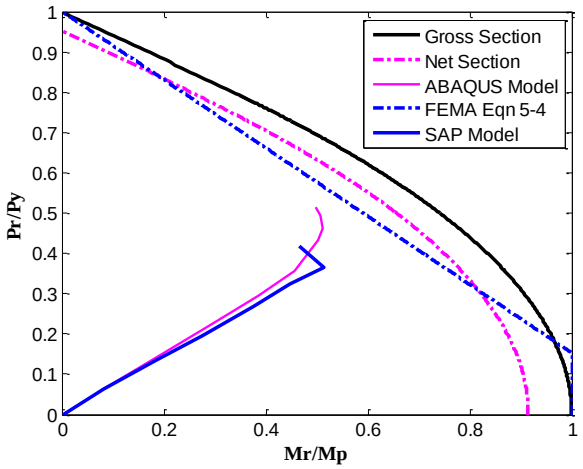

(a) Critical section near member end U8

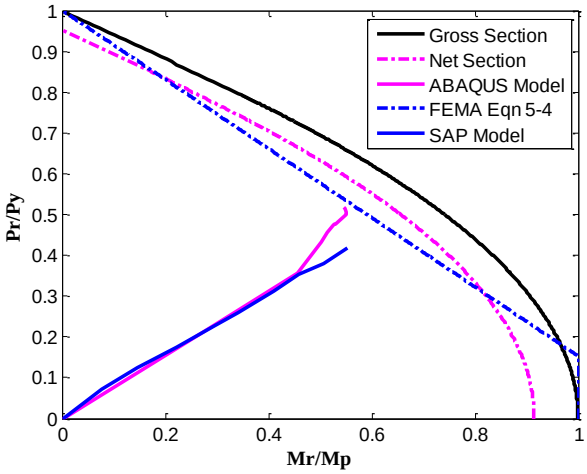

(b) Critical section near member end U9

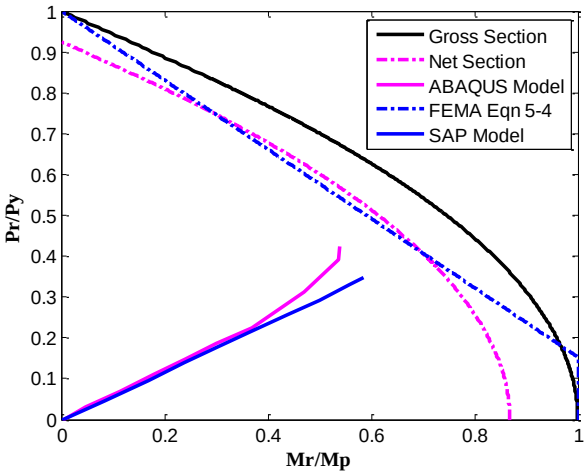

(c) Critical section near member end L8

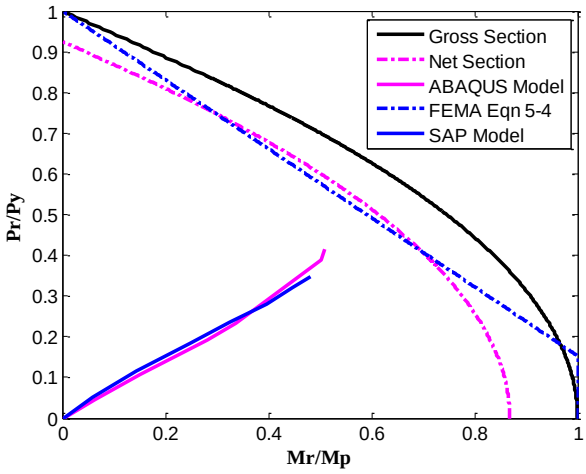

(d) Critical section near member end L9

Figure 7-21. Comparison of P-M interaction behavior at each plastic hinge location between SAP2000 model and ABAQUS model

7.4.2 M-Bridge

The system model for the undamaged bridge structure was verified by comparing the measured stresses for selected members with the stresses calculated by SAP2000. The test data for member stresses was obtained by multiplying the axial strains measured by strain gauges with an elastic modulus of 29,000ksi for the steel members (Cha et al. 2014). The loading condition in the field test includes self-weight of the bridge and 145kips of sand weight, which was uniformly distributed in the central three panels across the width of the deck as illustrated in Figure 7-22.

To simulate this loading condition, two steps were implemented in the SAP2000 model. The first step was simulating dead load. This was achieved by specifying a self-weight multiplier of 1 in the definition of dead load pattern so that the gravity load of the entire structure will be automatically calculated and applied to each member. It is important to note that self-weight of the deck had already been accounted for by applying effective loads on stringers and floor beams as discussed in Section 7.3.2. To avoid double counting of the deck weight, a factor of zero was assigned to both the mass modifier and the weight modifier of each shell element. The second step was applying the sand load to the system model. As the sand load was uniformly distributed in the central three panels of the deck, this area load was applied to the model in a similar way to the deck weight, which means that the area load was converted to effective line loads acting on the supporting stringers and floor beams.

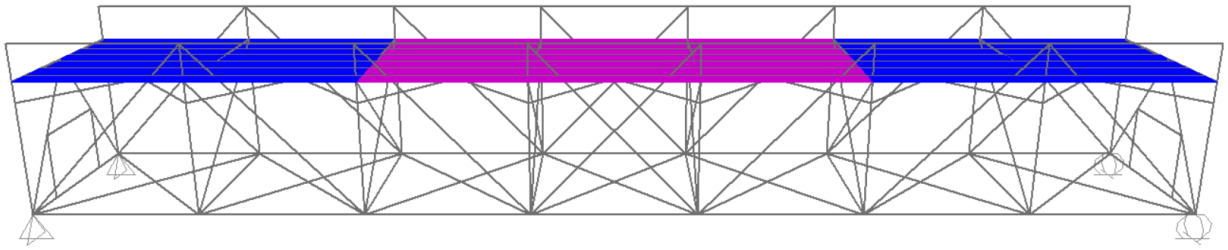

Figure 7-22. Sand load distribution on the deck (highlighted in pink)

Members selected for calibration included the main trusses, stringers, floor beams, and braces listed in Table 7-1 to Table 7-3. The nomenclature and locations of these members are displayed in Figure 7-23 to Figure 7-25.

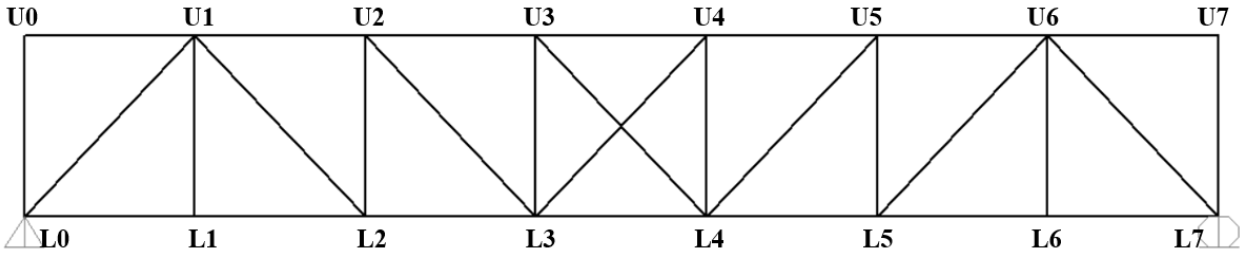

Figure 7-23. Nomenclature and location for each main truss member

Table 7-1. Member stress comparison on the main trusses in the undamaged structure (unit: ksi)

Main Truss Members	DL + Sand Load		Ratio of Model Result To Test Data
	SAP2000 model	Test Data	
L4L3-US	8.56	8.86	0.97
U4U3-US	-7.36	-8.27	0.89
L4L3-DS	8.56	9.15	0.94
U4U3-DS	-7.36	-8.61	0.85
L4L5-DS	8.25	8.76	0.94
U4L3-US	-0.89	-0.91	0.98
L4U3-US	-0.89	0.03	N.G.
U6L5-US	9.15	10.65	0.86
U6L5-DS	9.15	10.95	0.84
U4L4-US	-2.93	-2.65	1.11

Note: US=Upstream Side; DS=Downstream Side

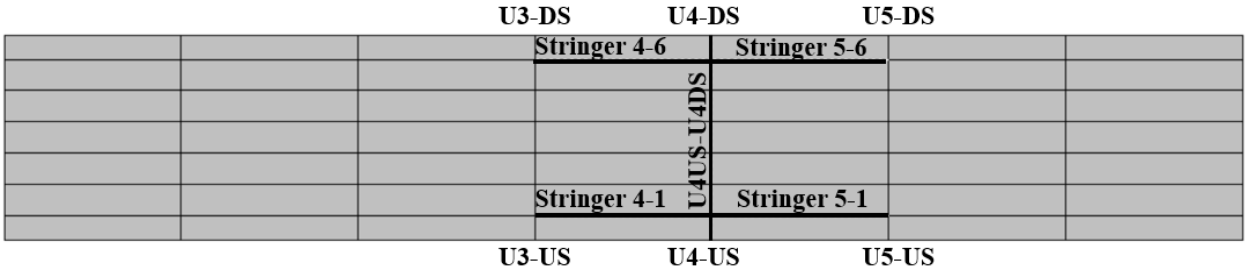

Figure 7-24. Nomenclature and locations for the selected stringers and floor beam

Table 7-2. Member stress comparison for the selected stringers and floor beam in the undamaged structure (unit: ksi)

Members		DL + Sand Load		Ratio of Model Result To Test Data
		SAP2000 model	Test Data	
Stringers	4-1	1.86	1.70	1.10
	5-1	1.86	1.49	1.25
	4-6	1.86	1.42	1.31
	5-6	1.86	1.70	1.10
Floor Beam	U4US-U4DS	2.03	2.25	0.91

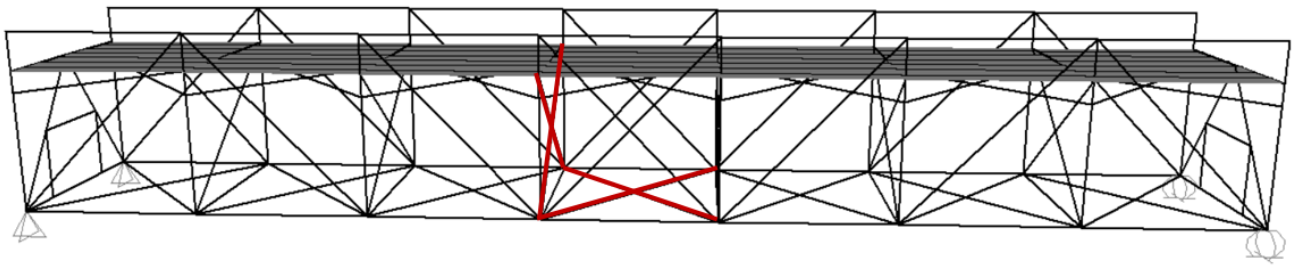

Figure 7-25. Locations for the selected braces

Table 7-3. Member stress comparison for the selected braces in the undamaged structure (unit: ksi)

Braces		DL + Sand Load		Ratio of Model Result To Test Data
		SAP2000 model	Test Data	
Lower Braces in Horizontal plane	L3US-L4DS	3.07	2.89	1.06
	L3DS-L4US	3.07	2.36	1.30
Sway Brace in Vertical plane	U4DS-L4US	1.37	0.45	N.G.

It can be seen from Table 7-1 to Table 7-3 that most of the ratios of the model results to the test data are close to 1. This indicates that the analytical model developed in SAP2000 is able to capture the real structural behavior measured during the controlled load testing. In the cases of members L4U3-US and U4DS-L4US, the model in SAP2000 predicts much higher stresses than the measured test data. However, these stress values obtained from both the model and the test measurement are less than 1.5ksi. With such small magnitude of stresses, it is reasonable to assume that these two cases are not significant factors to affect the overall quality of the model. Additionally, the significant difference observed in member U4DS-L4US is probably caused by the insufficient number of strain gauges installed on this angle member (Cha et al. 2014). Due to the limited project resources, the instrumentation was simply intended to get a feel for the forces transferred into the brace members in a damaged structure.

Considering that the cases with ratios greater than 1.2 are not found in main truss members but in secondary members (i.e. two stringers and one brace member) and that there are uncertainties associated with the experimental measurements as there was no duplication of measurements to ensure overall equilibrium, these cases can be assumed to not significantly influence the correlation between the model results and the measured member behavior.

The model for the damaged structure after losing the bottom chord member at the mid-span on the upstream side (L3L4-US) was calibrated to match the member strain data obtained from the destructive field test. This test was actually performed as a subsequent test on the bridge structure that was loaded with 145kips sand in the previous controlled load testing. The damaged structure was obtained by neatly severing one bottom chord member using shape charges. After this demolition the redistributed stresses on the remaining members were measured using the same strain gauges (Table 7-4 to Table 7-6).

Table 7-4. Member stress comparison on the main trusses in the damaged structure (unit: ksi)

Main Truss Members	DL + Sand Load		Ratio of Model Result To Test Data
	SAP2000 model	Test Data	
L4L3-US	Fractured		
U4U3-US	-7.64	-8.50	0.90
L4L3-DS	12.09	11.70	1.03
U4U3-DS	-8.69	-10.70	0.81
L4L5-DS	12.06	11.28	1.07
U4L3-US	10.25	9.28	1.10
L4U3-US	10.12	10.64	0.95
U6L5-US	6.70	N.A.	N.A.
U6L5-DS	10.85	12.60	0.86
U4L4-US	-6.08	N.A.	N.A.

Table 7-5. Member stress comparison for the selected stringers and floor beam in the damaged structure (unit: ksi)

Members		DL + Sand Load		Ratio of Model Result To Test Data
		SAP2000 model	Test Data	
Stringers	4-1	3.68	4.15	0.89
	5-1	3.68	3.52	1.05
	4-6	1.92	1.77	1.08
	5-6	1.92	2.20	0.87
Floor Beam	U4US-U4DS	4.18	3.32	1.26

Table 7-6. Member stress comparison for the selected braces in the damaged structure (unit: ksi)

Braces		DL + Sand Load		Ratio of Model Result To Test Data
		SAP2000 model	Test Data	
Lower Braces in Horizontal plane	L3US-L4DS	15.23	14.62	1.04
	L3DS-L4US	13.37	10.41	1.28
Sway Brace in Vertical plane	U4DS-L4US	6.27	4.02	1.56

As it can be seen from the ratios of model results to test data listed from Table 7-4 to Table 7-6, the model for the damaged structure is able to capture the stress behavior of most members except for the brace member U4DS-L4US. The reasons for the significant difference between the model results and the test data were discussed above.

7.5 Identification of Critical Members

Due to the large number of truss members and high complexity of the 3D structural system of the I-35W Bridge, it would be desirable if the redundancy analyses can be focused on a very limited number of truss members that are truly critical to this bridge system. As stated in AASHTO (2012), these members can be deemed as failure critical if failure of one of these members is expected to cause the collapse of the bridge. In a typical truss bridge, the critical members were selected amongst the main truss members, as they were designed to provide the primary load capacity for the entire bridge system. In a preliminary screening process, the critical members were identified as the main truss members with high demand to capacity (D/C) ratio for axial loads. This measure has been used by other researchers in similar studies. Hickey et al. (2009) and Azizinamini (2002) utilized the D/C ratio for axial loads as the measure to identify the most critical main truss member for an undamaged bridge structure.

A limitation of this approach is that stability-critical members such as vertical zero-force members can be missed due to their very small D/C ratios. To investigate the system effect of failure on one of the zero-force members, every single vertical member in the I-35W Bridge and M-Bridge as well as the diagonal member in the mid-span panel of the M-Bridge are also assumed as critical members.

Since the selection of the critical members as the first phase of a system analysis was aimed at determining the total number of critical main truss members, it was deemed satisfactory to compute the member D/C ratio using a simplified 2D elastic model, as the two lines of main truss was symmetric in an undamaged condition. The 2D model was validated through comparing the axial load demand for each main truss member between the predicted result and the member resultant

force under dead load provided from the original design drawing. This comparison of axial load demand was made for the I-35W Bridge and the M-Bridge respectively as displayed in Figure 7-26 to Figure 7-29.

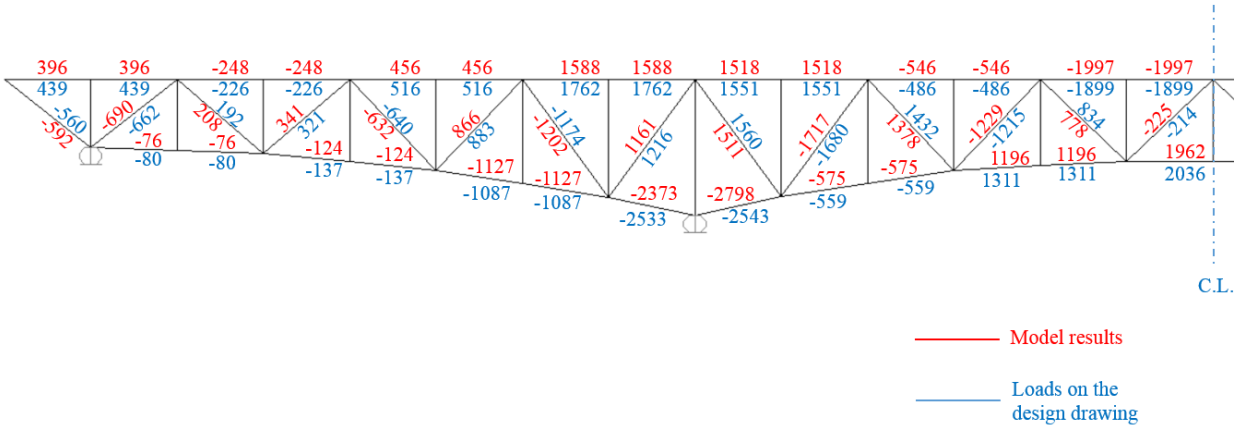

Figure 7-26. Comparison of axial load demand for the main truss members in the I-35W Bridge under design dead load

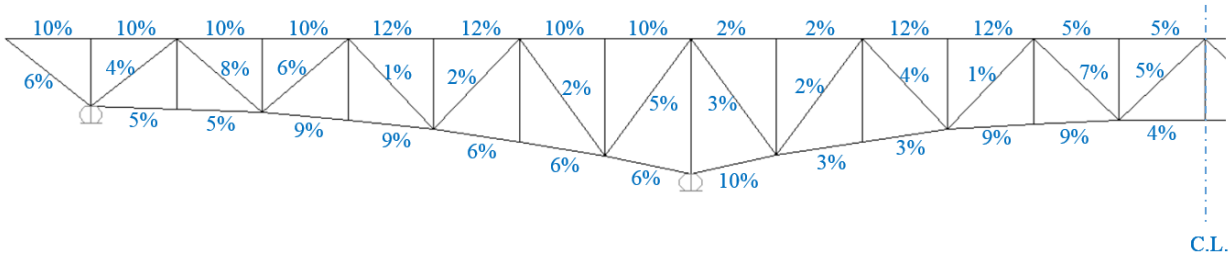

Figure 7-27. Difference between the results from the 2D model and design values on the drawing for the I-35W Bridge

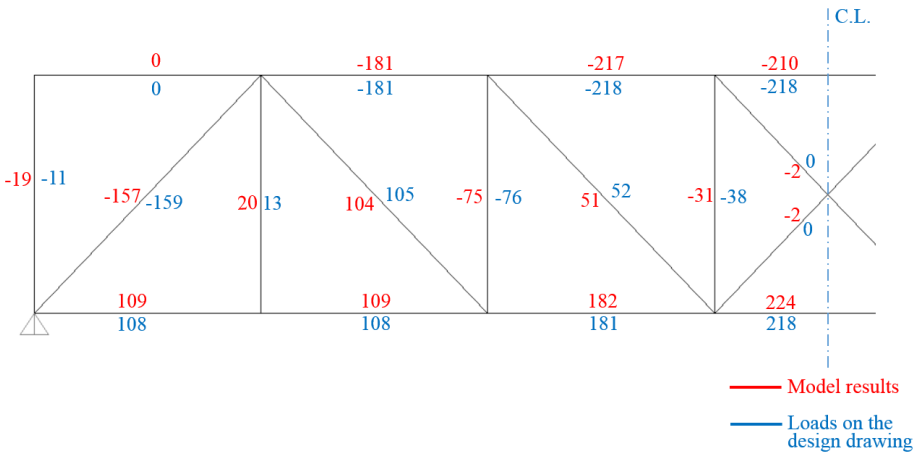

Figure 7-28. Comparison of axial load demand for the main truss members in the M-Bridge under design dead load

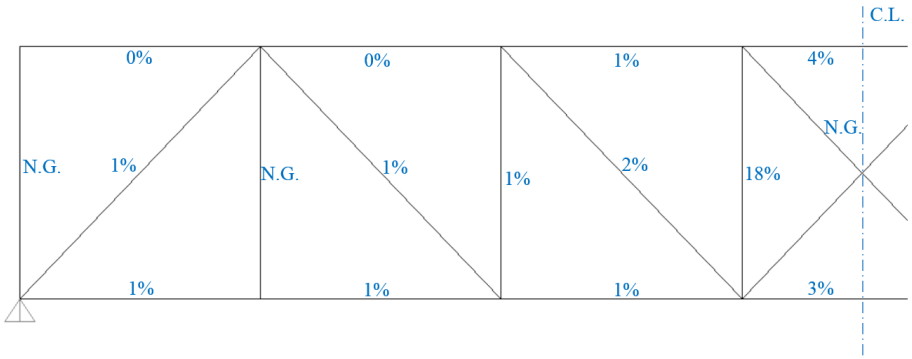

Figure 7-29. Difference between the results from the 2D model and design values on the drawing for the M-Bridge

Once the 2D elastic models are demonstrated their capability of matching the design data, the main truss member capacities were obtained using the geometric information automatically by SAP2000.

Considering that bridge system redundancy is usually evaluated through examining the ultimate load capacity of the bridge, the loading condition used in the determination of member load demand was supposed to represent a severe traffic loading condition that would maximize the live load response of the entire bridge system. For this reason, the national standard HL-93 load is selected as the live loads for the M-Bridge studies. This is in contrast to the I-35W Bridge for

which dead load alone are considered sufficient to identify critical members as the self-weight of steel members made approximately 93% of the total loads.

After the type of live load was determined for the M-Bridge, the next task is to identify the critical location of the truck loads as part of the HL-93 load. Since the system redundancy analysis focuses on the global behavior of a bridge structure, the truck loads need to be applied in the position that will produce the critical system capacity (Ghosn and Fiorillo 2013). Therefore, the truck loads used for this system redundancy analysis were applied to the mid-span. The spacing between each truck load was taken as 14 feet.

With the member capacities as well as load demands determined, the D/C ratio for each main truss member can be computed. Then the main truss members can be arranged in descending order of D/C ratio. A lower threshold of interest was arbitrarily set at the maximum D/C ratio divided by two. The main truss members with D/C ratios lower than one-half of the highest D/C ratio were not considered as critical members, as they were not expected to significantly affect the system redundancy. The exception is the vertical members for which all cases were checked. Following this selection criterion, the critical diagonal and chord members for the I-35W Bridge and the M-Bridge are highlighted in Figure 7-30 and Figure 7-31, respectively.

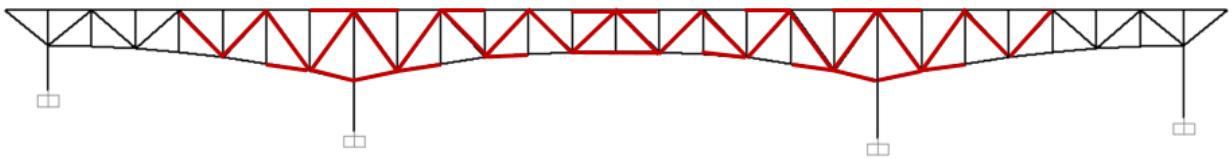

Figure 7-30. A 2D model in SAP2000 for the I-35W Bridge showing critical diagonal and chord members

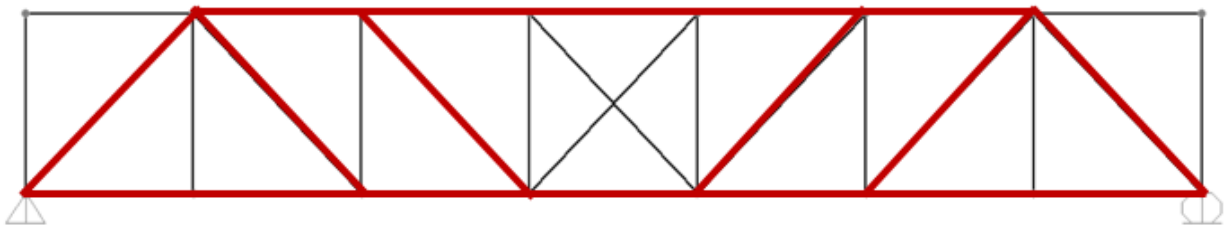

Figure 7-31. A 2D model in SAP2000 for the M-Bridge showing critical diagonal and chord members

The prioritization results of critical members using the previously mentioned criterion were compared with those determined using the load rating method as shown in Table 7-7 and Table 7-8. The load rating method is considered as a robust approach and will be discussed in detail in Section 7.6.1. Note that for length reason, column 1 in Table 7-7 and Table 7-8 merely shows the most critical vertical members whose failure are found to significantly affect the system redundancy.

Table 7-7. Comparison of the ranking for critical members between the D/C ratio based method and the load rating method for the I-35W Bridge

Member removed from a 3D model in a no-load condition	$DL_{,ultimate}$ / $DL_{,total}$	$LL_{,ultimate}$ / HL-93	Critical members in a 2D model for the undamaged structure	D/C ratio	Difference in the position between column 1 and column 4 (i.e. row# in column 1 – row# in column 4)
U8L9	0.20	0.00	U8L9	0.34	0
U10L9	0.23	0.00	U7U8	0.33	-8
L8L9	0.31	0.00	U8L7	0.33	-3
U10L11	0.38	0.00	U10L11	0.33	0
U8L8	0.43	0.00	U8U9	0.32	-8
U8L7	0.46	0.00	L8L9	0.32	3
U12L11	0.51	0.00	L7L8	0.32	-7
L7L8	0.52	0.00	L13L14	0.31	1

Member removed from a 3D model in a no-load condition	$DL_{,ultimate}$ / $DL_{,total}$	$LL_{,ultimate}$ / HL-93	Critical members in a 2D model for the undamaged structure	D/C ratio	Difference in the position between column 1 and column 4 (i.e. row# in column 1 – row# in column 4)
U6L7	0.63	0.00	U6L5	0.31	-6
U12L13	0.90	0.00	U10L9	0.30	-2
L11L12	1.00	0.14	U13U14	0.29	-5
L13L14	1.00	0.21	U12L13	0.29	4
U8U9	1.00	0.34	U8L8	0.28	8
U7U8	1.00	0.40	U12L11	0.28	12
L9L10	1.00	0.59	U6L7	0.28	-4
U14L13	1.00	0.93	L11L12	0.28	-7
U10U11	1.00	0.96	L6L7	0.27	-4
U13U14	1.00	1.02	U4L5	0.25	7
U4L5	1.00	1.08	L9L10	0.25	1
L6L7	1.00	1.11	U10L10	0.24	3
U6L5	1.00	1.15	U10U11	0.20	12
U10L10	1.00	1.18	U9L9	0.16	2
U9L9	1.00	1.19	U14L13	0.15	1

Table 7-8. Comparison of the ranking for critical members between the D/C ratio based method and the load rating method for the M-Bridge

Member removed from a 3D model in a no-load condition	$LL_{,ultimate}$ / HL-93	Critical members in a 2D model for the undamaged structure	D/C ratio	Difference in the position between column 1 and column 3 (i.e. row# in column 1 – row# in column 3)
U1U2	0.00	U2U3	0.46	-6
U2U3	0.00	U3U4	0.44	1
U1L0	0.18	L3L4	0.43	-5
U3U4	0.35	U2L3	0.42	2
U1L2	0.83	U1L2	0.41	0
U2L2	1.09	L2L3	0.40	-5
L3L4	1.11	U1U2	0.39	4
L2L3	1.18	U1L0	0.34	2
L1L2	1.36	L1L2	0.32	0
U2L3	1.39	L0L1	0.32	6
L0L1	1.42	U2L2	0.30	1
U0L0	1.45	U3L3	0.18	-3
U1L1	1.60	U3L4	0.17	-1
U3L3	1.60	U1L1	0.06	2
U3L4	1.63	U0L0	0.03	2

From Table 7-7 and Table 7-8, it can be seen that the ranking of critical members based on D/C ratios is quite different from that obtained using the load rating method. This difference is caused by two main reasons: First, the D/C ratio based ranking results were obtained from an undamaged structure under the design condition while the load rating method utilized various damaged structures to predict a ranking result; Second, the D/C ratio based method relied on a 2D model for one line of the main truss while in the load rating method the entire 3D system containing main

trusses, floor trusses, braces, and deck was used. Due to these reasons, the application of member D/C ratio concept was limited to identify critical members in a preliminary phase.

7.6 Rating of Critical Members

The sequential rating of critical members was used for the following two main purposes:

(1) If member X was rated as more critical than member Y, then member X was expected to affect the system redundancy more than the member Y.

(2) As rating of critical members requires the evaluation of the failure modes of particular damaged structures, the rating process can also be used to determine whether failure on one critical member is likely to trigger a progressive collapse.

The overall benefit of a proper ranking of critical members is an economic allocation of inspection resources, as careful inspection need only carried out for the most critical members.

Since the most critical member can be identified as the member whose failure is expected to cause the worst system effect, the approach of identifying the most critical member is to measure the ensuing change of system behavior due to the removal of critical members one at a time. As the removal of one critical member will make the two lines of the main truss structure no longer symmetric, a three dimensional model is needed to simulate the real bridge in a damaged condition. Furthermore, as the ultimate failure of bridge systems typically includes a combination of nonlinear effects such as yielding and buckling, the nonlinear features are required to be introduced into the 3D models.

In the following sections, two methods that measure the change of system strength and energy will be discussed. In the rating factor method, the change of system load capacity was studied through comparing the ultimate live load capacities between the original bridge and the damaged structure

after losing one critical member. In the strain energy method, the strain energy release on the main truss structure was measured through comparing the total strain energy of all main trusses in the original bridge with the total strain energy of the remaining main trusses in the damaged 3D system.

7.6.1 Rating Factor Method

The rating factor method was utilized to quantify the strength change of a bridge system due to failure of one critical member. The terminology of load rating was defined in the National Bridge Inspection Standards (NBIS) regulations as "The determination of the live load carrying capacity of a bridge using as-built bridge plans and supplemented by information gathered from the latest field inspection." The live load carrying capacity of a bridge is expressed as a Rating Factor (RF). This factor represents the number of a particular type of traffic loads that a bridge can carry when the ultimate limit state of the bridge is reached.

As the strength capacity of a bridge system can be expressed as a rating factor, the system effect of losing one critical member was evaluated through the comparison of the rating factors between the undamaged and the damaged bridge structures. Thus the most critical member to the system was thereby identified when the damaged structure without this member has the smallest rating factor.

It is also of great importance to note that a proper estimation of the ultimate limit state of a bridge system is essential in the load rating process. The ultimate limit state is often considered to be reached when failure of the first load carrying component occurs. It is crucial to identify the most vulnerable component to failure in the system. This identification was implemented through consideration of four main failure modes on all structural components, including axial-flexural interaction failure at ends of each main truss member, failure at truss member connections,

buckling of truss members, and damage on the reinforced concrete deck. To appropriately capture these failure modes different nonlinear features were incorporated into the 3D system models developed in SAP2000. A detailed description of simulation for each failure mode will be presented later in Section 7.7.

The approach for determining the rating factor for the bridge both in an as-built condition and in a damaged condition can be briefly summarized as follows:

(1) Select loading condition: The HL-93 load was selected as the traffic loads for rating the two example bridges in this research;

(2) Apply rating load: One HL-93 load was applied to the stringers and main truss members by assigning uniform frame loads and point loads to these members to simulate the effect of lane loads and truck loads respectively;

(3) Apply rating load to failure: A scale factor of 3 was chosen for amplifying the HL-93 load as three times of the HL-93 load was assumed large enough to initiate the collapse of a bridge. This was achieved by modifying the live load scale factor to 3 in the definition of the load case in SAP2000;

(4) Determine rating factor: The load rating factors for dead load and live loads were determined as the ratios of total reactions in the ultimate state of the structure to design dead load and the HL-93 load, respectively.

7.6.1.1 Load Rating for the I-35W Bridge

Through rating the I-35W Bridge in a damaged condition, ten damaged cases were found unable to sustain the full dead load when failure of the first component was observed. The load carrying capacities for the I-35W Bridge both in the damaged and the undamaged conditions were calculated as dead load factors and live load factors respectively. The critical damaged structures as well as the original intact structure is shown in Table 7-9 in ascending value of the dead and the live load factors. Note that a dead load factor less than one implies that the structure would collapse under its self-weight. Note also that for rating purposes, a live load factor of 1.0 is set as the minimum value for keeping a structure in a safe condition under normal traffic as specified by AASHTO (2012). Table 7-9 also shows the most critical remaining member. The position of such critical member is displayed in Figure 7-32.

Table 7-9. System load capacities and governing failure modes for the I-35W Bridge in the undamaged and damaged conditions

Member removed in a no-load condition	Member force in the undamaged Structure	$DL_{,ultimate}$ / $DL_{,total}$	$LL_{,ultimate}$ / HL-93	Most critical remaining member	Critical location	Governing failure mode	Group
U8L9-W	Tension	0.20	0.00	LB8-9E	Brace-main truss connection	Block shear	I
U10L9-W	Compression	0.23	0.00	LB9-10E			
L8L9-W	Compression	0.31	0.00	LB9-10E			
U10L11-W	Tension	0.38	0.00	LB10-11E			
U8L8-W	Compression	0.43	0.00	LB7-8E			
U8L7-W	Tension	0.46	0.00	LB7-8W			
U12L11-W	Compression	0.51	0.00	LB11-12E			
L7L8-W	Compression	0.52	0.00	LB7-8W			
U6L7-W	Compression	0.63	0.00	LB6-7W			
U12L13-W	Tension	0.90	0.00	LB12-13E			
L11L12-W	Tension	1.00	0.14	L10L11-W	Main truss	Buckling	II
L13L14-W	Tension	1.00	0.21	L10L11-W	Main truss	Buckling	
U8U9-W	Tension	1.00	0.34	U10U11-W	Main truss	Buckling	
U7U8-W	Tension	1.00	0.40	U10U11-W	Main truss	Buckling	
L9L10-W	Compression	1.00	0.59	U10U11-W	Main truss	Buckling	
U14L13-W	Compression	1.00	0.93	U12U13-W	Main truss	P-M interaction	III

Member removed in a no-load condition	Member force in the undamaged Structure	$DL_{,ultimate}$ / $DL_{,total}$	$LL_{,ultimate}$ / HL-93	Most critical remaining member	Critical location	Governing failure mode	Group
U10U11-W	Compression	1.00	0.96	L10L11-W	Main truss	Buckling	
U13U14-W	Compression	1.00	1.02	LB11-12E	Brace-main truss connection	Block shear	
U4L5-W	Compression	1.00	1.08	LB4-5W	Brace-main truss connection	Block shear	
L6L7-W	Compression	1.00	1.11	LB5-6W	Brace-main truss connection	Block shear	
U6L5-W	Tension	1.00	1.15	U5U6-W	Main truss	P-M interaction	
U10L10-W	Tension	1.00	1.18	L9L11-W	Main truss	P-M interaction	
U9L9-W	Compression	1.00	1.19	U9U10-W	Main truss	P-M interaction	
Undamaged	N.A.	1.00	1.21	U13U14	Main truss	P-M interaction	

Notes:

- Each damaged structure was simulated by removing one main truss member on the West side of the two-line main truss;
- The geometric position of each main truss member being removed can be identified in Figure 7-10;
- LB( )-( )E: the lower brace that connects the bottom chord of east main truss with the middle point of the bottom portal frame as illustrated in Figure 7-32.

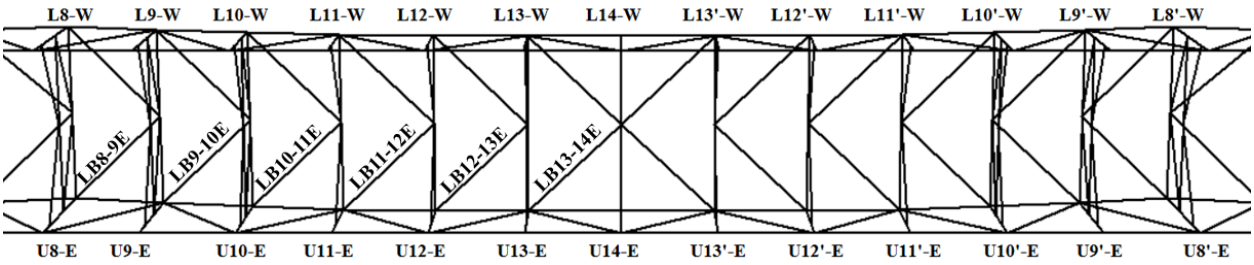

Figure 7-32. A top view of the main truss and brace systems in the I-35W Bridge showing the locations of critical lower braces

From Table 7-9, it is clear that the most critical member was U8L9, as the associated damaged structure without this member was found to have the lowest load capacity. Note that this member was the first diagonal member in tension from the interior support on the center span. This result was in good agreement with the conclusion made by Yamaguchi et al. (2010) who stated that the influence of the failing member was greatest when the truss diagonal member was near a support. Considering that the member U8L9 was found unable to sustain its self-weight, it can be reasonable to identify this member as a fracture critical member that is truly non-redundant to the bridge system.

Based on the values of load rating factors in Table 7-9, the critical members can be classified into three groups. The first group includes ten cases that have dead load factors less than 1, which means the structure is unable to carry full dead load, and needless to say, any amount of live loads. Most members in the first group were diagonal members and the vertical member U8L8, which connects to Pier 6. In the second group, with live load factors less than 0.9, all critical members were chord members. These results indicate that in this particular bridge configuration the diagonal members and the vertical member framing into the interior support were basically more critical to the system than most chord members. The structures in the third group were found to be capable of carrying more than 90% of the HL-93 load. Thus it can be inferred that the damaged structures

in this group will remain functional under normal traffic loads provided a typical level of material overstrength is present.

As far as the critical member location is concerned, it can also be noticed that the critical members in the first group were close to the interior support (Pier 6). In particularly, the vertical member that connects to the interior support was found to be most critical among all vertical members. Failure of any other vertical member did not significantly reduce the system redundancy. These results indicate that in a continuous span bridge members near an interior support needs careful attention in bridge system redundancy evaluation.

Table 7-9 also indicates which member becomes the critical one after the initial failure. In the first group, the ultimate failure of each damaged structure was triggered by failure on the connection between the bottom chord member and the lower brace member close to the undamaged side. The location and forces on the critical lower brace members are displayed in Figure 7-33 for the most critical case (failure at member U8L9). In this case, the Brace-main truss connection failure (failure at member LB8-9E connection) implies that there must be an increase in the axial load demand on the critical lower brace members. As the brace members were not expected to carry loads in design, the actual strength capacity of a brace member was not considered in designing the connection between the brace member and a main truss member. In other words, the connection was designed based on basic detailing requirements alone to provide a minimum stiffness. However, when member U8L9 was removed from the system, a failure mechanism would have developed if there was no load carrying members in the brace system. This means that to keep the damaged structure in a stable condition the load originally carried by the damaged member needs to be redistributed locally to the other truss through the brace member. This load redistribution is illustrated in Figure 7-33.

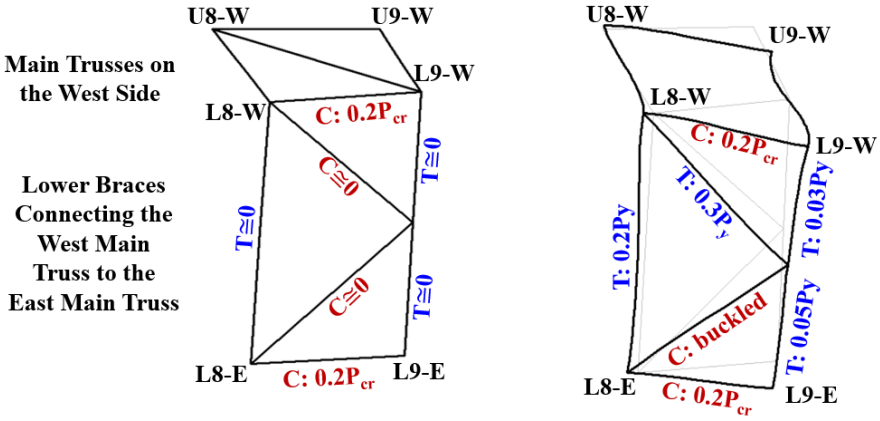

(a) U8L9-W undamaged (b) U8L9-W damaged

Figure 7-33. Comparison of load distribution on the critical brace members between an undamaged structure and a damaged structure with the removal of member U8L9-W both under the same loading condition (0.20*DL when failure occurs on the critical lower brace connection)

As seen from the diagram on the right of Figure 7-33, due to a large relative displacement between the two sides of main truss, the diagonal brace connecting the west main truss was stretched while the diagonal brace connecting the east truss was shortened. The shortening effect led to a buckling failure on the lower brace connecting to the east truss. As the post-buckling strength was considered in the analysis, this buckled member was still carrying loads in the ultimate state. Thus the equilibrium and stability was maintained in the damaged structure. The occurrence of a large relative displacement as displayed in Figure 7-33 was caused by asymmetric stiffness on each side of main truss structure. Therefore, the load path was quite different from that was expected in design. The large number of main truss members with a load rating factor less than 1 for dead load indicates that the I-35W Bridge was a particularly collapse-critical structure.

7.6.1.2 Load Rating for the M-Bridge

The load rating results for the northernmost approach span of the Milton-Madison Bridge structure are summarized in Table 7-10. The first two critical damaged structures were found unable to sustain the full dead load when the ultimate failure occurred. The most critical tension member U1L2 was found to be the first tension diagonal member from the support. As the failure of this tension diagonal member left the structure with a live load capacity less than the standard HL-93 load, this member can be identified as a fracture critical member.

In the most critical damaged structure, the system ultimate state was considered to be reached when two plastic hinges occurred on member U0L0 on the damaged side. The two hinges formed simultaneously as the resultant axial load and biaxial moment at both ends were equal in magnitude (Figure 7-34). Since the plastic hinge behavior was limited by the P-M-M interaction surface specified in FEMA 356 Equation (5-4), the formation of a plastic hinge indicated an ultimate interaction ratio at the hinge location. Further investigation revealed that in-plane bending dominated the interaction ratio. Therefore, the ultimate failure can be considered as being caused by a significant in-plane bending effect, which is illustrated in Figure 7-35.

As seen from Table 7-10, most damaged structures reached their ultimate state when failure due to large in-plane bending occurred on a vertical main truss members. One exception is the case of damage on the vertical member U2L2, which caused a buckling failure on a sway brace that connected the vertical members on both sides of the main truss. For the most damaged cases, failure on the vertical members controlled the ultimate state of the system. This result can be explained by the fact that the cross sections for these vertical members were the smallest among all main trusses. The most critical location on one of these members is highlighted in Figure 7-34. The failure mode on this critical location can be illustrated as shown in Figure 7-35. It was clear

that large in-plane flexure on the vertical member resulted in the bending about weak axis of the vertical member. With a very small flexural stiffness about the weak axis, it was not surprising that large in-plane bending behavior on these vertical members dominated the ultimate failure in most cases.

Table 7-10. System load capacities and governing failure modes for the M-Bridge in the undamaged and damaged conditions

Member removed in a no-load condition	Member force in the undamaged structure	$DL_{,ultimate}$ / $DL_{,total}$	$LL_{,ultimate}$ / HL-93	Critical main Truss	Failure mode
U1U2-US	Compression	0.85	0.00	U0L0-US	In-plane bending
U2U3-US	Compression	0.97	0.00	U2L2-US	
U1L0-US	Compression	1.00	0.18	U1L1-DS	
U3U4-US	Compression	1.00	0.35	U1L1 and U6L6	
U1L2-US	Tension	1.00	0.83	U0L0-DS	
U2L2-US	Compression	1.00	1.09	Sway Brace	Buckling
L3L4-US	Tension	1.00	1.11	U1L1 and U6L6	In-plane bending
L2L3-US	Tension	1.00	1.18	U7L7-DS	
L1L2-US	Tension	1.00	1.36	U0L0-US	
U2L3-US	Tension	1.00	1.39	U0L0-DS	
L0L1-US	Tension	1.00	1.42	U0L0-US	
U0L0-US	Compression	1.00	1.45	U7L7-US	
U1L1-US	Tension	1.00	1.60	U7L7-US	
U3L3-US	Tension	1.00	1.60	U0L0-DS	
U3L4-US	Compression	1.00	1.63	U0L0-US	
Undamaged	N.A.	1.00	1.63	U1L1 and U6L6	

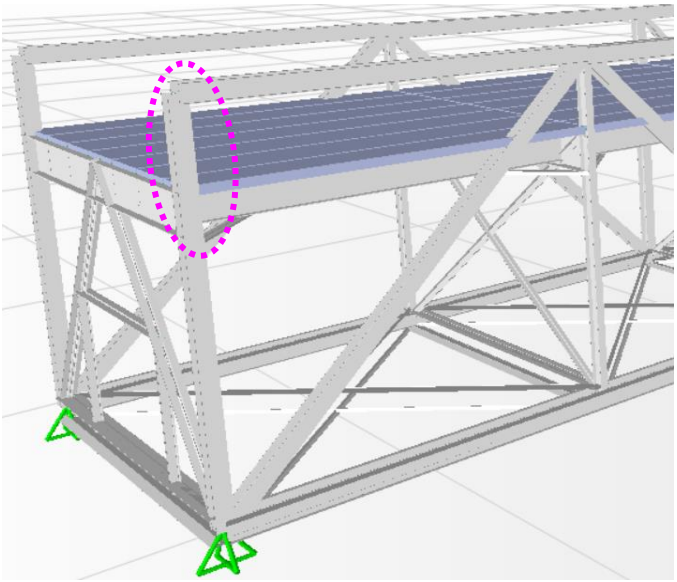

Figure 7-34. Critical location on member U0L0, where a large in-plane bending effect can be observed as the ultimate failure mode

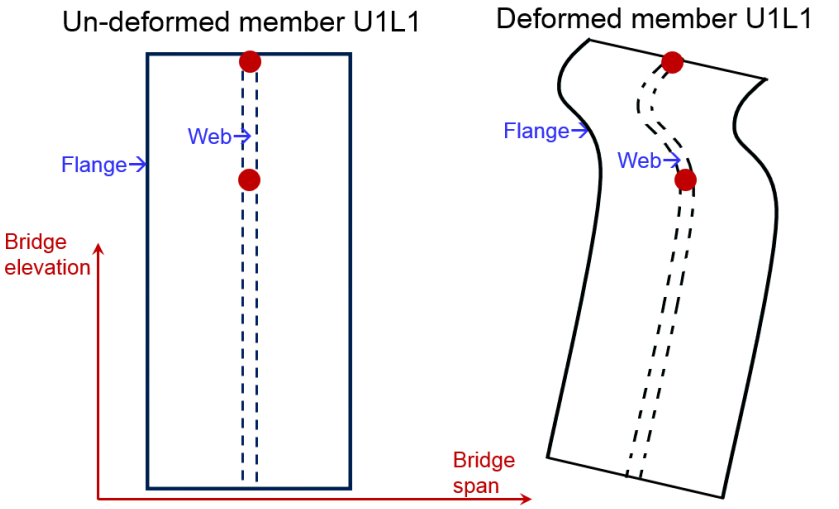

(a) Undeformed member U1L1 (b) Deformed member U1L1

Figure 7-35. A simple illustration of the undeformed shape and the deformed shape of member U1L1 (Note: the red dot represents the location of plastic hinges formed in the ultimate state)

A live load rating factor of 1.63 was obtained for the undamaged structure of the M-Bridge, indicating that the original undamaged structure can carry 1.63 times of the design live load (the HL-93 load) without failure. To ensure the accuracy of such high capacity a simple verification

was conducted. Since the ultimate failure of the undamaged structure was reached when most truss members in the system still behaved linear elastically (except the plastic hinge locations on the upper portions of the vertical members U1L1 and U6L6 where the plastic deformation just began to develop in a very early stage), an elastic system response can be assumed for the undamaged structure under full dead load and 1.63 times of the HL-93 load. As the test loads applied to the same structure were around 28% of the total loads in the rating analysis, including dead load plus 1.63 times of the HL-93 load (see Table 7-11), the behavior of each truss member measured in the test was also linear elastic. Therefore, the resultant member axial stress was expected to be linearly proportional to the applied loads on the undamaged structure. This also means that the ratio of member axial stress resulting from the test loads to the stress from the rating loads should be very similar to the ratio of the test loads to the rating loads. This expected result was confirmed through the comparison of axial stresses on members L3L4 on both sides of the main truss structure between test loads and rating loads (see Table 7-11). The reason to choose these two members for comparison is due to the fact that the member axial stresses under dead and sand loads were measured in the test.

Table 7-11. Comparison of member axial stresses in the undamaged structure under sand loads to the stresses under 1.63 times of the HL-93 load

Member for comparison	Member axial stress (ksi)		Ratio of (Sand/HL-93)		
	DL+Sand	DL+ 1.63·(HL-93)	(DL+Sand) / [DL+ 1.63·(HL-93)]	Member axial stress ratio = column 2 / column 3	Difference = column 4 / column 5
L3L4-US	SAP: 8.56	13.01	0.61	SAP: 0.66	0.93
	Test: 8.86			Test: 0.68	0.89
L3L4-DS	SAP: 8.56	12.99	0.61	SAP: 0.66	0.92
	Test: 9.15			Test: 0.70	0.86

Furthermore, Table 7-12 compared the load rating factor for each structure with the current load rating limit at the inventory level, which is specified by the current load rating standard published by FHWA (2012). This load rating limit provides a convenient screening of existing bridges. As the HL-93 load is used in such load rating process, bridges that can carry full HL-93 load will have adequate long-term capacity for all AASHTO loads and state legal loads. A factor of 1.0 was used as the minimum rating factor, which represents the standard HL-93 load. As the rating factors for the first five most critical damaged cases were less than 1.0, these damaged structures were considered to fail to meet the load rating requirement. In other words, the removal of any one of the top five critical members in the first column of Table 7-12 would leave the damaged system insufficient redundancy. Such critical members can therefore be classified as System Non-Redundant Members per new FHWA definition in the Technical Memo (2012).

Table 7-12 also shows that the removal of either one of the vertical members or the diagonal member in the mid-span panel (U3L4) does not reduce the system load capacity below the standard HL-93 load. In particularly, the reduction in system load capacity due to the removal of member U3L4 is less than 1%. These results indicate that in this simple-supported truss structure, the vertical members and the diagonal member in the mid-span panel are not critical to system redundancy.

Since tension members are deemed as fracture critical members, failure on one of these members is expected to lead to a bridge collapse. However, except member U1L2, the first tension diagonal from the support, failure on any one of the tension members will not reduce the system redundancy below the established minimum, thus keeping the bridge in a safe condition. These members could thereby be classified as System Redundant Members (SRMs) defined by the FHWA Technical Memo (2012). Hence, these tension members can be removed from the fracture critical designation.

Overall, only the tension member U1L2 in the M-Bridge will be considered truly fracture critical if using the criterion for classifying SRMs.

Table 7-12. Classification of critical members in the M-Bridge

Member removed in a no-load condition	Member force in the undamaged structure	$DL_{,ultimate}$ / $DL_{,total}$	$LL_{,ult}$ / HL-93	Member classification	Fracture critical members?
U1U2-US	Compression	0.85	0.00	System Non-Redundant Members	No
U2U3-US		0.97	0.00		
U1L0-US		1.00	0.18		
U3U4-US		1.00	0.35		
U1L2-US	Tension	1.00	0.83		Yes
U2L2-US	Compression	1.00	1.09	System Redundant Members	No
L3L4-US	Tension	1.00	1.11		Yes
L2L3-US		1.00	1.18		
L1L2-US		1.00	1.36		
U2L3-US		1.00	1.39		
L0L1-US		1.00	1.42		
U0L0-US	Compression	1.00	1.45		No
U1L1-US	Tension	1.00	1.60		Yes
U3L3-US	Tension	1.00	1.60		
U3L4-US	Compression	1.00	1.63		No

7.6.2 Strain Energy Method

As previously discussed in Section 2.5.2, the application of strain energy concepts could also provide a robust measure of the influence exerted by the failure of one critical member on system robustness. Unlike the rating factor method, which merely focuses on the strength of a system, the strain energy approach ideally will account for the change of both strength and stiffness of a system. To be specific, the ranking of critical members using the rating factor method was based on the ratio of axial force demand to the member strength capacity. The effect of member length that directly affects the member deformation was not accounted for. In contrast, the strain energy approach measures the member volumetric change. Thus the influence of both strength and stiffness of a system following the failure of one critical member can be assessed simultaneously.

The strain energy approach will utilize two steps to rate critical members. The first step requires measuring the strain energy release on the main truss system after a single member is damaged. In this step, the strain energy is measured as the difference between the undamaged and damaged structures when they just reaches their ultimate states. The ultimate state assumed herein is when the most critical remaining member begins to fail on two remaining members.

The strain energy for an undamaged structure (U_0) is computed as the sum of every main truss member's strain energy, given the fact that loads are primarily carried by the main truss structure. The member strain energy is computed as the superposition of strain energies due to axial, flexural, and shear forces. The torsion effects on the truss members are neglected, as the deck provides adequate stiffness to prevent significant torsion on the truss system.

Since the behavior of each critical structure in its ultimate state is close to elastic, the calculation of member strain energy follows the equations (7-1) to (7-3) as shown below:

$$U_P = \frac{P^2 L}{2EA} \tag{7-1}$$

$$U_M = \int_l \frac{M^2}{2EI} d_l \tag{7-2}$$

$$U_S = \int_l \frac{kV^2}{2GA} d_l \tag{7-3}$$

In the undamaged two example bridge structures, about 94% of member strain energy results from axial forces. In their corresponding damaged structures, the average contribution of axial force induced strain energy is approximately 91% and flexural moment induced strain energy is around 8%, leaving 1% of strain energy due to shear effect. The strain energy for each damaged structure (U_d) is calculated as the total strain energy of the remaining main trusses after one critical member is removed from the system. Then the strain energy release (ΔU) is expressed as the difference between U_0 and U_d. The calculation results are summarized in Table 7-13 and Table 7-14.

Table 7-13. System strain energies for the I-35W Bridge in both undamaged condition (U_0) and damaged conditions (U_d)

Member removed in a no-load condition	$U_{0,ult}$ (in-k)	U_d (in-k)	$\Delta U = U_0 - U_d$ (in-k)	$U_{0,d}$ (in-k)	$U'_d = U_d / U_{0,d}$ (in-k)
U8L9	84798	5427	79371	15228	0.36
U10L9	84798	5816	78982	17513	0.33
U8L8	84798	8246	76553	32741	0.25
L8L9	84798	8261	76537	23604	0.35
U10L11	84798	8527	76272	28934	0.29
U8L7	84798	10289	74509	35025	0.29
U12L11	84798	12132	72666	38832	0.31
L7L8	84798	12503	72295	39594	0.32
U6L7	84798	15805	68993	47969	0.33
U12L13	84798	31010	53788	68528	0.45
L13L14	84798	37237	47561	77143	0.48
L11L12	84798	39103	45695	77644	0.50
U8U9	84798	42889	41909	78574	0.55
U7U8	84798	44693	40105	79003	0.57
U13U14	84798	47021	37777	80363	0.59
L6L7	84798	55434	29364	82795	0.67
U10U11	84798	60951	23847	83010	0.73
U4L5	84798	62712	22086	83439	0.75
U6L5	84798	63102	21696	83868	0.75
L9L10	84798	71308	13490	84083	0.85
U9L9	84798	76939	7859	84655	0.91
U14L13	84798	81613	3185	84369	0.97
U10L10	84798	84307	491	84583	1.00

Notes:

- $U_{0,ult}$ in the second column is calculated on the undamaged structure when it is carrying full dead loads and 1.21 times of the HL-93 loads. This loading condition represents the ultimate load capacity of the undamaged structure;

- U_d in the third column represents the strain energy for a damaged structure when it reaches the ultimate state;

- $U_{0,d}$ in the fifth column is calculated on the undamaged structure when it is carrying the loads at which the ultimate state of the corresponding damaged structure is reached. This means that the loading condition in the calculation of $U_{0,d}$ is the same as that in the calculation of U_d.

Table 7-14. System strain energies for the M-Bridge in both undamaged condition (U_0) and damaged conditions (U_d)

Member removed in a no-load condition	$U_{0,ult}$ (in-k)	U_d (in-k)	$\Delta U = U_0 - U_d$ (in-k)	$U_{0,d}$ (in-k)	$U'_d = U_d / U_{0,d}$ (in-k)
U1U2	693	91	601	466	0.20
U2U3	693	121	572	533	0.23
U1L0	693	165	528	358	0.46
U3U4	693	219	474	399	0.55
U1L2	693	376	317	508	0.74
U2L2	693	456	237	570	0.80
L3L4	693	543	150	590	0.92
L2L3	693	543	150	630	0.93
L1L2	693	586	107	638	0.94
U2L3	693	601	92	574	0.95
L0L1	693	612	81	645	0.95
U0L0	693	612	81	652	0.94
U1L1	693	619	74	687	0.90
U3L3	693	682	11	687	0.99
U3L4	693	691	2	694	1.00

Notes:

- $U_{0,ult}$ in the second column is calculated on the undamaged structure when it is carrying full dead loads and 1.63 times of the HL-93 loads. This loading condition represents the ultimate load capacity of the undamaged structure;

- U_d in the third column represents the strain energy for a damaged structure when it reaches the ultimate state;

- $U_{0,d}$ in the fifth column is calculated on the undamaged structure when it is carrying the loads at which the ultimate state of the corresponding damaged structure is reached. This means that the loading condition in the calculation of $U_{0,d}$ is the same as that in the calculation of U_d.

In the second step of the strain energy approach, the critical members were prioritized based on the values of strain energy release (ΔU). The damaged structures are shown in Table 7-13 and

Table 7-14 in descending value of the strain energy releases. The goal of this arrangement was to indicate that one member would be considered more critical than another if the strain energy release due to the loss of this member was higher, as failure of the most critical member was expected to exert the greatest system effect. In addition, the last column in Table 7-13 and Table 7-14 also indicates that failure on the most critical member basically leads to the most significant reduction of strain energy from the undamaged structure to the damaged structure under the same loading condition.

In Table 7-15 and Table 7-16, the ranking of critical members based on ΔU are compared with that obtained from the rating factor method.

Table 7-15. Critical member prioritization results using load rating factor compared with the prioritization results based on strain energy release for the I-35W Bridge

Load rating factor (column 1 in Table 7-9)	Strain energy release (column 1 in Table 7-13)	Difference in terms of relative ranking (column 1 in this table as a baseline)
U8L9	U8L9	0
U10L9	U10L9	0
L8L9	U8L8	-1
U10L11	L8L9	-1
U8L7	U10L11	-1
U12L11	U8L7	-1
U8L8	U12L11	4
L7L8	L7L8	0
U6L7	U6L7	0
U12L13	U12L13	0
L11L12	L13L14	-1
L13L14	L11L12	1
U8U9	U8U9	0
U7U8	U7U8	0
L9L10	U13U14	-5
U14L13	L6L7	-6
U10U11	U10U11	0
U13U14	U4L5	3
U4L5	U6L5	1
L6L7	L9L10	4
U6L5	U9L9	2
U10L10	U14L13	-1
U9L9	U10L10	2

Table 7-16. Critical member prioritization results using load rating factor compared with the prioritization results based on strain energy release for the M-Bridge

Load Rating Factor (column 1 in Table 7-10)	Strain energy release (column 1 in Table 7-14)	Difference in terms of relative ranking (column 1 in this table as a baseline)
U1U2	U1U2	0
U2U3	U2U3	0
U1L0	U1L0	0
U3U4	U3U4	0
U1L2	U1L2	0
U2L2	U2L2	0
L3L4	L3L4	0
L2L3	L2L3	0
L1L2	L1L2	0
U2L3	U2L3	0
L0L1	L0L1	0
U0L0	U0L0	0
U1L1	U1L1	0
U3L3	U3L3	0
U3L4	U3L4	0

As seen from Table 7-15, the two different methods gave very similar ranking results. The differences in ranking occur on the less critical members. In Table 7-16, no differences were found for the M-Bridge studies. Thus the prioritization of critical members can be implemented through either the rating factor method or the strain energy method. Although the former merely considered the strength effect of a system, it still predicted a similar prioritization result as well as the latter one, which accounted for a combined effect of both strength and stiffness of a system. This fact implies that the strength effect played a dominant role in the prioritization of critical members at

least for these two example bridges. One can infer that using a strength based approach alone that focuses on the load capacity of a system can be sufficient for evaluating the system effect due to failure of one critical member. Moreover, as the strain energy concept is not emphasized in most bridge engineering practice and the energy calculation seems to be more complicated than the load calculation, the strain energy method will not be used for rating the critical members for the other truss bridges that will be studied in the remainder of this research. However, this methodology may be useful for structures with geometries and member strength distributions significantly different from a truss bridge.

7.6.3 Additional Findings from the Strain Energy Measures

In addition to the strain energy method, the individual member strain energy can also be used as a measure in the identification of a subsequent damage after one critical member was removed from the system. It was found that the most critical remaining main truss member kept absorbing the greatest member strain energy from the work done by the applied loads raising after failure on the first member occurred. This result implies that the first failure location could be predicted by tracking the maximum strain energy position without the need to actually load the structure up to the ultimate failure state.

As a trial to explore the feasibility of using the system plastic strain energy as a measure of rating critical members, the system plastic strain energy in ABAQUS models for the I-35W Bridge was studied. The reason to select the ABAQUS models is that one of the advanced features available in ABAQUS, but not in SAP2000, is the calculation of both the elastic and plastic strain energy for a set of members selected by the user.

As shown in Table 7-9, the ultimate states of some damaged structures were connection failure. As this failure mode was not incorporated in the system models developed in ABAQUS, these damaged structures were not included in this plastic strain energy study. Considering that the ultimate state of the rest of damaged structures were member failure on the main truss structure, the strain energy output from the ABAQUS models for these damaged structures was focused on the main truss members. To attain a better sense of the extent of member plasticity to the overall main truss system, a plasticity ratio (PR) was utilized:

$$PR = U_{plastic} / (U_{plastic} + U_{elastic}) \quad (7\text{-}1)$$

where

$U_{elastic}$=the sum of elastic strain energy for each main truss member;

$U_{plastic}$=the sum of plastic strain energy for each main truss member;

Furthermore, to investigate the effect of plastic strain energy on the system load carrying capacity, the *PR* versus the fraction of HL-93 load plus the full dead load are plotted in Figure 7-36 and Figure 7-37.

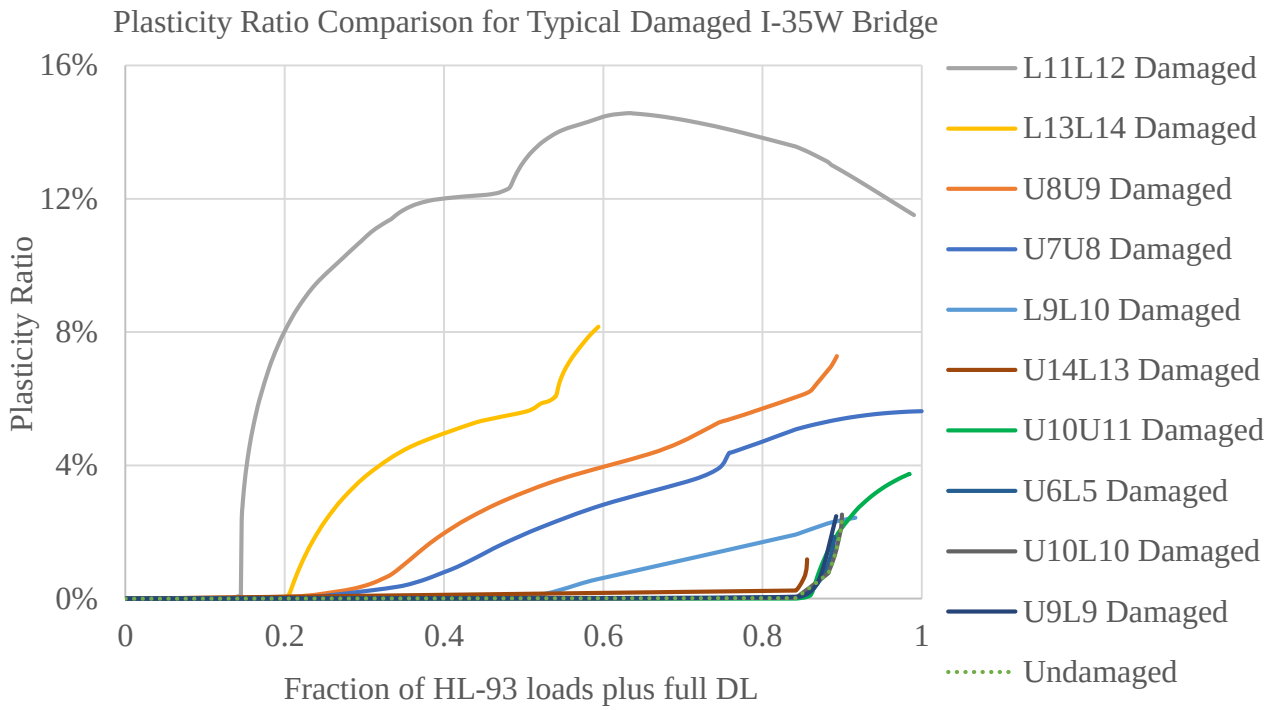

Figure 7-36. Comparison of the curves for the plasticity ratio versus loads on the ABAQUS models for the I-35W Bridge both in undamaged and damaged conditions

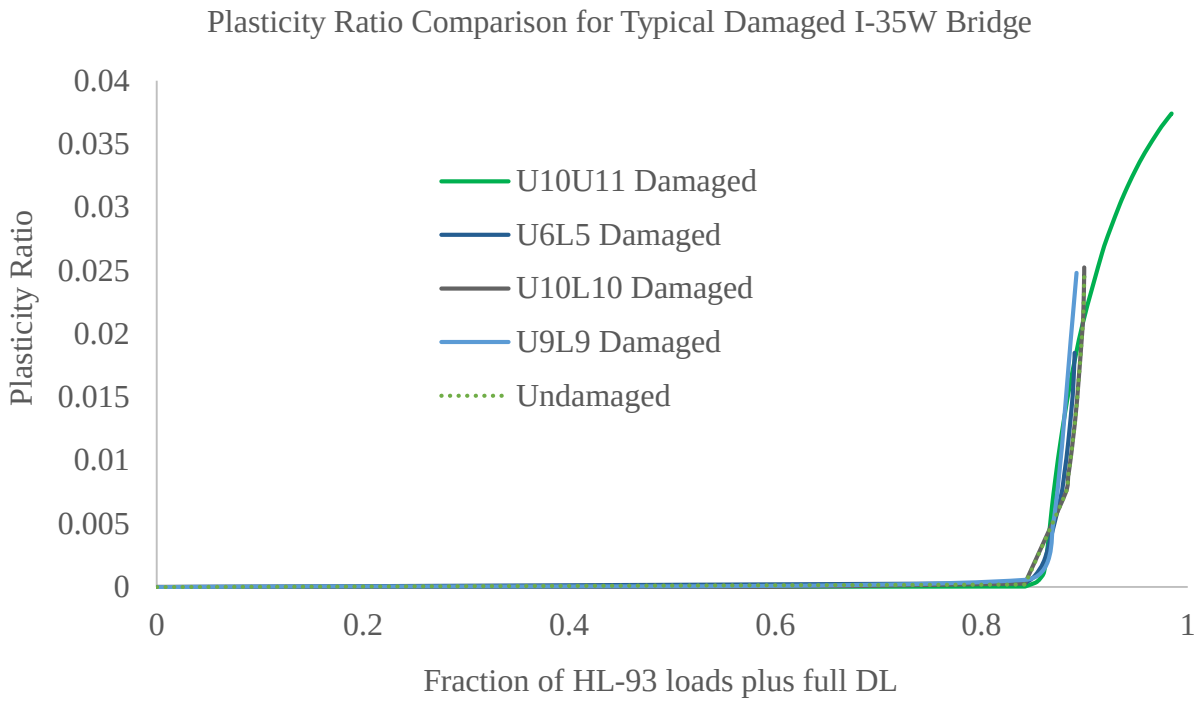

Figure 7-37. A close-up view for the cases: U10U11-damaged, U6L5-damaged, U10L10-damaged, U9L9-damaged, and Undamaged as plotted in Figure 7-36

Since the plasticity ratio can be used as an indicator of damage in a structural system, the first non-zero plasticity ratio will represent the onset of damage on the most critical member. In the damaged structures selected in this plastic strain energy study, the plastic behavior did not develop until the most critical remaining member started buckling. As it was expected that the system ultimate load capacity would be reached when the most critical remaining member began to buckle, it can be assumed that the initiation of plastic behavior is associated with the ultimate load capacity of a system. Following this assumption, the load factor that reflected a system ultimate load capacity was determined to be associated with the first non-zero plasticity ratio on each of the curves plotted in Figure 7-36 and Figure 7-37. Thus to prioritize the damaged structures, the load factor of each model was tabulated in an ascending order in Table 7-17.

Table 7-17. Prioritization of a selected number of critical damaged structures for the I-35W Bridge using load factors determined by the plastic strain energy based approach and the load rating method

Member being removed in a no load condition	Load factor associated with the first non-zero plasticity ratio based on ABAQUS models	Load factor determined using the load rating method based on SAP2000 models (selected from column 3 in Table 7-9)
L11L12	0.13	0.14
L13L14	0.18	0.21
U8U9	0.21	0.34
U7U8	0.21	0.40
L9L10	0.48	0.59
U14L13	0.84	0.93
U10U11	0.84	0.96
U6L5	0.84	1.15
U10L10	0.84	1.18
U9L9	0.84	1.19

Table 7-17 also presents the load factors for the damaged structures obtained using the load rating factor method. Although the load factors shown in the second and the third columns were determined using different methods, the trend for these load factors is similar. For the first five cases, the same ranking is found. This result indicates the possibility of extending the application of plastic strain energy to the rating of critical damaged structures. However, due to the limited number of case studies, this plastic strain energy based approach may not be viable for the engineering practice at the present time.

7.7 Redundancy Evaluation for the Damaged Bridge Systems

As stated previously, a proper estimation of the ultimate state of a system needs the consideration of all possible failure modes. In this section, four types of failures are explicitly discussed. At the member level, the axial-flexural interaction failure as well as the buckling failure were simulated via introducing plastic hinges and nonlinear axial springs into each critical truss member. At the connection level, the possible occurrence of either main truss connection failure or main truss to brace connection failure was accounted for by limiting the truss member peak resultant axial force in the system model. At the system level, the existence of plastic damage on deck was examined by comparing the maximum resultant principal stress among all the deck elements with the concrete deck elastic stress limit.

7.7.1 P-M Interaction Failure

To account for the failure due to significant axial-flexural interaction effects, plastic hinges were incorporated at the two member ends of each main truss where large bending moments were more likely to be detected in the damaged structures. The axial and flexural properties of each plastic hinge are shown in Figure 7-20. The curves in this figure reflect the load and moment variation of the hinge before an ultimate limit state was reached. To efficiently identify the failure due to large axial-flexural interaction on the cross section where a hinge was assigned, the ultimate interaction limit defined in FEMA 356 Equation (5-4) was selected from the available interaction surface options provided in SAP2000. In this way, the interaction failure can be observed as the plastic hinge begins to occur in the SAP2000 model. Without the need to manually check the interaction capacities for various cross sections of main truss members, this approach of modeling plastic hinges can be considered time-saving and practical. Although the predicted interaction limit using

the FEMA equation is lower than the actual capacity, it can be considered sufficient in comparing the relative severity of each damaged structure. Hence a reasonable ranking of critical members can be obtained by using such a conservative failure criterion.

7.7.2 Buckling of Truss Member

The buckling failure was simulated by introducing nonlinear axial springs into both main truss and brace members so that the member peak resultant compression force was limited to be no greater than the yield capacity. Since the average slenderness ratio (KL/r) for the truss members is 49 if K=1.0, this slenderness ratio is relatively small as compared to the non-compact limit (KL/r=113 for Grade 50 steel). Thus the member buckling capacity is close to the yield capacity. The force-deformation property of each nonlinear spring normalized by the yield behavior is illustrated in Figure 7-19. The accuracy of critical buckling load prediction in a damaged system model using the curve in Figure 7-19 in SAP2000 was examined by comparing it to the predicted critical member peak compression force in the ABAQUS model, as the ABAQUS program is capable of clearly displaying member post-buckling deformation.

The comparison results are summarized in Table 7-18. The buckling load comparison focused on the damaged I-35W Bridge after the removal of six chord members one at a time. Failure on these damaged structures are expected to occur due to buckling of one compression main truss member.

Table 7-18. The critical member buckling load comparisons among SAP2000 model results, ABAQUS model results, and the theoretical buckling strength and yield strength

Member removed in a no-load condition	Buckled member	P_{cr}, model (kips)			P_{cr}, theoretical (kips)	
		SAP	ABAQUS	SAP / ABAQUS	K=0.5	K=0.85
L13L14-W	L10L11-W	2770	3054	0.91	3084	2838
L11L12-W	L10L11-W	2755	3060	0.90	3084	2838
U10U11-W	L10L11-W	2675	3035	0.88	3084	2838
L9L10-W	L9L10-E	2874	2951	0.97	3084	2838
U7U8-W	U10U11-W	2934	3297	0.89	3442	3164
U8U9-W	U10U11-W	2947	3324	0.89	3442	3164

From Table 7-18, it can be seen that acceptable correlation exists in the results between the SAP2000 and ABAQUS models for each damaged case. This fact enhanced the level of confidence of using the nonlinear springs in the SAP2000 models to capture the buckling failure of truss members. To further justify the results from the ABAQUS models, the predicted buckling loads were compared with the theoretical buckling strengths based on an effective length factor of 0.5, as in the system model the main truss members were rigidly connected to one another assuming perfect fixed end conditions. It can be seen that the predicted buckling loads from ABAQUS models were close to the theoretical values. Moreover, as suggested by Ziemian (2010), a factor of 0.85 may be used for the compression chord if this truss member was continuously spanning across two panels. This condition represents the status of the buckled members in each damaged case in Table 7-18. Interestingly, it was found that the theoretical buckling loads calculated using a K factor of 0.85 were much closer to the predicted buckling loads in the SAP2000 models. This could further validate the results from SAP2000 models.

The initial imperfection on each truss member was determined to have an insignificant effect in the prediction of member critical buckling load. The maximum buckling strength reduction due to the introduction of an initial imperfection was merely 1.8% among the four buckled chord

members in the second column of Table 7-18. In the imperfection sensitivity studies, the out-of-straightness of the chord members were assumed to reach the maximum allowable value of L/1000 per the applicable ASTM A6 Standard (ASTM 2010).

7.7.3 Connection Failure

For the sake of computational efficiency, the truss member connection details were not simulated in the 3D system models constructed so far. To incorporate the consideration of connection failure into a system model, a two-step approach was implemented.

First, the load capacity for each truss member connection was determined through calculation of the unfactored nominal strength for the particular connection layout. This unfactored nominal strength was the minimum ultimate load capacity provided by the governing failure mode out of the possible failure modes. The main failure modes on a gusset plate include Whitmore section failure, bearing or tear out of the gusset plate, Block shear failure, gross section yielding, and net section rupture for tension member connections. Although buckling failure may also occur on a gusset plate if it is underdesigned, the incorporation of this failure is out of the scope of this research, assuming no design flaw existed in these example bridges. The failure modes that could occur on a rivet were shear rupture, tensile rupture, and shear-tension interaction failure. The tensile force on rivets in the two example truss bridges was caused by out-of-plane flexural deformation on the truss member connection. Since the out-of-plane bending moments were found to be on an average of an order of magnitude less than the in-plane bending moments at the critical truss connections among all the damaged cases, the tensile force was not expected to contribute to the failure on a rivet. Therefore shear rupture was determined as the controlling failure mode on rivets. It is also worth noting that in calculating the shear rupture limit the ultimate shear stress was determined as 0.75 times of the nominal tensile stress of 60ksi as suggested by Schenker et al.

(1954). After the calculation of the ultimate capacity for each failure mode, it was found that gusset plate Block shear would occur first on the truss member connections in the I-35W Bridge, while in the M-Bridge rivet shear rupture failure would control the truss member connection capacity. The typical connection layouts for the I-35W Bridge and the M-Bridge are presented in Figure 7-38.

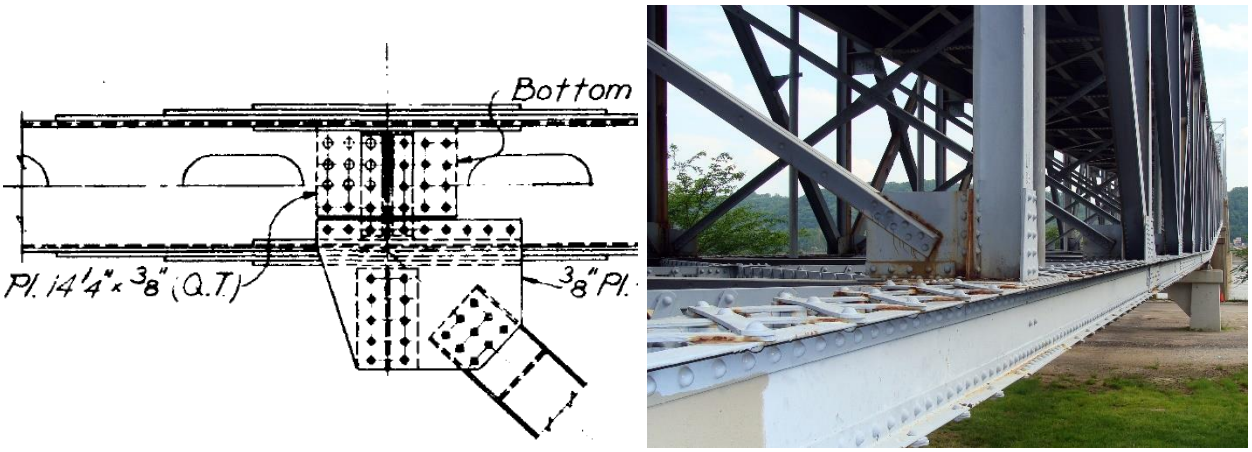

(a) (b)

Figure 7-38. Truss member connection details: (a) A shop drawing for a typical main truss to lower brace connection in the I-35W Bridge. Sverdrup & Parcel and Associates Inc. (1965). State of Minnesota Department of Highway Construction Plan for Bridge No. 9340 – Balance of Bridge and Approaches. St. Louis, MO. Used under fair use, 2015; (b) A photo showing a typical main truss connection and a typical main truss to sway brace connection in the M-Bridge (http://www.purdue.edu/newsroom/research/2011/110726ConnorBridge.html)

The effect of truss member connection failure was incorporated into the system models in SAP2000 by assigning tension and compression limits to selected members, whose connection capacities were less than the member yield strength. The reason to compare the connection capacity with the member yield strength alone came from the concern that before a load analysis one could hardly predict whether a particular member would be in tension or in compression. Hence if the connection capacity was higher than the member yield capacity, then there would be no possibility to see a connection failure prior to a member failure. Even if a member were to carry compression forces in the system under a particular load condition, the compression limit defined

herein would not affect the prediction of buckling failure on this member as long as a previously described nonlinear axial spring was assigned to this member.

The strength comparison results for the I-35W Bridge show that the member failure on the main truss will occur prior to a connection failure, while the failure on a typical main truss to brace member connection would occur before the yielding behavior began to develop in a brace member. Thus the tension and compression limits were applied to the brace members in the system models for the I-35W Bridge.

For the M-Bridge, the source that provided most information about the truss member connection details were from the photos taken on site as no structural drawings with plate dimensions were available. Thus the gusset plate dimensions were not clear. Based on engineering judgement, the governing failure mode at each truss member connection was assumed to be shear rupture on the rivets. A further comparison between the connection capacity and the truss member capacity reveals that the main truss connection failure would occur earlier than the onset of yielding on a main truss member. Brace member failure due to either yielding or buckling would control as the connections between braces and main trusses had higher ultimate capacities than the brace member yield strength.

7.7.4 Damage on Deck

The reinforced concrete decks in the two example bridges were considered in a damaged condition when nonlinear behavior such as cracking and crushing on the deck could be identified. The existence of nonlinear behavior on the deck was examined through checking the maximum principal stresses on the deck in each bridge system model. If the maximum principal stress exceeded the tensile stress limit, then there would be a need to introduce the effect of plastic damage on the deck to the system model.

In the models for I-35W Bridge the deck elements were assigned an equivalent elastic modulus to represent the smeared properties of the 4ksi plain concrete with Grade 40 reinforcing steel. This equivalent modulus of elasticity was verified by drilling a number of cores from above through the entire depth of the deck. When drilling these cores, reinforcing steel was encountered. This indicates that the property of each core could represent the smeared property of reinforced concrete deck. The average test value of the equivalent modulus of elasticity was 4800 ksi, which gave rise to a 7.09 ksi compressive strength as well as a 0.63 ksi tensile strength of the reinforced concrete per ACI 318-11 Section 8.5.1. Based on the assumption that concrete will remain linear elastic until one half of its compressive strength was reached in compression and until its full tensile strength is reached in tension, the elastic stress limits of the smeared reinforced concrete were thereby determined as 3.55 ksi in compression and 0.63 ksi in tension. Then these elastic limits were compared with the maximum principal stresses on the deck in each damaged case. The tabulated results were presented in Table 7-19.

Table 7-19. Comparison between the maximum principal stresses on decks in the system models and the elastic stress limits of the smeared reinforced concrete deck in the I-35W Bridge

Member removed in a no-load condition	$\sigma_{c,max}$ (ksi)	$\sigma_{c,elastic}$ (ksi)	$\sigma_{t,max}$ (ksi)	$\sigma_{t,elastic}$ (ksi)
U8L9	0.62	3.55	0.12	0.63
U10L9	0.36	3.55	0.14	0.63
L8L9	0.35	3.55	0.08	0.63
U10L1	0.46	3.55	0.15	0.63
U8L8	0.77	3.55	0.49	0.63
U8L7	0.33	3.55	0.13	0.63
U12L11	0.49	3.55	0.13	0.63
L7L8	0.54	3.55	0.16	0.63
U6L7	0.47	3.55	0.15	0.63
U12L13	0.61	3.55	0.17	0.63
L11L12	0.56	3.55	0.17	0.63
L13L14	0.40	3.55	0.14	0.63
U8U9	0.31	3.55	0.18	0.63
U7U8	0.35	3.55	0.13	0.63
L9L10	0.35	3.55	0.14	0.63
U14L13	0.40	3.55	0.14	0.63
U10U11	0.31	3.55	0.13	0.63
U13U14	0.29	3.55	0.18	0.63
U4L5	0.39	3.55	0.16	0.63
L6L7	0.38	3.55	0.22	0.63
U6L5	0.43	3.55	0.32	0.63
U10L10	0.41	3.55	0.13	0.63
U9L9	0.42	3.55	0.14	0.63

From the above stress comparison, it was clear that the deck behavior on each damaged structure was still elastic. This reflected that the removal of one critical member did not cause plastic damage on the deck. Therefore, it can be considered sufficient to model reinforced concrete decks with elastic properties for the I-35W Bridge system in a damaged condition.

In the M-Bridge system models, 4ksi plain concrete properties were used for the deck so that the predicted main truss member stresses can be better calibrated to the measured data in the field test. The effect of reinforcing steel is accounted for through using an equivalent plain concrete deck

with an increased deck thickness. This equivalent deck was determined such that it can provide the same weight of the reinforced concrete deck. With 4ksi plain concrete being selected, the deck elastic stress limits were determined as 2ksi in compression and 0.47ksi in tension. Then the stress comparison was performed for each damaged structure and tabulated in Table 7-20.

Table 7-20. Comparison between the maximum principal stresses on decks in the system models and the elastic stress limits of the plain concrete deck in the M-Bridge

Member removed in a no-load condition	$\sigma_{c,max}$ (ksi)	$\sigma_{c,elastic}$(ksi)	$\sigma_{t,max}$ (ksi)	$\sigma_{t,elastic}$(ksi)
U1L0	-0.21	2	0.08	0.47
U1U2	-0.23	2	0.01	0.47
U2U3	-0.33	2	0.01	0.47
U3U4	-0.35	2	0.01	0.47
L3L4	-0.27	2	0.03	0.47
L1L2	-0.25	2	0.03	0.47
L0L1	-0.26	2	0.03	0.47
U1L2	-0.31	2	0.09	0.47
U2L3	-0.30	2	0.02	0.47
L2L3	-0.29	2	0.05	0.47
U0L0	-0.23	2	0.03	0.47
U1L1	-0.28	2	0.06	0.47
U3L3	-0.26	2	0.04	0.47
U3L4	-0.21	2	0.01	0.47

Similarly, it can be found that the deck remain elastic even after losing one critical member from the system. It was thereby believed that modeling the deck elements with elastic properties alone would be adequate to properly capture the deck behavior in a damaged system.

7.7.5 Investigation of Ultimate State for Damaged Bridge Systems

After incorporating the aforementioned features to the bridge models in SAP2000, it was anticipated that the ultimate state of a bridge system could be captured as the first component reached its ultimate strength capacity. To verify that the occurrence of first component failure will

lead to the failure of an entire structural system, the behavior of each example bridge system in its ultimate state is investigated and discussed below.

7.7.5.1 I-35W Bridge

Since a highly detailed finite element model for the entire bridge system had been developed in ABAQUS and this model was validated in Section 3.4, the load-deformation behavior of this bridge modeled in SAP2000 can be compared with the predicted results from the ABAQUS model as an attempt to vet the accuracy of the SAP2000 model with the nonlinear features. To examine the correlation of load-deformation behavior of a bridge system between the SAP2000 and the ABAQUS models, the total loads carried by each structural system versus its mid-span deflection was plotted from Figure 7-39 to Figure 7-49. Noted that the damaged structures whose ultimate failure occurred at the connections between braces and main trusses were not included herein, because the connection failure was not incorporated in the system models developed in ABAQUS. The following remarks apply to the data shown in Figure 7-39 to Figure 7-49:

- The end of each curve represented the moment when SAP2000 failed to obtain a solution to satisfy equilibrium;
- The mid-span deflection is limited to span length/100 (i.e. 4.56ft for the center span of the I-35W Bridge), which is believed to be the maximum visible displacement that a bridge user or an observer can tolerate. The use of this limit is also agreed on by researchers and engineers (Ghosn and Moses 1998);
- The difference in stiffness between dead load and live load (the HL-93 load in this case) is due to the differences in load position and magnitude, not inelastic action;
- In each damaged system, the curve for the SAP model with two members damaged represents the load-deformation behavior of a system with the removal of the member shown in the title

of each plot as well as the member displayed in the legend, which is the most critical remaining member in the damaged system with a single member out.

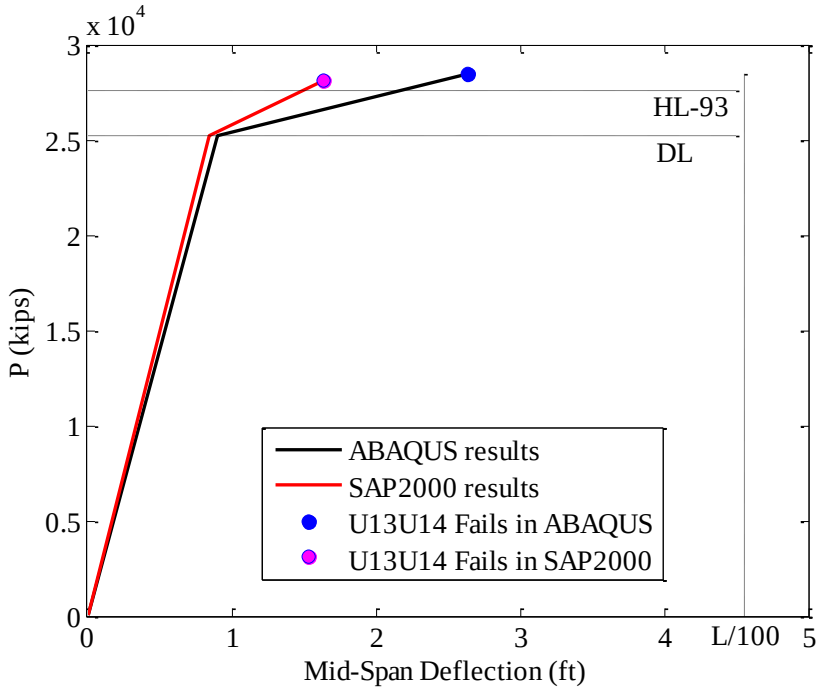

Figure 7-39. System load versus mid-span deflection curves for the I-35W Bridge in an undamaged condition

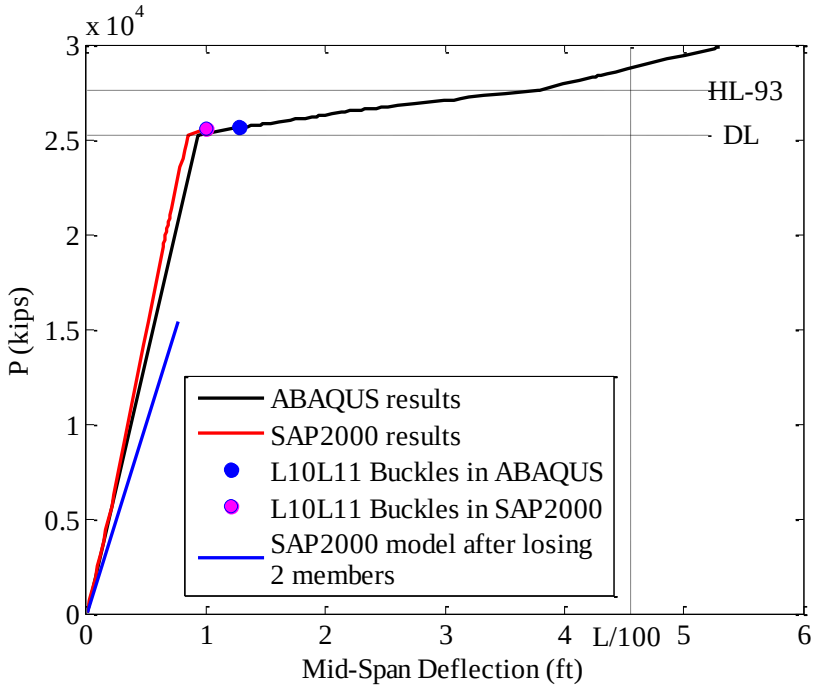

Figure 7-40. System load versus mid-span deflection curves for the I-35W Bridge with an initial damage on member L11L12

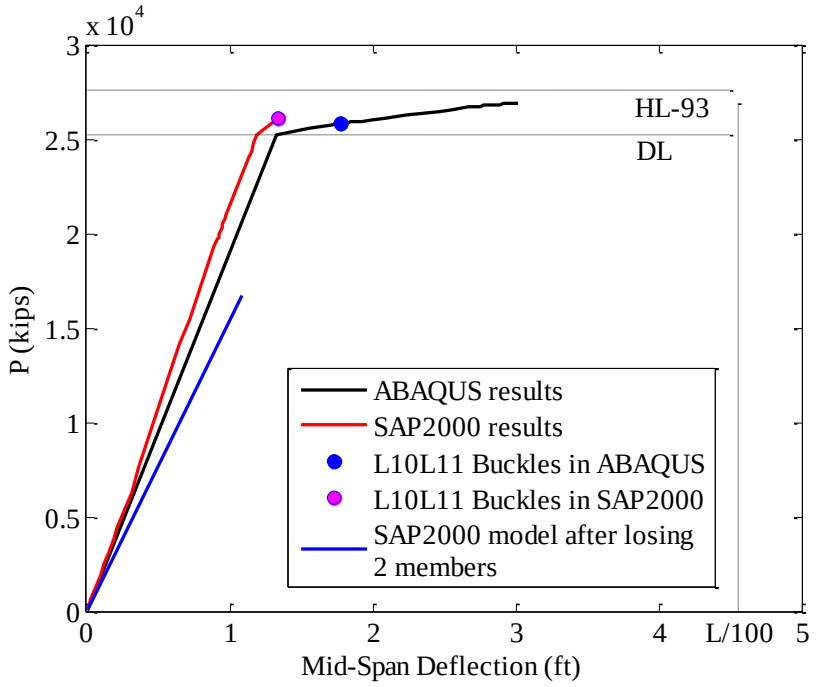

Figure 7-41. System load versus mid-span deflection curves for the I-35W Bridge with an initial damage on member L13L14

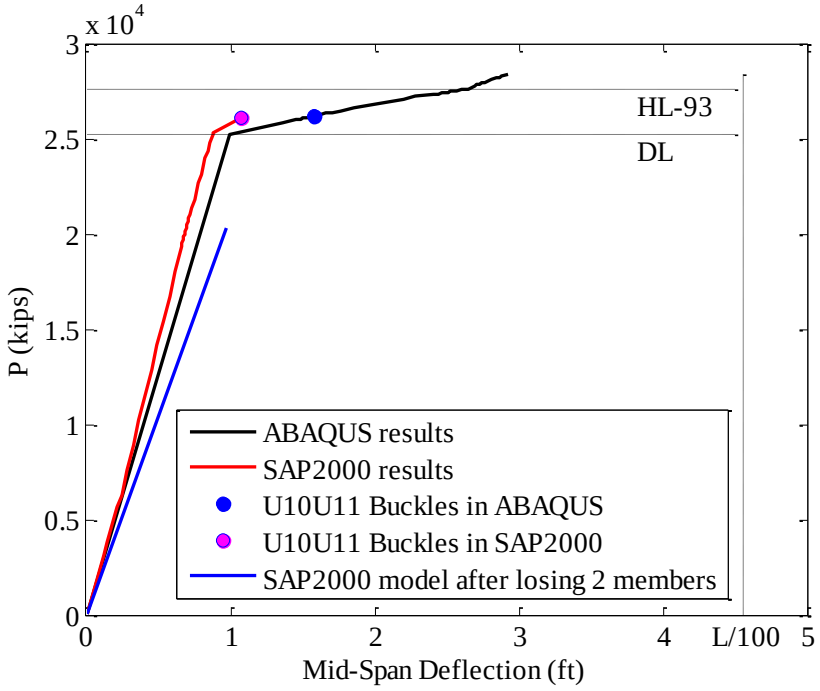

Figure 7-42. System load versus mid-span deflection curves for the I-35W Bridge with an initial damage on member U8U9

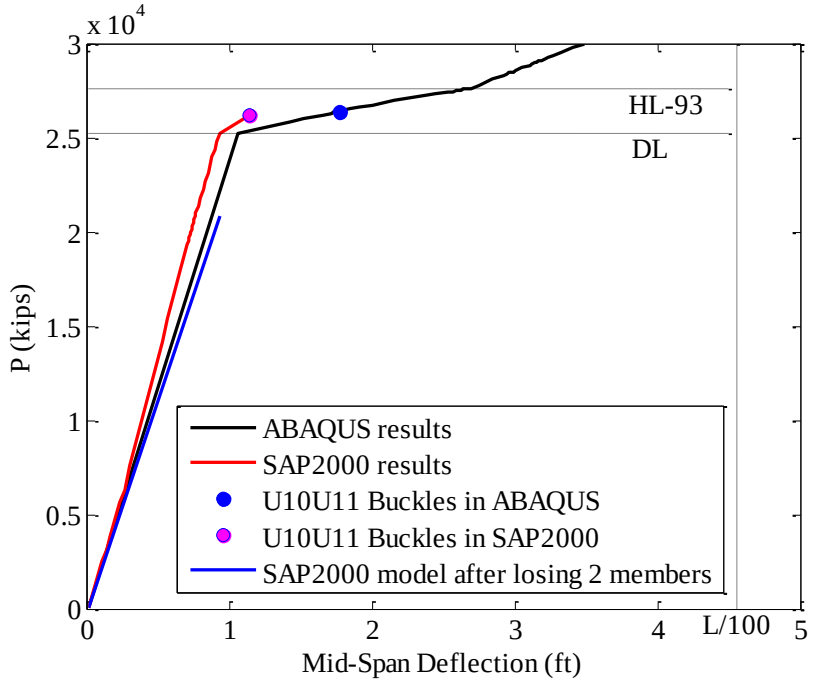

Figure 7-43. System load versus mid-span deflection curves for the I-35W bridge with an initial damage on member U7U8

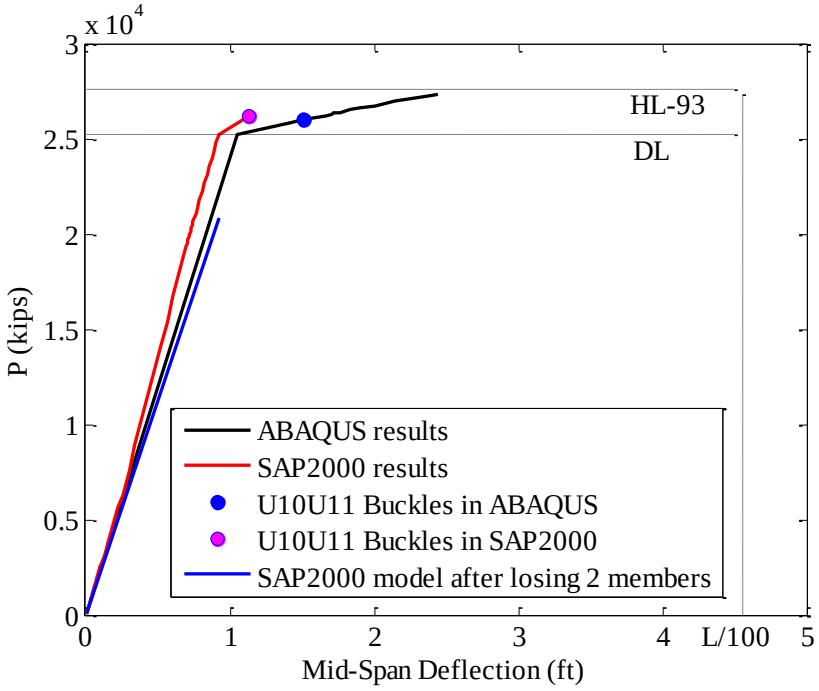

Figure 7-44. System load versus mid-span deflection curves for the I-35W Bridge with an initial damage on member L9L10

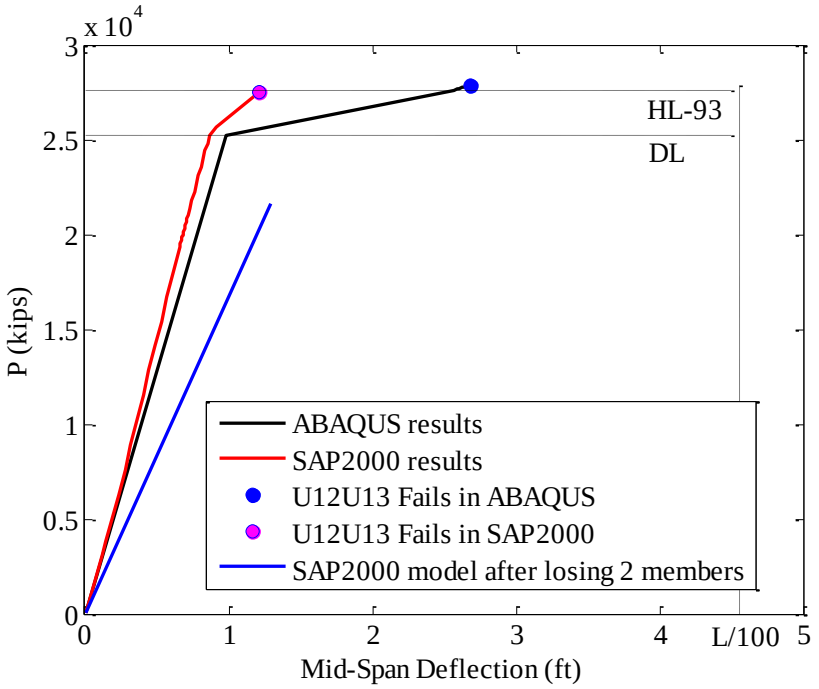

Figure 7-45. System load versus mid-span deflection curves for the I-35W Bridge with an initial damage on member U14L13

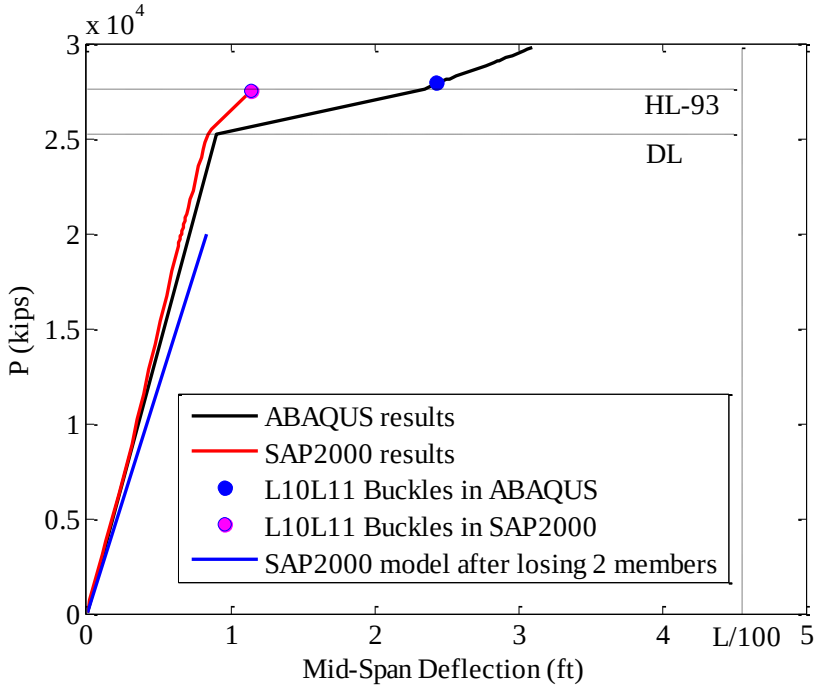

Figure 7-46. System load versus mid-span deflection curves for the I-35W Bridge with an initial damage on member U10U11

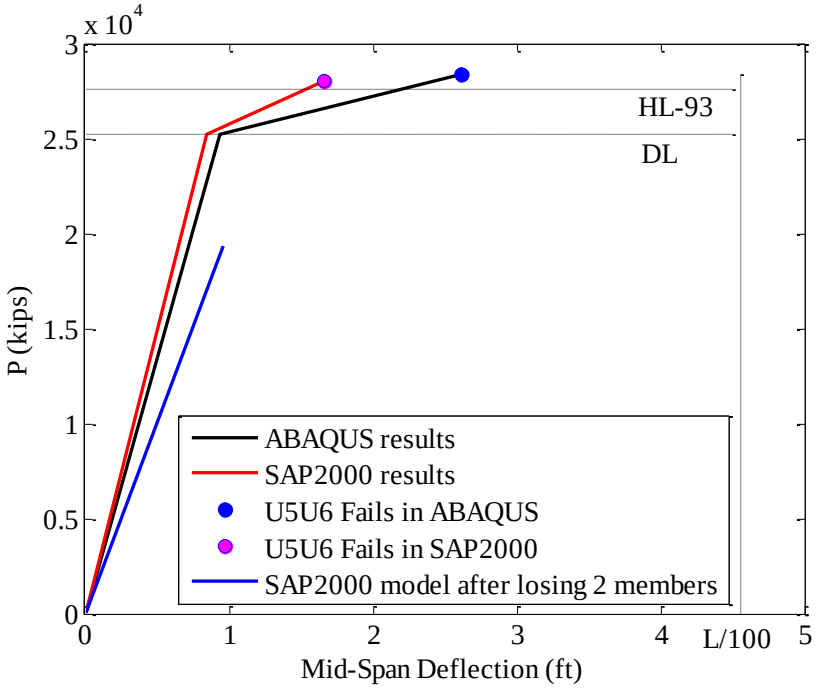

Figure 7-47. System load versus mid-span deflection curves for the I-35W Bridge with an initial damage on member U6L5

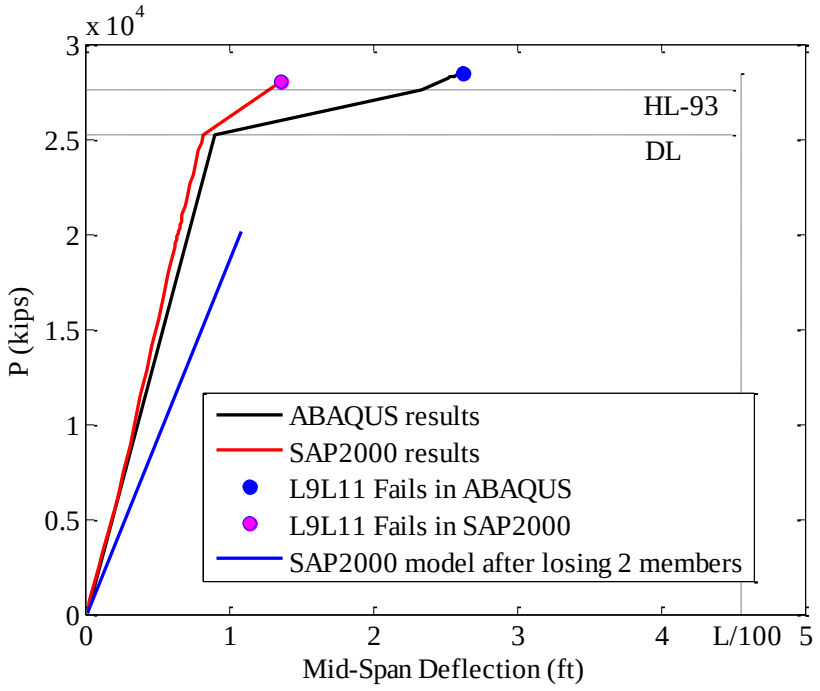

Figure 7-48. System load versus mid-span deflection curves for the I-35W Bridge with an initial damage on member U10L10

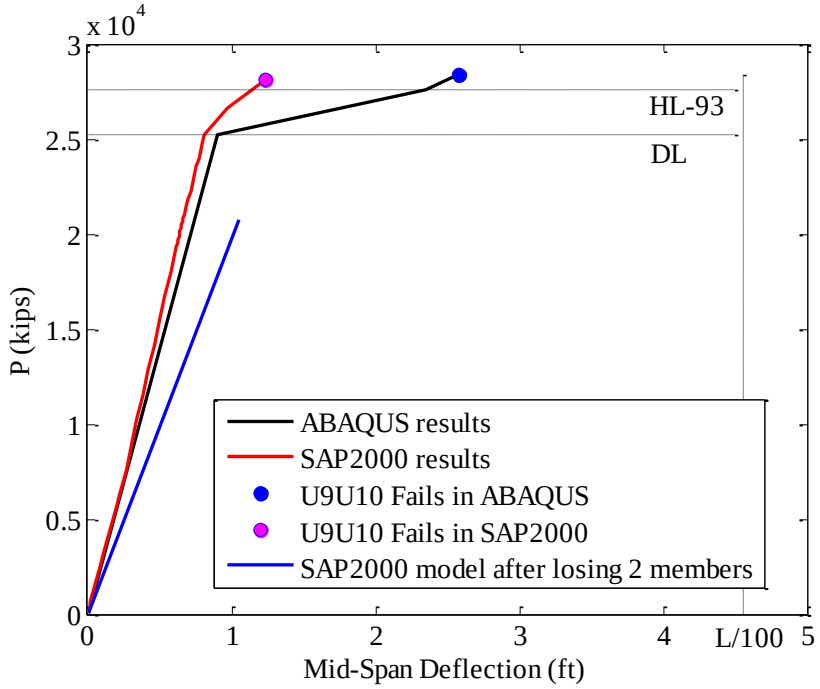

Figure 7-49. System load versus mid-span deflection curves for the I-35W Bridge with an initial damage on member U9L9

It is clear to see from Figure 7-39 to Figure 7-49 that the load-deformation curves predicted from the SAP2000 models have similar slopes to those obtained from the ABAQUS models from a no load condition to a full dead load condition. These figures also show that each SAP2000 model produces a higher stiffness than the corresponding ABAQUS model. This difference is primarily caused by the inability of the SAP2000 models to properly capture the second-order effects on the system especially when it approaches the ultimate state. In addition, the difference of mid-span deflection mainly results from the different approaches of incorporating plasticity to the truss members. In the SAP2000 models the member plastic behavior is lumped at the two ends of each member by assigning two zero-length plastic hinges, while in the ABAQUS models the member plastic behavior is continuously distributed along the member length by assigning plastic properties to the member cross section. As it is believed that ABAQUS has more robust features to properly capture the nonlinear behavior of a complex system, the deformation prediction from SAP2000 models was not considered reliable. Thus the deformation prediction can be regarded as one limitation of the simplified system analysis implemented in SAP2000. It is noted, however, that even the deflections obtained from complex ABAQUS models can only be regarded as providing an approximate bound.

From Figure 7-39 to Figure 7-49, it is also obvious that the mid-span deflection of each system model in the ultimate state was much less than the maximum allowable deflection (L/100). This result confirms that the controlling factor in determining the system ultimate failure was not the excessive deformation but the system strength capacity.

In addition, these figures also show that the load capacity of each system model in its ultimate state when the most critical member begins to fail is similar between the SAP2000 and the ABAQUS

models. The comparison of this ultimate load capacity is presented in percentage terms in Table 7-21.

Table 7-21. System ultimate load capacity comparison between the SAP2000 and ABAQUS models

System model	Results from the SAP2000 model (kips)	Results from the ABAQUS model (kips)	Difference
Undamaged	28125	28492	1.3%
L11L12-Damaged	25587	25661	0.3%
L13L14-Damaged	25753	25833	0.3%
U8U9-Damaged	26061	26199	0.5%
U7U8-Damaged	26204	26387	0.7%
L9L10-Damaged	26654	26922	1.0%
U14L13-Damaged	27461	27837	1.4%
U10U11-Damaged	27532	27905	1.4%
U6L5-Damaged	27983	28350	1.3%
U10L10-Damaged	28054	28493	1.6%
U9L9-Damaged	28082	28381	1.1%

Table 7-21 shows a negligible difference in system ultimate load capacity between the results from the SAP2000 and the ABAQUS models. This indicates a good correspondence between the SAP2000 and the ABAQUS results. Thus the SAP2000 models can be considered capable of predicting a reasonable system ultimate load capacity.

As an attempt to confirm that a bridge system will collapse after failure of the most critical remaining member in a damaged structure with a single member out, the load capacity reduction from an undamaged structure to a structure with two members damaged was investigated and tabulated in Table 7-22.

Table 7-22. Load capacity reduction from an undamaged structure to a structure with two members damaged

Two damaged members	Undamaged system strength (kips)	System with two members damaged	Load capacity reduction
L11L12 & L10L11	28492	15422	46%
L13L14 & L10L11	28492	21808	41%
U8U9 & U10U11	28492	20331	29%
U7U8 & U10U11	28492	20875	27%
L9L10 & U10U11	28492	21219	26%
U14L13 & U13U14	28492	21594	24%
U10U11 & L10L11	28492	19986	30%
U6L5 & U13U14	28492	19335	32%
U10L10 & U13U14	28492	20146	29%
U9L9 & U9U10	28492	20750	27%

As it can be seen from Table 7-22, the load capacity reduction from an undamaged structure to each of the structures with two members damaged is greater than 20%. Thus it is reasonable to expect that a bridge system cannot sustain the required loads after two member have been damaged. In other words, failure on the most critical remaining member in a damaged structure with a single member removed in the initial condition will lead to failure of the bridge system.

7.7.5.2 M-Bridge

As mentioned in Section 7.6.1, the failure mode for the M-Bridge structure both in an undamaged and a damaged condition was in-plane bending on a vertical main truss member. This in-plane bending failure was inferred from the axial-flexural interaction failure, which was observed as the formation of plastic hinges. To confirm that an axial-flexural interaction failure can be considered to occur when the plastic hinge defined by the FEMA 356 Equation (5-4) begins to occur, the interaction behavior of the critical remaining components in the SAP2000 models was studied. The interaction ratio at the location of each plastic hinge was calculated using the FEMA 356 Equation (5-4). Since the two hinges on the same member were found to have approximately the same interaction ratios, the interaction ratio at one of the two hinges is presented from Figure 7-50 to Figure 7-65.

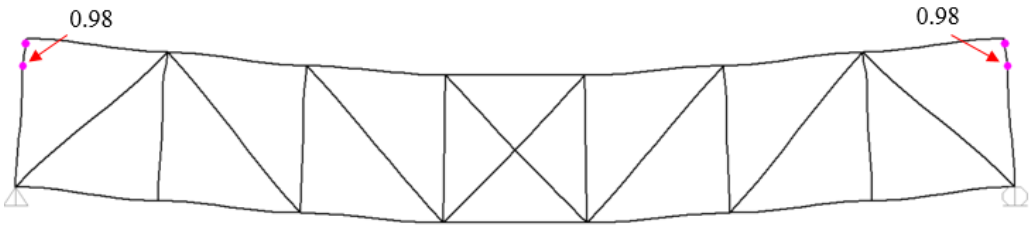

Figure 7-50. 2D view of one main truss of the undamaged M-Bridge model in its ultimate state

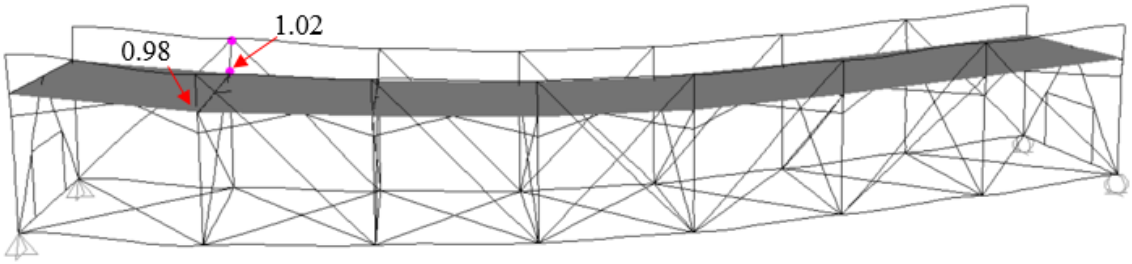

Figure 7-51. 3D view of the M-Bridge model with an initial damage on member U1L0 in its ultimate state

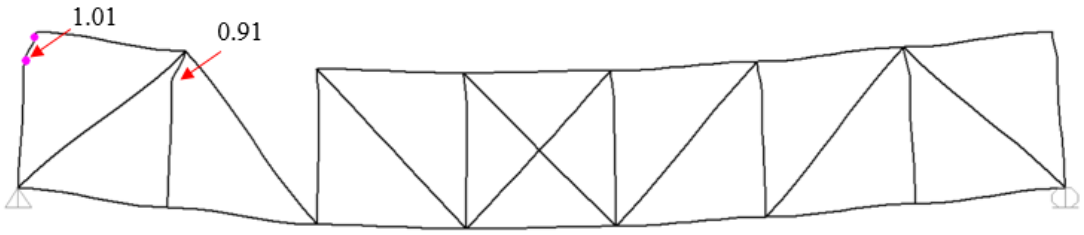

Figure 7-52. 2D view of the damaged side of main truss for the M-Bridge model with an initial damage on member U1U2 in its ultimate state

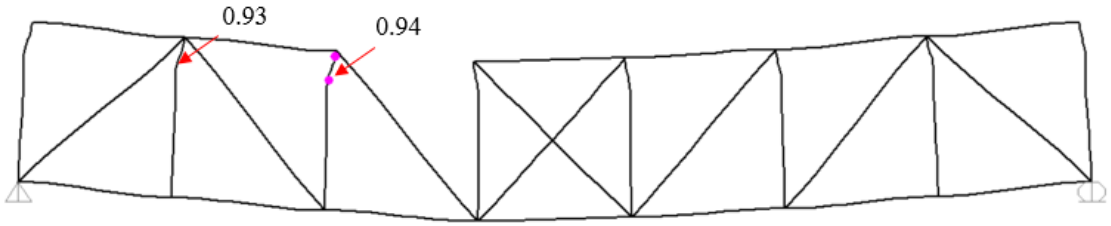

Figure 7-53. 2D view of the damaged side of main truss for the M-Bridge model with an initial damage on member U2U3 in its ultimate state

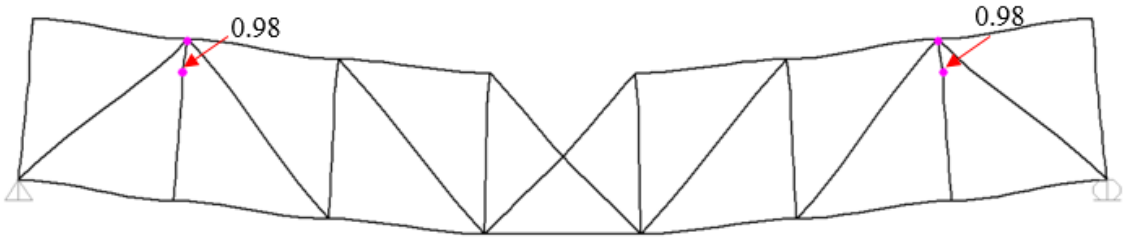

Figure 7-54. 2D view of the damaged side of main truss for the M-Bridge model with an initial damage on member U3U4 in its ultimate state

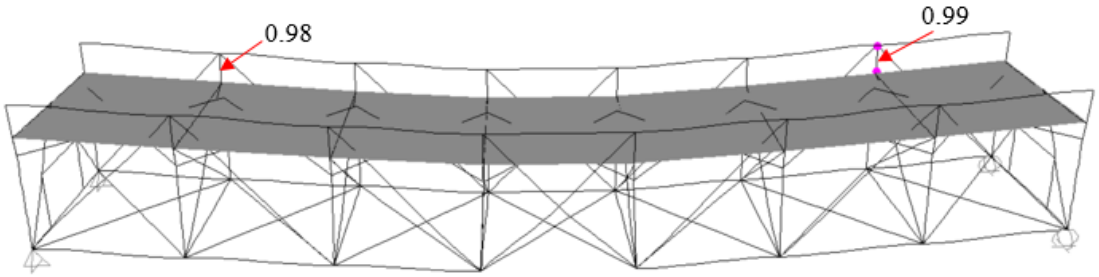

Figure 7-55. 3D view of the M-Bridge model with an initial damage on member L3L4 in its ultimate state

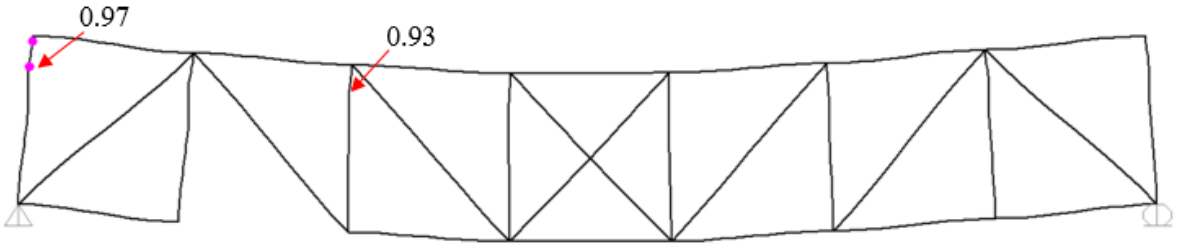

Figure 7-56. 2D view of the M-Bridge model with an initial damage on member L1L2 in its ultimate state

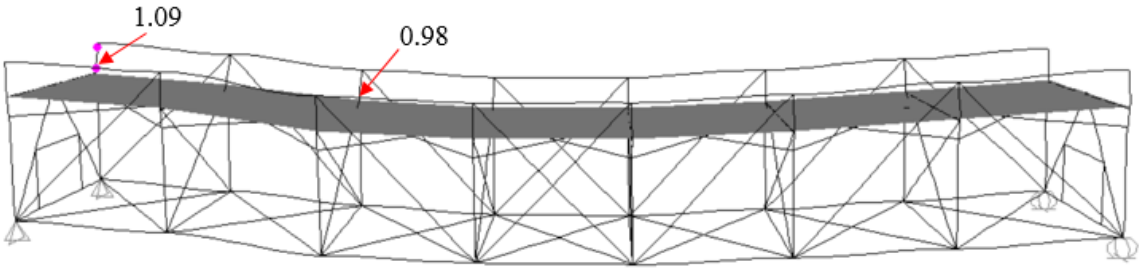

Figure 7-57. 3D view of the M-Bridge model with an initial damage on member U1L2 in its ultimate state

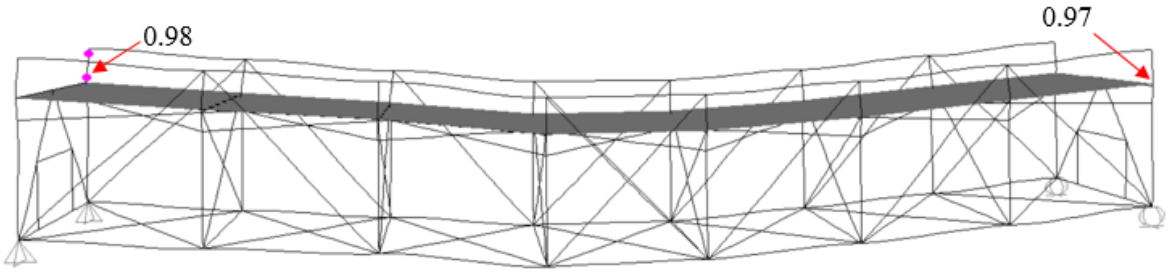

Figure 7-58. 3D view of the M-Bridge model with an initial damage on member U2L3 in its ultimate state

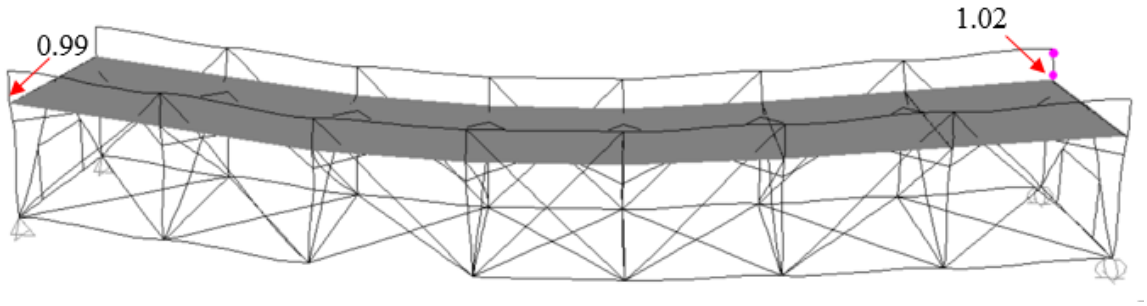

Figure 7-59. 3D view of the M-Bridge model with an initial damage on member L2L3 in its ultimate state

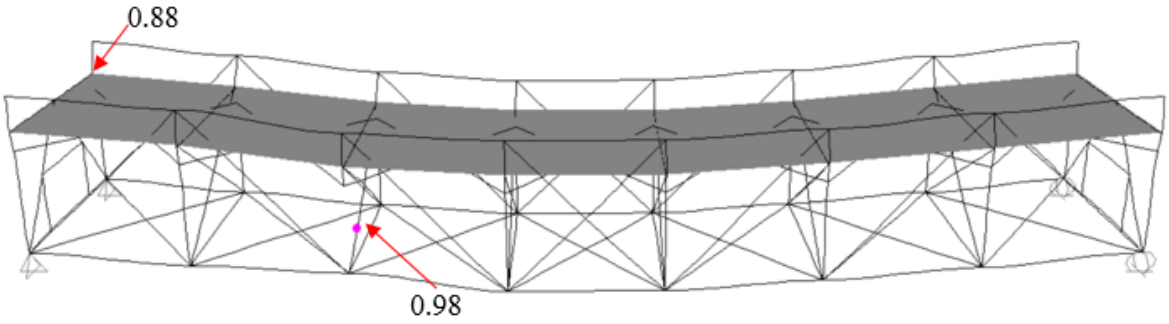

Figure 7-60. 3D view of the M-Bridge model with an initial damage on member U2L2 in its ultimate state

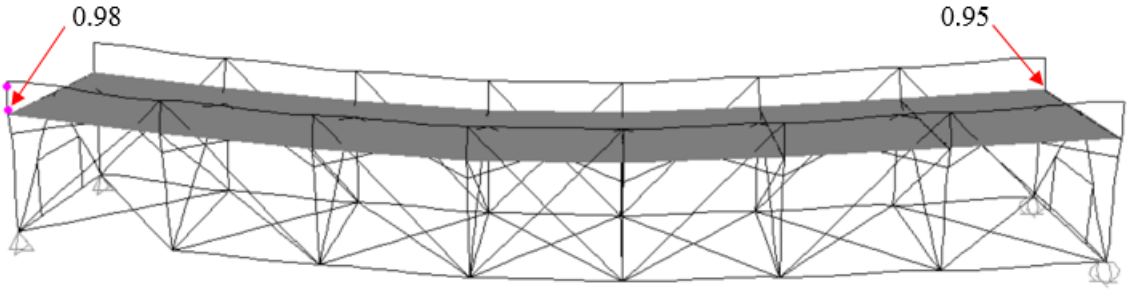

Figure 7-61. 3D view of the M-Bridge model with an initial damage on member L0L1 in its ultimate state

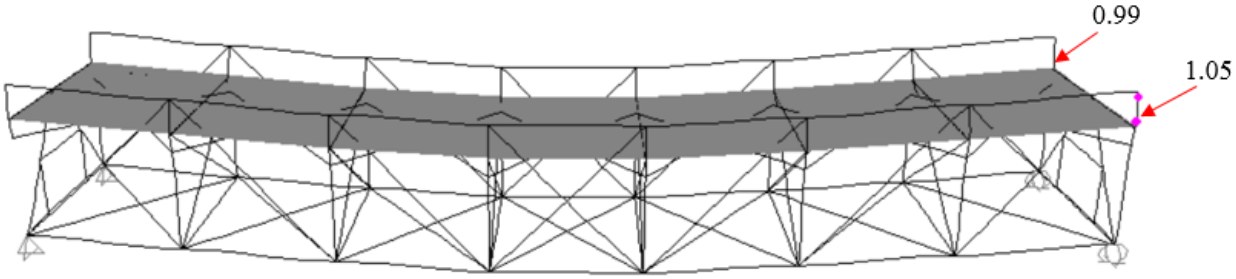

Figure 7-62. 3D view of the M-Bridge model with an initial damage on member U0L0 in its ultimate state

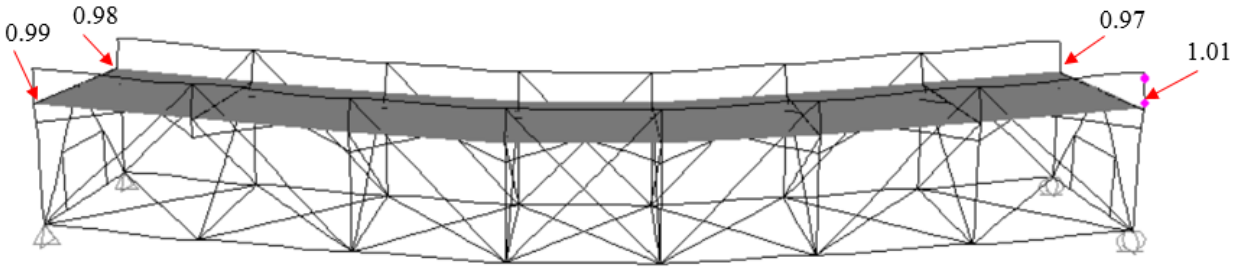

Figure 7-63. 3D view of the M-Bridge model with an initial damage on member U1L1 in its ultimate state

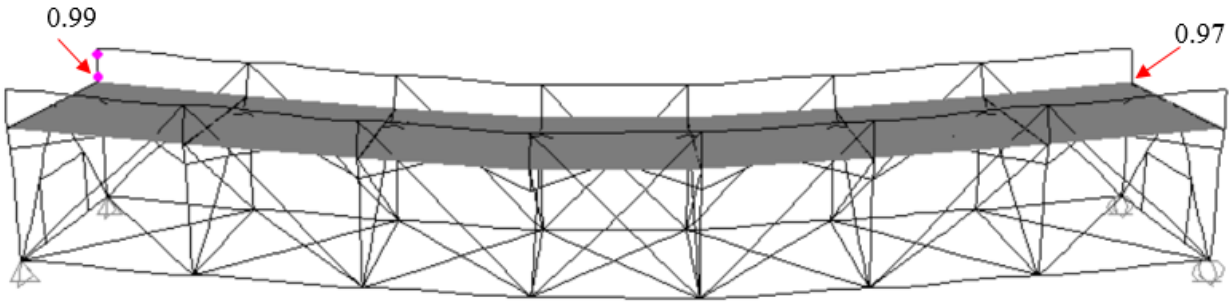

Figure 7-64. 3D view of the M-Bridge model with an initial damage on member U3L3 in its ultimate state

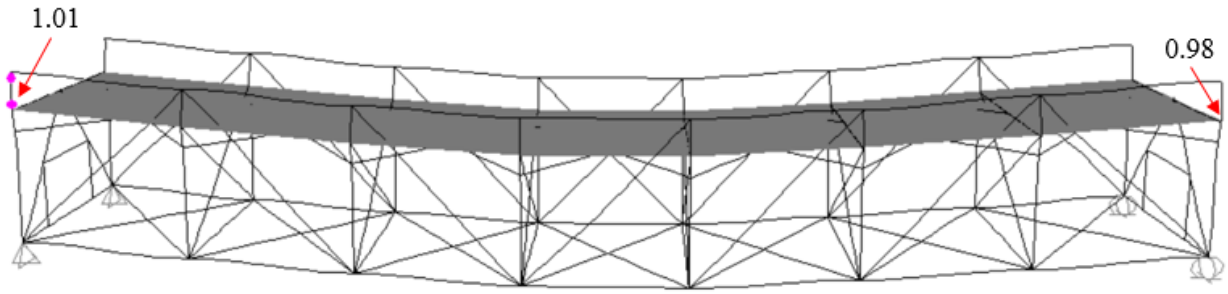

Figure 7-65. 3D view of the M-Bridge model with an initial damage on member U3L4 in its ultimate state

As seen from Figure 7-50 to Figure 7-65, the interaction ratios on the critical remaining members were close to 1, indicating that the interaction limit defined by FEMA 356 Equation (5-4) was reached at the hinge locations.

In the undamaged structure the plastic hinges were observed to form simultaneously on the upper portion of the four vertical main truss members as shown in Figure 7-50 due to symmetry. Since failure on four locations is shown in this figure, it is reasonable to expect that the system ultimate state is reached.

Figure 7-51 reflects the behavior of the structure after losing member U1L0, which was rated as the most critical member. As the interaction ratios on the remaining member U1L1 exceeded 1,

this indicates the loss of two members (U1L0 and U1L1) from the system. System failure was assumed at this point.

It can be seen from Figure 7-52 to Figure 7-65, that in each figure apart from the most critical remaining member where plastic hinges exist, there is one more critical member whose interaction ratio at the critical locations approaches the limit of 1. As the interaction ratios on these two critical members are close to each other, it is likely that these two members fail simultaneously when plastic hinges occur on either member. Therefore, the behavior shown from Figure 7-52 to Figure 7-65 can be considered to represent the system ultimate state. This ultimate state is also confirmed by the fact that the deflections at the mid-span in both undamaged and damaged system models at their ultimate states are much less than the deflection limit for collapse. The maximum mid-span deflection amongst all system models for the M-Bridge is 2.08 inches, while the deflection limit as span length/100 is 17.64 inches.

7.7.6 Examination of the Most Critical Live Load Condition for the Damaged Systems

As explained in Section 7.5, the I-35W Bridge was not sensitive to the variation of live load positions in that the dead load alone comprised 93% of total loads. Therefore, this section will discuss the effect of live load position on the system behavior of the M-Bridge.

For the M-Bridge, a typical simple span bridge, the HL-93 load that consist of lane loads and truck loads are believed to cause the worst system effect (AASHTO 2012). The truck loads positioned at the mid-span are assumed to be critical to the system capacity of an undamaged bridge structure. However, it is unknown if such truck load condition will still lead to the lowest system load capacity of the bridge structure after a particular member is damaged. Ascertaining which location of truck loads will produce the maximum influence on the damaged member, the system load

capacity under this truck load condition was compared with that under the truck loads on the mid-span, as summarized in Table 7-23.

Table 7-23. System load capacity comparison under various truck load conditions

Member damaged in a no load condition	Location of the centroid of truck loads	System Load Capacity	
		Centroid of truck loads applied to the location as shown in Column 2	Centroid of truck loads applied to the mid-span
U1U2	U2	0.85•DL	0.85•DL
U2U3	U3	0.98•DL	0.97•DL
U1L0	U1	0.35•(HL-93)	0.18•(HL-93)
U3U4	M.S.	0.35•(HL-93)	0.35•(HL-93)
U1L2	U2	1.06•(HL-93)	0.83•(HL-93)
U2L2	U2	0.95•(HL-93)	1.09•(HL-93)
L3L4	M.S.	1.11•(HL-93)	1.11•(HL-93)
L2L3	U2	1.51•(HL-93)	1.18•(HL-93)
L1L2	U1	1.72•(HL-93)	1.36•(HL-93)
U2L3	U3	1.48•(HL-93)	1.39•(HL-93)
L0L1	U1	1.89•(HL-93)	1.42•(HL-93)
U0L0	U0	1.46•(HL-93)	1.45•(HL-93)
U1L1	U1	1.62•(HL-93)	1.60•(HL-93)
U3L3	U3	1.61•(HL-93)	1.60•(HL-93)
U3L4	M.S.	1.63•(HL-93)	1.63•(HL-93)

Table 7-23 shows that most damaged systems would carry less load if the truck loads were applied to the mid-span as compared to the case with truck loads applied to cause the maximum influence on the damaged member. One exception is the structure with an initial damaged on the vertical member U2L2. In this damaged structure, it can be seen that the system load capacity under the truck loads at the mid-span is lower than the capacity under the truck loads applied to location that

will cause the maximum influence on the damaged member. Nevertheless, this exception can be considered insignificant considering two facts: (1) the overall ranking results under these two different truck load conditions are similar, indicating that the rating of critical members may not be changed even if the truck loads were moved from the mid-span to the locally critical location; and (2) the only exception that has an initial damage on vertical member U2L2 was not highly critical as the damaged structure can still sustain full dead load plus about one HL-93 load . The difference in the load capacity between these two different truck load conditions is 13%, which can be considered not significant. Therefore, the live load condition with truck loads applied to the mid-span can still be considered most critical to the system both in the undamaged and damaged conditions. Moreover, this live load condition was also used as the most critical loading condition in the system redundancy analyses for a typical simple span truss bridge conducted by Ghosn and Fiorillo (2013).

7.8 A Step-by-Step Procedure for System Redundancy Analyses

(1) As a summary, the proposed procedure for a system redundancy analysis requires the following steps:

(2) Develop a 2D model of the main truss structure;

(3) Determine critical live load position;

(4) Identify critical members with high demand-to-capacity ratios for axial loads;

(5) Model the full 3D bridge system;

(6) Incorporate nonlinear features to the 3D system model;

(7) Create damaged structures by removing the critical members identified in Step 3 as well as all vertical members one at a time from the 3D system model;

(8) Rate the load capacity for the undamaged and damaged 3D systems.

7.9 Application of System Redundancy Analysis Methodology to Two Other Simple Truss Bridges

As an effort to extend the application of the previously proposed methodology for system redundancy evaluation to general truss structures, two other simple truss bridges with different configurations will be studied in this section. Given the fact that most existing truss bridges have not been tested to develop an understanding of the system response to a single member damage, it will be useful to blindly apply the methodology to the truss to see if reasonable outcomes are predicted. The New River Bridge and the Span No.4 of the Milton-Madison Bridge were selected from the available bridge inventory in this research.

7.9.1 New River Bridge

In 1941, the bridge over the New River between Pulaski and Hillsville on Virginia Route 100 was constructed. The bridge is a steel deck truss bridge that carries two traffic lanes. With a total length of 846 ft, the bridge is comprised of two 150 ft main spans over the river and 7 approach spans. The main span truss structure that will be addressed in this research study is shown in Figure 7-66.

Figure 7-66. The main span truss structure of the New River Bridge. Hickey, L. J., et al. (2009). Live Load Test and Failure Analysis for the Steel Deck Truss Bridge Over the New River in Virginia. Report No.: FHWA/VTRC 09-CR8. Virginia Transportation Research Council. Charlottesville, VA. Used under fair use, 2015.

As seen from Figure 7-66, the bridge structure consists of two continuous spans. This structural configuration is different from the I-35W Bridge and the M-Bridge. Therefore, it is useful to conduct system redundancy studies on this particular truss structure to ensure that the previously proposed methodology is still applicable. This bridge had been instrumented and thus some baseline data for comparisons is available (Hickey et al. 2009).

The system redundancy analysis for this bridge was implemented following the steps summarized in Section 7.8 as shown below:

Step 1: Develop a 2D model of the main truss structure

As the first phase of the system redundancy analysis, critical members in a main truss system will be identified using a simplified 2D model that can reflect one line of the main truss structure in its design condition. The 2D model for one of the two symmetric main spans of the New River Bridge developed in SAP2000 is shown in Figure 7-67. This figure also shows the comparison of the resultant axial loads on each main truss member between the SAP2000 model results and the calculated loads on the original design drawing. The ability of the 2D model to properly capture the main truss behavior envisioned in the design condition was confirmed by the fact that the largest difference between the model results and the design values, as shown in Figure 7-68, is merely 6%.

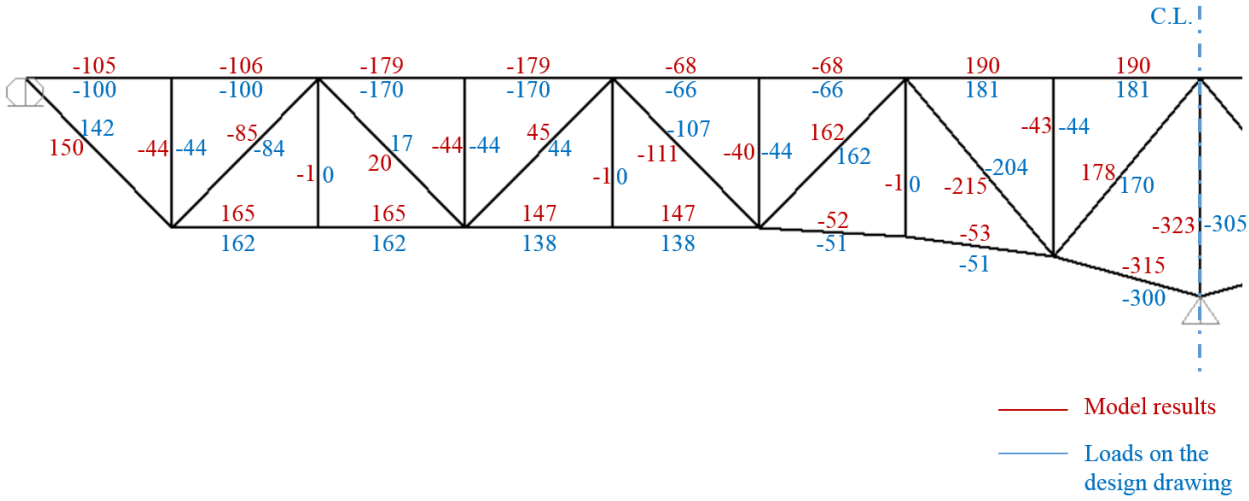

Figure 7-67. Comparison of axial load demand (unit: kips) for the main truss members in the New River Bridge under design dead load between the results from a 2D elastic model and the values on the design drawing

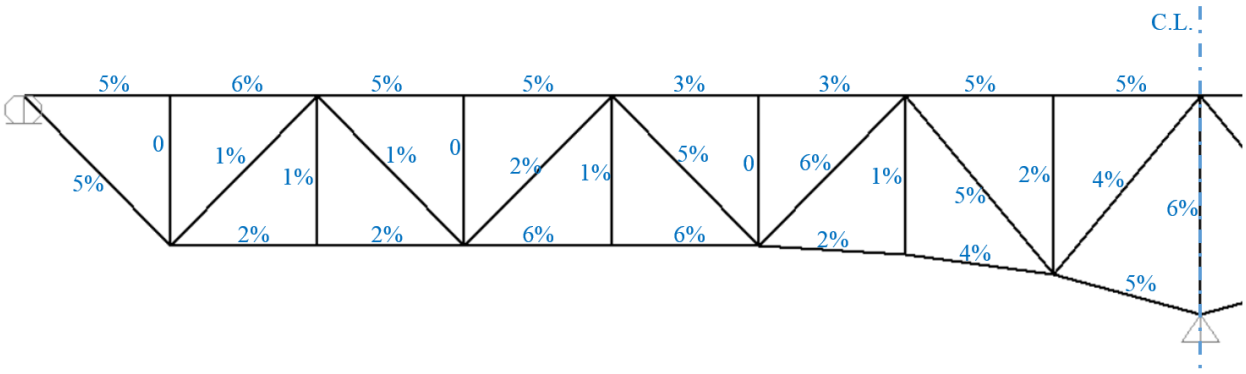

Figure 7-68. Difference between the results from the 2D model and design values on the drawing for the New River Bridge

Step 2: Determine critical live load position

After validating the 2D model for the New River Bridge, there is a need to determine the live load condition that will be critical to the system load carrying capacity. Given the fact that this bridge has two continuous spans and each span length is 150 ft, two loading conditions as illustrated in Figure 7-69 and Figure 7-70 were considered critical to the system capacity.

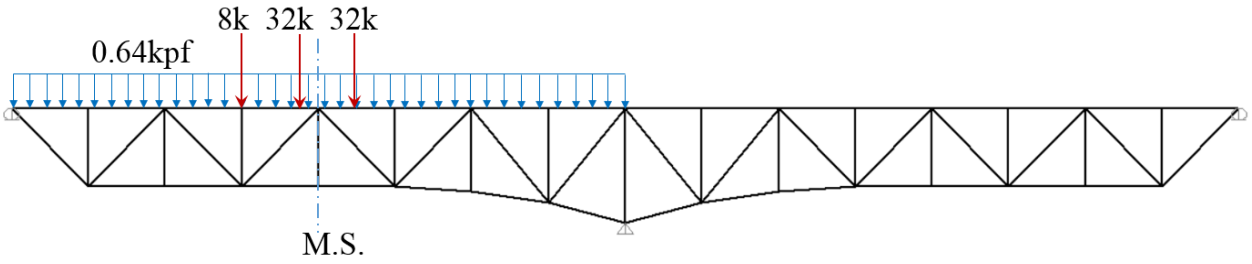

Figure 7-69. HL-93 load configuration I: only one span is assigned the HL-93 load

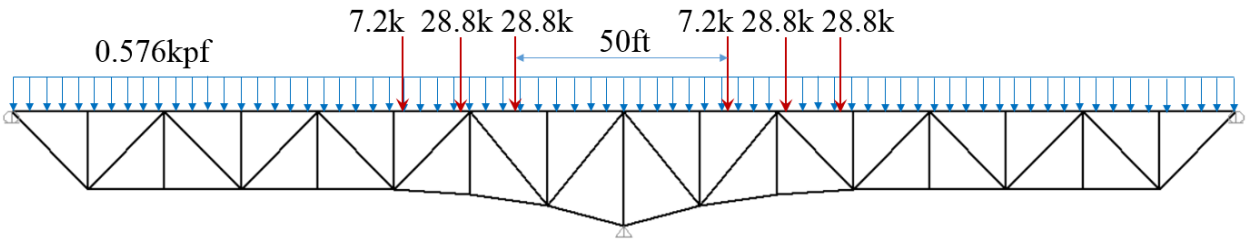

Figure 7-70. HL-93 load configuration II: two spans are assigned the HL-93 load (Note that both the truck load and the lane load in this model are 90 percent of their corresponding loads in the model shown in Figure 7-69 to account for a relatively low probability of this loading condition as specified by AASHTO (2012))

The calculation of system load capacity shows that the bridge structure can carry 1.82 times of the HL-93 load with configuration I while only 70% of the HL-93 load with configuration II. Therefore, the critical live load condition was determined as the HL-93 load with configuration II as illustrated in Figure 7-70. This loading condition will be used in the remainder of system redundancy study for the New River Bridge.

Step 3: Identify critical members with high demand-to-capacity ratios for axial loads

Once the critical loading condition was determined, the resultant axial load on each main truss member can be computed. Then the member D/C ratio can be obtained. Following the criterion proposed in Section 7.5, the critical members were identified as the members whose D/C ratios were not less than one half of the greatest value of member D/C ratio. Because the configuration of the bridge structure and the live load condition is symmetric about the interior support, the critical members were selected from one span of the main truss structure as shown in Figure 7-71.

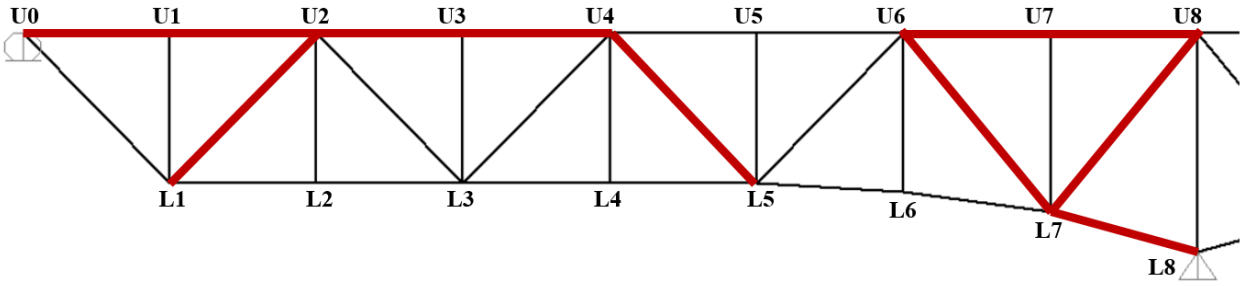

Figure 7-71. A 2D model in SAP2000 for the New River Bridge showing critical chord and diagonal members

Step 4: Model the full 3D bridge system

As stated in Section 7.6, the load capacity evaluation for damaged structures requires the modeling of a full 3D bridge system. In this regard, a 3D elastic model for the New River Bridge was developed as the first step. This 3D model was constructed using frame elements for the truss members, stringers, floor beams, and braces. The bridge deck was not expected to develop composite action in that substantial cracking across the deck was reported during the inspection (VDOT 2006). Thus the estimated weight of reinforcement and concrete was converted to equivalent line loads that were applied to the stringers in the 3D model. The stringers were assigned axial force release so that the axial forces carried by the top chord main truss members can come close to the design values. This modeling effort is to ensure that axial force induced by the loads on the deck can be carried by main trusses as primary members rather than stringers as secondary members. The connection between floor beams and top chord main trusses was modeled using rigid links, which can properly capture force and moment transfer from the floor system to the main truss structure. Moreover, the main truss member forces predicted from the model with rigid links were found to be much closer to the member design forces as compared to the models with partially rigid links.

The accuracy of the 3D model in predicting the main truss member forces was examined by comparing the member axial forces between the model results and the design values as shown in Figure 7-72 and Figure 7-73.

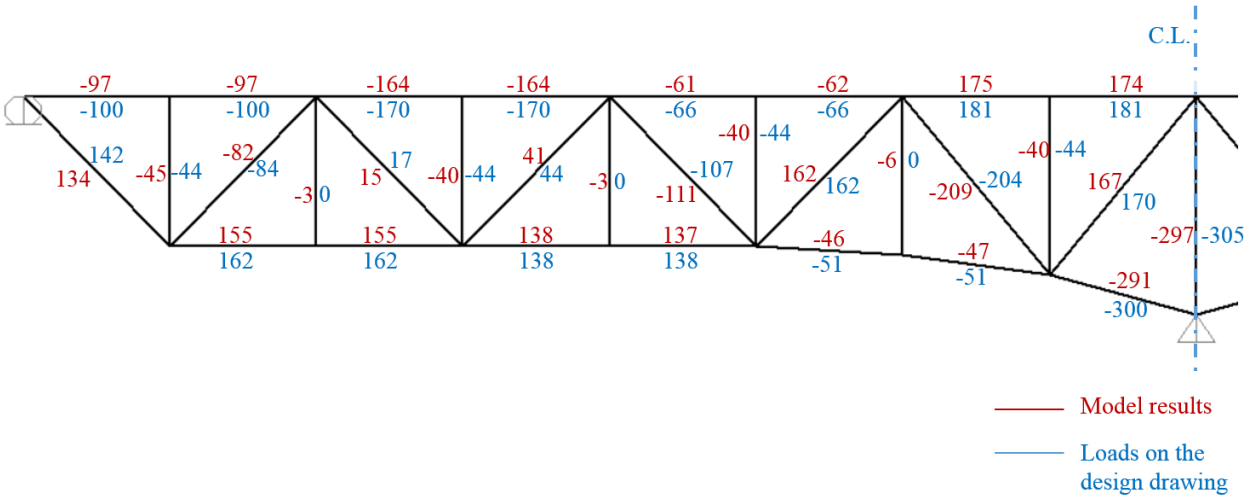

Figure 7-72. Comparison of axial load demand (unit: kips) for the main truss members in the New River Bridge under design dead load between the results from a 3D elastic model and the values on the design drawing

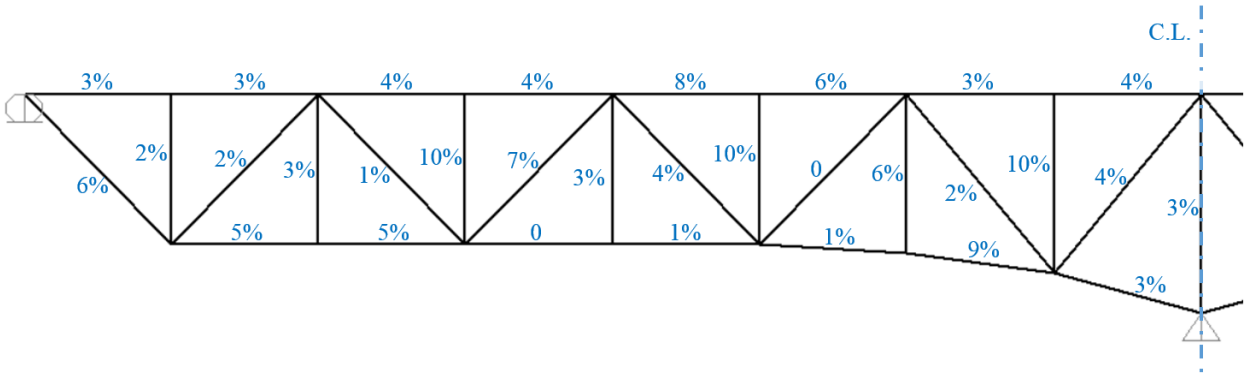

Figure 7-73. Difference between the results from the 3D model and design values on the drawing for the New River Bridge

Since the live load response for the New River Bridge in an undamaged condition was measured by Hickey et al. (2009), the accuracy of the 3D model was also verified by comparing the model results with the live data as illustrated in Figure 7-74 and Figure 7-75.

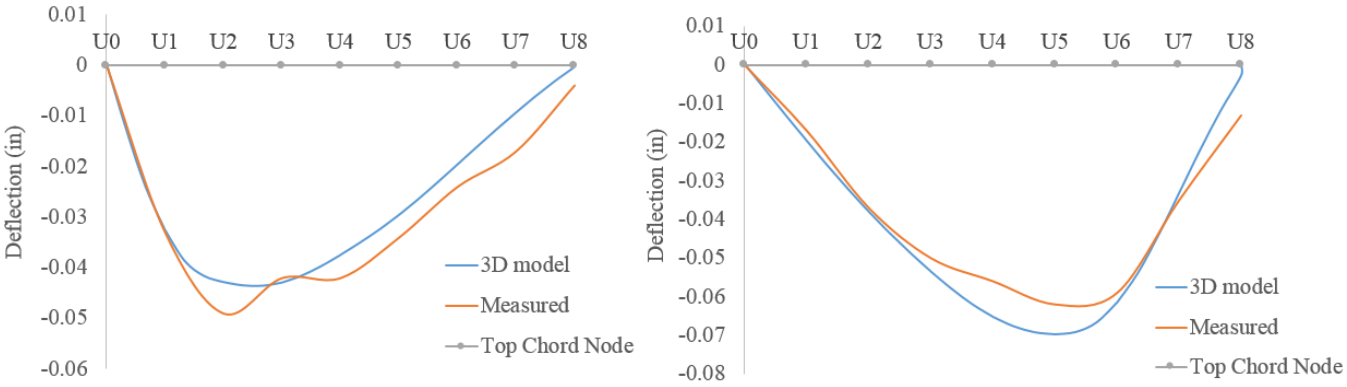

(a) Influence line for deflection at L1 (b) Influence line for deflection at L6

Figure 7-74. Model calibration of the influence line for nodal deflections when the two HS-25 truck loads were moving along the centerline of the deck

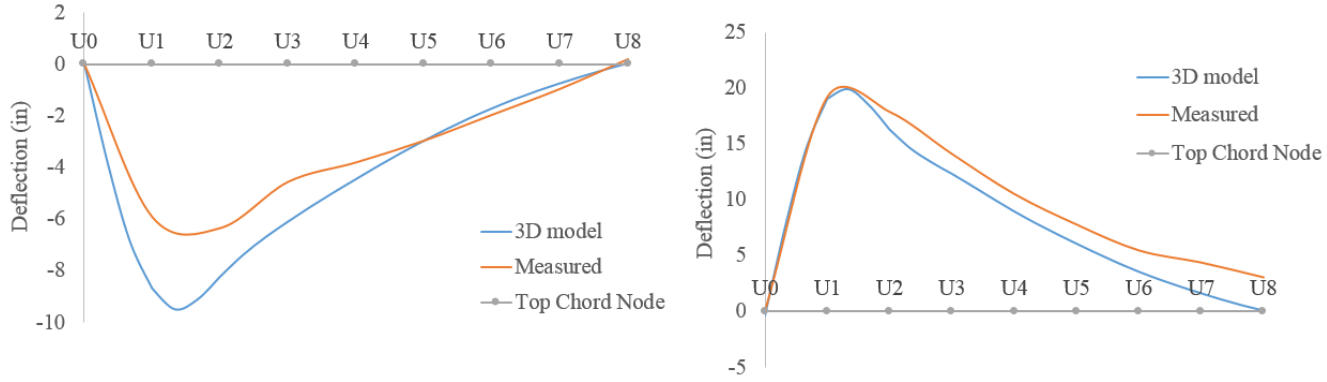

(a) Influence line for axial force on member U0U1 (b) Influence line for axial force on member U0L1

Figure 7-75. Model calibration of the influence line for member axial forces when the two HS-25 truck loads were moving along the centerline of the deck

As good correlation can be found between the model results and the measured data, it is believed that the current 3D elastic model is capable of capturing the system behavior for the New River Bridge in an undamaged condition.

Step 5: Incorporate nonlinear features to the 3D system model

The nonlinear features discussed in Section 7.7 were incorporated into the 3D system model. It was noted that in this bridge structure either main truss member yielding or brace member buckling was the controlling failure mode, the connection failure was therefore not incorporated into the SAP2000 models for this bridge.

Step 6: Create damaged structures by removing the critical members identified in Step 3 as well as vertical members one at a time from the 3D nonlinear system model

Using the nonlinear 3D models, the load capacity for the bridge structure in both undamaged and damaged conditions can be determined when the system reaches its ultimate state as discussed in Section 7.7.5.

Step 7: Rate the load capacity for the undamaged and damaged 3D systems

Since the load capacity is a measure of the system redundancy, the bridge system with less load capacity is considered to have less redundancy and is thereby rated more failure critical. The critical members in the New River Bridge were arranged in an ascending order of the load rating factors for their associated damaged structures as shown in Table 7-24. Note that the live loads used in the evaluation of the load capacities for both undamaged and damaged systems were the HL-93 load applied to two spans as illustrated in Figure 7-70, as this loading condition was found to be most critical to the system capacity.

Table 7-24. System load capacities and governing failure modes for the New River Bridge in the undamaged and damaged conditions

Member removed in a no-load condition	Member Force in the Undamaged Structure	$DL_{,ultimate}$ / $DL_{,total}$	$LL_{,ultimate}$ / HL-93	Most critical remaining member	Critical location	Governing failure mode
U8L8-US	Compression	0.22	0.00	U8US-L8DS	Sway brace	Buckling
L7L8-US	Compression	0.43	0.00	LB7US-8DS	Lower brace	Buckling
U6L7-US	Compression	0.69	0.00	U6US-L6DS	Sway brace	Buckling
U8L7-US	Tension	0.90	0.00	LB7US-8DS	Lower brace	Buckling
U0U1-US	Compression	1.00	0.27	U1US-L1DS	Sway brace	Buckling
U1U2-US	Compression	1.00	0.26	U1US-L1DS	Sway brace	Buckling
U4L5-US	Compression	1.00	0.15	U5US-L5DS	Sway brace	Buckling
U3U4-US	Compression	1.00	0.21	U3US-L3DS	Sway brace	Buckling
U2U3-US	Compression	1.00	0.21	U3US-L3DS	Sway brace	Buckling
U7U8-US	Tension	1.00	0.26	U8US-L8DS	Sway brace	Buckling
U2L1-US	Compression	1.01	0.26	U1US-L1DS	Sway brace	Buckling
U7L7-US	Compression	1.00	0.29	U7US-L7DS	Sway brace	Buckling
U6U7-US	Tension	1.00	0.31	LB7DS-8US	Lower brace	Buckling
U6L6-US	Compression	1.00	0.57	U8US-L8DS	Sway brace	Buckling
Undamaged	N.A.	1.00	0.70	U8US-L8DS	Sway brace	Buckling

From Table 7-24, it is apparent that the system for the New River Bridge both in the undamaged and damaged conditions cannot support 100% of the HL-93 load. This indicates that every critical member in this table needs to be regarded as system non-redundant member. The three critical tension members can be classified as fracture critical members. Furthermore, the most critical

tension member was identified as member U8L7 which was the diagonal member closest to the interior support. This location of the most critical tension member in the New River Bridge is also in consistent with the counterpart in the I-35W Bridge.

7.9.2 Span No.4 of the Milton-Madison Bridge

This structure is another of the approach spans of the Milton-Madison Bridge. This structure is selected as a case study because it is the only one approach span of the entire Milton-Madison Bridge that is in a through truss configuration, as shown in the right of Figure 7-1. Unlike the three example bridges that were previously discussed, this truss structure has a deck system that is located near the bottom chord main truss members.

The span length of this truss structure is 147 feet. This structure is a simple-supported structure consisting of five panels. The two end panels have an equal length of 29’ 4 7/8” and the center three panels have an equal length of 29’ 4 3/4”. The width of this structure is 24 feet and the truss height is 30 feet. The deck system is located 3.75 feet above the bottom chord of the main truss and the deck is supported by six lines of stringers. Floor beams are attached below the deck and therefore are not coincident with the bottom chord truss joints. The geometry of the 3D system for this structure can be seen from Figure 7-76.

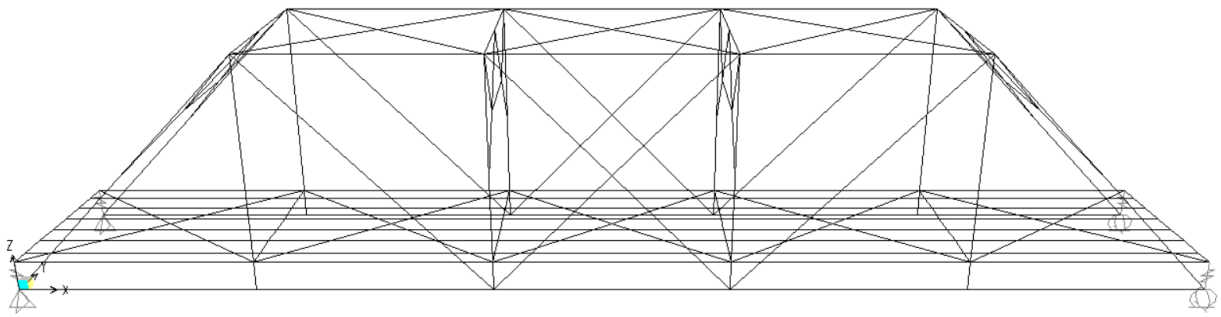

Figure 7-76. 3D system of the Span No.4 of the Milton-Madison Bridge modeled in SAP2000

Following the steps proposed in Section 7.8, the procedure for performing system analyses for this bridge structure is described as below:

Step 1: Develop a 2D model of the main truss structure

One line of the main truss structure of the Span No.4 of the Milton-Madison Bridge was modeled in SAP2000 and the axial force demand under design dead load on each main truss member predicted from the model was compared with the values shown on the design drawing. The comparisons are presented in Figure 7-77 and Figure 7-78.

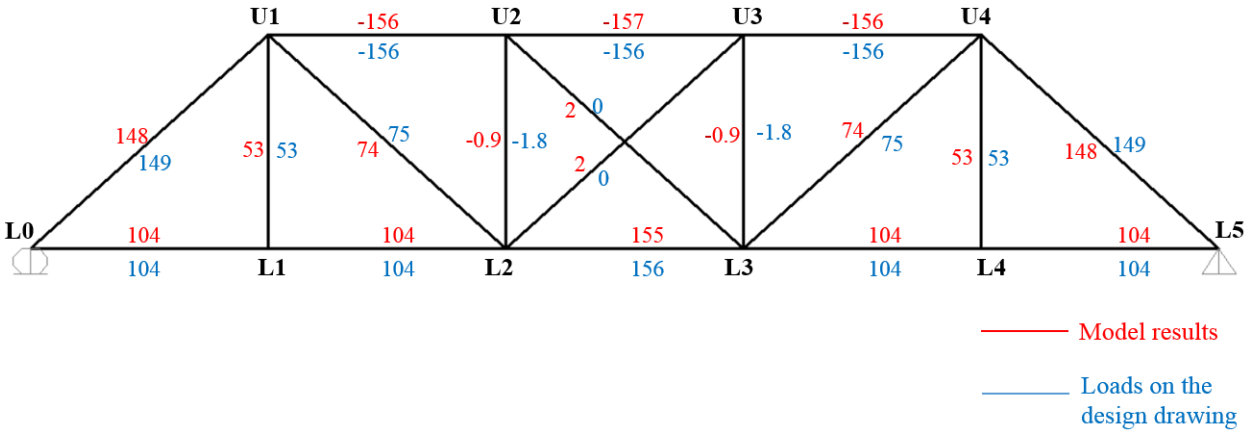

Figure 7-77. Comparison of axial load demand (unit: kips) for the main truss members in the Span No.4 of the Milton-Madison Bridge under design dead load between the results from a 2D elastic model and the values on the design drawing

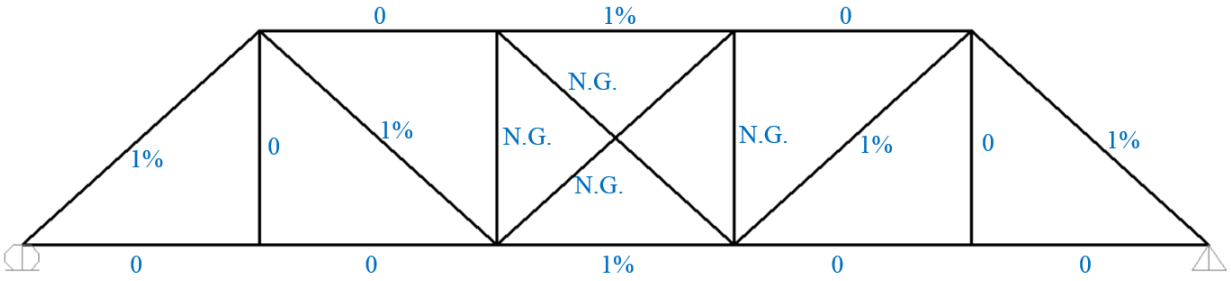

Figure 7-78. Difference between the results from the 2D model and design values on the drawing for the Span No.4 of the Milton-Madison Bridge

Note that Figure 7-78 does not show the difference of axial force demand on the vertical members and the diagonal members in the center panel, because the relative difference in percentage on these members are quite large. However, considering that these members are carrying the smallest axial forces amongst all main truss members and they are very close to zero force members under the design dead load, the difference between the model results and the design values on these members is still acceptable. Therefore, the 2D model can be demonstrated to have a good correlation with the behavior expected in the design.

Step 2: Determine critical live load position

Since the structure only has one simple-supported span, the critical live load condition was found to be the HL-93 load with truck loads applied at the mid-span and lane loads distributed to the entire span length.

Step 3: Identify critical members

Since both this loading condition and the geometry of this simple span structure are symmetric about the mid-span, there are actually ten main truss members that need to be analyzed. Due to the limited number of main truss members, each of the ten main truss member was treated as critical member.

Step 4: Model the full 3D bridge system

A 3D elastic model was first developed and the main truss member behavior was calibrated to match the values on the design drawing. The geometry of the 3D model can be seen from Figure 7-76. The accuracy of this 3D model in predicting the main truss members axial force demand under design dead load was evaluated through the comparison of main truss member force as shown in Figure 7-79 and Figure 7-80.

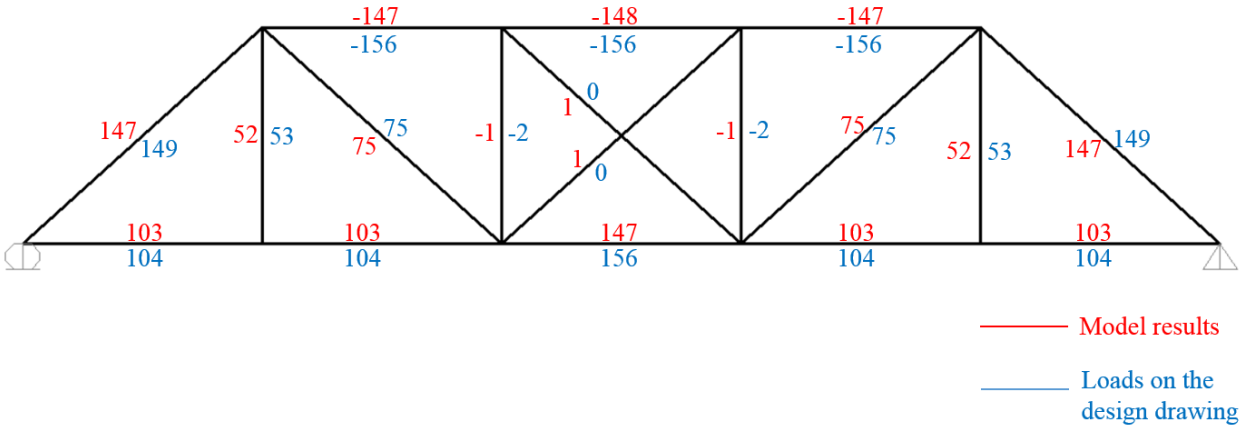

Figure 7-79. Comparison of axial load demand (unit: kips) for the main truss members in the Span No.4 of the Milton-Madison Bridge under design dead load between the results from a 3D elastic model and the values on the design drawing

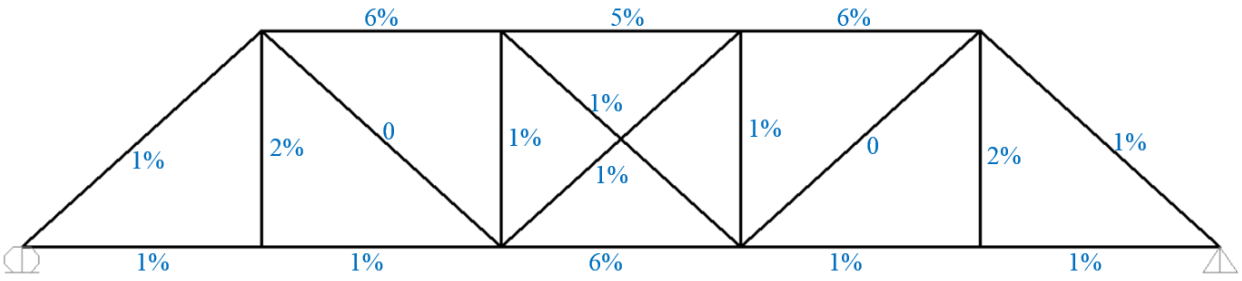

Figure 7-80. Difference between the results from the 3D model and design values on the drawing for the Span No.4 of the Milton-Madison Bridge

From Figure 7-79 and Figure 7-80, good correlation can be seen between the model results and the design values. Hence the 3D model can be utilized as a baseline model for the subsequent studies.

Step 5: Incorporate nonlinear features to the 3D system model

After the 3D elastic system model was validated, the nonlinear features discussed in Section 7.7 were incorporated into this model. As in this structure the connection details for both the main truss members and brace members were not available, it was assumed that a member failure would occur prior to a connection failure. Thus the nonlinear features incorporated to the 3D model were the plastic hinges for capturing the axial-flexural interaction failure at the ends of a main truss member, and the nonlinear axial springs for simulating the post-yielding and post-buckling behavior of main truss and brace members.

Step 6: Create damaged structures by removing all main truss members one at a time from the 3D system model

To simulate the damaged system with failure on a single critical member, the ten main truss members were removed from the nonlinear 3D model one at a time before applying loads.

Step 7: Rate the load capacity for the undamaged and damaged 3D systems

The system load capacity for each damaged structure was computed and expressed using the dead load factor and the live load factor as shown in Table 7-25.

Table 7-25. System load capacities and governing failure modes for the Span No.4 of the Milton-Madison Bridge in the undamaged and damaged conditions

Member removed in a no-load condition	Member Force in the Undamaged Structure	$DL_{,ultimate}$ / $DL_{,total}$	$LL_{,ultimate}$ / HL-93	Most critical remaining member	Critical location	Governing failure mode
U1U2-US	Compression	0.12	0.00	U2US-U3DS U2DS-U3US	Top diagonal braces	Buckling
U2U3-US	Compression	0.15	0.00	U2L3-US	Main truss	Buckling
U1L0-US	Tension	0.19	0.00	U1L1-US	Main truss	Buckling
L1L2-US	Tension	0.20	0.00	U1L1-US	Main truss	In-plane bending
L0L1-US	Tension	0.25	0.00	U1L1-US	Main truss	Buckling
U1L1-US	Tension	0.69	0.00	L1L2-US	Main truss	In-plane bending
U1L2-US	Tension	1.00	0.03	U2L3-US	Main truss	Buckling
U2L2-US	Compression	1.00	0.17	U2L3-US	Main truss	Buckling
L2L3-US	Tension	1.00	0.25	U2US-U3DS U2DS-U3US	Top diagonal braces	Buckling
U2L3-US	Tension	1.00	0.69	U2US-U3DS U2DS-U3US	Top diagonal braces	Buckling
Undamaged	N.A.	1.00	0.71	U2US-U3DS U2DS-U3US	Top diagonal braces	Buckling

From Table 7-25, it is worth noting that the live load capacity for the undamaged Span No. 4 of the Milton-Madison Bridge is less than the HL-93 load. This result is similar to what was shown in Table 7-24 for the undamaged New River Bridge. Thus it can be inferred that the Span No. 4 of the Milton-Madison Bridge is a particularly collapse-critical structure. All main truss members in

this structure are non-redundant to the system. Every main truss member in tension still needs to be regarded as fracture critical member.

Additionally, it is also obvious that the most critical tension member in this truss structure is member U1L0, the edge diagonal member that is connects to one support. This result agrees well with the findings from the previous three example bridges in that the most critical tension member is a diagonal member near the support and this member can be classified as fracture critical member.

Table 7-25 also shows that the top two most critical members are top chords. This result agrees well with the conclusion that in a simple-supported through truss structure top chords were more critical than bottom chords based on the study conducted by Yamaguchi et al. (2010).

Lastly, it can be seen from Table 7-25 that the removal of member U2L3, the diagonal in the mid-span panel, merely lead to 3% reduction in system load capacity. This result is in agreement with the result as shown in Table 7-10. Thus it can be confirmed that the diagonal members in an X-truss configuration in the mid-span panel of a simple-supported truss structure are not critical to system redundancy.

7.10 Evaluation of the Proposed System Analysis Methodology

7.10.1 Appropriateness of Load Models

In this research study, the HL-93 load as specified by AASHTO (2012) are expected to cause the most critical system response. Whereas the two side-by-side HS-20 truck load was utilized as the critical traffic load in previous redundancy studies for truss bridges (Ghosn and Moses 1998; Ghosn and Fiorillo 2013; Reese 2009). Ascertaining which loading condition will produce the maximum influence on a bridge system, the moment at the mid-span of a bridge resulting from the

two side-by-side HS-20 truck load is compared with that caused by the HL-93 load, as summarized in Table 7-26.

Table 7-26. Comparison of moment at the mid-span of the example bridges

Example Bridges	Span L (ft)	M_{Truck} (k-ft)	M_{Lane} (k-ft)	M_{HL-93} (k-ft)	Truck/HL-93
The Example Truss Bridge in NCHRP-406 (Ghosn and Moses 1998)	104	1573.33	865.23	2438.56	64.5%
Åby Bridge (Ghosn and Fiorillo 2013)	110	1681.33	967.94	2649.27	63.5%
Beech Creek Veterans Memorial Bridge (Reese 2009)	144	2293.32	1658.88	3952.20	58.0%
Milton Madison Bridge: Test Span	147	2347.33	1728.61	4075.95	57.6%
Milton Madison Bridge: Span No.4	147	2347.33	1728.61	4075.95	57.6%
New River Bridge	150	2401.33	1799.89	4201.22	57.2%
I-35W Bridge	456	7909.33	16634.78	24544.11	32.2%

Notes:

- M_{Truck} = Moment at the mid-span caused by two side-by-side HS-20 trucks;
- $M_{HL-93} = M_{Truck} + M_{Lane}$.

As seen from Table 7-26, it is clear that the HL-93 load result in a significantly higher moment at the mid-span of every example bridge as compared to the two side-by-side HS-20 truck load. This table also demonstrates that the load effect due to the two HS-20 trucks increases as the bridge span length decreases. This result indicates that the truck load may be critical to a short bridge but it cannot cause the worse load effect on a bridge longer than 100ft. In fact, aside from the truck load, the lane load also contributes to the mid-span moment a lot. Therefore, it is more appropriate to consider both the truck load and the lane load in the determination of critical system load capacity for a truss bridge.

7.10.2 Efficiency of Nonlinear Analyses

The advantages of using SAP2000 as an analytical tool for system redundancy evaluation are the simplicity of modeling and efficiency of computation, as demonstrated in Table 7-27. This table compares the nonlinear system model for the damaged I-35W Bridge with the removal of the most critical member (U8L9) developed in SAP2000 with that constructed in ABAQUS.

Table 7-27. Comparison of nonlinear system models developed in SAP 2000 and in ABAQUS

Nonlinear models	SAP 2000 model	ABAQUS model
Number of elements on one truss member	1	5
Total number of elements in the truss system, including the two-line main trusses and the lateral braces	546	2730
Consideration of plasticity (Nonlinear hinge assignment)	For every member in the main truss and bracing systems	For a limited number of main truss members and brace members in the vicinity of the damaged member (U8L9)
Computational time	8min	12hr

7.11 Sample Retrofit Strategies

It will be of great interest to determine if the proposed rating method can lead to selective strengthening of members, which will result in significant increase of system capacity, once a critical member is removed. This section provides some overview of such strategies for the bridges studied in this thesis.

7.11.1 I-35W Bridge

The strengthening schemes for the I-35W Bridge were considered for the damaged structures in Group I and II identified in Table 7-9. In Group I, each damaged structure failed to carry full dead load due to block shear on the gusset plate that connected a main truss member with a lower brace member. An initial attempt to retrofit the damaged structure addressed increasing the strength capacity of the gusset plate. This can be achieved by installing supplemental steel plate to increase the gusset plate thickness. A plate with a minimum thickness of 7/16 inches was the found adequate to prevent the block shear on the strengthened gusset plate. However, this strengthening scheme did not greatly improve the system load capacity in that buckling on the adjoining brace member had occurred before full dead load were applied to the retrofitted structure. The choice for an effective retrofit strategy was thereby aimed at avoiding the brace member connection failure as well as buckling on the critical braces. Considering the complexity of the connection configuration of the built-up box shape brace member as illustrated in Figure 7-81, it would be efficient to install a steel cable parallel to the critical brace members. The cable could be held in place by a stiffened steel angle member bolted perpendicular to the gusset plate. A simplified configuration of the retrofitted connection is illustrated in Figure 7-81.

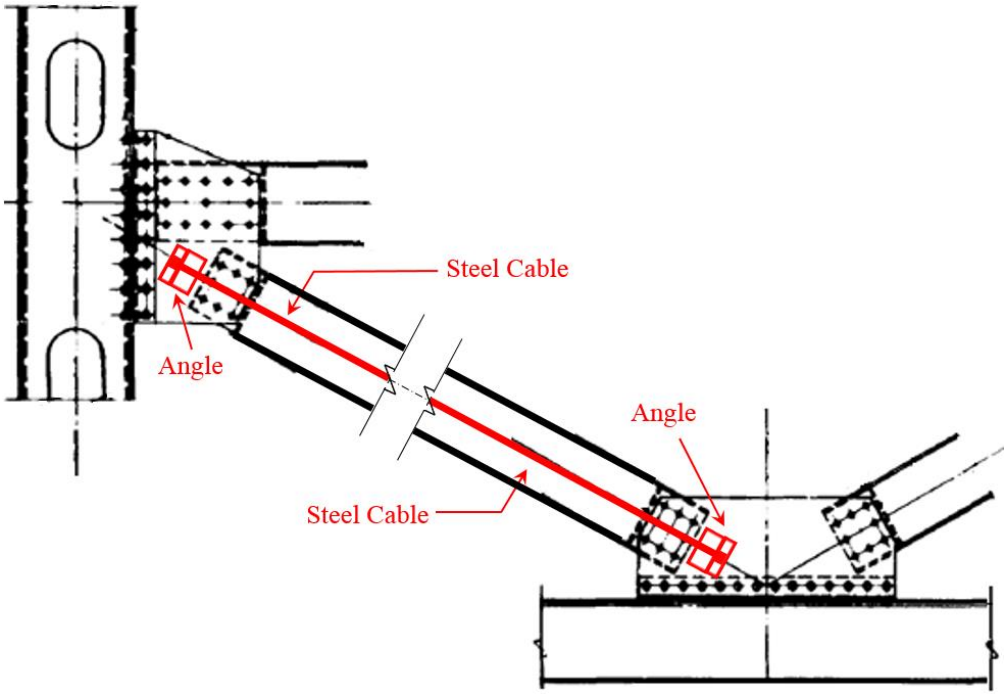

Figure 7-81. Illustration of steel cable installation

The axial force demands for designing the cable and the angle were assumed to be equal to the brace member yield strength. This design is to ensure that the critical locations in the transverse brace system will not get overstressed after one main truss member is damaged. The benefits of installing the cable and angle members may be described as:

(1) The connection force can be distributed to both brace member and the angle member leading to a reduction in the resultant axial force in the vicinity of rivet holes; and

(2) Brace member buckling could be prevented since the cable will restrain the lateral deformation of the brace member.

Assuming that after applying such retrofit strategy to the critical sway braces and lower braces, the ultimate failure of the damaged structures in Group I will take place in the main truss structure, the load capacity for each retrofitted structure is summarized in Table 7-29.

In Group II in Table 7-9, the damaged structures failed due to buckling of one of the chord members U10U12 and L9L11. As discussed in Section 7.7.2, the buckling capacities for these members were close to their yield strengths, an effective approach to enhance the member strength capacity would be increasing the area of the cross section. The new cross section should be optimized to ensure that the properties about weak axis can approach those about strong axis, in order to make full use of the cross section in both orthogonal directions. As the load rating analyses revealed that strengthening merely these two chord members could not help the structures in Group II sustain full HL-93 load, the retrofit work was extended to two more critical chord members (L8L9 and U12U14) whose end connections were subjected to significant axial-flexural interactions. The final strengthening scheme for these four critical chord members is summarized in Table 7-28, which shows the increase in both axial and flexural strength capacity of each critical chord member after the retrofit. Furthermore, the effectiveness of strengthening these chord members at once for each damaged structures in Group II is demonstrated by assessing the system load capacity increase from the original structures to the retrofitted ones, as shown in Table 7-29.

Table 7-28. Comparison of cross section and capacity for each retrofitted member in the I-35W Bridge

Retrofitted Members	Original Cross Section (unit: inch)	Optimized Cross Section (unit: inch)	Original Member Capacity (P_{cr} based on K=1)	Optimized Member Capacity (P_{cr} based on K=1)	Strength Capacity Increase
L8L9	B29 X 21 X 5/8 X 2 1/2 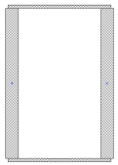	Add 4L8 X 8 X 5/8 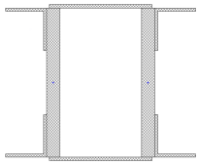	$P_{cr,orig}$ =6859kips $M_{p,orig}$ =67785in-kips	$P_{cr,new}$ =8635kips $M_{p,new}$ =89505in-kips	$\frac{P_{cr,new}}{P_{cr,orig}} = 1.26$ $\frac{M_{cr,new}}{M_{cr,orig}} = 1.32$
L9L11	B29 X 21 X 1/2 X 15/16 	Add 4L8 X 8 X 1 1/8 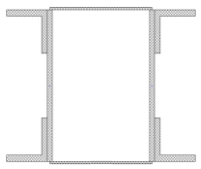	$P_{cr,orig}$ =3000kips $M_{p,orig}$ =32625in-kips	$P_{cr,new}$ =5846kips $M_{p,new}$ =71411in-kips	$\frac{P_{cr,new}}{P_{cr,orig}} = 1.95$ $\frac{M_{cr,new}}{M_{cr,orig}} = 2.19$
U10U12	B29 X 21 X 1/2 X 1 	Add 4L8 X 8 X 1 1/8 & C15 X 50 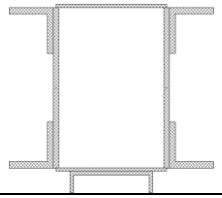	$P_{cr,orig}$ =3161kips $M_{p,orig}$ =33850in-kips	$P_{cr,new}$ =7013kips $M_{p,new}$ =85355in-kips	$\frac{P_{cr,new}}{P_{cr,orig}} = 2.22$ $\frac{M_{cr,new}}{M_{cr,orig}} = 2.52$
U12U14	B29 X 21 X 9/16 X 2 1/8 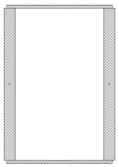	Add 4L8 X 8 X 9/16 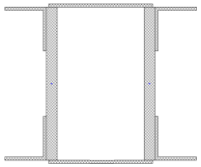	$P_{cr,orig}$ =5858kips $M_{p,orig}$ =57716in-kips	$P_{cr,new}$ =7542kips $M_{p,new}$ =78202 in-kips	$\frac{P_{cr,new}}{P_{cr,orig}} = 1.29$ $\frac{M_{cr,new}}{M_{cr,orig}} = 1.35$

Table 7-29. System load capacity comparison between the original and the retrofitted structures for the I-35W Bridge

Member removed in a no-load condition	Group	Retrofitted Members	$DL_{,ultimate}$ / $DL_{,total}$		LL_{ult} / HL-93	
			Original	Retrofitted	Original	Retrofitted
U8L9	I	LB 8-9 & Sway braces at panel point 9	0.20	1.00	0.00	1.03
U10L9		LB 9-10 & Sway braces at panel point 10	0.23	1.00	0.00	1.06
L8L9		LB 8-9 & Sway braces at panel point 9	0.31	1.00	0.00	1.12
U10L11		LB 10-11 & Sway braces at panel point 10	0.38	1.00	0.00	1.33
U8L8		LB 7-8 & Sway braces at panel point 7	0.43	1.00	0.00	1.31
U8L7		LB 7-8 & Sway braces at panel point 7	0.46	1.00	0.00	1.21
U12L11		LB 11-12 & Sway braces at panel point 12	0.51	1.00	0.00	1.24
L7L8		LB 7-8 & Sway braces at panel point 7	0.52	1.00	0.00	1.71
U6L7		LB 6-7 & Sway braces at panel point 7	0.63	1.00	0.00	1.46

Member removed in a no-load condition	Group	Retrofitted Members	$DL_{,ultimate}$ / $DL_{,total}$		LL_{ult} / HL-93	
			Original	Retrofitted	Original	Retrofitted
U12L13		LB 12-13 & Sway braces at panel point 12	0.90	1.00	0.00	1.89
L11L12	II	L8L9, L9L11, U10U12, and U12U14	1.00	1.00	0.14	1.35
L13L14			1.00	1.00	0.21	1.61
U8U9			1.00	1.00	0.34	1.24
U7U8			1.00	1.00	0.40	1.16
L9L10			1.00	1.00	0.59	1.73

7.11.2 M-Bridge

For the M-Bridge the first failure locations in most damaged structures were the vertical main truss members, as summarized in Table 7-10. Thus the retrofit was implemented through strengthening these members on both sides of the main truss. Since the governing failure modes on these members were identified as large plastic bending about the weak axis of an H-shape cross section, the strengthening scheme was determined as welding two steel plates to make a tube section on each side of the web as illustrated in Figure 7-82. As the cross section was changed into a tube-shape, the weak axis bending capacity could be effective improved to approach the strong axis bending capacity. The dimension of steel plates used in the retrofit is tabulated in Table 7-30. The stiffness increase reflected by the elastic section modulus from the original H-shape to the strengthened tube-shape is shown in Table 7-31.

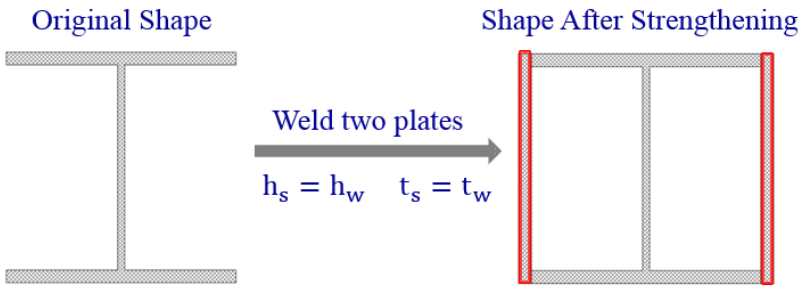

Figure 7-82. Illustration on how an H-shape cross section was strengthened

Table 7-30. Dimension of the critical member cross section and the steel plates used in the retrofit

Vertical Members	Original Cross Section	Steel Plates Used in the Retrofit (in. by in.)
U0L0 and U7L7	W10X49	10 X 9/16
U1L1 and U6L6	W10X31	10 1/2 X 1 1/4
U2L2 and U5L5	W10X56	10 X 1

Table 7-31. Elastic section modulus comparison between the original H-shape and the strengthened tube-shape

Vertical Members	M_y (in-k)	Original	Strengthened	Increase=Column4/Column3
U0L0 and U7L7	M_{weak}	19	73	3.87
	M_{strong}	54	73	1.36
U1L1 and U6L6	M_{weak}	6	78	13.82
	M_{strong}	32	84	2.62
U2L2 and U5L5	M_{weak}	21	94	4.51
	M_{strong}	60	119	1.99
U1L0 and U6L7	M_{weak}	40	158	3.92
	M_{strong}	112	164	1.47

Note: the member U1L0 was observed to buckle after the most critical member U1L1 failed due to large in-plane bending effect.

With the improved bending capacities about both strong and weak axes, these vertical main truss members were expected to fail later in the retrofitted structure than it did in the original damaged structure. This would lead to an increase in the system load carrying capacity.

As the last six damaged cases in Table 7-12 were found to have a live load rating factor greater than one, these damaged structures were considered to maintain adequate level of redundancy even after losing one critical member. Therefore, the structure did not need to be retrofitted for these six cases. Table 7-32 shows the results for the remaining cases. The final dimension of the steel plates used to strengthen the vertical members was determined through an iterative process, as the objective of the retrofit work is to increase the system live load capacity to meet the required minimum live load rating factor as 1.0. Moreover, it was observed that in the damaged structures listed in Table 7-32 the plastic hinge formation progressed from one remaining main truss member to another resulting in plastic damage on multiple members. The analysis stopped due to its inability of obtaining a solution to satisfy equilibrium and stability requirements. As far as such progressive collapse is concerned, more than one remaining member needs to be strengthened in some damaged structures.

Table 7-32. System load capacity comparison between the original and the retrofitted structures for the M-Bridge

Member removed in a no-load condition	Retrofitted Members	$DL_{,ultimate}$ / $DL_{,total}$		LL_{ult} / HL-93	
		Original	Retrofitted	Original	Retrofitted
U1U2-US	U0L0, U7L7, U1L1, U6L6	0.85	1.00	0.00	1.40
U2U3-US	U1L1, U6L6, U2L2, U5L5	0.97	1.00	0.00	1.36
U1L0-US	U0L0, U7L7, U1L1, U6L6, U1L0-DS, U6L7	1.00	1.00	0.18	1.80
U3U4-US	U1L1 and U6L6	1.00	1.00	0.35	1.39
U1L2-US	U0L0 and U7L7	1.00	1.00	0.83	2.49

7.11.3 New River Bridge

As shown in Table 7-24, the New River Bridge system even in an undamaged condition failed to carry full HL-93 load. This implies that this bridge structure lacks of system redundancy and cannot provide normal service according to the load rating standards (AASHTO 2012). To improve the bridge condition, retrofit strategies for the undamaged system were studied as the first step.

As Table 7-24 shows that the ultimate failure of the undamaged system for the New River Bridge was caused by buckling of a sway brace, a retrofit was implemented by strengthening this brace member to enhance its buckling capacity. The strengthening scheme consists of increasing the cross section of this member from 2L5 X 3 ½ X 5/16 to an equivalent 2L8 X 8 X 5/16 by welding plates to the two angle legs. After strengthening this critical member, it was found that buckling on brace members no longer controlled the ultimate failure state of the undamaged system. Instead, the retrofitted structure was found to fail due to buckling on the main truss member U6L7 under the approximately same load as that caused the buckling of a sway brace. A further investigation

reveals that the buckling capacity of this main truss member is approximately 96% of its yield capacity. This implies that the member cross section is fully utilized so that little benefit will be gained by improving the member buckling capacity. In this regard, the strengthening of this main truss member can be achieved by installing high strength steel plates parallel to this member.

Given the fact that the undamaged bridge structure after the proposed retrofit work could still have difficulty in sustaining full HL-93 load, one can infer that strengthening the critical brace member alone still failed to provide the undamaged bridge with sufficient system redundancy. Strengthening for the critical brace member as well as the critical main truss member on both spans and both sides of the main truss structure are required. If so, six members will be strengthened. Considering such number of critical members that need strengthening just for the undamaged structure, this retrofit strategy may not be a cost-effective option.

An alternative solution to increase the system load rating factor is decreasing the amount of dead load on the structure. This can be achieved by replacing the existing concrete deck system with a lightweight deck system. In addition, the replacement can also change the deck system from non-composite into composite to the truss structure. The new deck system can be constructed either utilizing lightweight concrete or normal weight concrete as there are three practical options proposed by one of the top bridge design company Modjeski and Masters (2011). Option 1 is using a steel grid deck fully filled with lightweight concrete plus 1.5 inches of overfill (Figure 7-83). Option 2 is filling the steel grid deck half with lightweight concrete and overfilling a 1.5 inches normal weight concrete (Figure 7-84). Option 3 is installing an Exodermic deck filled with normal weight concrete (Figure 7-85). An Exodermic deck is comprised of a lightly reinforced concrete slab composite with an unfilled grid. The benefits of utilizing the Exodermic deck are that the deck is not only lightweight but it also has similar durability and strength to normal weight reinforced

concrete deck. Moreover, this type of deck does not require field welding and it can be erected in a relatively short period of time. In addition, the application of the Exodermic deck can be found in the replacement of the deck for the test span of the Milton-Madison Bridge as mentioned in Section 7.2.2.

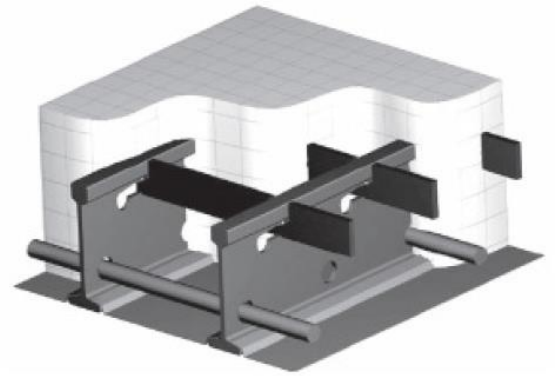

Figure 7-83. A steel grid deck fully filled with lightweight concrete. Modjeski and Masters (2011). Winona Bridge - Deck Rehabilitation Options. Used under fair use, 2015.

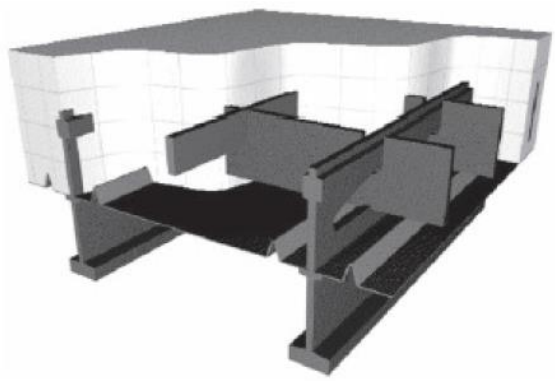

Figure 7-84. A half-filled steel grid deck. Modjeski and Masters (2011). Winona Bridge - Deck Rehabilitation Options. Used under fair use, 2015.

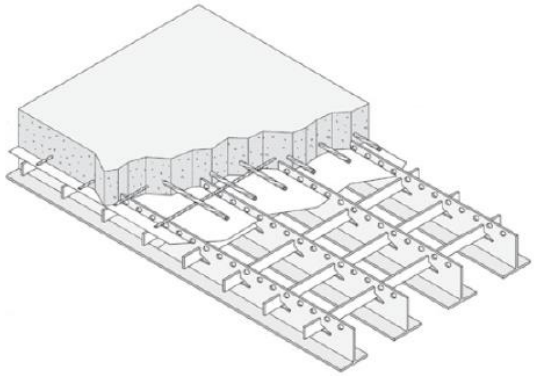

Figure 7-85. Exodermic deck. Modjeski and Masters (2011). Winona Bridge - Deck Rehabilitation Options. Used under fair use, 2015.

To determine which deck option will produce the lightest self-weight, the dead load on this bridge structure result from different deck options are compared in Table 7-33.

Table 7-33. Comparison of dead load on the New River Bridge with different deck options

Deck options	Deck Made	Deck Type	Deck Weight (psf)	$DL_{,total}$ Reduction
Original	Normal weight concrete	Non-Comp	108.76	0.00
Option 1	Fully filled with lightweight concrete	Composite	60.4	0.24
Option 2	Half-filled with lightweight concrete		60.5	0.24
Option 3	Normal weight concrete		47	0.31

It is clear that deck option 3, the Exodermic deck, has the lightest unit weight. Considering the benefits of the Exodermic deck as discussed in the previous paragraph, this type of deck will be selected for replacing the existing deck.

However, it is noted that although the weight of the Exodermic deck is less than half of the weight of the original deck, the total dead load that also include the weights of steel members and

reinforcement will merely reduce by 31% if the original deck is replaced by the Exodermic deck. A further investigation reveals that such replacement of the deck will lead to an approximate 39% increase in the live load capacity of the undamaged structure. An 8% additional increase is primarily caused by the composite action developed between the deck and the stringers if using the Exodermic deck. Eventually, the live load rating factor of the undamaged structure for this bridge will change from 0.70 to 1.09. This means that even after the deck is replaced the undamaged structure can barely sustain the HL-93 load given many uncertainties on the real structure. Therefore, any additional strengthening of this bridge will have limited benefits; this bridge should be (and was) replaced.

7.11.4 Span No.4 of the Milton-Madison Bridge

From Table 7-25, the first attempt to retrofit each structure should address increasing the strength capacity of the most critical remaining member. This can be achieved by optimizing the cross section of critical members, as shown in Table 7-34 and Table 7-35.

Table 7-34. System load capacity comparison between the original and the retrofitted structures for the Span No.4 of the Milton-Madison Bridge

Member removed in a no-load condition	Retrofitted Members	$DL_{,ultimate}$ / $DL_{,total}$		LL_{ult} / HL-93	
		Original	Retrofitted	Original	Retrofitted
U1U2-US	Top Diagonal Braces	0.12	1.00	0.00	0.75
U2U3-US	Top Diagonal Braces, U2L3, U3L2	0.15	1.00	0.00	3.36
U1L0-US	Top Diagonal Braces, U1L1, U4L4, U2L3, U3L2	0.19	1.00	0.00	0.57
L1L2-US	Top Diagonal Braces, U1L1, U4L4	0.20	0.70	0.00	0.00
L0L1-US	Top Diagonal Braces, U1L1, U4L4, U2L3, U3L2	0.25	1.00	0.00	0.30
U1L1-US	Top Diagonal Braces, L1L2, L3L4	0.69	1.00	0.00	1.75

Member removed in a no-load condition	Retrofitted Members	$DL_{,ultimate}$ / $DL_{,total}$		LL_{ult} / HL-93	
		Original	Retrofitted	Original	Retrofitted
U1L2-US	Top Diagonal Braces, U2L3, U3L2	1.00	1.00	0.00	1.28
U2L2-US	Top Diagonal Braces, U2L3, U3L2	1.00	1.00	0.17	2.14
L2L3-US	Top Diagonal Braces, U2L2, U3L3	1.00	1.00	0.25	0.80
U2L3-US	Top Diagonal Braces	1.00	1.00	0.69	2.53
Undamaged	Top Diagonal Braces	1.00	1.00	0.71	2.72

The location of each retrofitted member listed in Table 7-34 is illustrated in Figure 7-86.

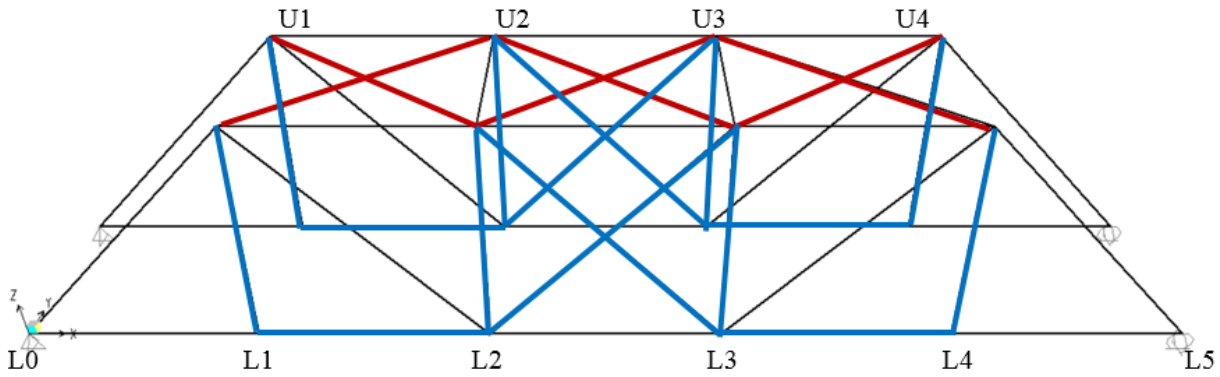

Figure 7-86. 3D view of the main truss members (highlighted in blue) and top diagonal brace members (highlighted in red) in the Span No.4 of the Milton-Madison Bridge

The optimized cross section of each retrofitted member and the member strength capacity increase from the retrofit are summarized in Table 7-35.

Table 7-35. Comparison of cross section and capacity for each retrofitted member in the Span No.4 of the Milton-Madison Bridge

Retrofitted Members	Original Cross Section (unit: inch)	Optimized Cross Section (unit: inch)	Original Member Capacity (P_{cr} based on K=1)	Optimized Member Capacity (P_{cr} based on K=1)	Strength Capacity Increase
Top Diagonal Braces	2L3 ½ X 3 ½ X 5/16 	Add 2L3 ½ X 3 ½ X 5/16 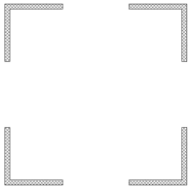	$P_{cr,orig}$ =24kips $M_{p,orig}$ =679in-kips	$P_{cr,new}$ =265kips $M_{p,new}$ =1357in-kips	$\frac{P_{cr,new}}{P_{cr,orig}} = 11$ $\frac{M_{cr,new}}{M_{cr,orig}} = 2$
U2L3, U3L2	1PL10 X 5/16 & 2L4 X 3 X 5/16 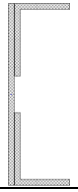	Add 2L4 X 3 X 5/16 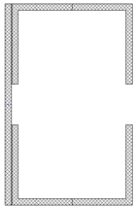	$P_{cr,orig}$ =19kips $M_{p,orig}$ =844in-kips	$P_{cr,new}$ =242kips $M_{p,new}$ =1407in-kips	$\frac{P_{cr,new}}{P_{cr,orig}} = 13$ $\frac{M_{cr,new}}{M_{cr,orig}} = 2$
U1L1, U4L4	1PL10 X 5/16 & 4L4 X 3 X 5/16 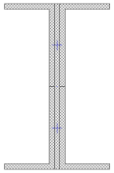	Add 2PL10 X 5/16 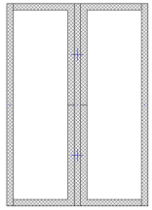	$P_{cr,orig}$ =416kips $M_{p,orig}$ =1430in-kips	$P_{cr,new}$ =667kips $M_{p,new}$ =2310in-kips	$\frac{P_{cr,new}}{P_{cr,orig}} = 2$ $\frac{M_{cr,new}}{M_{cr,orig}} = 2$
L1L2, L3L4	2PL12 X 5/16 & 4L3 ½ X 3 ½ X 5/16 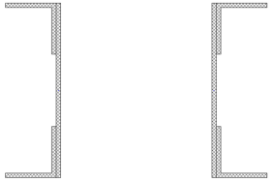	Add 2PL 12 5/8 X 5/16 & 2PL 18 X 5/16 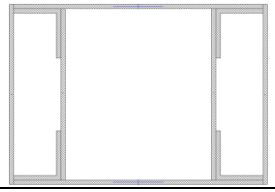	$P_{cr,orig}$ =379kips $M_{p,orig}$ =2318in-kips	$P_{cr,new}$ =948kips $M_{p,new}$ =5759in-kips	$\frac{P_{cr,new}}{P_{cr,orig}} = 3$ $\frac{M_{cr,new}}{M_{cr,orig}} = 2$

From Table 7-35, it can be seen that adding steel plates to optimize the cross sections of the critical members can increase both member buckling capacity and yield strength to at least twice as the original ones. However, considering the number of required steel plates as well as the difficulty in welding these plates in the retrofit, this retrofit strategy with an emphasis on strengthening the critical members may not be cost effective. In particularly, the system load capacity as shown in

Table 7-34 also shows that five out of eleven retrofitted systems after strengthening more than six members are still unable to carry full HL-93 load, which means that nearly half of the retrofitted structures cannot meet the current load rating requirement. Therefore, a complete bridge replacement is probably a better choice.

7.12 Conclusion

This chapter summarized the proposed procedures for performing a simplified system analysis to evaluate both the existence of critical members and the remaining load carrying capacity of a damaged bridge. The commercial program SAP2000 was selected as the analytical tool in the study, as it is widely used in current bridge engineering practice. Both the development and the calibration of full 3D models for the I-35W Bridge and the test span of the Milton-Madison Bridge are discussed. Good correlations between the model results and the real bridge behavior in an undamaged state and a damaged state were found, validating the modelling techniques utilized in this simplified system analysis.

The 3D system models with elastic properties alone were determined to be adequate in capturing the overall bridge response, as these elastic models matched the measured test data well. However, to reasonably predict the behavior of a damaged bridge, it was found necessary to selectively introduce nonlinear features into the truss members in the system models. These nonlinear features

include plastic hinges that simulate large axial-flexure interaction behavior before and after yielding on a particular cross section, nonlinear axial springs that can capture both post-yielding and post-buckling behavior, and the assignments of tension and compression limits as an effort to consider the connection failure that occurs prior to a member failure. It was also found that the decks in all example bridges remained elastic even after one critical member was damaged in the system. Therefore, the nonlinear features for deck elements were not needed.

To assess the various levels of importance of each critical member to a system, a rating factor method and a strain energy method were proposed and compared. As consensus can be found from the ranking results for the critical members using these two methods, either method is able to properly prioritize the critical members. Considering that the rating factor method is more likely to be readily accepted by bridge engineers, this method will be recommended as a practical approach for rating critical members for other truss bridges.

An additional application of a member strain energy based approach was explored. Through examining the strain energy distribution within a damaged main truss system, it was discovered that the location with highest strain energy throughout the entire loading history was most likely to fail first. This implies that the first failure location can be predicted by identifying the maximum strain energy position without the need to actually load the structure up to the ultimate state.

The proposed methodology for system redundancy analyses using nonlinear SAP2000 models were found to be effective in evaluating the bridge conditions for both the New River Bridge and the Span No.4 of the Milton-Madison Bridge. This fact increases the level of confidence in applying this methodology to more general truss bridges.

Reviewing the ranking results of critical members for these four example bridges (two separate spans of the Milton-Madison Bridge, the I-35W Bridge, and the New River Bridge), one key

common result can be found. That is the most critical tension member is the first tension diagonal member from the support. This result is also in consistent with the finding presented by Yamaguchi et al. (2010). This member can also be classified as fracture critical member. In addition, the ranking results also provide insights into the system effect of failure of one stability-critical member, whose axial load demand is close to zero in an undamaged structure. In both the I-35W Bridge and the New River Bridge, which represent typical continuous truss structures, the vertical member that connects to the interior support is most critical to system redundancy among all vertical members. Failure on this member will lead to bridge collapse, as the damaged structure is unable to sustain full dead loads. In contrast, failure on any other vertical member will not reduce the system load capacity below 1.0 of the HL-93 load. In both the test span and the Span No.4 of the Milton-Madison Bridge, which represent typical simple-supported truss structure, the diagonal members in an X-truss configuration in the mid-span panel can be considered as system redundant members, since failure on any one of these members is found to have negligible reduction in system load capacity.

Through examination of the ultimate failure modes in both the test span and Span No.4 of the Milton-Madison Bridge, it is found that failure of a single main truss member in a typical simple-supported truss structure will lead to large in-plane bending effects on a portion of the critical vertical main truss member. The critical portion is where the vertical member projects from the deck plane to the chord member that is closest to the deck. This finding may help to emphasize the need to pay special attention to the vertical main truss members in a damaged simple span truss bridge.

The system analyses performed using the proposed modeling techniques can provide a basis for an effective redundancy retrofit work. These system analyses were found capable of identifying

the most critical components where damage or complete failure existed in the ultimate state of a structure. The majority of retrofit resources can thereby be allocated to these critical components. Most of these critical components identified from the four example bridges in various damaged conditions are the brace members and their connections surrounding the damaged member as well as the main truss members designed as zero-force members. These main truss members include the vertical members adjoining a three-member joint, such as U1L1 in the test span of Milton-Madison Bridge (see Figure 7-23), as well as the diagonal members, which form an X-truss configuration in the mid-span panel. In fact, the strength capacity of these components was not a major concern in the design, but it could greatly affect the load capacity of a damaged structure after losing one main truss member. Therefore, careful examination of the behavior on these components is recommended. Moreover, the redundancy retrofit studies in this research indicated that increasing the strength capacity of the critical brace members and their connections could effectively improve the redundancy of a damaged structure. In contrast, the retrofit strategy of replacing deck to reduce the dead load and develop composite action could not greatly increase the system redundancy for a damaged structure.

Since the above discoveries came from the results for only four example bridges, they were too specific to be considered as generally valid conclusions. However, these results can provide valuable insights in support of any future improvements in allocating resources toward the members that are truly critical to the system redundancy.

8 Conclusions

8.1 Summary

Although truss bridges traditionally classified as fracture critical are perceived to be highly susceptible to collapse after a single member failure, no examples of catastrophic failures could be found from the truss bridge inventory. In particularly, a recent accident on the Matthews Bridge in Florida and a full scale test on one span of the Milton-Madison Bridge on the Route of US-421 revealed that these truss bridges possessed considerable 3D redundancy so that the bridges remained standing after one primary member was removed from the systems. However, this system redundancy is unaccounted for in bridge practice, as there is no clear guidance for assessing it. This research is intended to propose guidelines for system redundancy evaluation of existing truss bridges.

This research utilized the system load capacity in an ultimate state as a measure of system redundancy. The load capacity for a system was determined using a full 3D system model with nonlinear features that properly captured all the likely failure modes. The model was implemented in SAP2000, a commercially available analysis package commonly used in engineering practice; calibration studies and verification of member behavior were carried out using ABAQUS, a research finite element program.

The possible failure modes in a typical truss bridge were identified based on the results from the case study of the I-35W Bridge. The preliminary system redundancy study focused on the system behavior of the I-35W Bridge after losing the tension diagonal member identified as the most critical member to the system capacity. By observing the system behavior predicted from the ABAQUS model, critical locations with plastic damage as well as the possible failure modes at

these locations were identified. Thus an appropriate selection and assignment of nonlinear features was made in the SAP2000 models.

Considering that the system model would have difficulty in predicting connection failures, the connection capacity at the critical locations was examined through studying the local behavior predicted from highly detailed finite element models with very dense meshing in ABAQUS. The results of these local studies were then used to refine the nonlinear properties in the system model so that failure on either a critical member or a weak connection in a system could be properly captured.

From a practical implementation perspective, the ABAQUS software that provided the platform for a nonlinear system redundancy analysis is still a research tool and is not common for engineering use. Hence this research also proposes a methodology of performing system analysis in SAP2000, one of the most common program being utilized by the bridge engineering community. After confirming that the models developed in SAP2000 can properly capture the system behavior of the I-35W Bridge in an undamaged state, specific nonlinear features were introduced to the SAP2000 models to simulate the system response to a single member removal scenario.

Using these workable and validated SAP2000 models, the system load capacities for the I-35W Bridge and the test span of the Milton-Madison Bridge under various damaged conditions were predicted. The modeling techniques for analyzing the system load capacity were further applied to two other truss bridges with different configurations. This application demonstrated the efficiency and reliability of the prediction of system load capacity using nonlinear SAP2000 models.

8.2 Guideline for System Redundancy Evaluation

This section presents a preliminary guideline for system redundancy analysis of truss bridges based on the case studies discussed in this research. First and foremost, the need for performing a system redundancy evaluation should be decided by DOTs based on the current bridge condition.

8.2.1 System Analysis Procedures

When performing a system analysis, the following tasks are required:

(1) Identify members that are most critical for the bridge system:

These critical members can be identified as the members with high demand to capacity ratios for axial loads in an undamaged structure under a prescribed loading condition (see Section 8.2.2). The identification of critical members is carried out on an undamaged bridge model, and a 2D elastic model for the main truss structure is considered capable of reasonably predicting the system behavior for this stage.

(2) Conduct system analyses to study the effects of critical single member removal:

Since this study focuses on the behavior of a bridge system after a single member is removed from the structure, a 3D nonlinear model for the entire bridge including main trusses, braces, deck and floor systems is required in order to capture the progression of failure as well as possibly alternate load paths in the damaged structure. Failure modes to be considered include: yielding and buckling in both main truss members and brace members; axial-flexural interaction near the ends of main truss members resulting in a failure at the critical net section where rivet or bolt holes exist; truss member connections; and plastic damage on deck. To predict the occurrence of the aforementioned failure modes, the critical capacities of these

structural components need to be determined through local studies. Then the results of these local studies will be utilized to define properties of the nonlinear features in the system models.

(3) Calculate the load capacity of a system to examine the adequacy of system redundancy and classify critical members:

The load capacity of a system is calculated as the total loads that are carried by the structure under its ultimate state. The determination of an ultimate state will be explicitly described in Section 8.2.3. The adequacy of system redundancy is examined by comparing the system load capacity with the AASHTO load rating standards at the inventory level and operating level respectively. If a system can be found to possess sufficient redundancy after a member is removed from the system, then this member can be considered as a system redundant member. And if this member is in tension, then it may be re-classified as a non-fracture-critical member for in-service inspection.

8.2.2 Critical Loading Condition

The HL-93 load is chosen as the live load for system analysis as this loading condition represents the current standard for bridge design and inspection. In addition, it is also found that the HL-93 load will produce a more critical system response as compared to the two side-by-side HS-20 truck load, which was utilized by other researcher in similar studies. From the case studies of the four example bridges in this research, the critical loading condition for a given bridge configuration can be summarized as below:

(1) For a short truss bridge with a single span, the HL-93 load that is placed to cause the worst mid-span deflection are most critical to the system load capacity both in an undamaged and a damaged states;

(2) For a long truss bridge, there is little difference in the system response to the variation of live load position. Because the dead load on the structure take account of the majority of total loads, the contribution of live loads to the system is less critical.

(3) For a truss bridge with continuous spans, the HL-93 load positioned so as to induce the worse negative moment effect on one of the interior supports are most critical for the load capacities of both undamaged and damaged systems.

8.2.3 Redundancy Criteria

The redundancy in a system is measured by the load capacity of this system under its ultimate state. An undamaged system is considered to reach its ultimate state when two structural components reach their critical capacities. The progression of failure to the next critical locations is not accounted for as damage on more than two structural components is not considered a practical situation for continued bridge operation in current bridge practice.

The load capacity of a system under its ultimate state can be expressed as a dead factor and a live load factor. The former one will be equal to 1 if the magnitude of total loads carried by a system in an ultimate condition is greater than the full dead load. This indicates that the system can support the structure itself when there is no traffic. The live load factor is then calculated as a ratio of the available live load capacity to the HL-93 load, which is expected to cause the worst live load effect among all current AASHTO loads and state legal loads in a long term. A bridge structure with a live load factor greater than one can be considered capable of remaining functional under normal traffic. If failure on one member in the bridge structure will not reduce its live load factor below 1, this member can thereby be considered redundant to the system. If this member is in tension, then it can be removed from the Fracture critical designation.

8.3 Key Findings from Example Bridge Studies

Key findings observed from the case studies for the four truss bridges can be briefly summarized as below:

(1) Not all tension members are fracture critical. A number of the case studies indicate that failure of a single tension member may not significantly affect the system load capacity. The tension members with low demand-to-capacity ratios for axial loads in an undamaged structure are less likely to affect the system redundancy. Thus these members can be regarded as system redundant members that may not require a fracture critical inspection.

(2) It is clear that the most critical tension member in each of the example bridge study is the first tension diagonal member from the support. Failure on this diagonal member will cause a bridge collapse under the self-weight of the structure. Hence this member can be considered truly fracture critical. Greatest attention needs to be paid on this member in a fracture critical inspection.

(3) In a typical continuous truss structure, the vertical member that connects to the interior support is most critical to system redundancy among all vertical members. Failure on this vertical member will also lead to a bridge collapse under the self-weight of the structure. Therefore, this member needs to be classified as a system non-redundant member even though the demand-to-capacity ratio for axial loads on this member is low in an undamaged structure. The rest of vertical members can be considered as system redundant members, since failure on any one of them will not reduce the system load capacity below 1.0 of the HL-93 load.

(4) In a typical simple-supported truss structure, the diagonal members in an X-truss configuration in the mid-span panel can be classified as system redundant members, as the removal of any one of these members will result in little reduction in system load capacity.

(5) A subsequent failure, after a main truss member is damaged, will most likely occur at the ends of the main truss members in the vicinity of the damaged member due to excessive axial-flexural interaction effect. For a tension truss member, the ultimate failure mode is controlled by rupture at the critical net section under a combination of tension and flexure. This failure mode will deactivate the member suddenly at low elongation.

(6) The strength and deformation capacities at the critical net section that is subjected to high tension-flexural loading effect can be predicted through a fracture simulation approach using strain controlled failure criteria available in ABAQUS program. This procedure is complex and computationally expensive but no reliable simplified techniques could be found to predict the actual capacity for this failure mode in complex built-up members.

(7) In a combined tension and flexure loading condition, a net section rupture will occur prior to a gross section yielding if the area of holes is no more than 15% of the gross area. This statement is corroborated by the results from the case study for the net section interaction capacity of one side plate on the tension member U8U9 in the I-35W Bridge. This 15% rule also agrees well with the current steel design practice.

(8) The study for the net section interaction capacity for the entire built-up cross section on member U8U9 demonstrates that the capacity reduction from a gross section to a net section is primarily caused by the presence of regularly spaced access holes on the bottom cover plate. When this cover plate is in tension, it will lose strength capacity due to net section rupture as the cover plate has a ratio of net to gross area less than 0.85. The effects of these access holes on the bottom cover plate can be estimated using either of two equivalent sections obtained by:

a. replacing the bottom cover plate with a solid plate without access holes and assigning this solid plate a reduced thickness, which is determined to provide the same tensile stiffness as that of the original cover plate; or

b. by deducting the net area of an access hole while keeping the original cover plate thickness. Since using the latter cross section is specified by AASHTO (2012) as a standard approach for calculating the strength capacity of a net section under either pure tension or pure flexure, it is possible to extend this AASHTO specification to the calculation of the net section interaction capacity under a combined tension and flexure.

(9) The net section rupture due to axial-flexural interaction effect can be captured from a system model by incorporating plastic hinges to the ends of a truss member. The properties of the plastic hinges can be determined by either developing robust local models for a single truss member with net section details or conducting experiments to measure the local behavior of critical sections.

(10) System analysis results from the studies of both the test span and Span No.4 of the Milton-Madison Bridge indicate that in a typical simple span truss structure excessive in-plane flexural deformation may lead to plastic damage on a vertical main truss member as a consequence of failure on one main truss member. The most critical section on the vertical member is where the vertical member projects from the deck plane to the chord member that is closest to the deck. This result not only highlights the importance of a vertical member in a damaged structure after losing one main truss member, but it also provide insights of the locations on which inspection and retrofit work need to be focused.

(11) Brace members are susceptible to overstress in response to failure on a main truss member. Thus the actual strength capacity of brace members, which is typically not accounted for in a bridge design, must be carefully considered in a system redundancy analysis.

(12) The study of system effect due to failure on a gusset plate connection reveals that the same system consequences are observed either from failure on a truss member or from failure on the connection of this truss member. A connection failure due to shear rupture along the chord line on a five-member joint is unable to impair the structural integrity, so the damaged system can still behave elastically. This result may eliminate the need of considering the shear rupture failure on a main truss member in a system redundancy analysis.

8.4 Redundancy Retrofit

The advantages of a refined system analysis are not limited to the improvement in classifying system non-redundant members and identifying fracture critical members. This analysis will also benefit the redundancy retrofit work. As the ultimate failure mode of a structure can be properly predicted by performing a system analysis with a selective number of nonlinear features, retrofit work can be focused on the most critical components.

Examination of the most critical components identified from the four example bridges provides insights into the location where special attention needs to be paid to in a redundancy retrofit process. Results from the redundancy retrofit case studies would lead to the following conclusions:

(1) In a damaged structure after one primary load carrying member is removed, truss members mainly designed for providing stiffness require careful inspection and some of them often need strengthening. These members include brace members in the vicinity of the removed member and the main truss members that were designed as zero-force members.

(2) Strengthening critical brace members and their connections could significantly improve the redundancy of a damaged structure after failure on one main truss member, as these components primarily contribute to providing alternate load path in the damaged structure.

(3) Replacing deck may not be an effective retrofit strategy. Based on the retrofit study for the New River Bridge, it is clear that the system load capacity cannot be greatly enhanced even filling the deck with lightweight concrete and developing composite action between the deck and floor systems.

8.5 Recommendations for Further Research

Further improvements toward a robust and practical guide specification for performing system redundancy analysis can be achieved in the following directions:

8.5.1 Probability of Failure on Each of the Critical Members

The calculation of system load capacity for a damaged structure performed in this research is based on an assumption that each critical member identified in the preliminary screening process is equally susceptible to be completed deactivated. In fact, the likelihood of failure on a particular member is affected by multiple factors, such as the corrosion deterioration on this member, the actual fatigue resistance on the critical sections, the variability of actual traffic loads, exposure to impact, to name but a few. Studies to quantify the vulnerability of typical bridge members are needed. With an appropriate evaluation of the key factors that may significantly alter either the load demand or the capacity of a specific member, the member whose failure is most likely to occur will be inspected with the shortest time interval. Meanwhile, the inspection and retrofit work can be highly focused on the critical locations identified from the study of the damaged structure behavior after losing this member using the approach proposed in this research.

8.5.2 Model Sensitivity Studies

Since this research utilizes 3D system models to predict the ultimate load capacity of a bridge structure, the robustness of the model depends on their user's abilities to properly calibrate it to the behavior of a real structure. Given the formidable constraints in conducting tests to measure the real structural response to failure on different truss members one at a time, the development of a robust system model needs comprehensive investigations of the relevant variables to reduce the uncertainties in the analyses. Further research should study the model sensitivity to the variable

parameters that include the randomness of material properties and truck loads with various dynamic impacts, possible differential support settlements, changes in the boundary conditions from the design, and the effect of skew angles.

8.5.3 Reliability-Based Measure of System Redundancy

As an alternative measure of the redundancy in a bridge system, the reliability indices expressed as β factors are utilized by the current LRFD criteria in AASHTO (2012). The reliability indices of a bridge system can be estimated based on the knowledge regarding the probability of occurrence of a single member damage as well as the associated system load capacity. Then the adequacy of system redundancy can be checked by comparing the reliability indices for the specific structure with the target values of reliability indices as suggested by Ghosn and Moses (1998). Although the framework for conducting reliability assessment was provided by G. Washer et al. (2014), the feasibility and potential limitations of applying the methodology proposed in this report to a real truss bridge still need to be explored through extensive case studies.

8.5.4 Further Experimental Studies for the Net Section Capacity under Combined Tension and Flexure

In this research, the net section capacity under a combination of tension and flexure was explored based on a specific cross section configuration and the study was performed using finite element modeling tools. The level of confidence for the predicted net section capacity will be greatly enhanced if similar behavior at this cross section can be observed from robust experiments. To further generalize the net section capacity prediction, it is necessary to conduct a series of parametric studies for analyzing the effects of various cross section configurations, net section details and material ductility.

8.5.5 Improvement of Ultimate State Prediction in the Analytical Models

This research studies one example bridge system behavior using two analytical tools, one is ABAQUS and the other is SAP2000. The latter one is a recommended choice for bridge engineers to perform system redundancy evaluation. One major concern in using the results from a SAP2000 model is identified as the inability of these models to properly capture the deformation of a system in its ultimate state. Further research effort will be spent in providing more realistic deformation prediction from SAP2000 models. This can be achieved by improving the nonlinear features in SAP2000.

8.5.6 Improve the Design for New Truss Bridges with the Consideration of System Redundancy

Due to the lack of a clear guidance on the evaluation of system redundancy, the benefits of utilizing system redundancy are not accounted for in current bridge design practice. As a continuation of the current research which aims to appropriately measure the redundancy in a truss bridge system, future studies can be focused on the development of robust methodologies to incorporate the system redundancy evaluated using the approach proposed in this research into the design of new truss bridges. This will be a leading effort towards a more economic design for new truss bridges, as the concept of considering system redundancy in bridge design is presented by Ghosn et al. (2014) but the example truss bridge applications have not been studied thus far.

References

A. Astaneh, and Asla "Progressive Collapse of Steel Truss Bridges, the Case of I-35W Collapse." Proc., 7th International Conference on Steel Bridges, Guimarães, Portugal.

AASHTO (1978). "AASHTO's Guide Specification for Fracture Critical Nonredundant Steel Bridge Members." American Association of State Highway and Transportation Officials, Washington D.C.

AASHTO (2012). "AASHTO Load and Resistance Factor Design (LRFD) Bridge Design Specifications." American Association of State Highway and Transportation Officials, Washington D.C.

AASHTO (2011). "Manual for Condition Evaluation of Bridges." American Association of State Highway and Transportation Officials, Washington D.C.

AASHTO/NSBA (2011). "Guidelines for Steel Girder Bridge Analysis." NSBA SGBA-1, National Steel Bridge Alliance, Chicago.

AISC (2011). "Manual of Steel Construction, Load & Resistance Factor Design" American Institute of Steel Construction, Chicago.

Altstadt, S. A. (2004). "Tensile Strength and Ductility of High Performance Steel Girders." Master, University of Minnesota.

Altstadt, S. A. (2006). "Net Section Failure Criteria of Bolted Connections under Bi-axial Moment and Tensile Axial Loading." First International Conference on Fatigue and Fracture in the Infrastructure - Bridges and Structures of the 21st Century, Philadelphia.

Areias, P. M. A., and Belytschko, T. (2005). "Analysis of Three-dimensional Crack Initiation and Propagation Using the Extended Finite Element Method." International Journal for Numerical Methods in Engineering, 63, 29.

ASTM (2010). "Standard Specification for General Requirements for Rolled Structural Steel Bars, Plates, Shapes, and Sheet Piling " ASTM A6/A6M-2010American Society for Testing Material (ASTM)

Azizinamini, A. (2002). "Full Scale Testing of Old Steel Truss Bridge." Journal of Constructional Steel Research, 58(5–8), 843-858.

Bao, Y., and Wierzbicki, T. (2004). "On Fracture Locus in the Equivalent Strain and Stress Triaxiality Space." International Journal of Mechanical Sciences.

Bažant, Z. and Verdure, M. (2007). ”Mechanics of Progressive Collapse: Learning from World Trade Center and Building Demolitions.” J. Eng. Mech., 133(3), 308–319.

Beshah, F., Wright, W., and Graybeal, B. (2008). "Mechanical Property Test Report: I-35W over the Mississippi River." Federal Highway Administration, Turner-Fairbank Highway Research Center.

Bursi, O. S., and Jaspart, J. P. (1998). "Basic Issues in the Finite Element Simulation of Extended End Plate Connections." Computers & Structures, 69(3), 361-382.

CAN/CSA-S6 "Canadian Highway Bridge Design Code." Canadian Standards Association (CSA), Toronto.

CEN (2005). "Eurocode 3: Design of Steel Structures." Brussels: European Committee for Standarization

Cha, H., Lyrenmann, L., Connor, R. J., and Varma, A. H. (2014). "Experimental and Numerical Evaluation of the Post-fracture Redundancy of a Simple Span Truss Bridge." Journal of Bridge Engineering.

Charney, F. A. (2003). "Economy of Steel Framed Buildings through Identification of Structural Behavior." American Institute of Steel Construction, Inc.

Chi, W., Kanvinde, A., and Deierlein, G. (2006). "Prediction of Ductile Fracture in Steel Connections Using SMCS Criterion." Journal of Structural Engineering, 132(2), 171-181.

Citipitioglu, A. M., Haj-Ali, R. M., and White, D. W. (2002). "Refined 3D Finite Element Modeling of Partially-restrained Connections Including Slip." Journal of Constructional Steel Research, 58(5–8), 995-1013.

Connor, R. J., and Altstadt, S. A. (2013). "After-fracture Reserve Strength of Two Four-Chord Aluminum Sign Trusses." Journal of Structural Engineering.

Connor, R. J., Dexter, R., and Mahmoud, H. (2005). "Inspection and Management of Bridges with Fracture-Critical Details." NCHRP Synthesis 354, Transportation Research Board, Washington D.C.

Connor, R. J., Kaufmann, E. J., Jin, J., and Davies, C. H. (2004). "Forensic Investigation of the SR422 over the Schuylkill River Girder Fracture." Proceedings of the Twenty-First International Bridge Conference.

Dexter, R. J., Alttstadt, S. A., and Gardner, C. A. (2002). "Strength and Ductility of HPS70W Tension Members and Tension Flanges with Holes." University of Minnesota.

Diggelmann, L. M., Connor, R. J., and Sherman, R. J. (2012). "Evaluation of Member and Load-Path Redundancy on the US-421 Bridge over the Ohio River." Purdue University.

FEMA, P. (2000). "Commentary for the Seismic Rehabilitation of Buildings." FEMA-356, Federal Emergency Management Agency, Washington, DC.

FHWA (2012). "Clarification of Requirements for Fracture Critical Members", Federal Highway Administration, Washington D.C.

FHWA (2012). "Load Rating of Steel Bridges", Federal Highway Administration, Washington D.C.

FHWA (2012). "Steel Bridge Design Handbook: Bracing System Design", Federal Highway Administration, Washington D.C.

Fisher, J. W. (1984). "Fatigue and Fracture in Steel Bridges", New York.

Frank, Barsom, and Hamburger (2000). "State of the Art Report on Base Metals and Fracture" FEMA-355A, SAC Joint Venture.

G. Washer, R. Connor, A. Ciolko, R. Kogler, P. Fish, and Forsyth, D. (2014). "Proposed Guideline for Reliability-Based Bridge Inspection Practices" NCHRP Report 782, Transportation Research Board.

GB50017-2003 (2003). "Code for Design of Steel Structures." Administrative Group of the National Standard, Beijing, China.

Ghosn, M., and Fiorillo, G. (2013). "Nonlinear Redundancy Analysis of Truss Bridges." the City College of New York.

Ghosn, M., and Moses, F. (1998). "Redundancy in Highway Bridge Superstructures." Transportation Research Board, National Cooperative Highway Research Program.

Ghosn, M., Yang, J., Beal, D., and Sivakumar, B. (2014). "Bridge System Safety and Redundancy." NCHRP Report 776, Transportation Research Board.

Girão Coelho, A. M. (2013). "Rotation Capacity of Partial Strength Steel Joints with Three-dimensional Finite Element Approach." Computers & Structures, 116(0), 88-97.

Guo, W., and Gilsanz, R. (2003). "Simple Nonlinear Static Analysis Procedure for Progressive Collapse Evaluation." AISC Conference Proceedings.

Gurson (1976). "Continuum Theory of Ductile Rupture by Void Nucleation and Growth: Part I—Yield Criteria and Flow Rules for Porous Ductile Media." Journal of Engineering Material Technology, 99(1), 14.

Hancock (1976). "On the Mechanics of Ductile Failure in High-strength Steel Subjected to Multi-axial Stress States." Journal of the Mechanics and Physics of Solids, 24(3), 14.

Hickey, L. J., Roberts-Wollmann, C., Cousins, T., Sotelino, E., and Easterling, S. (2009). "Live Load Test and Failure Analysis for the Steel Deck Truss Bridge Over the New River in Virginia." Master of Science, Virginia Polytechnic Institute and State University.

Hill, H. J., McGormley, J. C., Koob, M. J., and Nugent, W. J. (2008). "I-35W Bridge over the Mississippi River Collapse Investigation." Minneapolis, Minnesota.

JRA (2002). Specifications for Highway Bridges Part I: Volume on Common Matters. Japan Road Association.

JSCE (2010). "Standard Specifications for Steel and Composite Structures." Committee on Steel Structures of Japanese Society of Civil Engineers.

K.Yamaguchi, Yoshida, Y., and Iseda, S. (2010). "Analysis of Influence of Breaking Members of Steel through Truss Bridges." Japan Bridge Engineering Center.

Kanvinde, and Deierlein (2004). "Micromechanical Simulation of Earthquake Induced Fractures in Steel Structures." Blume Center TR145, Stanford University, Stanford, California.

Khandelwal, K. (2008). "Multi-scale Computational Simulation of Progressive Collapse of Steel Frames." Doctor of Philosophy, University of Michigan.

Lemaitre, J. (1985). "A Continuous Damage Mechanics Model for Ductile Fracture." Journal of Engineering Materials and Technology, 107(1), 83-89.

Liao, M., and Okazaki, T. (2009). "A Computational Study of the I-35W Bridge Collapse." Center for Transporation Studies, National Technical Information Services.

Lora, M. A. R. (2013). "Study of the I-35W Highway Bridge Collapse Mechanism." Master of Science, Virginia Polytechnic Institute and State University.

Madison, R. B., and Irwin, G. R. (1974). "Dynamic KIc testing of Structural Steel." Journal of the Structural Division: American Society of Civil Engineers.

Mahmoud, H. (2005). "Inspection and Management of Bridges with Fracture-Critical Details." NCHRP Synthesis 354, Transportation Research Board, Washington D.C.

Mizzen, D. R. (2011). "Development of Subassembly Test Methods for Evaluation of Prefabricated Bridge Decks." Master of Science, Purdue University.

Mn/DOT (2009). "I-35W Bridge Original Plans and Details." Minnesota Department of Transportation, http://www.dot.state.mn.us/I-35Wbridge/history.html.

Modjeski, and Masters (2011). "Winona Bridge Deck Rehabilitation Options." Modjeski and Masters, Inc.

Mohr, B. A. (2005). "Investigation of Ultimate Bending Strength of Steel Bracket Plates." Masters of Science, Virginia Polytechnic Institute and State University.

Munse, W. H. (1970). "Riveted and Bolted Structural Joints." Illinois Cooperative Highway Research Program, University of Illinois.

Nagai, M., and Miyashita, T. (2009). "Recent Topics on Steel Bridge Engineering in Japan: Design and Maintenance." Nagaoka University of Technology.

NTSB (1971). "Collapse of U.S. 35 Bridge, Point Pleasant, West Virginia, December 15, 1967." Report NTSB-HAR-71-1, National Transportation Safety Board, Washington, D.C.

NTSB (2009). "Collapse of I-35W Highway Bridge, Minneapolis, Minnesota, August 1, 2007." National Transportation Safety Board.

Ocel, J. (2013). "Evaluation of Member and Load-Path Redundancy on the US-421 Bridge Over the Ohio River." Federal Highway Administration (FHWA).

Ocel, J. M. (2013). "Guidelines for the Load and Resistance Factor Design and Rating of Riveted and Bolted Gusset-Plate Connections for Steel Bridges." NCHRP Project 12-84, Federal Highway Administration, Turner-Fairbank Highway Research Center, McLean, VA.

Ocel, J. M., and Wright, W. J. (2008). "Finite Element Modeling of I-35W Bridge Collapse ", Turner-Fairbank Highway Research Center.

O'Connell, H. M., Dexter, R. J., and Bergson, P. (2001). "Fatigue Evaluation of the Deck Truss of Bridge 9340."University of Minnesota, Department of Civil Engineering. St. Paul, MN: Minnesota Department of Transportation.

Okui, Y., Nagatani, H., Akashi, N., Matsuda, T., Obata, M. Y. Y., Ishii, H., Miyamori, M., and Hirayama, H. (2010). "After Fracture Redundancy Analysis of Steel Truss Bridges in Japan." IABSE-JSCE Joint Conference on Advances in Bridge Engineering-II.

Panontin (1994). "The Relationship between Constraint and Ductile Fracture Initiation as Defined by Micromechanical Analyses." Doctor of Philosophy, Stanford, California.

Reese, L. D. (2009). "Critical Member Removal and Load Redistribution of a Deteriorated Truss Bridge." Master of Science, Pennsylvania State University.

Rice, and Tracey (1969). "On the Ductile Enlargement of Voids in Triaxial Stress Fields." Journal of Mechanics and Physics of Solids, 17(3), 17.

Scanlan, D., and Gilliam, D. (2013). "Jacksonville's Mathews Bridge Shut Down After Ship Hits It." The Florida Times – Union, http://members.jacksonville.com/news/crime/2013-09-27/story/jacksonvilles-mathews-bridge-shut-down-after-ship-hits-it.

Schenker, L., Salmon, C. G., and Johnston, B. G. (1954). "Structural Steel Connections." AFSWP Report No. 352.

Simulia (2010). "ABAQUS Analysis User Manual", Version 6.10, Providence, RI.

Starossek, U. (2009). "Progressive Collapse of Structures", Hamburg University of Technology.

Sverdrup & Parcel and Associates Inc. , I. (1965). "State of Minnesota Department of Highway Construction Plan for Bridge No. 9340 - Balance of Bridge and Approaches." St. Louis, MO.

Szyniszewski, S., and Krauthammer, T. (2012). "Energy Flow in Progressive Collapse of Steel Framed Buildings." Engineering Structures, 42, 10.

Tavakoli, H., and Kiakojouri, F. (2012). "Energy-based Assessment of Robustness in Progressive Collapse Scenario." 14th International Conference on Computing in Civil and Building Engineering, ISCCBE, Moscow, Russia.

VDOT (2006). "2006 Bridge Inspection Report, Route 100 (Wysor Highway) Over New River." Virginia Department of Transportation.

Wipf, T. J., and Phares, B. M. (2002). "Evaluation of Interstate 80 Sign Truss." The Iowa Department of Transportation, the Bridge Engineering Center at the Center for Transportation Research and Education-Iowa State University.

Wisniewski, D., Casas, J. R., and Ghosn, M. (2006). "Load Capacity Evaluation of Existing Railway Bridges based on Robustness Quantification." Structural Engineering International.

Wright, W. J. (2002). "Fracture Toughness Requirements for Highway Bridges: Past and Future Trends." Progress in Structural Engineering and Materials.

Yoshiaki Okui, H. N., Naomitsu Akashi, Takenori Matsuda, Masahiro Yasuda, Yasuhiro Obata, Hironori Ishii, Masayuki Miyamori, Hiroshi Hirayama (2010). "After Fracture Redundancy Analysis of Steel Truss Bridges in Japan." IABSE-JSCE Joint Conference on Advances in Bridge Engineering-IIDhaka, Bangladesh.

Zhou, T., Li, W., Yu, G., and Liang, B. (2013). "Damage Analysis of Steel Frames under Cyclic Load Based on Stress Triaxiality." Engineering Mechanics (In Chinese).

Ziemian, R. D. (2010). "Guide to Stability Design Criteria for Metal Structures", 6th Edition.

Appendices

The appendices provide information of the dimensions and design loads of the truss members in the full 3D system of the I-35W Bridge, the test span of the Milton-Madison Bridge, the New River Bridge, and Span No.4 of the Milton-Madison Bridge.

Appendix A: Details of the I-35W Bridge

Table A-1. Dimensions of the main truss members

Members	Length (ft)	Depth (in)	Width (in)	t_f (in)	t_w (in)	Shape
L1-L3	76.04	29	21	3/8	1/16	Box
L1-U2	48.41	25	21	1/2	1 1/8	Box
L5-U6	55.17	22	18 3/4	1 1/8	7/16	H
U0-U2	76	29	21	1/2	5/8	Box
U1-L1	30	16	21	1/2	3/4	Box
U2-L2	31.25	15	20	1/2	3/8	H
U2-L3	50	18	19 7/8	9/16	3/8	H
U2-U4	76	29	21	1/2	1	Box
U3-L3	32.5	16	21	1/2	3/4	Box
U4-L4	36.25	15	20	1/2	3/8	H
U4-U6	76	29	21	1/2	5/8	Box
U5-L5	40	16	21	9/16	3/4	Box
U6-L6	46	15	20	1/2	3/8	H
U6-L7	64.41	29	21	9/16	1 7/16	Box
U6-U8	76	29	21	1/2	1 5/8	Box
U7-L7	52	17	21	9/16	7/8	Box
U8-L8	60	33	21	3/4	2 3/8	Box
U8-L9	64	24	17 1/2	1 3/4	1/2	H
U9-L9	51.5	17	21	9/16	7/8	Box
L9-U10	64	29	21	11/16	2	Box
U8-U10	76	29	21	1/2	1 7/16	Box
L1'-L3'	76.04	29	21	7/16	7/8	Box
L1'-U2'	48.41	25	21	1/2	1 1/4	Box
L11-U12	55.17	29	21	9/16	1 7/16	Box
L3'-L5'	76.37	29	21	1/2	15/16	Box
U0'-L1'	48.41	25	21	1/2	1 7/16	Box
U0'-U2'	76	29	21	1/2	15/16	Box
U10-L11	55.17	24	17 3/4	1 5/8	9/16	H
U10-U12	76	29	21	1/2	1	Box
U11-L11	40	16	21	1/2	3/4	Box
U12-L12	38	15	20	1/2	3/8	H
U12-L13	52.35	22	18 3/4	7/16	1 1/8	H
U12-U14	76	29	21	9/16	2 1/8	Box
U13-L13	36	16	21	1/2	3/4	Box
U14-L14	36	15	20	1/2	3/8	H
U2'-U4'	76	29	21	1/2	1	Box
L3-L5	76.37	29	21	1/2	15/16	Box

Members	Length (ft)	Depth (in)	Width (in)	t_f (in)	t_w (in)	Shape
L3-U4	50	18	20 1/4	3/8	9/16	Box
L5-L7	76.94	29	21	1/2	1 5/16	Box
L7-L8	38.83	29	21	5/8	2 1/2	Box
L7-U8	64.41	24	18 1/4	1 3/8	7/16	H
L8-L9	38.94	29	21	5/8	2 1/2	Box
U0-L1	48.41	23	21	1/2	15/16	Box
U4-L5	55.17	25	21	1/2	15/16	Box
U8-L9	64	24	17 1/2	1/2	1 3/4	H
L9-L11	76.87	29	21	1/2	15/16	Box
L11-L13	76.11	29	21	1/2	1 7/16	Box
L13-U14	52.35	23	21	7/16	3/4	Box
L3'-U4'	50	19	21	3/8	9/16	Box
U10-L10	45.75	15	20	1/2	3/8	H
U2'-L3'	45.75	18	19 3/4	5/8	3/8	H
L13-L13'	76	29	21	1/2	2 1/8	Box

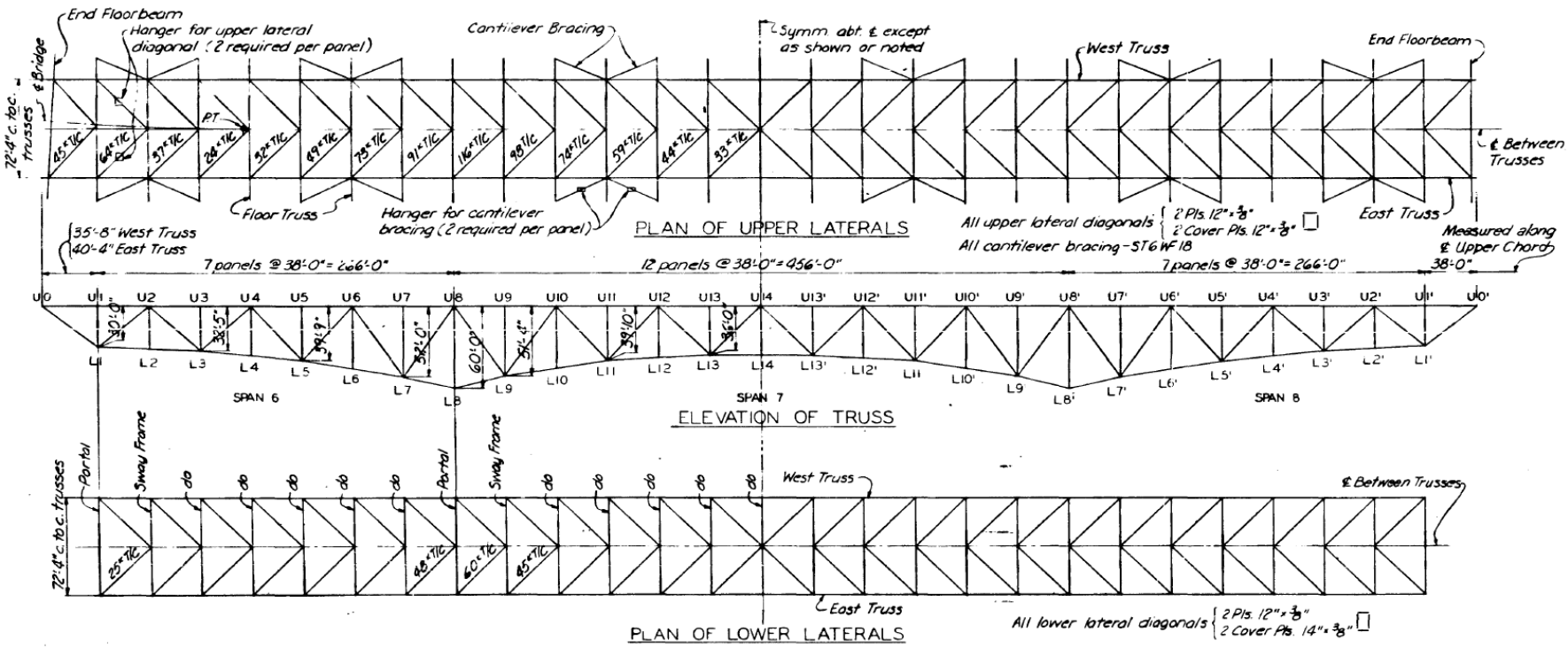

Figure A-1. Overall geometry of the truss system. Sverdrup & Parcel and Associates, Inc. (1965). State of Minnesota Department of Highway Construction Plan for Bridge No. 9340 – Balance of Bridge and Approaches. St. Louis, MO. Used under fair use, 2015.

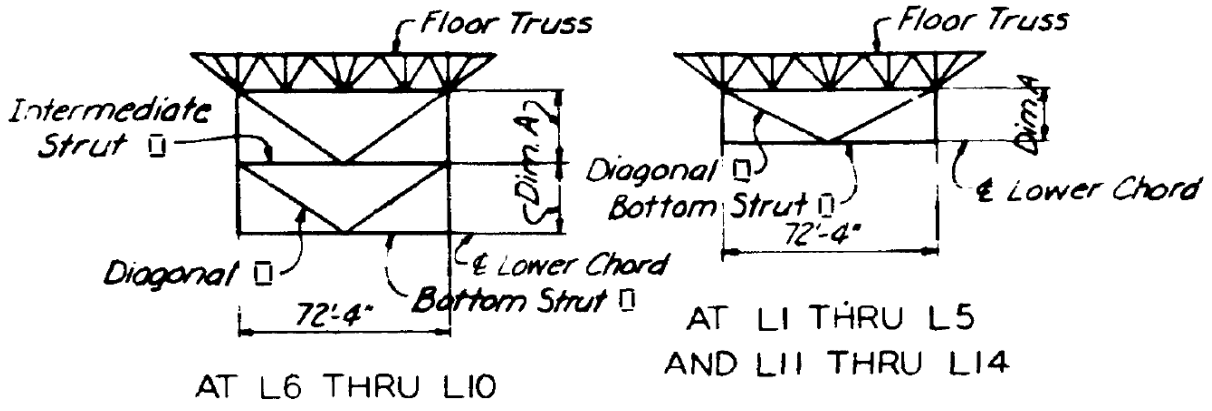

TABLE OF MEMBERS

	Panel Pt.	Inter. Strut	Bott. Strut	Diagonal
3 way frames	L2 thru L5 & L11 thru L14	—	2 Pls. 14" x ½" & 2 Cov. Pls. 12" x ⅜"	2 Pls. 12" x ⅜" & 2 Cov. Pls. 12" x ⅜"
	L6, L7, L9 & L10	2 Pls. 14" x ½" & 2 Cov. Pls. 12" x ⅜"	do	do
Portals	L1	—	2 Pls. 15" x ½" & 2 Cov. Pls. 12" x ⅜"	2 Pls. 12" x ⅜" & 2 Cov. Pls. 12" x ⅜"
	L8	2 Pls. 14" x ⅜" & 2 Cov. Pls. 12" x ⅜"	2 Pls. 15" x ½" & 2 Cov. Pls. 12" x ⅜"	2 Pls. 14" x ½" & 2 Cov. Pls. 12" x ⅜"

Panel Pt.	Dim. A
L1	19'-9⅜"
L2	21'-0⅛"
L3	22'-2⅝"
L4	25'-10⅝"
L5	29'-6⅝"
L6	17'-10 1/16"
L7	20'-10 13/16"
L8	24'-10 13/16"
L9	20'-6 9/16"
L10	17'-8 5/16"
L11	29'-7⅜"
L12	27'-8⅝"
L13 & L14	25'-9⅝"

Figure A-2. Dimensions of brace members. Sverdrup & Parcel and Associates, Inc. (1965). State of Minnesota Department of Highway Construction Plan for Bridge No. 9340 – Balance of Bridge and Approaches. St. Louis, MO. Used under fair use, 2015.

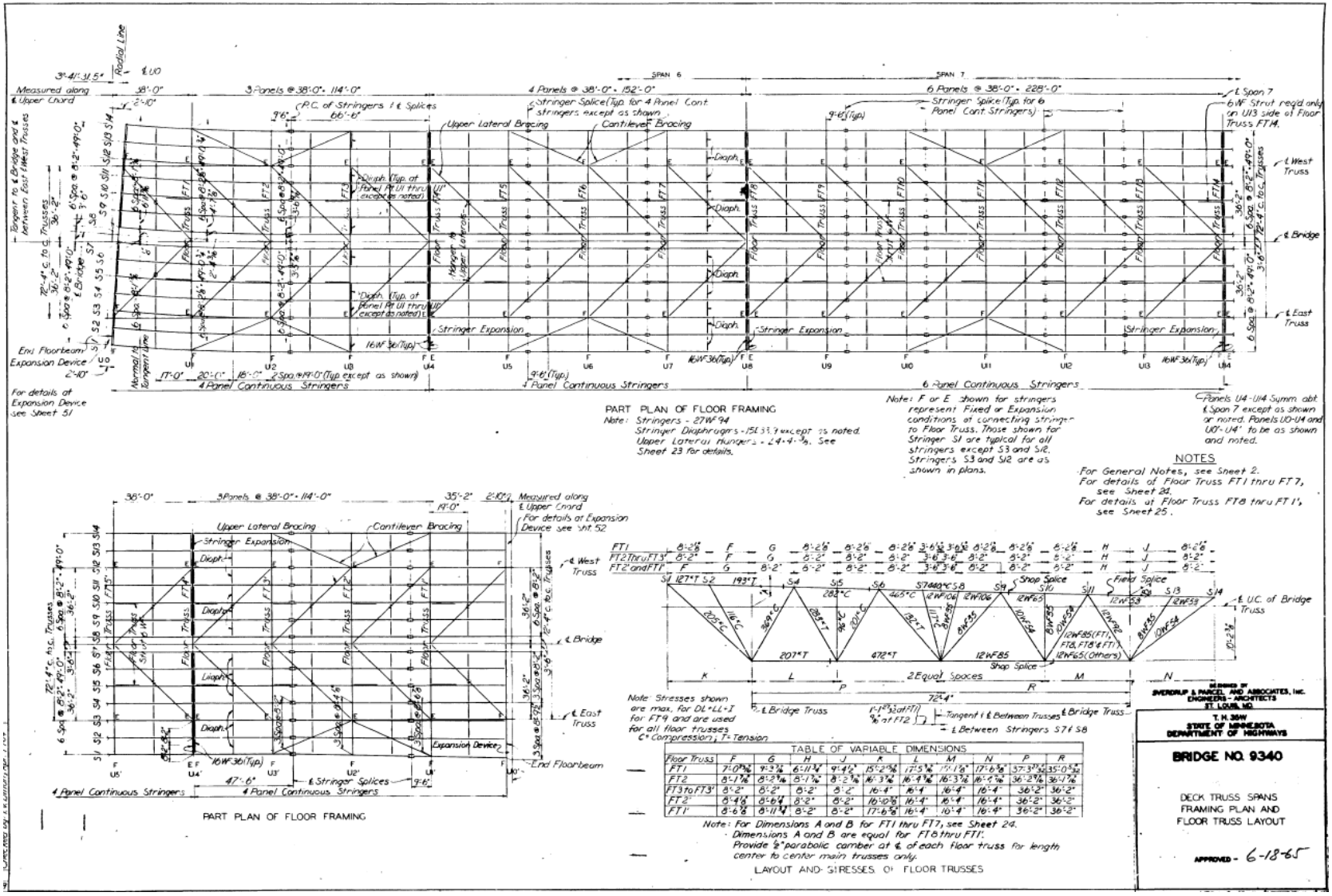

Figure A-3. Dimensions of floor truss members. Sverdrup & Parcel and Associates, Inc. (1965). State of Minnesota Department of Highway Construction Plan for Bridge No. 9340 – Balance of Bridge and Approaches. St. Louis, MO. Used under fair use, 2015.

Appendix B: Details of the Test Span of the Milton-Madison Bridge

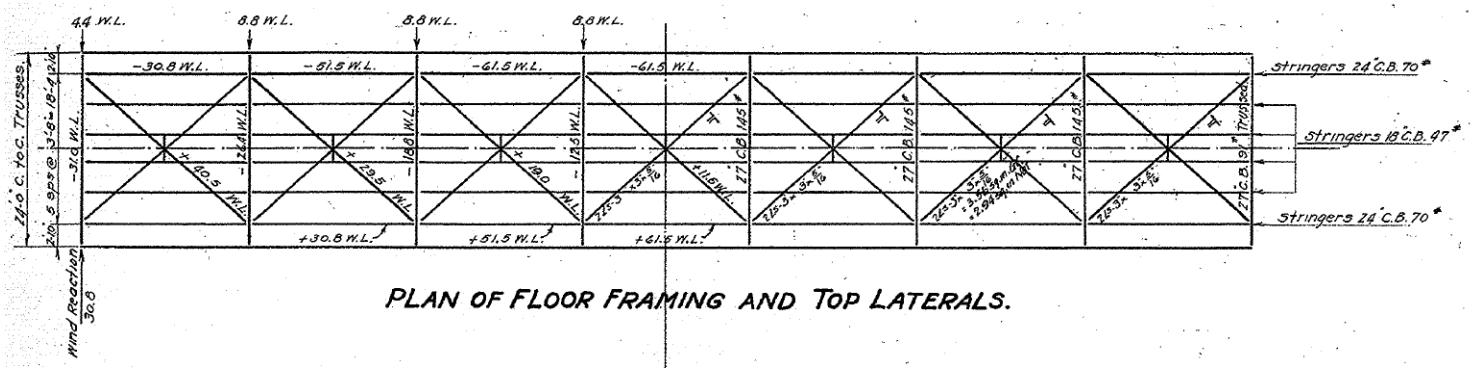

Figure B-1. Dimensions and design loads for floor truss members, stringers, and top lateral braces. J.G. White Engineering Corporation (1928). Used under fair use, 2015.

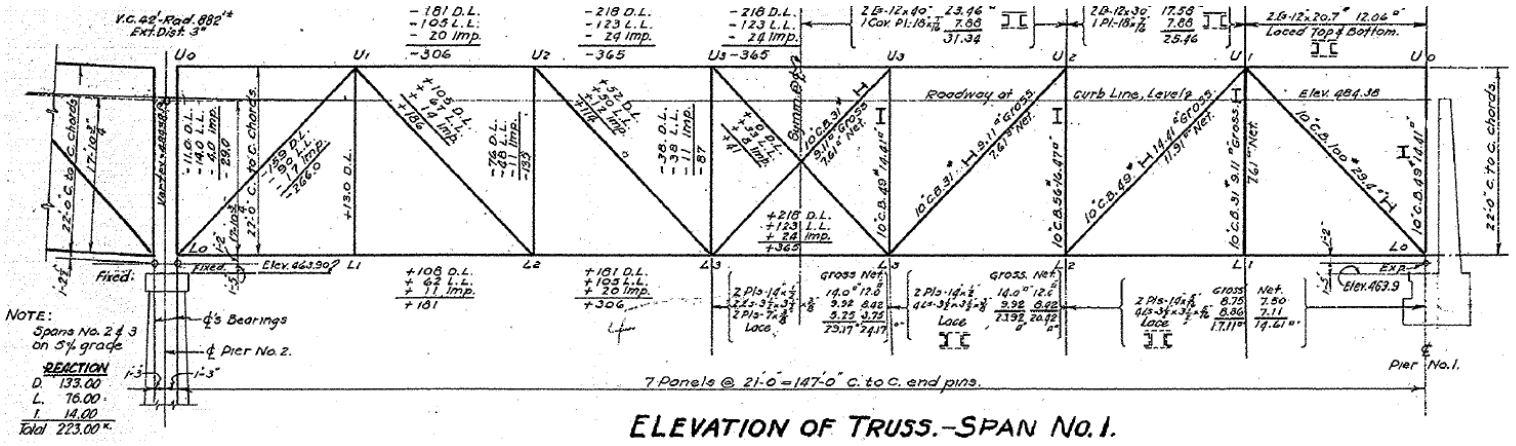

Figure B-2. Dimensions and design loads for main truss members. J.G. White Engineering Corporation (1928). Used under fair use, 2015.

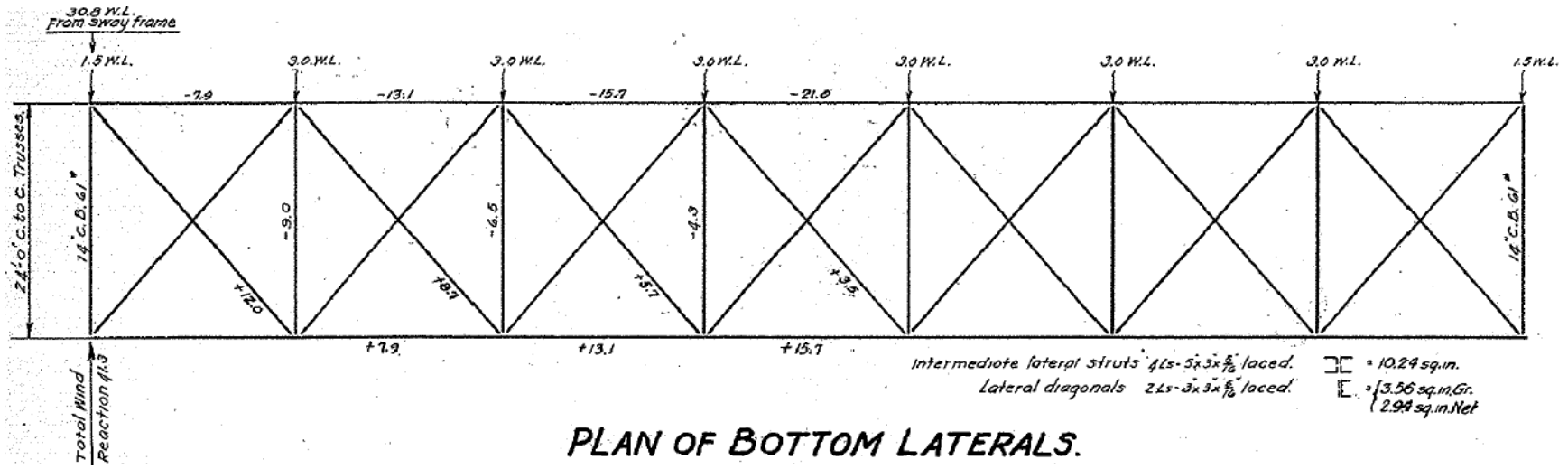

Figure B-3. Dimensions and design loads for bottom lateral braces. J.G. White Engineering Corporation (1928). Used under fair use, 2015.

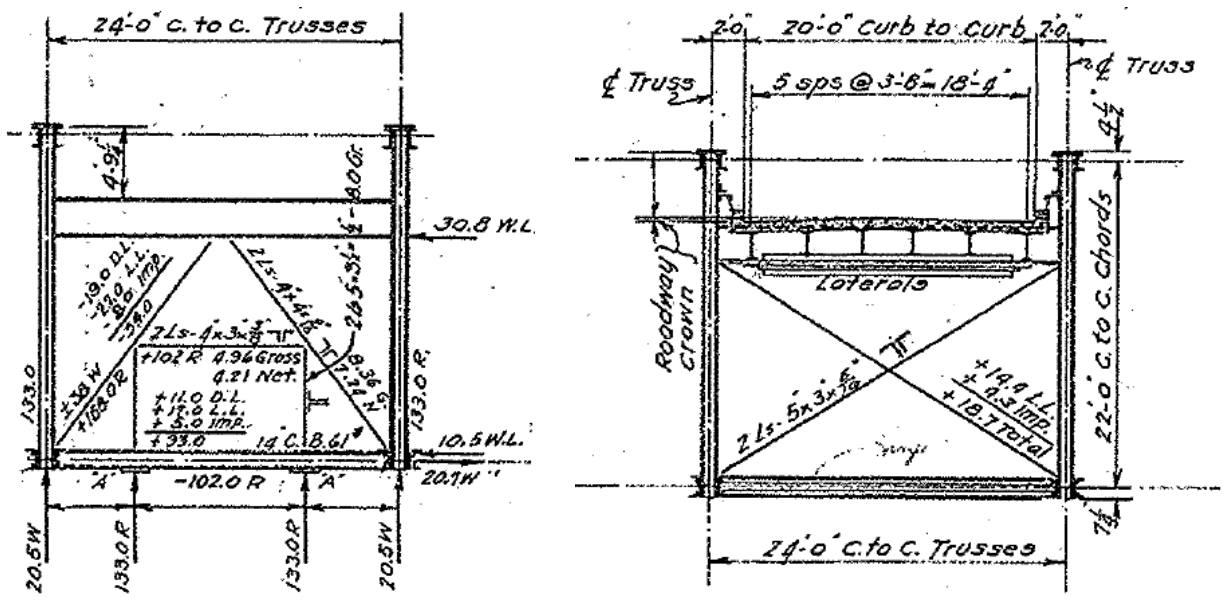

(a) (b)

Figure B-4. Dimensions and design loads for typical sway braces: (a) at the end panel points (U0 and U0'); (b) at intermediate panel points (U1 through U1'). J.G. White Engineering Corporation (1928). Used under fair use, 2015.

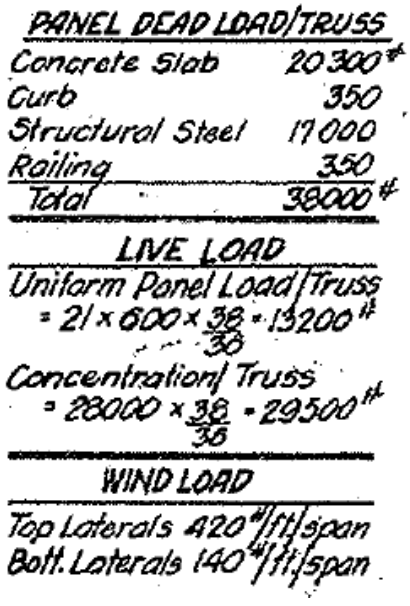

Figure B-5. Design loads for main truss members and lateral braces. J.G. White Engineering Corporation (1928). Used under fair use, 2015.

Appendix C: Details of the New River Bridge

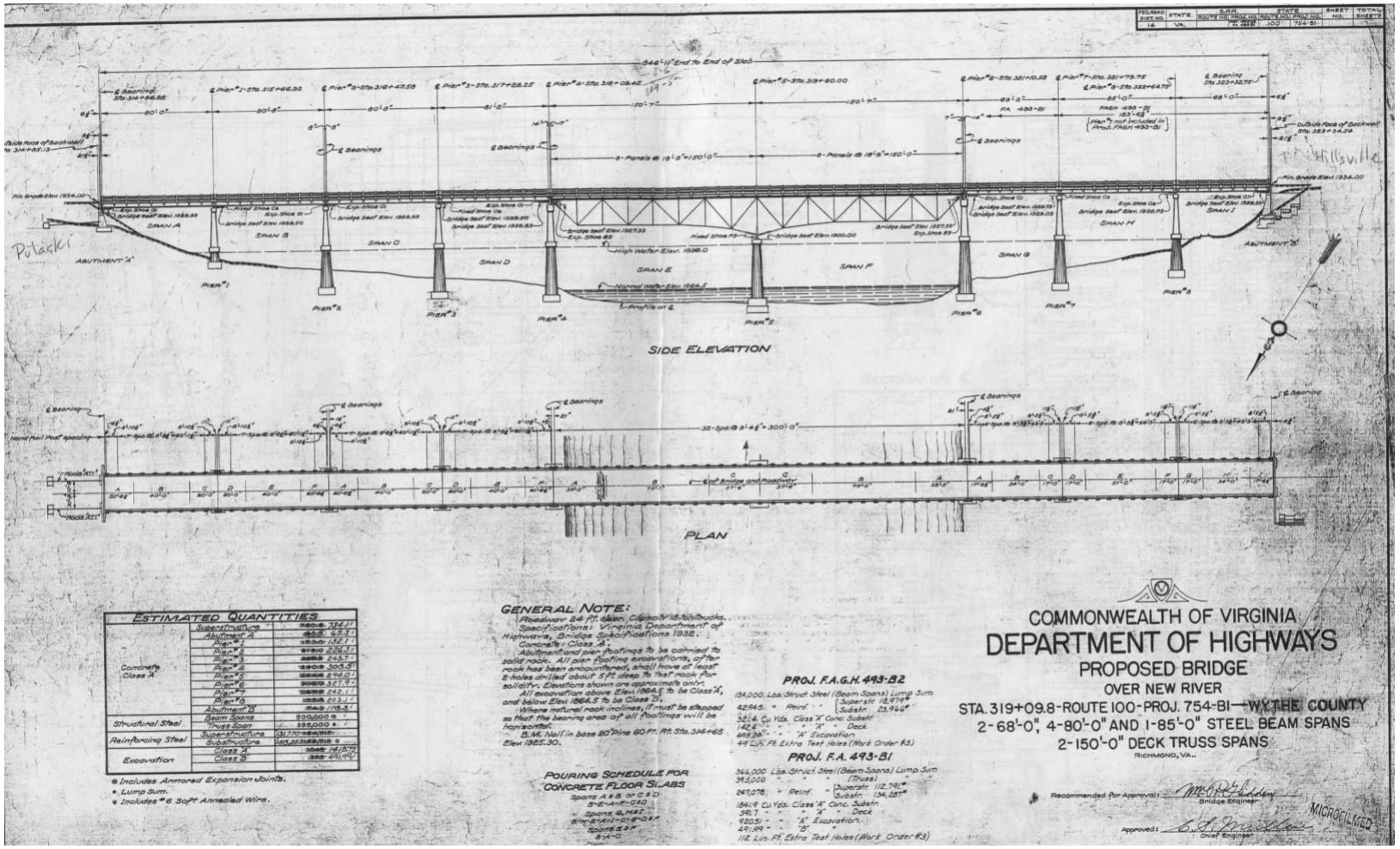

Figure C-1. General information of the bridge geometry. The Commonwealth of Virginia, Department of Highways, Virginia Transportation Research Council (1941). Used under fair use, 2015.

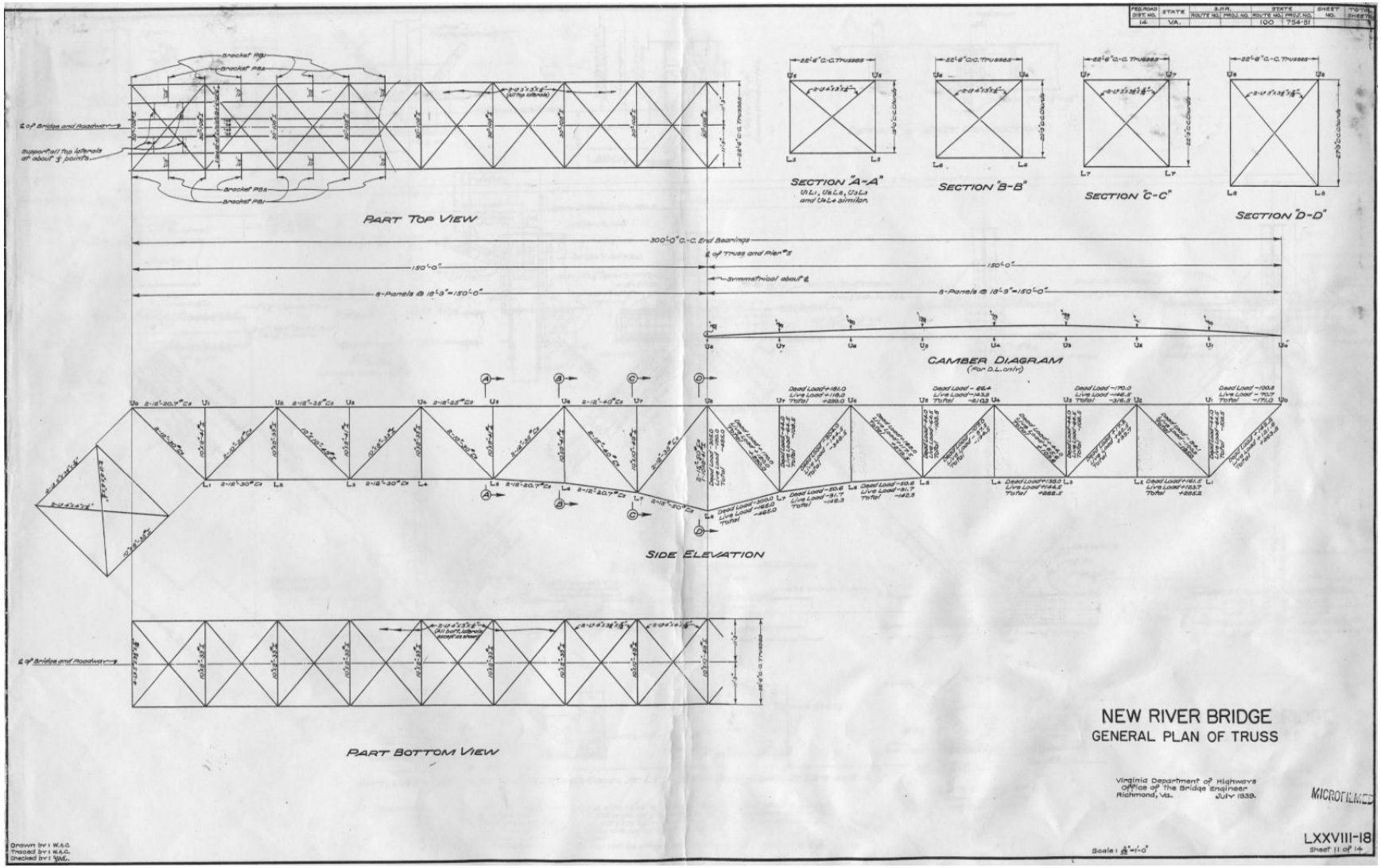

Figure C-2. Dimensions and design loads for truss members. The Commonwealth of Virginia, Department of Highways, Virginia Transportation Research Council (1941). Used under fair use, 2015.

Appendix D: Details of Span No.4 of the Milton-Madison Bridge

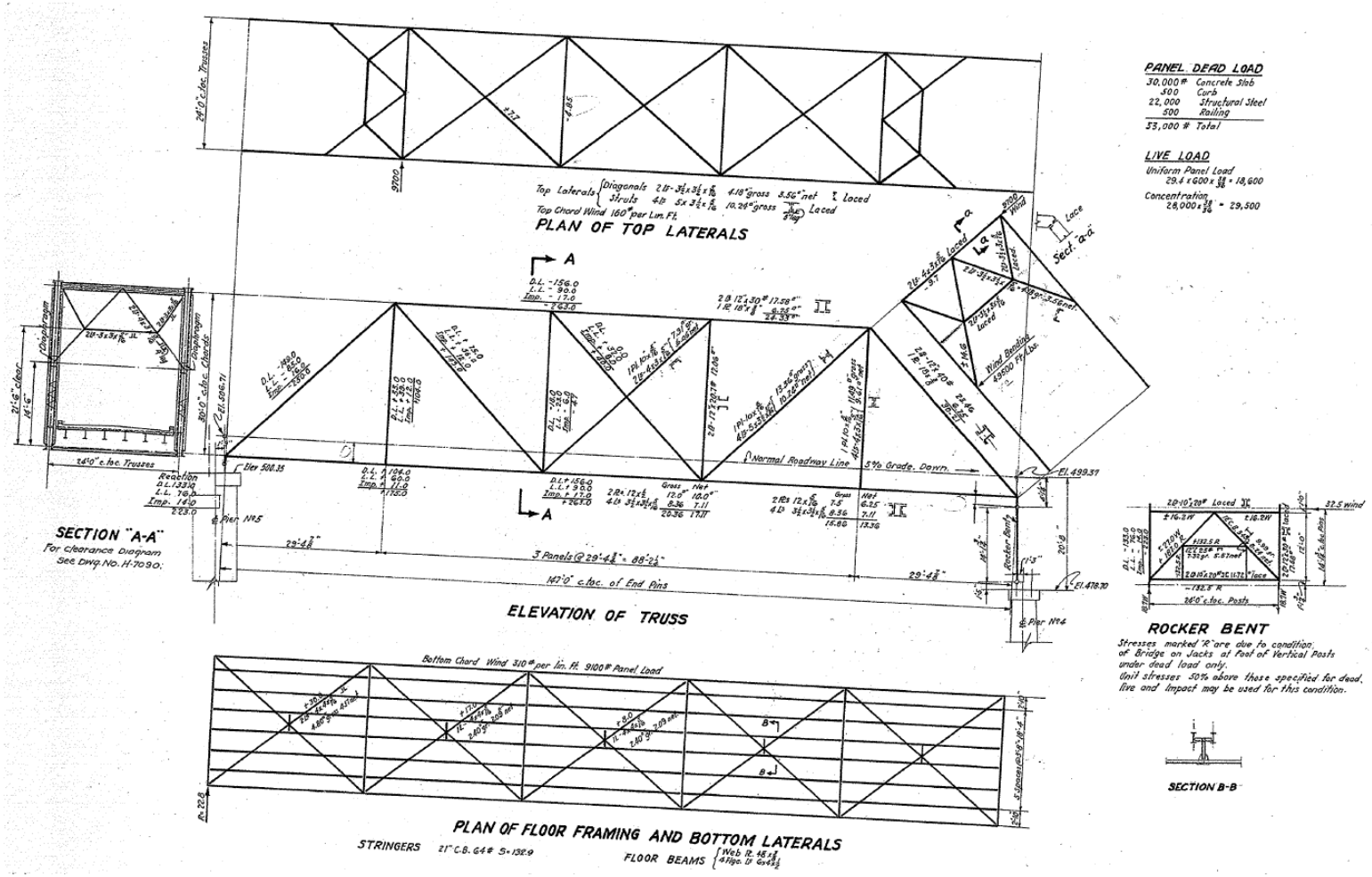

Figure D-1. Dimensions and design loads for truss members. J.G. White Engineering Corporation (1928). Used under fair use, 2015.